Guard cell shape change and the role of expansins and ARP2/3 in stomatal function

Eleanor G. Healicon

A thesis submitted in partial fulfilment of the requirements for the degree of Doctor of Philosophy

The University of Sheffield

Faculty of Science

Department of Animal and Plant Sciences

September 2019

Acknowledgements

Firstly, I would like to express my appreciation and thanks to my supervisors Professor Andy Fleming and Professor Julie Gray, for all their advice, guidance and feedback. I am grateful to BBSRC for funding this project. Thanks also to my thesis writing mentor, Sophie Nyberg, for her useful productivity suggestions during my writing process.

I would like to thank all members of D59, past and present, for their support and input into the project. It's been a pleasure to work in such a friendly lab group. This research would not have been possible without Marion Bauch, who has been an incredible help in the lab, and Jen Sloan, for technical support and who has been great when I've needed to bounce ideas off someone. Thanks to Matt Wilson for being generous with his time in providing training and help on the Li-cors and assistance with LithographX. Thanks to Shauni McGregor and Sarah Carroll for keeping an eye on my plants towards the end, for answering all my silly questions and for putting up with my mess in the Annexe. I am very grateful to Alice Baillie for her endless help and guidance both during her time in D59 and afterwards, as well as being a great host. Thanks to Naomi Cox and to Marion Tout, who have both been there when I've needed someone to listen.

My former housemates Antonia, Tom and Becca provided me with lots of moral support during our time at Fulton Road, and thanks to Rachel and Jordan for all their encouragement. Sabbie has been a constant source of positive words and life advice for which I am very grateful. My friends Yasmin and Emma have been a stronghold of emotional support during the last four years and have always been there for me when I've needed it. I feel very lucky to have their friendship in my life.

Thanks to my family for their love and caring words. A special thanks to Gary for his kindness, for making me laugh, and for always celebrating the small things with me. His company in the last few months made writing this thesis bearable. Finally, thanks to my mum and dad, who are the most supportive and kind people, who have shown me so much love and encouragement, and without whom I wouldn't have gotten through the last four years.

Collaborations

The work presented in this thesis could not have been done without the generous help offered by the following people.

One replicate of the *arp3* and Col-0 immunolabelling was carried out by Dr Alice Baillie, with whom I collaborated on the *arp3* project and who provided lots of useful guidance, advice and help. The *arp3* CO_2 bioassay in Chapter 4 was performed by Sarah Carroll, who gave me the resulting images and data for my own analysis.

A number of transgenic lines, data and other equipment were kindly gifted from numerous people.

Dr Firas Bou Daher from the Sainsbury Laboratory at the University of Cambridge kindly gave me seeds for the transgenic line myr-YFP which was fundamental to my work on the confocal microscope in Chapter 3.

Dr Raymond Wightman from the Sainsbury Laboratory at the University of Cambridge sent me the myr-YFP construct in agrobacteria which was also used in Chapter 3 and will be very useful in the continuation of this project.

Dr Lee Hunt from the Julie Gray lab in Sheffield gave me the APKa::GFP and APKb::GFP lines used in Chapter 3 for use on the light sheet fluorescent microscope. He also generated the microarray data and shared with me the results, which were used in Chapter 5 to identify expansin genes expressed in guard cells.

Professor Kathryn Ayscough and Dr Iwona Smaczynska-de Rooij from the Department of Biomedical Science at The University of Sheffield kindly gave me a sample of FM4-64 for use on the confocal microscope in Chapter 3.

Dr Gary McClean generously helped me with my statistical analyses.

Abstract

Stomata are microscopic pores that are critical for plant survival by regulating plant gas exchange and water regulation. They do this by moderating the aperture of the pore through the two flanking guard cells, which change shape in response to large changes in internal turgor pressure. The extent to which guard cells change shape is dependent on the anisotropic growth and deformation of the guard cell wall, and it is this shape change that is fundamental to the opening and closing of the stomata. Modellers of guard cell mechanics and function are increasingly realising that guard cell shape is crucial for understanding how guard cells can function under such conditions, yet there has been little detailed characterisation of guard cell shape change.

In this thesis, I present a novel method of imaging Arabidopsis guard cells using confocal microscopy and a way of processing these images to create 3D reconstructions of the guard cells. These reconstructions provide novel quantitative data on guard cell volume, surface area and other geometric parameters when the stomata are both open and closed. These data provide a novel insight into the type of shape changes that guard cells undergo to control pore aperture. I then report on a series of genes implicated in the control of guard cell shape, focussing on a subunit of the ARP2/3 complex, and a family of proteins implicated in regulating cell wall extensibility, the expansins. By a combination of mutant analysis and stomatal functional bioassays, as well as thermal imaging and gas exchange analysis, I provide evidence for a role of the ARP2/3 complex and expansins in guard cell function.

Table of contents

Table of figures

Table of tables

Table of equations

Abbreviations used

ABA	Abscisic acid
ABP	Actin binding protein
AFM	Atomic force microscopy
CMF	Cellulose microfibrils
CSC	Cellulose synthase complex
F-actin	Filamentous actin
FC	Fusicoccin
FEP	Fluorinated ethylene propylene
GalA	Galacturonic acid
GMC	Guard mother cell
HG	Homogalacturonan
IRGA	Infrared gas analyser
iWUE	Instantaneous water use efficiency
LGX	LithographX
LSFM	Light sheet fluorescent microscopy/microscope
mAB	Monoclonal antibody
MGX	MorphographX
MMC	Meristemoid mother cell
MP	Milk protein
PI	Propidium iodide
PBS	Phosphate buffered saline
PME	Pectin methyl esterase
PMEI	Pectin methyl esterase inhibitor
RB	Resting buffer
RGI	Rhamnogalacturonan I
RGII	Rhamnogalacturonan II
SA:V	Surface area: volume ratio
SEM	Scanning electron microscopy/microscope
SLGC	Stomatal lineage ground cell
WUE	Water use efficiency

Chapter 1: Introduction

Ensuring future food security is one of the most important international issues. A growing global population combined with the threat of climate change and increased competition for land and water means that it will be necessary to produce more food from less land area and water resources (Eckardt et al., 2009; Parry et al., 2004, 2007). This must be achieved to improve the future for humanity in a world where one in eight of the global population are already undernourished (Food and Agriculture Organization of the United Nations, 2013).

To confront this, attention has turned to modifying crops to produce a higher yield with the same given amount of land. This includes looking to improve water use and nutrient efficiency, as well as disease resistance and tolerance of other abiotic stressors (Godfray et al., 2010). Water use efficiency (WUE), defined as the ratio of the rate of carbon assimilation to the rate of transpiration, has been identified as a key factor in gaining crop productivity and reducing stress during periods of drought (Sinclair et al., 1984).

Amongst other mechanisms, plants can optimise their WUE through stomatal control (Bertolino et al., 2019; Franks et al., 2009). Stomata are pores on the surfaces of plants through which water is lost via transpiration and carbon dioxide is taken up for photosynthesis. In the short-term, most plants control their WUE by opening and closing these pores, whereas over longer time periods, some plant species produce leaves with altered stomatal size or density (Doheny-Adams et al., 2012; Franks et al., 2009). Each stomatal pore is flanked by two highly specialised cells named guard cells, which inflate and deflate to adjust the aperture of the pore and therefore control gas and water flux between the plant and the aerial environment.

Guard cells are distinct from other epidermal cells in size, shape and many other aspects. The structure and physical properties of the guard cells are important in stomatal function (Franks and Farquhar, 2007), which is essential for the survival of many plants. This thesis aims to contribute to our growing knowledge of how stomata are able to balance water use and photosynthetic assimilation, by developing a novel method of assessing guard cell shape change, and investigating the role of specific guard cell wall components in stomatal function.

1.1 Stomatal function

Stomata are key to determining the balance between maximising gas exchange for carbon assimilation and restricting it to conserve water. Stomata are responsible for both short-term and long-term control over the rate at which CO_2 is assimilated into and water lost from the plant. This control is essential in order for the plants to maintain a certain degree of plasticity for survival in changing environments (Hetherington and Woodward, 2003).

There is much morphological diversity in stomata across plant clades. Dicots typically have kidney bean-shaped stomata and do not have neighbouring subsidiary cells (Figure 1.1A and B). Monocots can have kidney bean-shaped stomata or, as with graminaceous monocots, can have stomata that are dumbbell-shaped and are paired with two flanking cells called subsidiary cells (Figure 1.1C and D), which are thought to play a role in support and the exchange of solutes and ions to and from the guard cells (Franks and Farquhar, 2007).

The aperture of the pore affects the rate of transfer of gases and water between the plant and its environment. Guard cell shape change in response to various signalling events can manipulate the pore in order to react to fluctuations in the plants' environment (Kollist et al., 2014; Schroeder et al., 2001). These signalling events trigger a change in internal turgor pressure within the guard cells. An increase in turgor pressure leads to cell swelling and bowing or moving outwards, therefore opening the pore, and a decrease in turgor pressure results in the cells shrinking and closing the pore (Hetherington and Woodward,

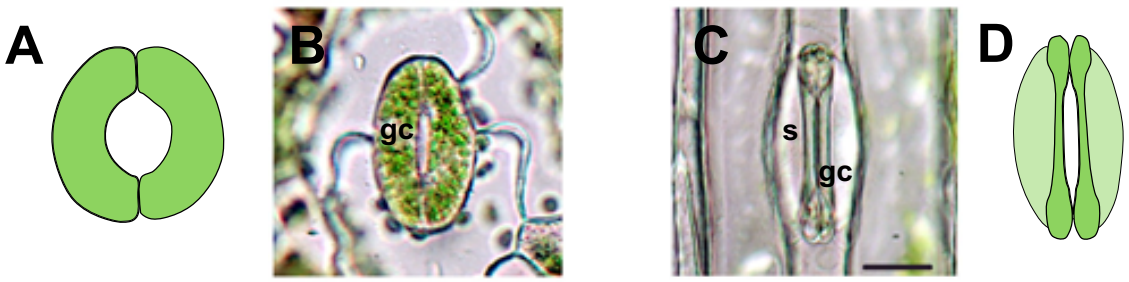

Figure 1.1 The morphological diversity of stomata. Stomata can be kidney bean-shaped (**A** and **B**) or dumbbell shaped (**C** and **D**). **A** and **D** are (respectively) schematics of **B**, micrograph of fern *Nephrolepis exaltata*, and **C**, micrograph of wheat *Triticum aestivum*. Guard cell indicated by **gc**, subsidiary cell indicated by **s**. Scale bar = 20μm, micrographs are at the same scale and were modified from Franks and Farquhar, 2007.

2003). These signalling events are highly coordinated in order to maximise the amount of CO_2 that can be assimilated for photosynthesis whilst also reducing effects of water loss.

Over longer periods of time, some plant species can produce a more systemic response to changes in the environment by moderating both the size and the number of stomata that develop (Casson and Gray, 2008; Doheny-Adams et al., 2012; Woodward, 1987). This is believed to have had a large effect on the maximum stomatal conductance during past changes in atmospheric CO_2 concentration (Franks and Beerling, 2009).

The significance of stomata also goes beyond plant physiology as their evolution is said to have been a key driver in the conquering of terrestrial environments for plants (Haworth et al., 2011). Furthermore, stomata have been implicated as a part of a vast system that regulates global carbon and water cycles, playing a key role in sensing, adapting to, and driving environmental change (Hetherington and Woodward, 2003).

1.2 Stomatal development

Stomata develop via a series of cell differentiation events and cell-state transitions which are shown in Figure 1.2 (Bergmann and Sack, 2007; Pillitteri and Torii, 2012; Zhao and Sack, 1999). This lineage begins with protodermal cells which are fated to become either epidermal pavement cells or meristemoid mother cells (MMCs), which are the first precursors on the guard cell differentiation pathway. MMCs undergo an asymmetric entry division to form a stomatal lineage ground cell (SLGC) and a smaller triangular meristemoid cell. SLGCs can either differentiate to form a pavement cell, or undergo further asymmetric divisions which are oriented in order to properly space out meristemoids (Geisler et al., 2000). This process upholds the 'one cell spacing rule' which ensures that the developing stomata are at least one cell away from each other (Geisler et al., 2000; Hara et al., 2007) which is thought to maximise CO_2 uptake (Rowe and

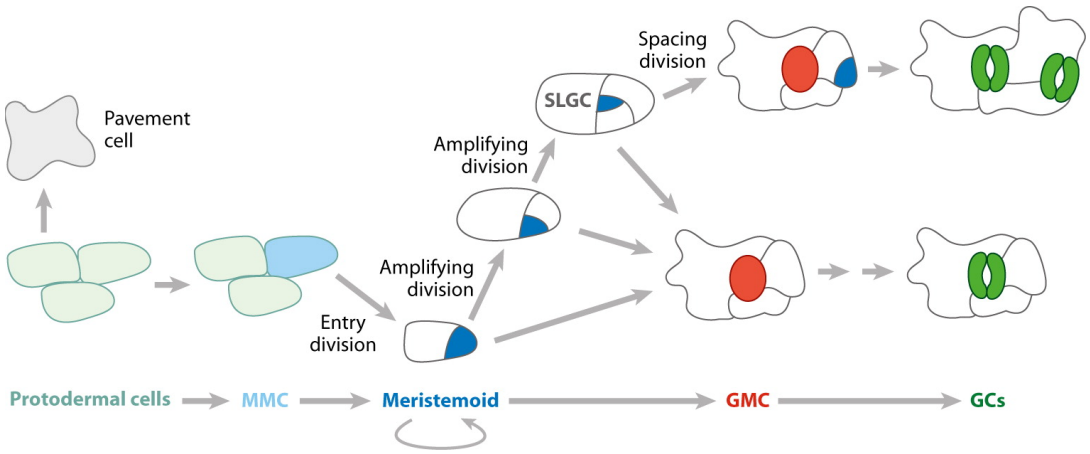

Figure 1.2 Cell differentiation events and cell-state transitions involved in Arabidopsis stomatal development. Protodermal cells transition into either pavement cells or meristemoid mother cells (MMCs). MMCs divide to form a meristemoid and a stomatal lineage ground cell (SLGC). Meristemoids then transition into guard mother cells (GMCs) which then differentiate into guard cells (GCs). Diagram from Pillitteri and Torii, 2012.

Bergmann, 2010). A series of amplifying divisions by the meristemoid means that additional SLGCs can be generated, whereas spacing divisions are orientated divisions which produce additional meristemoids (Geisler et al., 2000). It has been estimated that most of the cells that make up the leaf epidermis come from divisions of the guard cell lineage (Bird and Gray, 2003; Geisler et al., 2000). After a varying number of amplifying divisions, the meristemoid then undergoes a cell state transition into a guard mother cell (GMC). Unlike the previous asymmetric cell division events, the GMC divides evenly to form two cells which go on to mature into guard cells.

This process of guard cell development is highly controlled and has been the subject of thorough investigation in recent years. Experiments with the model plant species, *Arabidopsis thaliana*, have elucidated a series of transcription factors and signalling components that control the divisions of guard cell precursors by characterising the corresponding mutants in terms of their final stomatal phenotype (see Bergmann and Sack, 2007).

The density and number of stomata on a leaf is dependent on the number and frequency of the asymmetric spacing divisions of the SLGCs (Bergmann and Sack, 2007; Pillitteri and Torii, 2012). If multiple spacing divisions occur, then one daughter cell can produce generations of stomata from the same lineage. This, and the number of initial entry divisions, provides a developmental mechanism for the control of stomatal density.

Together these can result in the distinctions seen in different regions of plant tissue: for example, precursor cells that cease to form earlier in the adaxial epidermis than the abaxial epidermis (Geisler and Sack, 2002).

The environment of the plant can have a significant effect on the process of stomatal development and density (Casson and Gray, 2008; Lake et al., 2001; Schoch et al., 1980). Further study into the effects of stomatal density has shown that manipulation of stomatal density in common crop plants such as barley and rice can enhance water use efficiency without deleterious effects on yield (Caine et al., 2019; Doheny-Adams et al., 2012; Franks et al., 2015; Hughes et al., 2017).

1.3 Guard cell signalling

Guard cells control the aperture of the stomatal pore through changes in turgor pressure within the guard cells, which varies greatly. For example, internal turgor pressure in *Vicia faba* (broad bean) guard cells ranges between 0 and 5kPa (Franks, 2003). To open the stomatal pore, guard cells must accumulate ions and solutes in order to raise the osmotic potential of the cell, and to close the pore, the guard cells must do the opposite (Figure 1.3).

Stomatal opening requires the uptake of osmolytes such as K^+ into the guard cells (Fischer, 1968). During stomatal opening, H^+ ions are pumped out of the guard cell by membrane-bound H^+ ATPases in response to stimuli such as light (Lohse and Hedrich, 1992; Shimazaki et al., 2007). This forms an electrochemical gradient across the membrane which promotes the activation of inward-pumping K^+ channels (K^+_{in}) (Schroeder et al., 1984). This entry of positively-charged K^+ into the cell is counterbalanced by anions such as malate and Cl^- (Jezek and Blatt, 2017; Schmidt and Schroeder, 1994). The increase in ions and solutes within the guard cell causes the cell's water potential to decrease, resulting in an influx of water into the cell which increases the internal turgor pressure and results in cell swelling and eventual pore opening (Jezek and Blatt, 2017; Schroeder et al., 2001).

One of the major routes to stomatal closure involves an increase in internal calcium (Ca^{2+}) within the guard cells (Roelfsema and Hedrich, 2010). As an outline, this inhibits the H^+

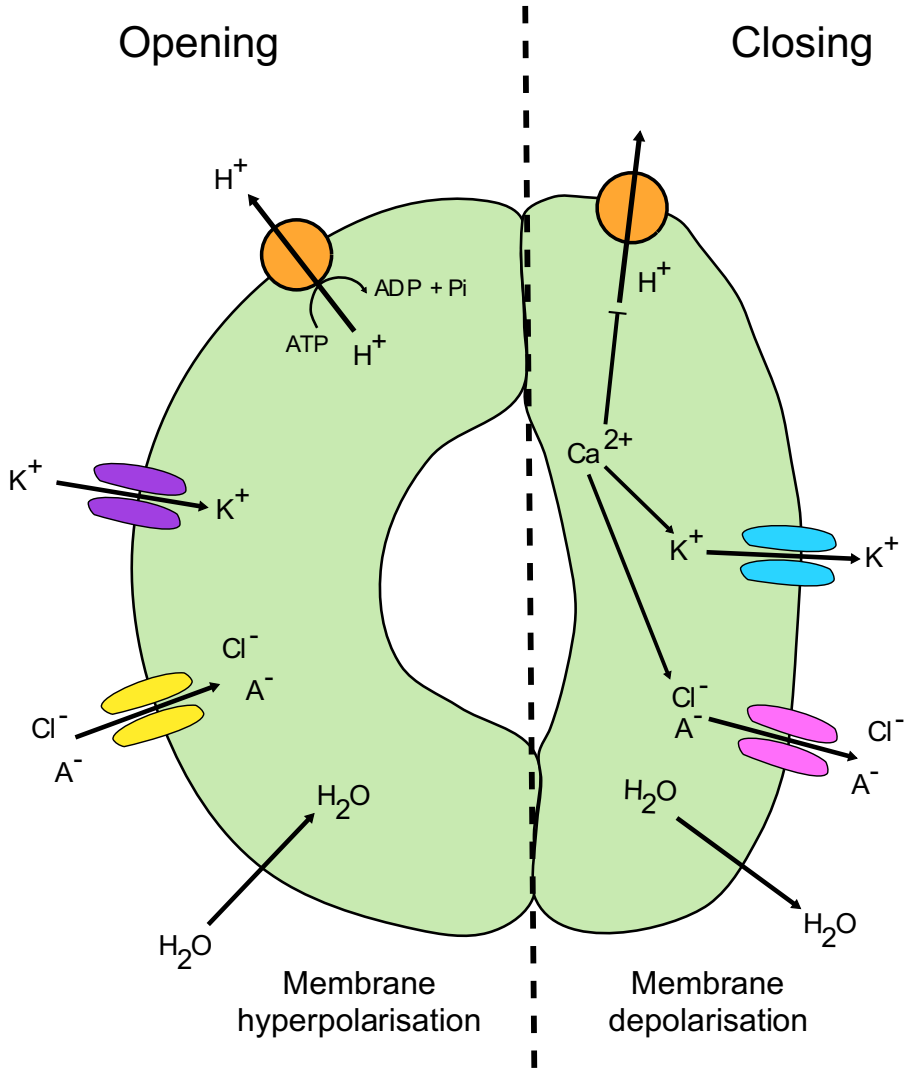

Figure 1.3 Schematic showing simplified signalling mechanisms for the opening (left) and closing (right) of stomata. During stomatal opening, an extrusion of H^+ ions via a proton pump (orange) causes membrane hyperpolarisation. This electrochemical gradient stimulates inward-pumping K^+ channels (purple) to let K^+ ions into the guard cell, as well as Cl^- and other anions (A^-) to counter the positively-charged potassium ions (yellow). This accumulation of ions and solutes decreases the water potential of the cell, causing an influx of water which increases guard cell turgor pressure and therefore cell expansion and stomatal opening. When stomata close, a stimulus increases intercellular Ca^{2+} which inhibits the proton pump and stimulates outward-pumping anion channels (pink) to release anions (A^-) and solutes from the cell. This results in membrane depolarisation, which causes outward-rectifying K^+ channels to expel K^+, leading to a decrease in cell water potential and an efflux of water which closes the pore.

pumps and the K^+_{in} channels (McAinsh et al., 1990). Elevated Ca^{2+} also activates anion channels that promote the release of anions from the guard cells (Schroeder and Hagiwara, 1989). This efflux of anions causes depolarisation of the plasma membrane, which further inhibits K^+_{in} channels and H^+ pumps (Schroeder et al., 1987), and is critical

for the release of water from the cell and its resulting reduction in turgor pressure which closes the pore (Jezek and Blatt, 2017; Schroeder et al., 2001).

Stomatal opening and closure is regulated by a complex signalling network. Stimuli from the neighbouring cells, the environment of the plant, and also the metabolism of starch (Horrer et al., 2016) and lipids (McLachlan et al., 2016) within the guard cells themselves can initiate a change in the stomatal pore aperture. Stomata must integrate a mixture of signals, such as light, plant hormones, CO_2, water status and pathogen presence, in order to balance plant water loss with overall CO_2 intake (Schroeder et al., 2001). Those studying stomata can use these stimuli to manipulate stomata in experiments to test opening and closing responses. In this thesis three main stimuli are used in various experiments: ABA, CO_2 and fusicoccin.

Abscisic acid (ABA) is a plant stress hormone that stimulates stomatal closure on drought. It induces the elevation of levels of guard cell Ca^{2+} which opens the outward-acting anion channels (McAinsh et al., 1990), allowing the extrusion of protons, Cl^-, K^+, and malate out of the cell which causes the efflux of water. This shrinks the guard cell due to the decrease in turgor pressure, which therefore closes the pore. The signalling pathway that induces stomatal closure in response to high concentrations of CO_2 initially uses a similar mechanism, whereby if the external CO_2 concentration is at a level that requires a smaller stomatal aperture for sufficient CO_2 influx, or if internal CO_2 rises at night as a result of plant respiration, there is an increase of Ca^{2+} inside the guard cells which initiates closure (Schroeder et al., 2001). It has been shown that stomatal responses to CO_2 are ABA-dependent (Chater et al., 2015; Dittrich et al., 2019) which further reinforces the idea of a convergence of the ABA and CO_2 signalling pathways, although this is not without some controversy (Kim et al., 2010; Leymarie et al., 1998). Investigations into this area have identified some components that are shared with the guard cell ABA response pathway such as the guard cell anion channel SLAC1 (Vahisalu et al., 2008), and also identified novel CO_2 response components, such as the kinase HT1 (Hashimoto et al., 2006), and carbonic anhydrases βCA1 and βCA4 (Hu et al., 2010).

During evolution, stomatal signalling pathways have been exploited by pathogens. An example of this comes from the fungal pathogen *Fusicoccum amygdali* which causes wilt disease in the *Prunu*s genus (in almonds and peach trees). It produces fusicoccin, a fungal

toxin which causes the opening of the stomatal pore in order for the fungus to gain entry to the plant. Fusicoccin constitutively activates the membrane-integral proton pump (Johansson et al., 1993) which is pivotal for stomatal opening. Constitutive activation of the H^+ ATPases means the guard cell plasma membrane is continuously hyperpolarised. It also causes the acidification of the area surrounding the plasma membrane which results in acid growth of the guard cell wall (Rayle and Cleland, 1992), which is believed to allow the cell wall expansion seen during stomatal opening.

1.4 Plant cell walls

The plant cell wall is a dynamic and complex extracellular matrix that surrounds the cell membrane, providing support, structure and protection to virtually all plant cells. Indeed, the word 'cell' in its biological capacity was coined by Robert Hooke in 1663 after viewing the thick cell walls of cork down a microscope. The main constituents and basic structure of the plant cell wall have been known for a long time (Carpita and Gibeaut, 1993) and research over the last two decades has revealed a considerable amount about the biosynthesis, organisation, mechanics, and interaction of cell wall components across plant taxa. This research into the synthesis, evolution and function of cell walls has highlighted their economic and ecological importance (Niklas, 2004), as they are valuable in industrial production of biofuels, paper, food and pharmaceuticals among many others (Rubin, 2008; Sticklen, 2008).

Plant cells are highly variable in size; within one plant species the size of a cell can vary 10,000-fold (Cosgrove, 2005) with guard cells being amongst the smallest. For a plant cell to change shape, such as in cell expansion and growth, turgor pressure within the cell pushes against the cell wall. The change in cell size is entirely dependent on the cell wall, where cell wall extensibility and elasticity determine the degree of yield to the internal pressure. Cell growth is also almost always anisotropic, meaning that the degree and rate at which cells grow is uneven across the cell, which explains in part why plant cells are not all spherical (a shape that is a product of isotropic growth) (Braidwood et al., 2014). Furthermore, the precise location and degree to which cell swelling occurs is due to the restrictions of the cell wall, meaning that it is key when considering eventual cell shape and shape change during growth.

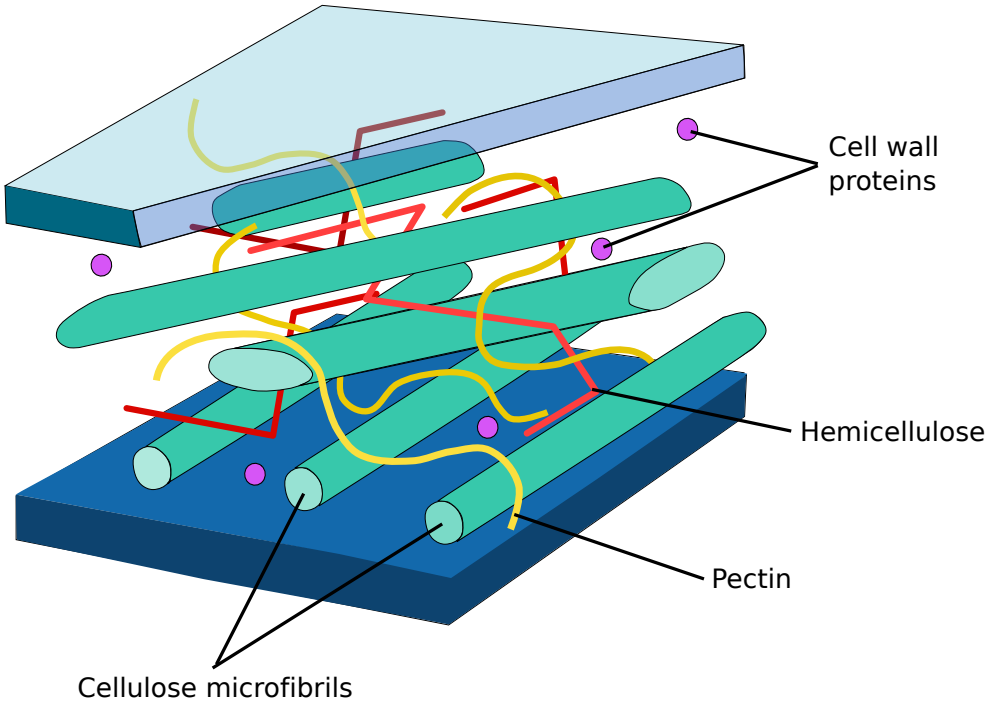

Figure 1.4 Simplified diagram of the primary plant cell wall. Cellulose microfibrils (blue) are cross-linked with hemicelluloses (red), providing tensile strength to the cell wall. These are embedded in a pectin matrix (yellow) along with other cell wall proteins (purple), such as expansins, which are endogenous modifiers of plant cell wall polysaccharides.

Cellulose, hemicelluloses and pectins are three main groups of polysaccharides that comprise the primary plant cell wall, along with other non-carbohydrate components such as cell wall proteins (Figure 1.4). The secondary cell wall is deposited between the protoplasm and the primary cell wall and is associated with woody tissue. It is lignin-heavy, which is tough and confers mechanical support, allowing plants such as trees to reach such great heights (Meents et al., 2018; Schuetz et al., 2013). In this thesis my focus will be on the primary cell wall and its constituents, as guard cells do not have a secondary cell wall.

1.4.1 Cellulose

Cellulose is the most abundant polymer in the world and has significant economic importance (Klemm et al., 2005), used in paper products, pharmaceuticals, biofuels and building materials. It is the main load-bearing constituent of the cell wall (Geitmann, 2010) and has a crystalline structure made up of β-1,4 glucose chains (Nishiyama, 2009). These chains are synthesised at the plasma membrane by the cellulose synthase complex

(CSC), a large rosette-shaped molecule of 6 subunits (Mueller and Brown, 1980). CSCs build these glucan chains which are then assembled into long unbranched cellulose microfibrils (CMFs) that are 3nm in diameter and can measure up to 7μm in length (Somerville et al., 2004). As the CSC has 6 subunits, it is assumed that CMFs are synthesised from glucan chains in multiples of six; traditionally, it was thought that 36 glucan chains make up a CMF, but more recent data propose that it is 18 (Newman et al., 2013). Cellulose synthesis is reviewed extensively in a review by McFarlane, Döring and Persson (2014).

The orientation and organisation of CMFs is largely due to the cell cytoskeleton and microtubules (Bashline et al., 2014; Palevitz and Hepler, 1976). The CMFs in the first layers of the cell wall (therefore closest to the plasma membrane of the cell) are oriented in parallel to the microtubules near the cell surface (Helper and Newcomb, 1964). The direction in which the CMFs is organised is thought to direct cell growth, with CMFs being laid down in a transverse orientation to the direction of growth (Roelofsen and Houwink, 1951). It has been observed that the direction of orientation can change over time (Anderson et al., 2010).

1.4.2 Hemicelluloses

Hemicelluloses interact with cellulose molecules in the cell wall by forming hydrogen bonds, tethering to the CMFs and therefore strengthening the cell wall (Scheller and Ulvskov, 2010). They are a heterogeneous class of cell wall polysaccharide around which there has been some debate as to what should be included. This is because the term was coined when there was very little known about the plant cell wall and the composition of hemicelluloses were not well understood (Scheller and Ulvskov, 2010). For example, sometimes arabinans and galactans are listed as hemicelluloses, but they are also frequently associated with pectin, and so overlaps between the plant cell wall categories is frequently seen. Vergara and Carpita (2001) use the alternative term cross-linking glycans to better define the hemicelluloses, however it has been observed that not all of these polysaccharides have cross-links. Scheller and Ulvskov (2010) suggest that the term hemicellulose should continue to be used for simplicity, but they define hemicelluloses as polysaccharides that are not cellulose or pectin and have a β-(1→4)-linked backbone structure of glucose, mannose or xylose, as this means the group has some degree of

structural similarities. This definition will be used in this thesis; meaning hemicelluloses include xylan, xyloglucan, mannan, and glucomannan. The relative quantity of the these diverse polysaccharides vary between dicots, monocots, conifers and algae (Scheller and Ulvskov, 2010).

Xyloglucans are widespread across plant taxa and represent the most abundant hemicelluloses in dicot primary cell walls (Popper et al., 2011; Scheller and Ulvskov, 2010). They are highly branched, with different side branch conformations conferring different functional properties (Scheller and Ulvskov, 2010). They are synthesised in the Golgi and have been observed to co-localise with CMF-containing regions of the cell wall (Moore and Staehelin, 1988). It is thought that this cross-linking between xyloglucan and cellulose provides the main load-bearing network within the primary cell wall, an idea which is supported by the relative abundance of cellulose and xyloglucan (Peaucelle et al., 2012). Interestingly though, Arabidopsis mutants deficient in xyloglucan have aberrant root hairs but do not have a distinct whole plant phenotype (Cavalier et al., 2008).

Mannans have backbones made entirely of β-(1→4)-linked mannose, and the backbones of glucomannans are made from repeated β-(1→4)-linked mannose and glucose. They are the most common hemicellulose in green algae cell walls (Popper, 2008). Despite being found in variable but low amounts in dicots (Scheller and Ulvskov, 2010), it is known that they are important in Arabidopsis growth, as a knock-out mutant of a glucomannan synthesis gene *CSLA7* results in embryo death (Goubet et al., 2003). Knock-outs of mannan synthesis genes result in dwarfed Arabidopsis plants (Bernal et al., 2007).

Xylans share the common feature of having a β-(1→4)-linked xylose backbone and are characteristic of secondary cell walls in dicots. They are the most common hemicellulose in the cell walls of commelinid monocot species (Scheller and Ulvskov, 2010).

1.4.3 Pectins

Pectins are a diverse family of polysaccharides characterised by galacturonic acid (GalA) residues in their backbone, making up to 35% of the dicot primary cell wall (Mohnen, 2008; Ridley et al., 2001). Their diverse structures indicate that pectins have varied roles within the plant, and they are known to play a part in cell-cell adhesion, plant defence, signalling (Ridley et al., 2001), and fruit ripening (Tieman and Handa, 1994). Pectins are also of economic importance, being used as stabilising and gelling agents in food and

cosmetics, and also in products such as adhesives, medical devices and as a component in drug delivery services (Mohnen, 2008).

Pectins are categorised into three main groups: homogalacturonan (HG), rhamnogalacturonan I (RGI) and rhamnogalacturonan II (RGII; Figure 1.5) (Ridley et al., 2001). HG is a predominantly linear polysaccharide consisting of a linked GalA backbone wherein the GalA residues can be methyl- or acyl-esterified (Caffall and Mohnen, 2009). The degree and distribution of esterification of HG is developmental- and tissue-specific (Caffall and Mohnen, 2009; Willats et al., 2001) and has been observed to confer specific function to cell walls (Amsbury et al., 2016). It is the most abundant of pectin types in Arabidopsis (Caffall and Mohnen, 2009). In contrast to HG, RGI and RGII are highly branched and are particularly enriched with arabinan and galactan (Ridley et al., 2001). Arabinan side chains have been linked to specific cell wall properties in fruit ripening, whereby the loss of RGI side chains is closely followed by a loss of firm texture in apples

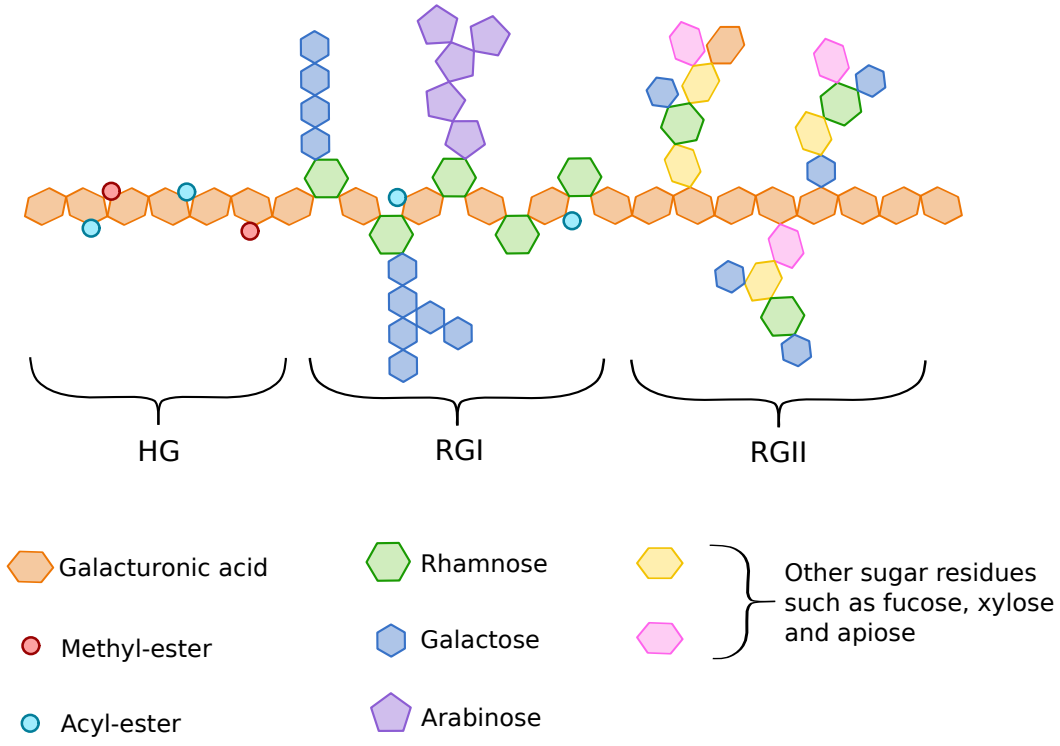

Figure 1.5 A schematic to show the simplified structure of three groups of pectin. Homogalacturonan (HG) is a linear form of linked galacturonic acid with occasional esterification. Rhamnogalacturonan I (RGI) contains both galacturonic acid and rhamnose within its backbone, and is branched with galactose and arabinose side chains. Rhamnogalacturonan II (RGII) is highly branched too, with side chains potentially consisting of multiple possible residues such as rhamnose, xylose, galactose and arabinose.

(Peña and Carpita, 2004). HG and RGII can be covalently linked, likely because they share a similar GalA backbone (Ridley et al., 2001; Willats et al., 2001) whereas RGI frequently self-dimerises.

Evidence indicates that pectin is synthesised in the Golgi apparatus by glycosyl transferases (Mohnen, 2008; Ridley et al., 2001). Pectin biosynthesis is a multifaceted and complicated process involving at least 67 enzymes (Mohnen, 2008), therefore the complexity of this process makes it difficult to study. However some pectin biosynthesis mutants have been identified, for example a glycosyl transferase called QUASIMODO1 (QUA1) where the mutant *qua1* exhibited a 25% reduction in GalA levels and a stunted growth phenotype has been reported (Bouton et al., 2002).

HG, the main pectin constituent of Arabidopsis cell walls, is synthesised in the Golgi and then transported to the cell wall in a highly esterified form. It is then de-esterified to varying degrees at the cell wall by pectin methylesterases (PMEs) (Pelloux et al., 2007). The level of pectin esterification and its effects on cell wall mechanics is contested. There are multiple competing hypotheses about the potential effects de-methylesterification of pectin can have on the cell wall (Wolf and Greiner, 2012).

It is known that de-esterification of cell wall pectin means that the HG can form Ca^{2+}-pectate cross links (Grant et al., 1973). Some think that these cross-links influence cell wall porosity, which can then indirectly affect the cellulose-hemicellulose network by allowing cell wall loosening proteins, such as expansins, into the cell wall (Cosgrove, 1999; Peaucelle et al., 2012; Wolf and Greiner, 2012). It is also a possibility that cross-linked pectin increases cell wall hydration which further increases cell wall flexibility. In contrast, Wolf and Greiner (2012) also hypothesise that the formation of Ca^{2+} cross-links after de-methylesterification may stop cell wall creep and therefore decrease cell wall pliancy. For example, some studies show that an increase in PME activity, and therefore a decrease in methylation of pectin, decreases cell wall elasticity (Derbyshire et al., 2007; Pelletier et al., 2010; Pelloux et al., 2007). However, a *PME* knockout, *pme35*, which would be expected to increase pectin methylesterification, had reduced mechanical strength in its stem (Hongo et al., 2012), and a knockout of *PME6* decreases cell wall flexibility in the guard cell wall (Amsbury et al., 2016). Other studies show otherwise and provide evidence that decreased pectin methylation led to increased pliancy of the meristematic

cell wall (Peaucelle et al., 2011, 2008). Thus, it remains unclear whether pectin esterification causes an increase in cell wall flexibility, a decrease in flexibility, or perhaps under differing circumstances can affect both. The situation is further complicated by the structure of a subgroup of PME proteins which contain a domain that is predicted to have pectin methyl esterase inhibitor (PMEI) activity (Wang et al., 2013).

It is clear that the mechanical consequences of pectin methylesterification status in the plant cell wall is a complex issue, and is likely dependent on developmental stage, cell type and many other influencing factors. Furthermore, other pectin epitopes also affect cell wall flexibility, for example, a loss of RGI arabinans has been shown to reduce guard cell mobility due to increased cell wall rigidity (Jones et al., 2003).

1.4.4 Cell wall proteins

Cell wall proteins have historically been difficult to study, because they are both comparatively low in number (Keller, 1993), but they are also embedded in a complex matrix of polysaccharides with which they interact (Albenne et al., 2014). They primarily exist to modify cell wall polysaccharides post-deposition and therefore they have the potential to allow changes to the cell wall in response to new stimuli (Braidwood et al., 2014). PMEs, discussed previously in section 1.4.3, are one of the most prominent groups of cell wall modifying proteins, along with extensins and expansins.

Extensins are a part of a larger hydroxyproline-rich glycoprotein (HRGP) family (Liu et al., 2016; Tierney and Varner, 1987) that are more abundant in dicots than monocots. They are a diverse family of glycoproteins thought to form cross-links with pectin (Lamport et al., 2011) by forming a positively-charged scaffold to which negatively-charged pectin binds to form extensin pectate, allowing assembly of a new cell plate during cell division (Cannon et al., 2007). Knock-out mutants of Arabidopsis *EXTENSIN3* (*AtEXT3*) display cell wall defects both in seedlings and embryos, wherein the frequency of "floating" walls (walls unconnected to cell walls) was much greater than in wildtype, and the likelihood of new cell walls being successfully connected to the mother cell wall was greatly decreased (Cannon et al., 2007; Hall and Cannon, 2002). Extensins have also been shown to be involved in plant defence (Castilleux et al., 2018).

Expansins are a large cell wall protein family with multiple subgroups (Li et al., 2002; Sampedro and Cosgrove, 2005) that are involved in cell wall loosening, doing so non-

enzymatically by breaking the hydrogen bonds that link cellulose and non-cellulose components of the cell wall (McQueen-Mason et al., 1992). Expansins are associated with cell growth due to their cell wall loosening properties, and have been implicated in fruit ripening (Brummell et al., 1999; Harrison et al., 2001), leaf expansion (Sloan et al., 2009) and root elongation (Lee et al., 2003).

1.5 Guard cell shape

Stomatal opening and closing is, fundamentally, a mechanical process, which must integrate three main factors: the physical properties of the guard cell wall, the internal turgor pressure of the guard cell, and overall cell shape (Woolfenden et al., 2018). As previously discussed, stomata are morphologically diverse (Figure 1.1). Size and shape of guard cells is essential to stomatal function, and the role of the surrounding cells is also important (Franks and Farquhar, 2007). However, this thesis will principally consider the mechanics of kidney bean-shaped guard cells without specialised subsidiary cells, as seen in Arabidopsis.

The shape of guard cells is critical to their function. In order to control the aperture of the stomatal pore and therefore provide a response to the plants' changing internal and external environment, guard cells must quickly and repeatedly shrink and inflate, therefore changing the shape of the cell (Meckel et al., 2007; Shope et al., 2003; Woolfenden et al., 2017). They do this in response to changes in internal turgor pressure, and the degree to which the guard cell changes its shape is influenced by its cell wall. Therefore, it is impossible to discuss guard cell shape change without also considering the guard cell wall.

The cell wall of guard cells is one of the few examples of cell wall deformation that is reversible, in contrast to the one-way growth of most plant cells. The guard cell wall, therefore, must have certain properties which will allow for this repeated stretching and shrinking, and that will be able to withstand the varying and often massive internal pressures that guard cells have been measured to contain. For example, *Vicia faba* (broad bean) and *Tradescantia virginiana* guard cells have an internal pressure that fluctuates between 0 and 5 kPa (Franks, 2003; Franks et al., 2001). The guard cell wall has been implicated in plant responses to biotic and abiotic stressors (Houston et al., 2016) and some research links guard cell wall composition specifically to altered transpiration

efficiency (Amsbury et al., 2016; Liang et al., 2010) and, therefore, WUE. Because of this, there has been significant interest in the specific properties of the guard cell wall.

1.5.1 Guard cell shape change and the guard cell wall

Early work approximated the guard cell as a thin-shelled torus with a highly elastic cell wall (Cooke et al., 1976), which more recent work has built upon. Woolfenden et al. (2017) used a biomechanical model to investigate a specific feature of the specialised guard cell wall: the rings of cellulose microfibrils (CMFs). These CMF rings wrap the circumference of the guard cell and are thought to guide the growth of the cells as turgor pressure increases (Figure 1.6A). This restricts cellular expansion widthways and ensures that the guard cells instead expand lengthways (Palevitz and Hepler, 1976; Shope et al., 2003). This makes growth of the guard cell anisotropic (direction-dependent), which has been observed experimentally (Meckel et al., 2007). Mutants with deficiencies in cellulose synthesis exhibit a wider stomatal pore and more isotropic cell growth (Rui and Anderson, 2016). The model used by Woolfenden and colleagues showed that without these CMF hoops, growth of the guard cell was isotropic and increasing turgor pressure was predicted to actually close the stomatal pore through the width-ways expansion of the guard cells.

Studies using immunohistochemistry have highlighted the important role of pectins in guard cell function. For example, guard cell walls have been shown to be rich in arabinan epitopes that assist in normal stomatal function. When arabinans are removed via enzymatic treatment, the stomata fail to open and close as normal, suggesting that the arabinans provide a degree of cell wall flexibility (Jones et al., 2005, 2003). This observation has been supported by biomechanical modelling of the guard cell (Woolfenden et al., 2017). A study into the distribution of highly methyl-esterified homogalacturonan (HG) and unesterified HG revealed that unesterified HG was present in guard cells and highly methyl-esterified HG was largely absent. Further investigation of a pectin methylesterase (*PME*) mutant *pme6*, which showed an increased amount of

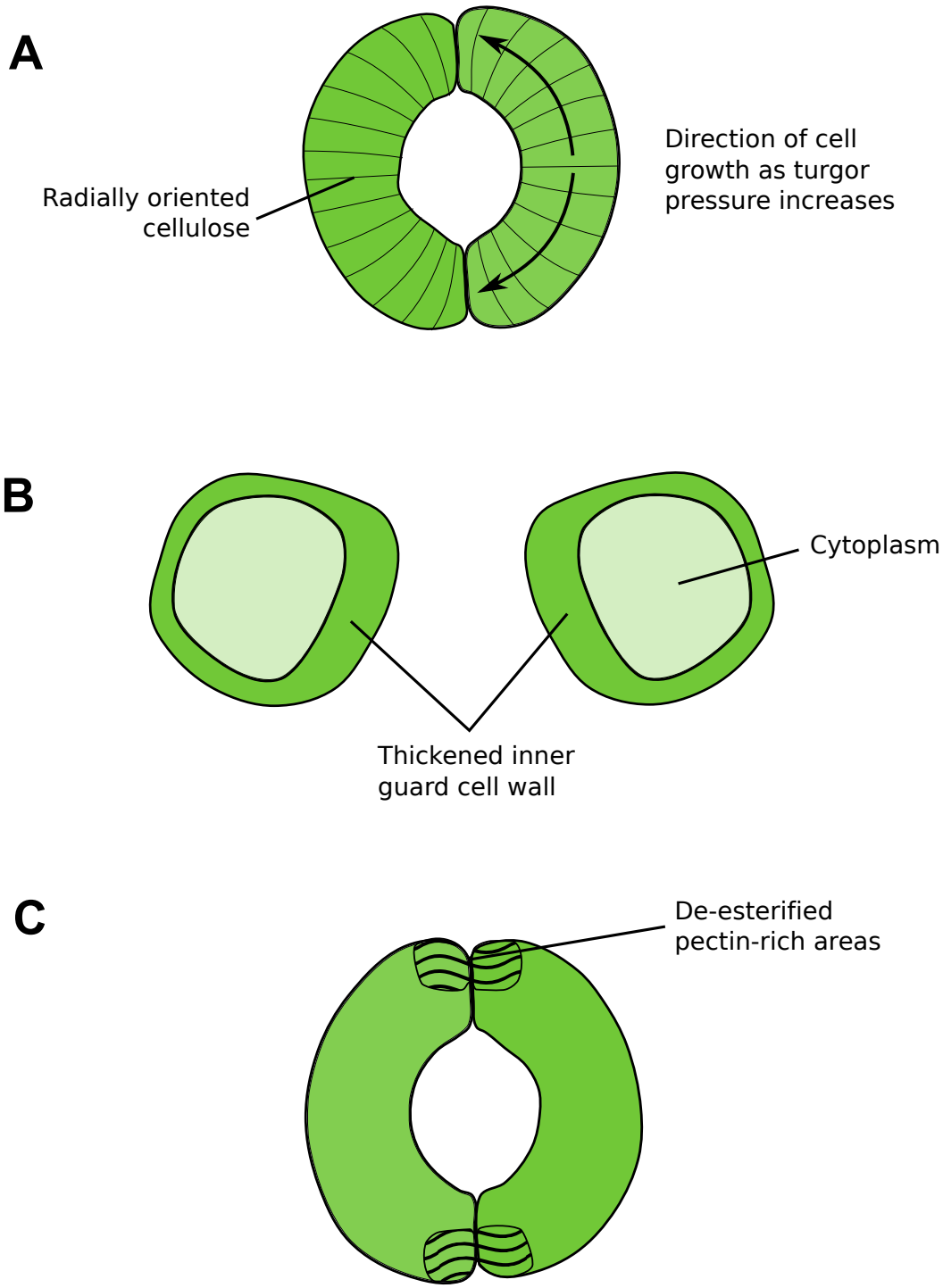

Figure 1.6 Schematics to illustrate different components of the guard cell wall which provide distinctive properties that aid stomatal function and shape the guard cell. (A) Radial rings of cellulose microfibrils ensure that the guard cells grow longitudinally rather than increasing in width. **(B)** The thickened inner guard cell wall was originally thought to be needed for the bending outwards of the guard cells during cell expansion, but is now thought to reinforce the cell wall against the stresses of repeated cell wall shrinking and stretching. **(C)** Deposits rich in de-esterified pectin at the guard cell tips coincides with areas of comparative cell wall stiffness. These pin the guard cells in place so that the stomatal complex does not change length during opening and closing, which results in a wider pore and a change in guard cell shape.

methylesterified HG in its guard cells compared to wild-type, lacked the ability to open and close its stomata fully (Amsbury et al., 2016). This provides more evidence to suggest that the role of pectins is important for normal stomatal function and further highlights the importance of the guard cell wall in stomatal function.

A study published by Carter et al. (2017) identified 'hotspots' of physical stiffness at the tips of the guard cells using atomic force microscopy (AFM), which they correlated with areas of de-esterified HG using a de-esterified HG probe. Using pore aperture measurements in combination with different cell wall enzymes, they found that these stiffer hotspots 'pinned down' the guard cell tips to ensure that the complex did not lengthen during opening or closing (illustrated in Figure 1.6C). Modelling indicated that this pinning down of the stomatal poles would result in a wider stomatal aperture when stimulated to open, and also suggested that the stomata may open faster. This work highlights not just the importance of the guard cell wall in stomatal function and efficiency, but also shows the importance of the precise location of the cell wall components within the guard cell wall. Furthermore, guard cells have been shown experimentally to lengthen during stomatal opening (Meckel et al., 2007). Therefore, this suggests that in order to comply with both the observation that the stomatal complex as a whole does not lengthen when opening the pore and the data showing that the component guard cells do lengthen when opening the pore, there must be a must change in the guard cell shape itself.

The same 2017 study by Carter and colleagues also explored the function of the commonly-observed thickening of the inner guard cell wall that lines the pore (Zhao and Sack, 1999). Early botanical studies identified a thickening of the inner guard cell wall which was presumed to be needed for the bending outwards of the guard cells as the stomata open (Figure 1.6B). However, Carter et al. showed that young stomata do not have this thickened inner cell wall yet can still open and close, therefore indicating that this inner cell wall thickening is not needed for normal stomatal function. Finite element modelling indicated that strain and stress on the guard cell wall is focussed around the inner guard cell wall, a finding that is supported by data from Woolfenden et al. (2017). Thus, the current hypothesis for the function of inner guard cell wall thickening is to alleviate the pressure stresses of repeated stomatal opening and closing, rather than to facilitate a shape change in the guard cell.

Other non-carbohydrate components of the cell wall have been shown to play a role in guard cell function. For example, the gene encoding Arabidopsis α-expansin 1, *AtEXPA1*, was overexpressed in Arabidopsis which resulted in accelerated light-induced stomatal opening (Zhang et al., 2011). The elastic modulus of the guard cell wall was measured and found to decrease, suggesting that the cell required less internal turgor pressure to open the stomata. This suggests that the overexpression of *AtEXPA1* affects the mechanics of the guard cell wall, making it more flexible and less resistant to yielding under increasing turgor pressure. However, these results were based on overexpression of an expansin gene and, to date, there has been no report on the outcome of decreased expansin activity in guard cells. Such loss of function data are required to prove a role for expansins in stomatal function.

The link between cell wall components, guard cell mechanics and guard cell shape change is clear. However, whilst there is now a growing amount of research into the specialised properties of the guard cell wall, the picture is far from complete. The effects of expansins on guard cell wall function in particular seems a promising area of research, especially considering that guard cell wall modifying proteins could provide a feasible explanation for short-term changes to the guard cell wall during rapid opening and closing (Cosgrove, 2005).

Similarly, although there is significant evidence that guard cell shape changes during pore opening and closing, most imaging of stomata has been performed using classical microscopy, yielding essentially 2D data. There have been only a few examples in the literature of using microscopy techniques for 3D reconstruction of guard cells (Meckel et al., 2007; Shope et al., 2003; Yi et al., 2018) and these studies were limited in terms of the guard cell shape characterisation, and the sample sizes small. Moreover, these investigations have rarely fully exploited the range of genetic mutants in the cell wall now available. Thus, despite the importance of guard cell shape in stomatal function (Woolfenden et al., 2018, 2017), a thorough characterisation of guard cell shape change in Arabidopsis is lacking, and new microscopy approaches provide prospective methods to extract 3D data on cell volume, surface area and other shape parameters during stomatal function.

1.6 Project aims

The overall aim of this project was to characterise guard cell shape change in greater detail than previous work, whilst furthering our understanding of how guard cell wall components can affect stomatal function.

I. I first aimed to apply new microscopy techniques, including light sheet fluorescence microscopy, to develop a novel method of imaging guard cells in 3D to obtain quantitative data on cell shape change during stomatal function.

II. I also aimed to investigate the role of two gene families implicated in guard cell wall function (expansins and the ARP2/3 complex), using a combination of molecular genetics and physiology techniques to characterise relevant mutants in terms of their stomatal function and whole plant physiology.

The aims were ultimately addressed as follows.

I. Confocal microscopy was used along with post-processing in LithographX to generate 3D images of guard cells. These 3D reconstructions provided data on guard cell volume, surface area and other geometric parameters whilst the stomata were in a closed, open or resting state, to further our knowledge of guard cell shape change.

II. A transgenic knockdown line of *ARP3*, a major subunit in the ARP2/3 complex, was analysed to assess alterations of its stomatal function, whole plant physiology and cell wall composition. This was achieved using standard techniques such as epidermal strip bioassays, gas exchange analysis and immunohistochemistry.

III. A transcriptomic approach was used to identify candidate α-expansin genes which may play an important role in stomatal function.

IV. α-expansin knock-out mutants were analysed for differences in stomatal function and whole plant physiology using tissue-based and whole plant methods.

Chapter 2: Materials and Methods

2.1 Plant material

2.1.1 Wildtype plants

The Columbia (Col-0) ecotype of *Arabidopsis thaliana* was used as a control for comparison to mutant lines and descriptive work.

2.1.2 Loss of function mutants: NASC

Loss of function T-DNA insertion mutant lines for expansin work in Chapter 5 are in the background Col-0 and were obtained from the Nottingham Arabidopsis Stock Centre (NASC). These were verified by PCR genotyping (below), and seeds of homozygous plants were propagated and used for further experimental work.

Loss-of-function T-DNA insertion mutant *arp3* was in the Col-0 background and phenotype was confirmed by previous members of the lab and through SEM imaging (see 2.10) of the distorted trichomes.

2.1.3 Fluorescent-tagged mutants

Homozygous seeds for the transgenic line myr-YFP in a Col-0 background were obtained from Firas Bou Daher (Sainsbury Laboratory, Cambridge and was originally generated by Raymond Wightman (Willis et al., 2016). APKa::GFP and APKb::GFP lines were acquired from Lee Hunt from the Gray lab group. The phenotype of these lines was confirmed by presence of GFP or YFP signal when viewed under a fluorescence microscope.

2.2 Plant growth

2.2.1 Germination on media

Seeds were surface-sterilised using a mixture of 1:5 bleach to water with 0.05% Tween-20 (Sigma). After several washes with water, the seeds were left to stratify in water at 4°C for 4-7 days. The seeds were then sown onto ½ MS agar (0.22% (w/v) MS salts (Sigma); 1% (w/v) sucrose (Sigma); 0.8% (w/v) plant agar (Duchefa Biochemie); pH 5.8) on 12 x 12 x 1.7cm plates. Plates were left in a controlled environment chamber under long day

conditions (16h light/8h dark, 150µmol s^{-1} m^{-2}, 22°C) and seedlings were maintained on plates for 7-10 days before transferring to soil.

2.2.2 Germination on soil

Seeds were left to stratify in microcentrifuge tubes of distilled water at 4°C in the dark for 4-7 days before being transferred to soil.

2.2.3 Growth conditions

M3 soil was mixed with perlite at a ratio of 3:1 and soaked with water before transfer of seeds or seedlings.

Plants for genotyping and seed collection were grown in 5 x 5 x 5cm pots of lightly compressed soil and perlite mixture and were grown in a controlled environment chamber under long day conditions (16h light/8h dark, 150µmol s^{-1} m^{-2}, 22°C, 60% relative humidity). Seeds were collected using Aracons and Aratubes (Arasystem, Belgium) once plants had bolted.

Plants for phenotypic analysis such as confocal imaging, stomatal aperture bioassays, immunolabelling, and Licor analysis, were grown in 7 x 7 x 8cm pots of lightly compressed soil and perlite mixture and were grown in a controlled environment chamber under short day conditions (12h light 22°C/12h dark 15°C, 150µmol s^{-1} m^{-2}, 60% relative humidity).

Plants for floral dipping were grown in 9 x 9 x 11cm pots lightly compressed soil and perlite mixture and were grown in a controlled environment chamber under long day conditions.

A transparent plastic lid or plastic bag was placed over the pots for the first 7 days after transferring seeds or seedlings to soil, to help germination and establishment through elevated humidity. The lid or bag was propped open once seedlings were established to ensure a gradual acclimatisation of the plants to the external humidity of the chamber. At around 14 days after sowing, plants were thinned out to one plant per pot, and from then on pots were regularly rotated in the tray as were the trays in the chamber.

2.2.4 Seedling viability assays

To assess the germination rate and the proportion of viable seedlings, seeds were stratified as in 2.2.2. The number of seeds sowed per pot was recorded and seeds were left to germinate and grow as normal. After 14-17 days after sowing, before thinning out seeds, the number of seedlings or plants was counted. Plants were classed as either viable (green tissue and at the expected developmental stage) or non-viable (significantly smaller than the other plants, exhibiting abnormal colour or dead). This was compared against the number of seeds sown to get % of viable and non-viable/not germinated plants.

2.3 PCR

2.3.1 Extraction of genomic DNA

Leaf tissue of 4-week-old Arabidopsis plants were harvested and flash frozen in liquid nitrogen. Samples were ground with 500µl extraction buffer (0.2M Tris/HCl pH9, 0.025M EDTA, 0.4M LiCl, 1% (w/v) SDS) and spun at 13krpm for 10 minutes. 350µl of the supernatant was transferred to 350µl of isopropanol and spun at 13krpm for 10 minutes. The supernatant was discarded and 350µl 70% ethanol was added to the pellet. This was then spun at 13krpm for 10 minutes and the supernatant discarded. The ethanol was allowed to evaporate and then 200µl TE buffer (0.01M Tris/HCl pH 7.5, 0.01M EDTA) added. The genomic DNA was left to resuspend at 4°C overnight and then kept at -20°C for future analysis.

2.3.2 PCR

All genotyping PCR reactions were assembled using standard Taq DNA polymerase (NEB Biosystems) in 0.2ml PCR tubes (Thermo Scientific) (Table 2.1). An extension time of 1 minute per kilobase of DNA was allowed. PCR genotyping reactions are described in more detail in Chapter 5.

Primers used for all PCR reactions are listed in Appendix section 8.1.

Table 2.1 Components of a 25µl PCR reaction using Taq DNA polymerase.

Component	Volume (µl) per 25µl reaction	Final concentration
10X Standard *Taq* reaction buffer	2.5	1X
10mM dNTPs	0.5	200µM
10µM Forward primer	0.5	0.2µM
10µM Reverse primer	0.5	0.2µM
Template DNA	2	variable
Taq DNA polymerase	0.125	1.25 units/50µl PCR mix
Nuclease-free water	18.875	

2.3.3 Agarose gel electrophoresis

PCR products were checked by running them on an agarose gel. Agarose gels were prepared by dissolving 1% agarose (w/v) in TAE buffer (40mM Tris, 20mM acetic acid, 1mM EDTA) with 1µg/ml ethidium bromide. 6x loading dye (0.25% bromophenol blue, 0.25% xylene cyanol, 30% glycerol) was added to the PCR product at a ratio of 1:5, and samples were ran at 70V. Gels were imaged with a Uvitec system.

2.4 Generation of transgenic lines

2.4.1 Transformation of *Arabidopsis* via floral dip

arp3 knock-out lines were germinated on soil and grown as described in 2.2.3.

Once the plants had bolted to 10cm, floral dip was used to transform the plants with the myr-YFP construct (Clough and Bent, 1998). Agrobacteria (strain GV3101) containing the myr-YFP construct (promUBQ10::acylYFP in pUB-DEST vector) (Willis et al., 2016) was grown on low-salt LB agar with 0.5µl/ml gentamycin and 0.5µl/ml spectinomycin at 28°C for 24 hours. A single colony was picked and used to inoculate 10ml low-salt LB containing gentamycin and spectinomycin at the same concentrations and was left shaking at 200rpm at 28°C overnight. 4ml of the minicultures was used to inoculate a bigger culture of 200ml low-salt LB containing gentamycin and spectinomycin as well as 2µl/ml rifampicin which was left for 24 hours shaking at 200rpm at 28°C overnight. Samples of the miniculture were also taken for glycerol stocks for long term storage at -

80°C and for minipreps (New England Biolabs). OD of the culture was measured, and once it had reached 0.8, cells were harvested by centrifugation at 3500rpm for 15 minutes at 4°C. Cells were resuspended in an MS solution (0.22% MS medium (w/v), 5% sucrose (w/v), 10% MES (v/v), 0.05% Silwet (v/v)). Siliques, flowers and stems were dipped in the bacterial solution twice before being laid in trays with damp tissue and covered in cling film to ensure a moist environment. After 24 hours, holes were cut into the cling film and then 2 hours later plants were stood upright, contained in Aratubes and watered as normal. Seeds were collected once plants had dried.

2.4.2 Selection of transgenic plants

Seeds from transformed plants were harvested, surface sterilised (as in 2.2.1) and stratified in the dark at 4°C for 4 days. Plastic trays of were filled with a ratio of 3:1 M3 soil and perlite, and soil was soaked with a mixture of 1:1000 glufosinate herbicide (brand name BASTA) in water. Surviving seedlings were transplanted to individual pots and grown in long day conditions. Seeds of these plants were collected.

2.5 Immunohistochemistry

2.5.1 Fixing, embedding and sectioning plant tissue

Leaf tissue was harvested from 5-week-old plants grown in short day conditions and rectangular 3 x 6mm sections were cut from the leaves before submerging in a fixative solution of 4% (v/v) formaldehyde in PEM buffer (50mM Pipes, 5mM EGTA, 5mM $MGSO_4$, pH 7.0) for 1 hour under vacuum and then overnight. Samples were washed in PEM buffer three times, before dehydration using an ascending ethanol series (20, 30, 50, 70, 90 and 100% (v/v) EtOH in water) for 1 hour in each. Dehydrated leaf samples were then infiltrated with LR White hard grade resin (London Resin Company) at increasing concentrations of resin in ethanol (10, 20, 30, 50, 70, and 90% (v/v) resin in EtOH) for 1 hour each and then 3 for 8 hours in 100%. The leaf samples were then transferred to gelatine capsules filled with resin which were sealed and left to polymerise at 37°C for at least 5 days. Once hardened, the gelatine capsules were removed from the resin and 2µm sections of embedded leaf tissue were cut using a Reichert-Jung Ultracut E ultramicrotome using glass knives. The sections were transferred to Vectabond-coated (Vector Labs, UK) multiwell microscope slides.

2.5.2 Immunolabelling and imaging of sectioned tissue

Sectioned tissue adhered to microscope slides was incubated in 3% (w/v) milk protein (MP; Marvel, Premier Beverages, UK) in phosphate buffered saline (PBS, 8% (w/v) NaCl, 0.2% (w/v) KCl, 1.44% (w/v) Na_2HPO_4, 0.24% (w/v) KH_2PO_4) to prevent nonspecific binding of antibodies in later steps. Sections were washed for 5 minutes in PBS, and then incubated with a chosen primary monoclonal antibody diluted tenfold in 3% MP in PBS for 1 hour. As a control, the MP/PBS solution without antibodies was added to control sections. After 3 washes in PBS for 5 minutes each, sections were incubated with an anti-rat fluorescein isothiocyanate (FITC) secondary antibody (Sigma-Aldrich) in the MP/PBS solution for 1 hour, and from this point onwards slides were kept in the dark. Further washes in PBS of 5 minutes each were performed and then a 1/10 dilution of 0.025% Calcufluor White (Fluorescent Brightener 28, Sigma-Aldrich) in PBS was applied to the sections for 5 minutes. The sections were washed 3 times with PBS, and then Citifluor AF1 anti-fade solution (Agar Scientific) was added to the slides which also served as a coverslip mountant. Slides were imaged using an Olympus BX51 microscope equipped with an Olympus DP71 camera and a CoolLED fluorescence system and images were captured using CellB software.

2.6 Stomatal density measurements

Whole leaves were taken from 5-week-old plants grown in short day conditions and dental paste (Whaledent) was applied to the abaxial side and left to solidify for 30 minutes (Weyers and Johansen, 1985). The leaf tissue was peeled off and discarded, leaving the dental paste impressions behind. Clear nail varnish was applied to the dental paste and was left to harden for 20 minutes before peeling off and placing onto a microscope slide. A coverslip was placed on top of the nail varnish and the nail varnish impressions were imaged using an Olympus BX51 microscope with an Olympus DP71 camera and CellA software. 5 viewpoints were imaged per leaf impression, and 3 leaves from 3 independent plants were analysed. All visible stomata for each viewpoint were counted using ImageJ software (Schneider et al., 2012) using the ObjectJ plugin (Bolte and Cordelières, 2006; Vischer and Nastase, 2009). Stomatal density was calculated using the following equation.

Equation 1 Equation used for stomatal density.

$$Stomatal\ density = \frac{No.of\ stomata}{Area}$$

2.7 Stomatal aperture bioassays

2.7.1 Effect of CO_2 on stomatal aperture

Abaxial leaf epidermal peels were taken from mature leaves of 5-week-old plants grown in short day conditions using fine forceps. 3 peels from 3 different plants were used for each CO_2 condition and experiments were replicated 3 times using different plants each day. Peels were floated in round 6cm petri dishes filled with opening buffer (50mM KCl, 10mM MES, pH 6.2), which were sealed using micropore tape and placed in an open-topped glass tank next to a light source of 200µmol m^{-2} s^{-1}. Needles were pierced through the tops of the petri dishes, in order to bubble air of different CO_2 concentrations through the opening buffer. For high CO_2, air from a cannister of 1000ppm CO_2 was used. For low CO_2, the air was forced through a tube of self-indicating sodalime which removed the air of CO_2. For ambient CO_2, air from the room in which the experiment was conducted was used and varied between 400 and 500ppm. These differing CO_2 conditions acted as triggers to change stomatal aperture in the peels.

Peels were left for 2.5 hours in the opening buffer and CO_2 treatment before being removed from the buffer and imaged using an Olympus BX51 microscope with an Olympus DP71 camera and CellB software. Images were analysed using ImageJ with the ObjectJ plugin (Bolte and Cordelières, 2006; Schneider et al., 2012; Vischer and Nastase, 2009). Stomatal pore width, stomatal pore length, stomatal complex width and stomatal complex length were measured. This was done for 3-5 stomata per peel. Pore area was estimated by equating the area of the pore to an ellipse and calculated using the following formula.

Equation 2 Equation used for stomatal pore area where *A* = pore area, *W* = pore width and *H* = pore height.

$$A = \pi \times \left(\frac{W}{2}\right) \times \left(\frac{H}{2}\right)$$

2.7.2 Effect of fusicoccin on stomatal aperture

Similarly to the methods described in section 2.7.1, epidermal peels were taken from control and mutant plants and were added to either opening buffer or a solution of opening buffer with 2μM fusicoccin added to it. Peels were left for 2 hours in ambient CO_2 and were imaged and analysed in the same way.

2.7.3 Effect of mannitol on stomatal aperture

To investigate the effect of mannitol on stomatal aperture for viability on the light sheet fluorescent microscope, cotyledons from media-grown Col-0 seedlings were removed and mounted on glass microscope slides. Approximately 1ml of 0.5M mannitol was applied to the slides before a coverslip and slides were immediately mounted on a BX51 light microscope. Images were taken every 5 minutes using a 40x objective and CellA software. Stomatal aperture changes over time were calculated from the images using Equation 2.

2.8 Whole plant physiology

2.8.1 Rosette area

Rosette area was calculated for 5-week-old plants grown in short day conditions. Images of plant rosettes were taken from above and scale bar was processed using ImageJ. Rosette area was then calculated using open source software Easy Leaf Area (Easlon, 2013).

2.8.2 Stomatal conductance and assimilation via CO_2 shifts

Measurements for CO_2 shifts were taken on a LICOR-6800 infrared gas exchange analyser (IRGA) using 5-week-old plants grown in short day conditions. A $6cm^2$ circular area was used and in cases where the leaf did not fill the sample chamber, leaf area was calculated and corrected for during analysis of the data. Temperature was held at 21°C, relative humidity at 60% and flow rate was 300 μmol s^{-1}. Photon flux density was maintained at 300 μmol m^{-2} s^{-1} with 10% blue light and 90% red light.

To assess stomatal response to CO_2, leaves were first stabilised at 400ppm for 40 minutes. CO_2 was then shifted to an elevated CO_2 concentration of 1000ppm for 50 minutes, and then was decreased to 100ppm for a further 50 minutes. Measurements of stomatal

conductance and assimilation of CO_2 were taken every 2 minutes throughout the experiment.

2.8.3 Stomatal conductance and assimilation via shifting light intensity

This method followed a similar one seen in Penfield et al. (2012). Measurements for light shifts were taken on a LICOR-6800 IRGA using 5-week-old plants grown in short day conditions. A 6cm^2 circular area was used and in cases where the leaf did not fill the sample chamber, leaf area was calculated and corrected for during analysis of the data. Temperature was held at 21°C, relative humidity at 60% and flow rate was 300 μmol s^{-1}. CO_2 remained constant at 400ppm.

To assess stomatal response to light, leaves were stabilised using the growth light intensity of 200 μmol m^{-2} s^{-1}. The light intensity was then switched to 0 μmol m^{-2} s^{-1} (i.e. total darkness) for 5 minutes, at the end of which a measurement of stomatal conductance and assimilation was taken. The light was then increased to 1500 μmol m^{-2} s^{-1} for 5 minutes, after which again a measurement of stomatal conductance and assimilation was taken. This dark/high light shifting every 5 minutes was repeated 10 times with measurements taken after every 5 minute period.

2.8.4 Thermal imaging after application with ABA

5-week-old plants grown in short day conditions were positioned 1 metre underneath a FLIR T650SC thermal imaging camera under 150μmol s^{-1} m^{-2} light. After an initial adjustment period of 30 minutes, 1 image was taken every minute for 1 hour. Two solutions were prepared: 5μM ABA (5μM ABA in ethanol, 0.012% (v/v) Silwet), or a mock solution (the equivalent volume of ethanol, 0.012% Silwet). These were applied to plant rosettes using a spray bottle and imaging continued for 1 hour.

For the analysis of the images, 3 leaves were selected per plant imaged, and a small region of interest (ROI) on each leaf was chosen, of which mean temperature was measured. The same ROI was used to measure average temperature from every image taken before and after the application of ABA or mock solution to obtain a continuous measurement of leaf temperature over the 2 hour time period. From this, plant averages could be calculated, as well as genotype averages and temperature difference before and after the application of ABA.

2.8.5 Thermal imaging after droughting

5-week-old well-watered plants grown in short day conditions were positioned 1 metre below a FLIR SC660 thermal imaging camera in a growth chamber to minimise changes to the plants' environment. Images were taken every 1 minute for 30 minutes. The plants were then returned to the initial growth conditions and were not watered for 5 days. After 5 days of drought treatment, the thermal imaging process was repeated and images analysed.

Three leaves per plant were chosen and average temperature was calculated using the method described in 2.8.4. This was done with the undroughted and droughted images to allow for comparison between genotypes.

2.9 Light sheet and confocal imaging and 3D rendering of guard cells

Please note that an in-depth discussion on light sheet fluorescent microscopy and confocal method development can be seen in Chapter 3.

2.9.1 Light sheet fluorescent microscopy

Fluorinated ethylene propylene (FEP) tubes with a 2mm inner diameter were cut into sections between 2 and 3cm in length. The tubes were inserted into ½ MS agar that had set in a Petri dish so it was 1cm thick. The tubes were used to scoop up the agar so that 1cm of agar was suspended in the bottom of the tube, and the FEP tube was placed into a 1.5ml Eppendorf tube so that it stood in an upright position.

Arabidopsis seeds were surface sterilised in the dark following the protocol listed in 2.2.1. After a period of stratification in water, the seeds were distributed into the FEP tubes so that germination of the seed would occur in the FEP tube on top of the MS media. One seed per section FEP tube was used. Tubes were then sealed with micropore tape to allow for some degree of air transfer within the Eppendorf tubes whilst preventing contamination of the media.

Seeds were left to germinate in a cabinet with long day conditions (16h light/8h dark, 150μmol s^{-1} m^{-2}, 22°C) and were left in the controlled environment between 1 and 2 weeks. Once seedlings had germinated and were big enough so that the cotyledon adaxial

surface were pressed against the inner sides of the FEP tubes, the seedlings were taken to be imaged.

A Zeiss Z.1 lightsheet microscope was used to image the cotyledons.

2.9.2 Confocal microscopy

Adhesive rectangular microscope slide wells (125µl Gene Frame, ThermoFisher Scientific) were applied to standard microscope slides and between 75-125µl of buffer was pipetted into the wells. Buffer was chosen depending on whether stomata were being stimulated to open, close or neither: resting buffer was used as a buffer without an opening or closing chemical trigger (RB; 10mM MES, pH 6.2), opening buffer with fusicoccin (FC; 10µM fusicoccin, 50mM KCl, 10mM MES, pH 6.2) was used for stomatal opening, and resting buffer with 5µM ABA was used to trigger stomatal closure. Epidermal peels of 4-week-old myr-YFP Arabidopsis leaves grown in short day conditions were taken and placed onto the buffer in the microscope slides and a coverslip was applied.

An Olympus FV1000 with a 60x oil lens was used to image abaxial epidermal peels using a 514nm laser between 4% and 10% power and an eYFP filter set. Z-stacks were taken in parallel with a step size of 0.3µm from approximately 3µm above to 3µm below the guard cells to ensure the whole cell was captured. HV was variable between 400 and 800 depending on signal strength and images were zoomed in to between 1x and 3x. The resolution of each image was 640x640 pixels per image and scan speed was 4µs per pixel.

2.9.3 Image processing on LithographX

Image files from the confocal were converted from .oif files to .tif files using Fiji (Schindelin et al., 2012) and then opened in LithographX (Barbier de Reuille et al., 2015). The voxel size was then updated and for each z-stack, the contrast was enhanced (using the Brighten/Darken function); the stack was autoscaled; and a Gaussian blur of value 0.3 applied to blur cell edges. This ensured that the cell membrane signal remained constant throughout the cell and reduced the chance of any gaps in the cell wall. The stacks were then segmented using the ITK Watershed function (value 1500). Any non-guard cell objects were removed and if a guard cell was split into multiple segments, these were merged to create one cell. Any guard cells that looked as if the cell shape was not accurately reflected in the segments were deleted so as not to skew the data. A mesh was

then made from the cell segmentation using the Marching Cubes 3D function and from this a heat map was created for both cell surface area and cell volume. These data were used to provide guard cell surface area and volume data for each guard cell imaged. Images of the midpoint of guard cells in cross section were also exported.

2.10 Scanning electron microscope imaging of leaf surface

Col-0 and *arp3* plants were grown in short day conditions and at 5 weeks after sowing, mature leaves were removed and 2-3mm^2 sections of leaf tissue were cut out. These were placed individually onto a small drop of Cryogel on the mounting stage of a Hitachi TM3030Plus Benchtop Scanning Electron Microscope (SEM). Images of the abaxial leaf surface were taken between 50x and 250x magnification with particular focus on the trichomes.

Chapter 3: Imaging guard cells to obtain qualitative data on stomatal opening and closure

3.1 Introduction

The main function of stomata is to open and close in order to control gas exchange and water loss. Many important and interesting questions are explored about how guard cells respond to various stomatal triggers by measuring stomatal aperture, and one can do this through light microscopy. In a typical CO_2 stomatal aperture bioassay, epidermal peels are taken from a leaf, immersed in a buffer through which different concentrations of CO_2 are bubbled, and then left for a set period of time. Afterwards, the peels are imaged using a compound light microscope and parameters such as pore width, pore length, stomatal complex width and stomatal complex length measured (Webb and Hetherington, 1997). These all provide useful and important information on stomatal response, as one can calculate average pore area in ambient CO_2 and see how this differs to low and high CO_2. This can be used as a point of comparison to see how stomatal opening/closing changes when, for example, a gene is knocked out or an enzyme degrades a specific cell wall component (Jones et al., 2003). This can therefore provide information about the specific role of cell wall components in stomatal function (e.g. Zhang et al., 2011; Amsbury et al., 2016).

However, guard cells are 3D structures and do not exist solely in the 2D plane of a microscopic image. During stomata opening and closing, the pressure inside guard cells can shift dramatically which results in the opening and closing of the pore, and in order to change the aperture, guard cell shape change must occur (Shope et al., 2003). Internal pressure changes in *Vicia faba* (broad bean) guard cells has been observed to change by a factor of 16 during stomatal opening (Franks et al., 2001), which results in a cell volume change of approximately 25% and a surface area change of 15% (Meckel et al., 2007). In the paper by Meckel and colleagues, confocal microscopy was used to show that these

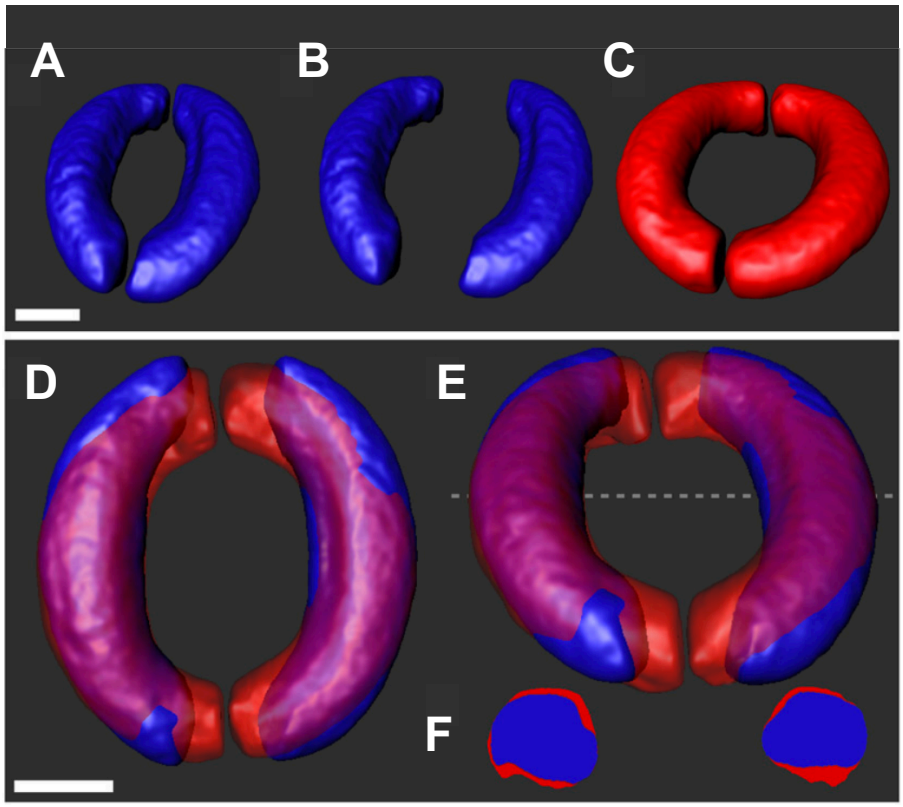

Figure 3.1 A figure illustrating 3D imaging of guard cell reconstructions by Meckel *et al.*, 2007. 3D reconstructions of closed **(A)** and **(B)** and open **(C)** stomata. The guard cells have been separated in **(B)** to match the aperture of the open pore to allow for the overlaid images in **(D)** and **(E)**. The purple colour represents overlap between the open and closed guard cells. There is significant shape change in the tips of the guard cells and a change in cross section shape **(F)**. Scale bar is 10µm. Images taken and modified from Meckel *et al.* 2007.

volume and surface area differences were reflected in a cell shape change that occurred primarily in the tips of the guard cells (Figure 3.1A-E). The work also showed that a degree of cross-sectional shape change occurred (Figure 3.1F), which has been observed in other work (Bidhendi and Geitmann, 2018; Cooke et al., 1976), however this cross-sectional shape change was not well characterised. Nevertheless, this landmark paper from Meckel and colleagues shone a new light on a system of guard cell shape change that strays from the traditional view of a curved tubular cell that inflates and deflates proportionally whilst maintaining a circular cross section (e.g. Rui and Anderson, 2016; Carter et al., 2017; Marom, Shtein and Bar-On, 2017).

Increasingly it is being realised that guard cell shape change is a more nuanced mechanism than can be captured fully by using 2D microscopy. Despite the work by Meckel et al., there remains a surprising gap in our knowledge when it comes to guard cell shape change in 3D during stomatal opening and closure. In particular, recent computational modelling approaches have shown that the shape of the guard cell and

wall have a major influence on the mechanics of stomatal function (Carter et al., 2017; Woolfenden et al., 2018, 2017; Yi et al., 2018) yet in most analyses the guard cells are assumed to be tubular in shape with a circular cross section, potentially limiting the validity of the models. In this chapter I aim to bridge this knowledge gap by developing a method of imaging guard cells in 3D, using these data to give us more accurate geometric information regarding guard cell shape change during opening and closure.

My hypotheses about imaging guard cell shape change are as follows:

I. Imaging methods can be utilised to image guard cells and these imaged can be processed to produce 3D reconstructions of stomata.
II. These reconstructions will make it possible to accurately map and quantify shape changes and the relative movement of guard cells that occur during stomatal opening and closing.

My objectives for this part of the project are as follows:

I. To develop a procedure using fluorescent microscopy to image guard cells in 3D.
II. To generate 3D images of stomata in opened and closed states.
III. To use these 3D images to give us quantitative data on guard cell volume and shape change during stomatal opening and closure.
IV. To use this method as a mode of comparison to see how guard cell shape change differs between wildtype and mutants with a known stomatal phenotype.

3.2 Light sheet fluorescence microscopy

To acquire 3D data from cells in a tissue, the signal of the cell outline must be strong, clear, continuous and visible from all angles to allow full segmentation of the cell (Barbier de Reuille et al., 2015). There are multiple ways to approach image acquisition with this in mind. Light sheet fluorescence microscopy (LSFM) is a relatively new type of fluorescence microscopy that uses a laser light sheet to illuminate and optically section a sample. Most light sheet microscopes allow easy and quick imaging of the sample from multiple angles and so this may be beneficial for capturing a continuous cell outline. Another more established method is confocal microscopy, which is a method of creating high-resolution

images that allow close examination. This could be useful for capturing the potentially complex small changes within guard cell wall movement.

Light sheet fluorescence microscopy (LSFM) offers intermediate resolution at a high speed. The novel principle of LSFM is that the detection and emission lenses are uncoupled at perpendicular axes, whereas conventional epifluorescence and confocal microscopes use the same lens for both. In LSFM the sample is illuminated on one side by a laser light-sheet beam, formed by a cylindrical lens and focussed in only one direction, which illuminates a thin plane of the specimen. The detection camera is arranged perpendicular to the beam. This means that the plane of illumination and the detection system meet and overlap only at the region of interest of the sample (Greger et al., 2007; Huisken et al., 2004). The perpendicularity of the emission source and detection lens minimises the area of the sample that is exposed to the laser beam, and this provides multiple benefits for the microscope user. Firstly, when compared to epifluorescence microscopy, much of the unwanted out-of-focus fluorescence is eliminated, meaning only the required view of the sample is detected. A second advantage is conferred because only one plane of the specimen is imaged at any one time, which decreases the exposure of the sample to the laser and therefore reduces photobleaching of the sample and results in a lower laser power being used overall. Thirdly, when imaging live tissue or a whole organism, decreasing the laser power and therefore minimising exposure to the laser reduces damage to the health of the sample and maintains longevity, which means long-term imaging of live samples becomes easier without potential damage to the tissue.

Another novel advance of LSFMs is that some models allow control of the internal conditions in the microscope. The Lightsheet Z.1 (www.zeiss.com) was the first light sheet microscope to become commercially available. The user can set or alter the internal CO_2 concentration, temperature, and the liquid that fills the sample chamber can be easily changed. This means the user can have a finer control of the environmental conditions of the sample, which again appeals to those doing long-term imaging with live organisms.

LSFMs are also quick and can confer intermediate resolution to users. Samples can be imaged at multiple angles, and they are ideal to generate 3D images that, when taken over a period of time, can be merged into 3D timelapses – to create 4D videos. This makes LSFMs a credible choice for those doing long-term imaging of large samples such as

whole organisms, and as such has been received well in areas such as developmental biology, with developed protocols and research papers published for many developmental model species, such as *C. elegans*, zebrafish and *Drosophila* (e.g. Huisken et al., 2004; Wu et al., 2011; Tomer et al., 2012).

However, plant scientists have been slower on the uptake, despite the fact that LSFMs allow vertical loading of samples (as opposed to horizontal loading stages of most confocal and epifluorescent microscopes) which is obviously beneficial for gravitropic growers such as plants (Ovečka et al., 2018). There have been multiple studies that use LSFM to visualise root development due to roots being relatively transparent when compared to aerial tissue and therefore easier to image deep into the tissue (e.g. Maizel et al., 2011; von Wangenheim et al., 2014; Berthet and Maizel, 2016). However, there have been few studies on leaf tissue and even fewer on stomata; indeed, there have only been two published examples to date (that I am aware of) that show stomata imaged on a LSFM (Ovečka et al., 2018, 2015). The first of these papers provided the first in-depth protocol on sample preparation and microscope set-up for imaging Arabidopsis on the Lightsheet Z.1. However, this paper focused on root development, and the images shown of stomata on the cotyledon surface functioned to demonstrate the capabilities of the Lightsheet Z.1 but did not investigate any aspect of stomatal structure or function. The second of the papers was a review which again highlighted the useful and increasingly important role of LSFM in recording plant development, especially in roots and seedlings, but again drew upon the images in the 2015 paper as an example of stomatal imaging using this method.

Therefore, imaging Arabidopsis to study stomatal function on a light sheet microscope remains to be fully explored. I chose to investigate the potential of light sheet microscopy to develop a method for this project in which guard cells can be imaged live over extended periods and rendered into 3D models post-imaging. Access to a Lightsheet Z.1 was considered beneficial due to the ability to control internal conditions, raising the possibility of changing the environment of the plant to manipulate the stomata into opening and closing whilst on the microscope, for example by changing CO_2 concentration, or adding a buffer containing known stomatal triggers, e.g. ABA.

3.3 Method development: light sheet microscopy

3.3.1 Sample preparation and seedling germination

Biological samples for most light sheet fluorescent microscopes (LSFMs), including the Zeiss Z.1 used for this work, are suspended in narrow tubes made out of fluorinated ethylene propylene (FEP) in the sample chamber (Figure 3.2), that is around 6cm cubed. FEP is chosen for this purpose as it has a refractive index very close to water (FEP: 1.344, water: 1.355; (Flurotherm.com, 2019)) which therefore reduces the chances of distortion in the images produced by the LSFM. The typical inner diameter of the FEP tubing used for LSFMs is between 1.6 and 2.0mm. Samples such as zebrafish are commonly mounted through a syringe mechanism by which the fish are taken up into the tubing and suspended using low w/v agarose (0.6-1% w/v), that prevents movement of the fish but will keep them alive during the imaging process.

Using the protocol detailed in Ovečka et al. (2015) as an outline, my first step was to work out how I would be able to get Arabidopsis plants into the FEP tubing to image them. It was clear early on in the method development process that only the smallest of plants

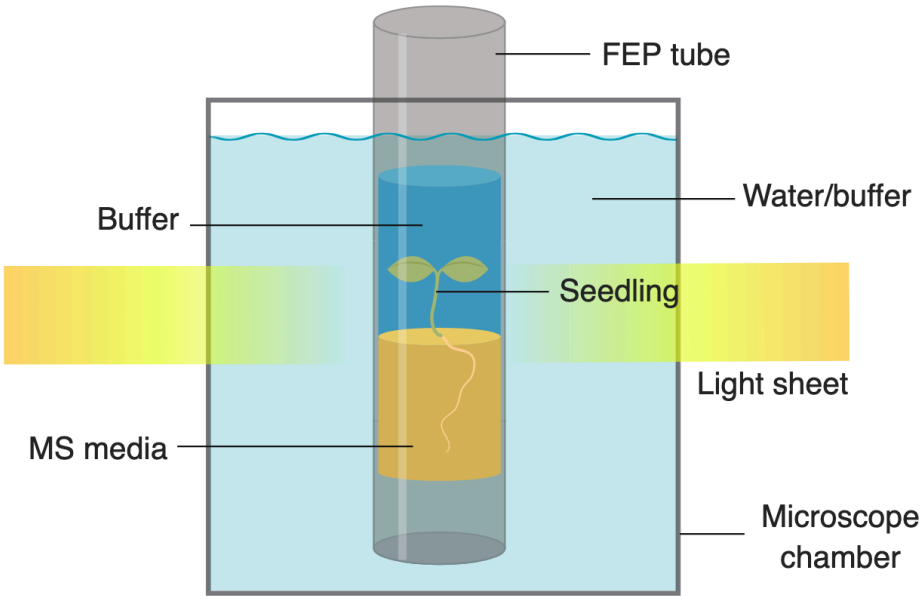

Figure 3.2 Internal set up of the LSFM. The seedling is germinated on ½ MS media inside the FEP tubing and buffer is pipetted in to cover the seeding. The tubing is inserted directly into the imaging chamber and a light sheet penetrates the sample, providing 'optical sectioning'. Schematic not to scale. Created with BioRender.

would be able to be contained within the narrow tubing, and so I decided to try and image Arabidopsis seedlings as young, and therefore as small, as possible.

I firstly sought to assess how I could transfer a small plant into such a thin tube, for example by pressing a 2-3cm long section of the tube over the plant from above and scooping up the seedling and some of its media to 'plug' the bottom of the tube. When this proved impossible without damaging the plant, I then turned to investigating whether I could germinate the seeds in the tube. To do this, I inserted around 1cm of ½ MS media into a 2-3cm cutting of tubing. I then pipetted in one pre-stratified Arabidopsis seed per tube and tapped the tube gently until the seed slid down and lay on top of the media. I left the FEP tube standing upright in a 1.5ml Eppendorf tube that was covered with Micropore tape to minimise infection of the media but to allow exchange of gases to and from the plant and the environment. When left to germinate in appropriate conditions (see Section 2.9.1 – LSFM germination), nearly all seeds germinated.

3.3.2 Imaging stomata on the LSFM

Once it was clear I was able to germinate seedlings to be imaged inside the FEP tubing, the next step was to investigate which method to use to make the stomata visible on the microscope. As there are so few papers in the literature that have used LSFM to image stomata, I explored a range of approaches to illuminating the stomata.

For the purposes of using the images of stomata to gain data on 3D guard cell shape, it is logical that the cell edges and surfaces must be clear in order for the 3D shape to be rendered (Barbier de Reuille et al., 2015). A choice must therefore be made as to how the cell edges can be made visible. Initially I looked into different fluorescent reporter gene-cell membrane constructs expressed in transgenic plants.

ARABIDOPSIS PROTEIN KINASE 1A (AT1G07570) and ARABIDOPSIS PROTEIN KINASE 1B (AT2G28930) (APK1a and APK1b) are both protein kinases located at the plasma membrane and are reported to be expressed predominantly in guard cells (Elhaddad et al., 2014). The seeds of two transgenic lines in which each APK1 protein had been tagged with GFP were made available (lines APK1a::GFP and APK1b::GFP were a gift from Lee Hunt in the Julie Gray lab at the University of Sheffield).

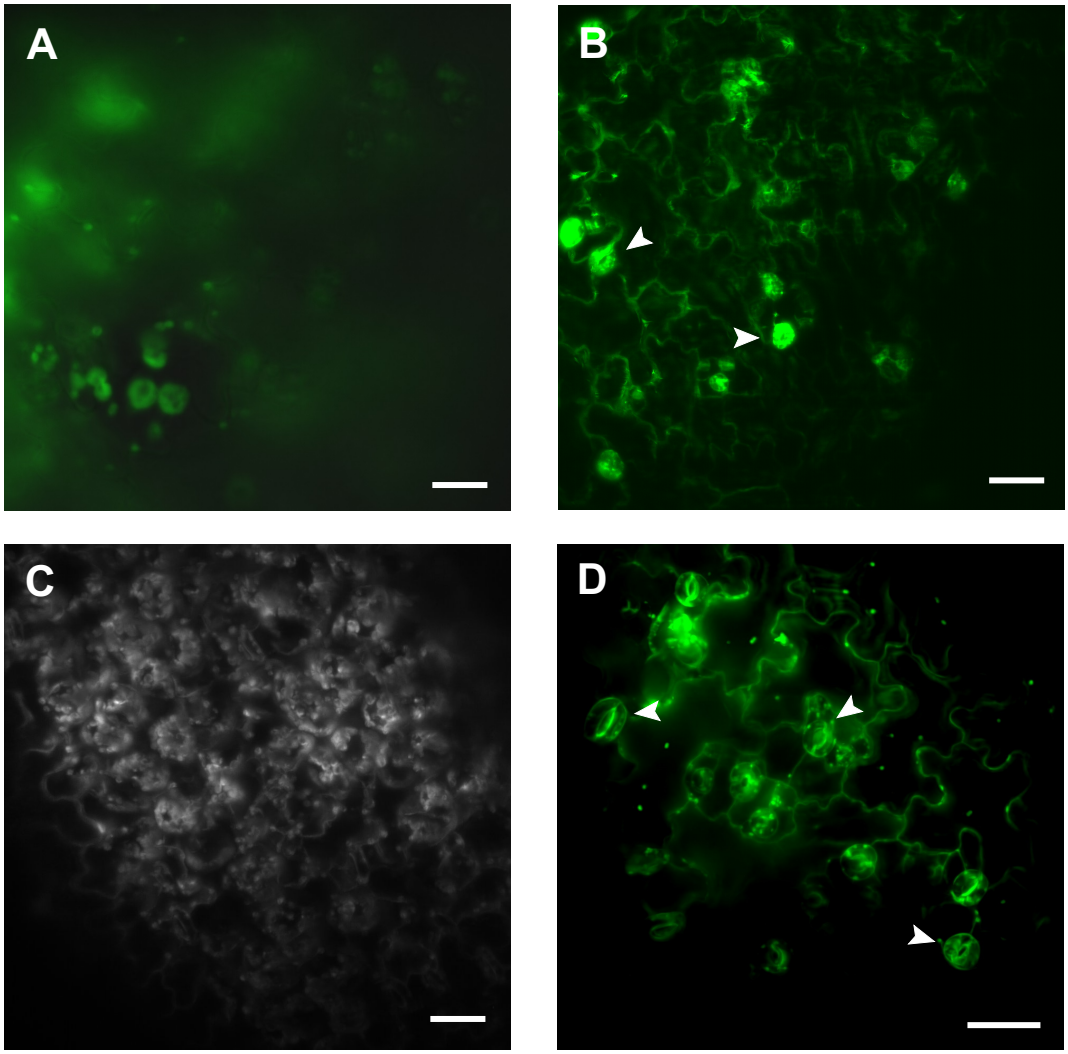

Figure 3.3 Images of Arabidopsis cotyledon epidermises taken on a LSFM. (A) APKa::GFP line imaged in air without any buffer. **(B)** APKa::GFP line imaged with buffer (PBS). Stomata are present however they appear 'blotchy'. **(C)** APKb::GFP line does not show any stomata. **(D)** Col-0 seedling stained with 100µg/ml PI 10 minutes before imaging submersed in PBS. Arrowheads highlight some of the stomata seen in each image. Scale bars represent 50µm.

I germinated the transgenic seeds in FEP tubing and once the seedlings were between 7 and 10 days old, I set them up to image on the LSFM. I then discovered that without a suitable buffer inside the FEP tubing, the images appeared blurry and out of focus (Figure 3.3A). This was because of the difference in refractive index between the fluid in the sample chamber and the air inside the FEP tubing (Figure 3.2), so I sought to find a suitable buffer in which the plants would remain viable, but that also allowed for sharper images. The use of PBS led to clearer, better quality images.

Images of APK1a::GFP and APK1b::GFP in PBS taken on a LSFM are shown in Figure 3.3B and 3.3C. Stomata were clearly seen on the epidermis of APK1a::GFP seedlings, however

for unknown reasons the stomata were not seen on the surface of APK1b::GFP seedlings. This line was discounted from further investigations on the LSFM. In contrast, the stomata were seen clearly on the APK1a::GFP seedings and were easy to locate. However, the signal appeared to be 'blotchy' and the guard cell membrane and therefore the outline of the cell was not clear. This would likely make it very difficult for any post-processing software to recognise the true cell membrane and therefore would not allow reliable 3D image reconstruction.

I then tried a different method of staining stomata. Propidium iodide (PI) is a fluorescent agent that accumulates in the cell walls of live cells and is often used as a cell wall stain in plants, including stomata (Melotto, 2010). It can be applied to live tissue only minutes before use on the microscope, making it a quick and easy way to image cell walls in plant tissue.

PI was applied to Col-0 seedlings 10 minutes before imaging and the results can be seen in Figure 3.3D. The cell walls on cotyledons stained with PI were visible and the stomata were easily located. The guard cell walls appeared to be stained relatively uniformly which I assumed would be beneficial when using the microscope images to render these guard cells in 3D.

3.3.3 Timelapse videos on the LSFM

Once I had seen that PI staining of the guard cell walls looked like it would have a reasonable chance of producing images capable of providing 3D data on guard cells, I decided that the next step was to try and stimulate the stomata to open or close and image in real time. This would provide proof that the cells were viable and could respond to external stimuli, and that the image capture time was appropriate for potentially capturing opening/closing dynamics of stomata in real-time.

As previously discussed, the Lightsheet Z.1 has the ability for CO_2 and temperature control as well as automatic changes to the liquid that fills the sample chamber. My initial plan was to either increase or decrease the CO_2 concentration in the chamber to induce stomatal opening and closing, whilst taking z-stacks of the stomata at periodic intervals to create a timelapse video, hopefully capturing the stomata responding to changes in CO_2 in 'real time'. However, due to equipment and facility constraints I was unable to change the CO_2 in the chamber.

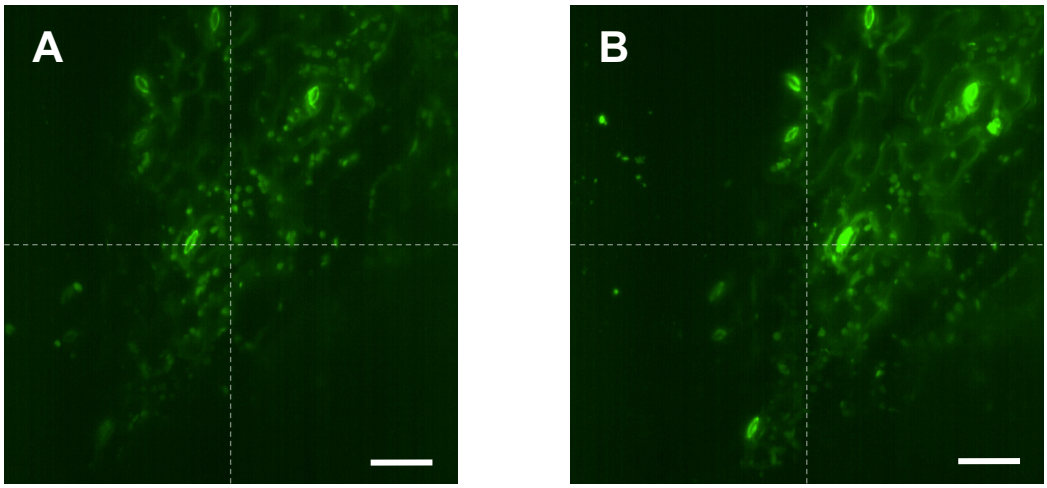

Figure 3.4 Cotyledon epidermis shifts during video capture. (A) The start point before PBS was removed to be replaced with buffer containing mannitol. **(B)** The end point after approx. 30 mins. Dashed lines are for positional reference. Col-0 cotyledon epidermis stained with PI 10 minutes before imaging. Scale bars represent 50µm.

A second method to manipulate stomatal opening/closure would be to change the buffer in the chamber to one containing a known stomatal trigger, for example ABA or fusicoccin. However, since in my experimental set-up the sample is contained within FEP tubing, the seedling would not actually be exposed to the liquid in the sample chamber (Figure 3.2). I therefore decided to change the buffer in which the seedling was immersed to one containing a stomatal trigger. This would allow direct access of the plant to the stomatal stimuli, and also would avoid changing any of the internal chamber conditions. To do this, a long and thin gel-loading pipette tip was used to draw up and discard the 'resting' buffer out of the FEP tube, and to replace that with the stomatal stimuli, all without removing the sample from the imaging chamber.

I chose mannitol as the first buffer reagent to induce stomatal closure. Mannitol is a sugar that has a strong known osmotic effect. It draws water out of the guard cells by decreasing their internal osmotic pressure, thus forcing the pore to close, but at certain concentrations allows recovery of stomata after prolonged exposure (Asai et al., 1999) which makes it suitable for long-term imaging of live plants.

10µl of 0.5M mannitol was added to the FEP tubing and then the cotyledons were imaged for 30-60 minutes. However, the results were variable, with the main problem being that changing the buffer caused the cotyledon to drift during imaging, thus shifting the stomata during image capture. An example of this can be seen in Figure 3.4.

Another issue was that the stomata did not visibly close when exposed to mannitol. This could have been for several possible reasons. Firstly, there are doubts as to whether stomata on cotyledons respond to triggers in a comparable manner to stomata on mature leaves. Secondly, it took approximately three to five minutes between setting up the sample with mannitol in the microscope and starting the imaging, and the time series lasted for between 30 minutes and 1 hour. It was unclear as to whether these time frames were appropriate for capturing stomatal closure on the light sheet microscope.

3.3.4 Assessing cotyledon viability and stomatal response

To investigate whether the stomata on cotyledons responded as expected to solutions that affect stomatal aperture, assays were conducted that measured stomatal aperture at different time points.

I first visualised Col-0 seedling cotyledons on a standard light microscope to assess the rate of stomatal closure after application of 0.5M mannitol. I took cotyledons from Col-0 seedlings and immersed them in 0.5M mannitol on microscope slides and imaged them on a standard light microscope on a brightfield setting. Using the method described in section 2.7.3, I took images every 5 minutes and afterwards calculated mean pore area using the formula seen in section 2.7.1.

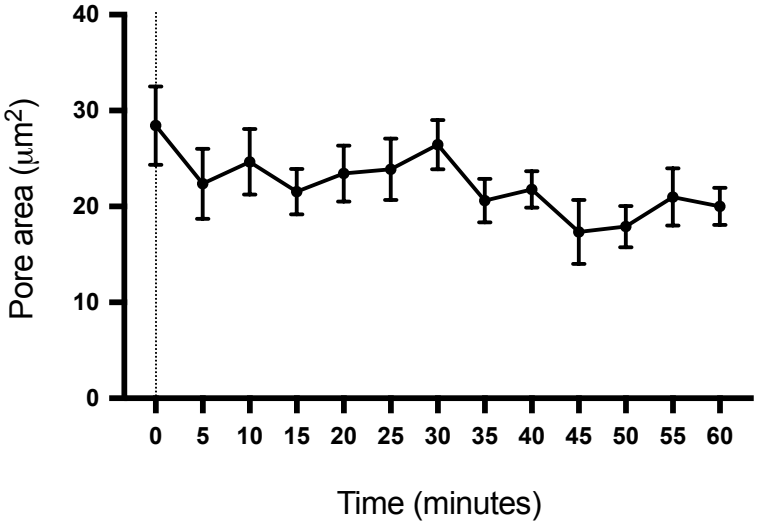

Figure 3.5 Effect of mannitol application on stomatal aperture on Col-0 cotyledons. 0.5M mannitol was applied to cotyledons at time point 0 as indicated by the dotted line and were imaged on a light microscope every 5 minutes after application of mannitol. Average pore area was then calculated from the images taken. Mean ± SEM. $n = 10$.

Figure 3.5 shows the results of this experiment. As seen, average pore area decreased over time from 28.4μm^2 immediately after mannitol application to 20.0μm^2 at 60 minutes after mannitol application which indicates the stomata are closing over that time period. This suggests that imaging the cotyledons on the LSFM over 60 minutes would be a suitable amount of time for a difference in stomatal aperture to be observed.

Cotyledon stomatal pore area did not decrease to less than approximately 20μm^2 which, according to my own data (see stomatal aperture bioassay data in sections 5.3.2 and 5.4.1) is slightly lower than what is normally seen for 'closed' stomata in response to low CO_2 concentration. However, full closure in response to mannitol is seen commonly in mature leaves, so the lack of total closure in the data shown here suggests that although the cotyledon stomata are responding to mannitol by decreasing the mean pore area, they lack the full response seen in mature leaves.

On the other hand, according to the same bioassay data, the initial pore area for "resting" stomata in mature leaves is much higher than observed here in cotyledons. In cotyledons the resting aperture was approximately 28μm^2 whereas a resting stomatal aperture of around 40μm^2 was commonly observed in mature leaves (sections 5.3.2 and 5.4.1). There are many potential reasons why the cotyledon stomata did apparently respond to the mannitol-induced closing stimulus. The first is that perhaps the stomata on the cotyledons were smaller than stomata found on mature leaves. There is also a possibility that technical aspects linked to the imaging process led to a drifting process, shifting the imaging angle and thus inaccuracies in the aperture measurements. It is also possible that the sample preparation required for analysing plant tissue in the light-sheet microscope was inherently not appropriate for the tissue, involving both long-term submergence in liquid and laser illumination. Indeed, Ovečka et al., 2018 admit that embedding or submerging aerial plant tissue for long-term imaging is "not ideal". Due to the unforeseen challenges of applying light sheet microscopy, I decided to try a more well-established technique as a point of comparison with the LSFM. For example, confocal microscopy has long been at the forefront of plant imaging (Wymer et al., 1999) and indeed, there are a number of successful examples of stomata being imaged in such a way (e.g. Franks et al., 2001; Meckel et al., 2007; Yi et al., 2018).

3.4 Method development: confocal microscopy

3.4.1 Confocal microscopy

Confocal laser scanning microscopy (CLSM) is a well-established and popular method of producing high resolution and high-quality images of biological specimens.

Figure 3.6 shows a diagram of a confocal microscope. A beam of light goes through a filter which only allows through light of a given wavelength; for example, to detect YFP in a sample, this will be 514nm. The light is reflected by a dichroic mirror onto the sample, which then emits light of a shifted wavelength depending on the fluorophore(s) present in the sample – for example, for YFP the emission peak is 527nm. The emitted light passes back through the dichroic mirror and passes through a second filter that lets through only

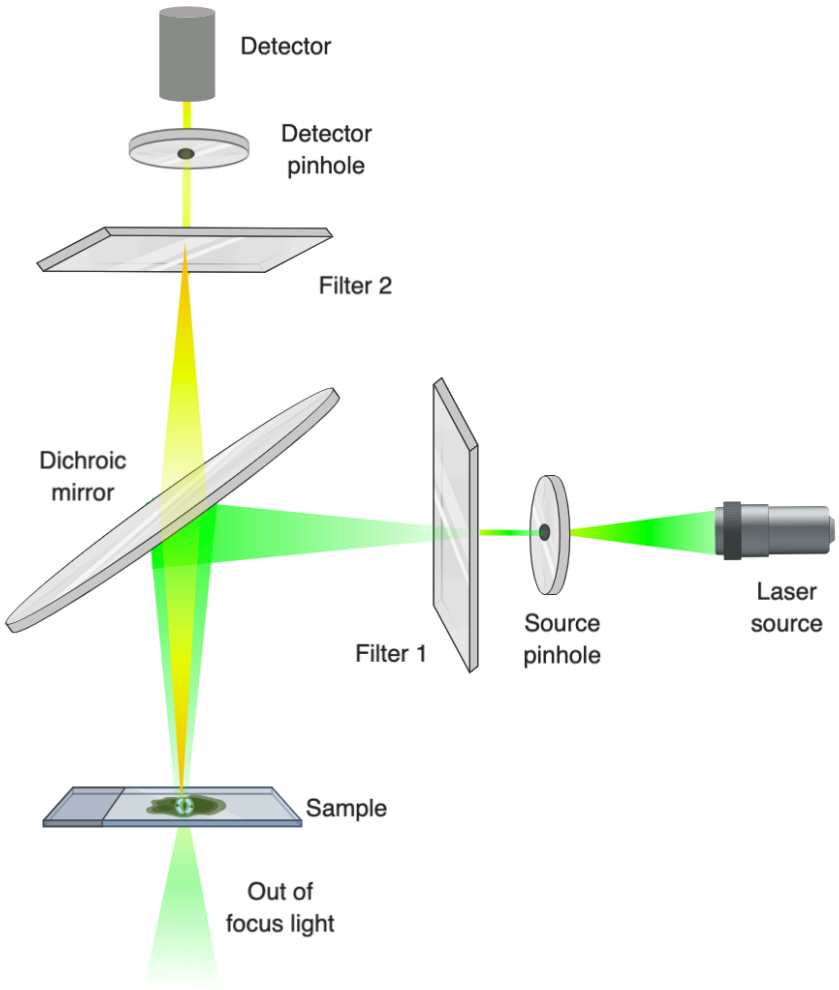

Figure 3.6 Simplified diagram of the internal architecture of a confocal microscope. The light beam travels from the laser source to the sample and then up to the detector. Green light represents the excitation beam and yellow light represents the emission beam. Schematic not to scale. Created with BioRender.

certain wavelengths of light (barrier filter), which then continue to the detection lens. Using the appropriate filter sets and dichroic mirror, the microscope can be set to detect sources of specific fluorophores, with the spatial distribution of the fluorophore captured via the lens set up in the microscope (Paddock, 2000).

A unique feature of the confocal microscope is the pinhole, the feature that allows the method to achieve such high resolution. A pinhole is placed both before the first filter and after the second filter, focussing the light beam so that only a very small proportion of the sample is illuminated and detected at any one time. This eliminates any out-of-focus light from above or below the plane of view, enabling extremely sharp and high-resolution imaging of the illuminated fluorophore.

A 2D image of the sample is then created by scanning the sample, either by moving the sample underneath the beam or moving the beam across the sample. Fluorescence that is emitted is detected by a digital camera, or before the camera a photomultiplier tube (PMT; this amplifies the fluorescent signal from the sample), allowing reconstruction of a 2D image at a given height. If this process is done at different vertical heights, one can obtain 'slices' (z-stacks) through the specimen from which a high-resolution 3D image of the sample can be constructed.

3.4.2 LithographX

The open-source image analysis software platform LithographX (hereafter referred to as LGX), and its parental programme MorphographX (MGX), were developed as a tool to recreate 3-dimensional models of morphogenesis from 2-dimensional images and time-lapse videos of living cells, and, once processed, to export the data into a variety of user-friendly formats (Barbier de Reuille et al., 2015). The software was developed initially to study plant morphogenesis, however it has been since shown that it can be used for a variety of purposes across various biological disciplines, for example in mammalian intestinal cells (Sumigray et al., 2018) and for the water flea *Daphnia* (Horstmann et al., 2018). Unlike many other models of morphogenesis that often rely on 2D templates, LGX extracts data from 3D images, such as z-stacks of a sample taken from a microscope, and recreates these in 2D. This is useful especially for those studying morphogenesis, as many developmental events happen in a 3-dimensional way because the sample tissue itself is curved.

Consequently, LithographX was chosen for this project because of its ability to extract 3D cellular data from 2D images, and it being Opensource software. In this project my ultimate aim was to obtain 3D data that could be interrogated to derive various guard cell parameters such as volume and surface area. This requires the software to efficiently and robustly identify guard cells from the z-stacks taken on a microscope. To do this, the programme seeds and then segments the guard cells, creates a mesh that represents the surfaces of the segmented cells from which quantitative data on cell parameters can be extracted, as required. This means that LGX needs to be able to recognise and trace cell boundaries within z-stack images accurately, so that individual cells can be recognised as separate objects and do not blur together or leak out.

3.4.3 Confocal workflow optimisation

There are many stages in developing and optimising a microscopy method for a specific purpose, from choosing the correct sample to analysing the final data. The confocal method I used can be broadly separated into three parts (Figure 3.7). Firstly, the input to the microscope consists of assessing which fluorophore to choose and then subsequent sample preparation. Secondly, the confocal imaging itself involves many adjustments and optimisation of parameters on the microscope. And thirdly, post-image analysis and processing comprises multiple small steps and alterations in order to obtain reliable and representative 3D guard cells. All three steps are interlinked and a literature review indicated that one of the most important factors in successful 3D segmentation in LGX is the quality and strength of the cell outline signals (Barbier de Reuille et al., 2015).

To ensure a clear and strong cell boundary signal, one must choose a suitable fluorophore carefully, and this can vary depending on many factors such as sample size, sample type, and what information is needed from the final images. From the review of the literature (see Appendix 8.2 for more details), approximately a fifth of papers fixed and cleared

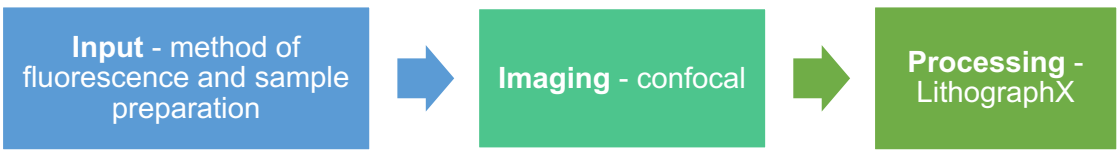

Figure 3.7 Workflow showing the different stages of optimisation for the confocal imaging method.

their samples, and from these, all but one used PI as the main fluorophore, with the other using a transgenic GFP line to illuminate cell boundaries. That fixed and cleared tissue is in the minority is unsurprising as the majority of papers used confocal imaging and subsequent MGX and LGX processing to track plant development at a cellular level, so live samples were crucial. As I was looking to image fresh tissue in order to see the opening and closing of guard cells, I ruled out sample fixation/clearing and instead focussed on the papers that used living tissue. Most papers using live tissue or whole organisms used transgenic lines with fluorescent proteins as reporter tags, including GFP, YFP and mCherry. These were mostly plasma membrane markers that could be easily recognised in processing, as seen in the YFP-tagged plasma membrane marker used in Kirchhelle *et al.* (2016) to track Arabidopsis root development. Nine studies used PI as a way to mark cell wall boundaries, and eight used another kind of membrane stain or dye, including six that used FM4-64, a red membrane-selective dye most commonly used to image yeast cells (Fischer-Parton et al., 2000).

3.4.4 Input – sample preparation and fluorescence

Standard microscope slides were used to mount the samples, but with the addition of a three-sided rectangular adhesive well to the slides in which the sample and some liquid could be contained, with the coverslip on top to create a small chamber (Figure 3.8). This was done because it stops the leaf sample from drying out, it raises the height of the coverslip so thicker leaf tissue can be accommodated, and it also allows buffer changes to be performed. Resting Buffer (RB; see section 2.9.2) was used as a 'neutral' in-medium for maintenance of tissue viability. The fungal toxin fusicoccin (FC) mixed with opening buffer (see section 2.7.1) was used to trigger stomatal opening (Eun and Lee, 2000), and

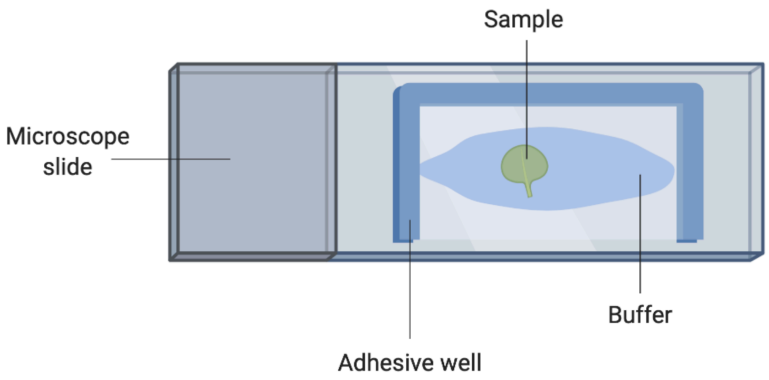

Figure 3.8 Schematic of microscope slide set up used for confocal microscopy. A standard 75 x 26mm microscope slide with a three-sided adhesive well created a small chamber in which the epidermal peel (sample) and the buffer used were contained. Image created with Biorender.

ABA in RB was used to stimulate the stomata to close. This method of mounting the samples remained consistent throughout the confocal optimisation.

A range of methods to illuminate the stomata were tested during the optimisation of guard cell confocal imaging. This included the GFP-tagged line APK1a described in section 3.3.2, and a transgenic *Arabidopsis* line containing the vector pUBQ10::acyl-YFP in a Col-0 background (the plants hereafter referred to as myr-YFP) which was described in Sapala et al., 2018 (a gift from Firas Bou Daher from the Sainsbury Laboratory in Cambridge). In addition to PI staining, I also explored the use of Calcofluor White (a fluorescent stain that binds to cellulose and therefore cell walls) and FM4-64 (a membrane selective fluorescent dye commonly demonstrated in the literature as a way to segment cells using LGX, e.g. Shope, DeWald and Mott, 2003; Kiss et al., 2017; Jones et al., 2017). Out of all the different methods of cell wall/membrane fluorescence marking, the transgenic myr-YFP line produced images in which the guard cells segmented the most successfully and consistently with LGX and so this was used in all further investigations.

3.4.5 Taking images on the confocal microscope

Confocal microscope and software settings that were adjusted during optimisation of this technique included scan speed, image size, HV (which boosts the signal), laser power %, lens type, and zoom factor. Many of these were adjusted in order to get the best possible image from the sample and this depended heavily on what type of fluorescence was being examined.

For the myr-YFP line, HV was optimal between 500 and 800, depending on signal strength. A magnification factor between 1 and 2.5 times often produced images of between 2 and 4 stomata per scan, thus increasing useful data acquisition. Originally I used images of 8 or more μs/pixel and canvas sizes of 1024x1024 pixels/image, however because of changes made to the image in post-processing (e.g. application of Gaussian blur) 4μs/pixel on 640x640 or 800x800 pixels/image was considered sufficient in terms of the trade-off between speed and image quality. Laser power was generally between 5 and 10% and the excitation wavelength was 514nm.

Z-stack size was always set to 0.3μm and stacks started and ended a few μm above and below the point at which the guard cells came in focus, so as to ensure the whole cell would be enclosed in the final z-stack. There were normally between 50 and 100 images per guard cell z-stack.

3.4.6 Image processing on LithographX

LGX requires images to be in a .tif file format and so all z-stacks from the confocal were converted to .tifs using FIJI (Schindelin et al., 2012) before being imported into LGX. From there voxel size details were adjusted as this information was lost when importing the files into LGX.

After loading a .tif into LGX and adjusting voxel size, there are many settings and parameters that can be changed in LGX according to user needs and image requirements. In many cases, the settings can be adjusted on such a massive scale that it would be impractical to assess the impact of every variation on final cell segmentation – for example, the ITK Watershed function can take any value between 1 and 65,000 although is automatically set to 1500. However, I found that once I started using myr-YFP epidermal peels to create z-stacks of stomata then most of the automatic recommended settings (such as ITK Watershed at 1500) worked with very few readjustments needed, which made the process easy and quick. This significantly benefitted the efficiency of the workflow.

The most common that were changed during LGX processing of guard cells z-stacks from myr-YFP epidermal peels are as follows:

i) The “Autoscale” function was applied to scale the intensity of the stack. This comes in use later on during segmentation.

ii) The “Gaussian Blur” function is an image processing technique that results in the blurring of an image to reduce detail and noise. It is typically used in conjunction with edge detecting algorithms which can be sensitive to noise. Increasing “Gaussian blur” can often result in more successful segmentation of cells in LGX due to the fact that it will decrease the likelihood of gaps or inconsistencies in the cell walls, however if blurred too much the cell wall signal can often be lost and undistinguishable from other features of the image. For myr-YFP z-stacks, “Gaussian Blur” was set between 0.25 and 0.3.

iii) The “Brighten Darken” function increases the contrast of the image. It does this by assigning all pixels a number between -1 and 1 based on how bright or dark the pixel is. If a pixel has a value between -1 and 0 the pixel will be darkened, relative to its original value, and likewise, if it has a value between 0 and 1 the pixel will be lightened proportional to its original value. This again makes the edges of the cells easier to detect by the software which will result in more successful cell segmentation. However, if the z-stack has too high a contrast then the cell walls will be too saturated for the software to detect. For myr-YFP z-stacks, “Brighten Darken” was set between 1.5 and 2.5 but most often at the standard 2.

iv) The “ITK Watershed” function is set to 1500. This binarises the image, i.e., sets what is cell wall and what is not. Increasing and decreasing this function can vary your final segmentation massively as this function determines how many or how few ‘cells’ the software detects.

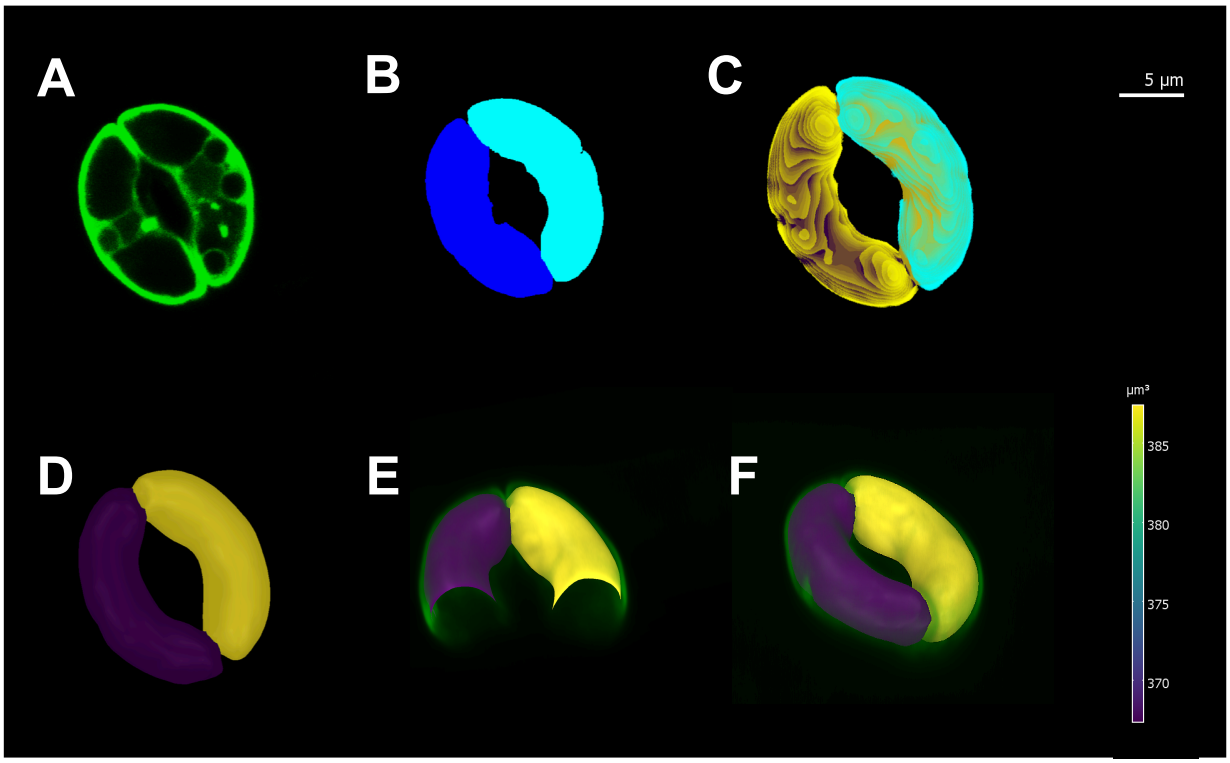

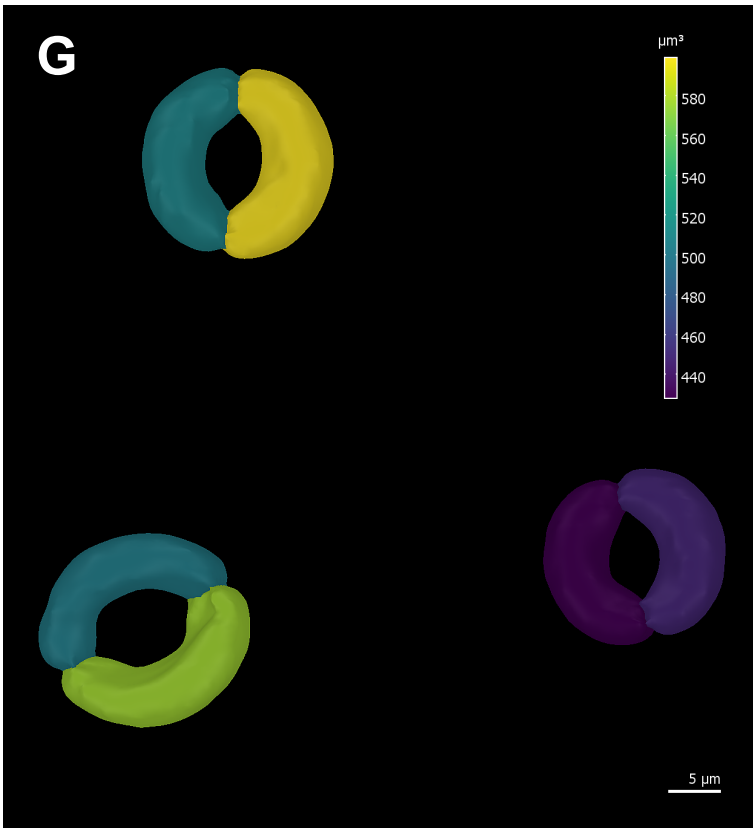

Figure 3.9 Screenshots from LithographX showing the process of 3D guard cell segmentation. (A) A single slice from a z-stack of a stomate, showing the strong membrane signal of the myr-YFP line. **(B)** Segmentation of the stomate, with each guard cell a different colour. **(C)** A mesh generated to recognise cell shape. **(D)** the stomate at the final 3D heat map stage where volume is represented by colour. **(E)** and **(F)** show the stomate heat map from different angles with the original YFP boundary overlayed (green). **(D-F)** Volume of cells represented by the heat map adjacent to **F**. **(G)** Multiple stomata as a heat map showing the volume variations, illustrating how the volume heat map works with multiple segmented cells. **(A-F)** are all on the same scale and the scale bar represents 5µm. **(G)** Scale bar represents 5µm.

3.4.7 Final method overview

For details of the full method, see methods section 2.9.

Epidermal peels from myr-YFP leaves were taken and mounted onto microscope slide wells with either ABA, RB or FC at the concentrations given. These were then imaged on an Olympus FV1000 confocal microscope using an eYFP filter set and a 514nm laser to acquire z-stacks that encapsulated either one or several (maximum 5) whole stomata. These z-stacks were then processed in LGX to seed and segment guard cells, producing 3D reconstructions of guard cells. An example of this process in shown in Figure 3.9. From this, volume and surface area data were generated by LGX, and images of midpoint cross sections were also taken and exported for further image analysis.

3.5 Results

3.5.1 Exposure to opening and closing stimuli changes guard cell volume and surface area

The average volume of guard cells imaged on epidermal peels in resting buffer (RB) was 464 ± 107μm^3 (mean ± SD, n = 100 cells). When exposed to ABA, the average guard cell volume decreased by 24% to 353 ± 68μm^3 (n = 84 cells). In contrast, when exposed to fusicoccin (FC), the average guard cell volume increased by 11% to 514 ± 111μm^3 (n = 84 cells). The difference in means of the three average cell volumes was statistically significant (Tukey test, F=62.19, p<0.001; Figure 3.10A).

The average surface area of guard cells imaged on epidermal peels also changed as the stomata opened and closed (Figure 3.10B). In RB the average cell surface area was measured as 375 ± 54μm^2 (n = 100 cells). When exposed to ABA, the average guard cell surface area decreased by 15% to 318 ± 36μm^2 (n = 84 cells). In contrast, when exposed to FC, the average guard cell surface area increased from RB by 8% to 404 ± 48μm^2 (n = 84 cells). These changes were also statistically significant (Sidak's multiple comparisons test, F=72.66, p<0.0001).

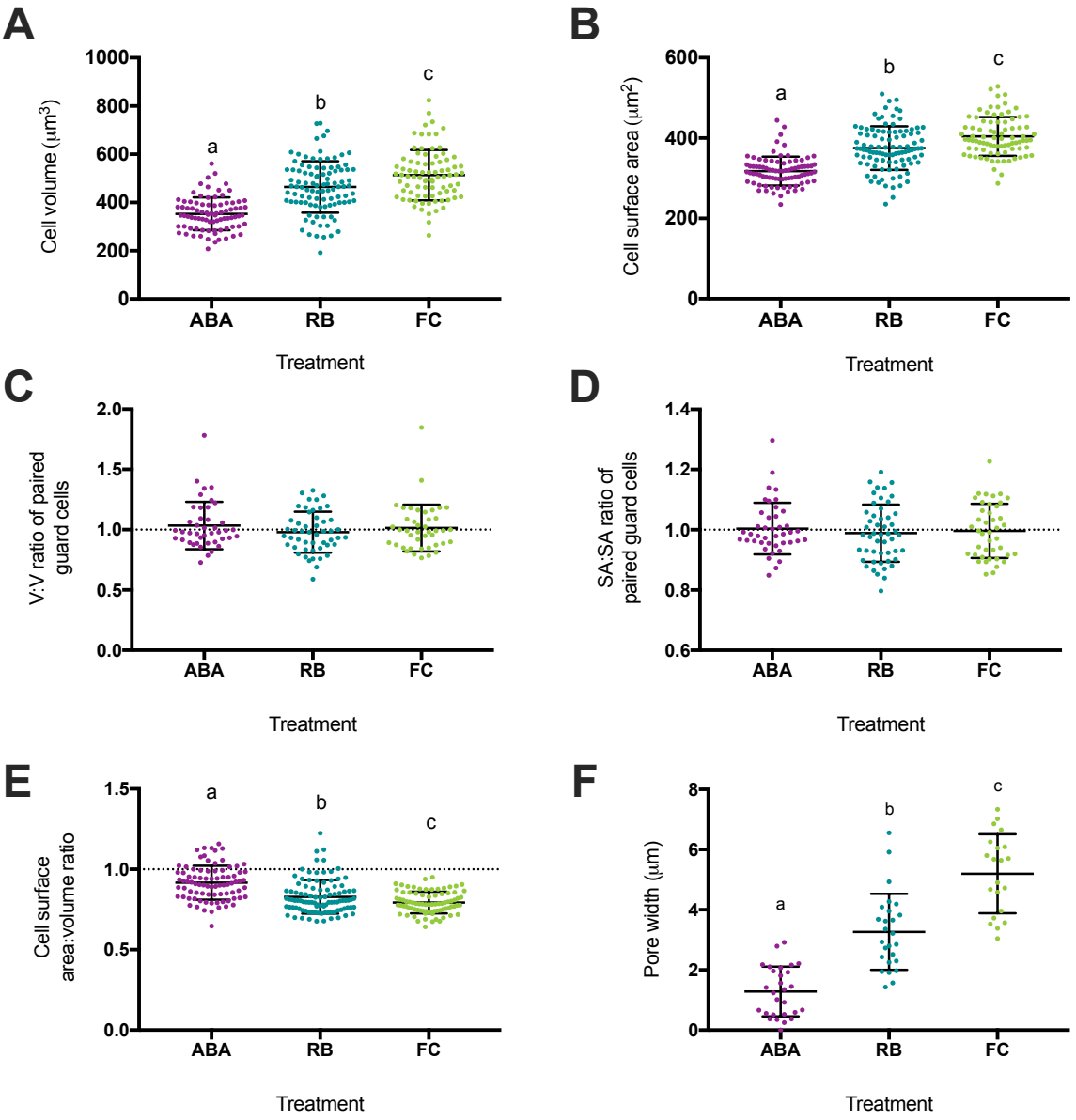

Figure 3.10 Changes in guard cell volume, surface area and stomatal pore width when exposed to ABA (purple), resting buffer (RB; blue) or fusicoccin (FC; green). (A) Average volume and **(B)** average surface area of guard cells. **(C)** Volume: volume (V:V) ratio of paired guard cells exposed to ABA, RB and FC. **(D)** Surface area: surface area (SA:SA) ratio of paired guard cells. **(E)** Surface area: volume ratio of guard cells. **(F)** Pore width of stomata. A one-way ANOVA was performed on each data set, followed by a Sidak's multiple comparisons test (as appropriate). Within a data set, samples indicated with the same letter cannot be distinguished from each other ($p<0.05$). Central horizontal line indicates mean and bars = SD. *n* = between 88 and 100 cells per treatment except for (F) where there are between 21 and 28 stomata per treatment. Stomata were exposed to ABA, RB or FC (as indicated) with each data point representing single guard cell (A-B) or stomate (C-F).

3.5.2 Paired guard cells show no relative difference in volume or surface area

Meckel et al., 2007 observed that in every stomate one guard cell seemed smaller than its pair. When looking at the initial confocal images and the subsequent 3D renderings of the cells, I too noticed that in casual observation paired cells did not always look identical in shape and size. To see if this was true and reflected in the data collected from the confocal images, I analysed the volume: volume (V:V) ratio and the surface area: surface area (SA:SA) ratio between each pair of guard cells from the confocal data. Paired guard cells in ABA, RB and FC all had a V:V ratio of 1:1, with an apparently equal spread of values around the means, suggesting that on average paired cells of a stomatal complex have a similar volume (Figure 3.10C). There were no significant changes in either mean ratio or spread of cell volume ratio between the treatments (one-way ANOVA, $F=1.044$, $p>0.05$). This pattern was also seen in SA:SA ratio, which also had a mean value of approximately 1 for all treatments (ABA, RB and FC) with a similar spread of values around the mean (one-way ANOVA, $F=0.3228$, $p>0.05$; Figure 3.10D). This indicates that during stomata opening and closing, paired guard cells on average stay matched both in volume and in surface area, with no evidence of significant disparity between paired cells.

3.5.3 Guard cell surface area: volume ratio increases as stomata close

The SA:V ratio of each guard cell was calculated. The average SA:V ratio of guard cells in RB was 0.828, which increased in ABA to 0.916, and decreased in FC to 0.793 (Figure 3.10E). The difference in SA:V ratio between ABA and RB and between RB and FC was statistically significant (Sidak's multiple comparisons test, $F=19.05$, $p<0.0001$). This means that in ABA, when stomata were more closed, the SA:V ratio of cells was larger than in RB and FC so there was more surface area to every unit of volume for the cells, reflecting the decrease in volume required to close the stomatal pore. In contrast, when stomata opened, their comparative surface area decreased compared to their volume, which reflects their increase in volume. This indicates that the cells are likely increasing in size, because as an object gets larger, its SA:V ratio gets smaller.

To confirm that the guard cells were opening and closing in each of the treatments, pore width was also measured (Figure 3.10F). Average pore width was statistically different in

each of the treatments (Sidak's multiple comparisons test, $F=72.03$, $p<0.0001$), and increased from an average of 1.10μm in ABA to 3.27μm in RB and finally to 5.20μm in FC.

So guard cells increase in overall size as they open and decrease in size as they close, which is supported by an increase in both surface area and volume during stomatal opening. However, it is clear that guard cell shape change during opening/closing is more than just an alteration on surface area and volume (Franks et al., 2001) with differences in cross sectional shape being observed in Meckel et al., 2007 between open and closed stomata. To investigate whether the changes in cell surface area and volume were related to guard cell shape, I looked at cross sections from my 3D guard cell reconstructions to see if they indicated whether any change in cell geometry was occurring during stomatal movement.

3.5.4 There are cross sectional shape changes in guard cells between open and closed stomata

Images of cell cross sections were taken at the vertical midpoint of each guard cell (Figure 3.11A), with Figure 3.11B showing some representative images of guard cell cross sections from stomata after incubation in ABA, RB or FC. Clear trends in shape differences are apparent. Cross sections of stomata in ABA have angled, elliptical cells that meet their pairs towards the bottom of the cells, whilst in FC cross sections appear more circular, and some seem almost quadrangular in shape.

There was more diversity in shape for cross sections of guard cells incubated in RB and FC, however there seems to be a trend towards the cross sections becoming less elliptical and more circular, which is especially seen in FC-treated cells.

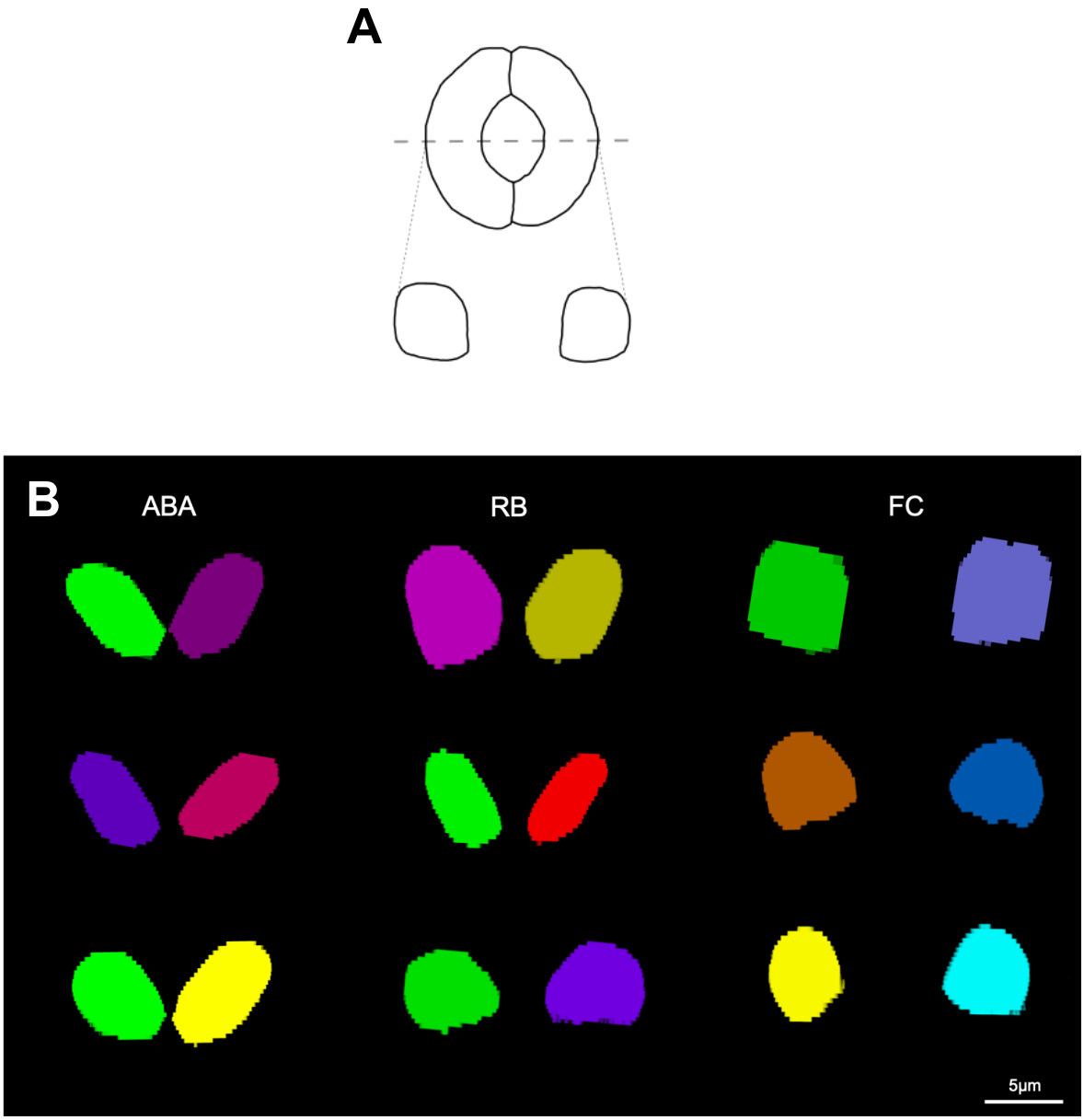

Figure 3.11 The morphological diversity of guard cell cross sections. (A) Schematic showing that guard cell cross section images were taken at the vertical midpoint of each cell. All diagrams of cross sections are shown with the periclinal (outer epidermal) surface to the top of the image. **(B)** The confocal method was followed and stomata were imaged after incubation in ABA (left hand column), RB (centre column) and FC (right hand column). z-stacks of guard cells were segmented in LGX and screenshots were taken of cross sections. Image is an amalgamation of 9 individual stomatal complexes. No meaning is inferred from cell colour. Scale bar = 5µm.

3.5.5 Guard cell cross sections become more circular when stomata open

Cross section shape circularity was measured in ImageJ from each of the cross section images. A circularity of 1 indicates a circular shape and shapes which are less circular (more elliptical) are described by a measurement tending towards 0. ImageJ calculates circularity using Equation 3.

Equation 3 Equation to measure circularity of a shape used by ImageJ.

$$Circularity = 4\pi\left(\frac{area}{perimeter^2}\right)$$

The frequency of cross sections with a circularity of 1 increased in RB and FC treatment, indicating that as stomata opened, the cross section of the guard cells became more circular; 7% of cell cross sections incubated in ABA had a circularity of 1, compared to 27% incubated in RB and 46% in FC (Figure 3.12A).

To test whether the differences in circularity were statistically different between treatments, statistical tests were carried out. However as the data were on a finite scale of 0–1, I questioned whether a standard ANOVA would be appropriate. An ANOVA is a robust test against both normally and non-normally distributed data (Glass et al., 1972), however the variances between treatments in the data must be equal. A Fligner-Killeen test, appropriate for non-normally distributed data such as these, was used to test for homogeneity of variance and found that there was heterogeneity of variance (median chi-squared=10.929, $p<0.05$). This can be seen when looking at the whiskers in the plots in

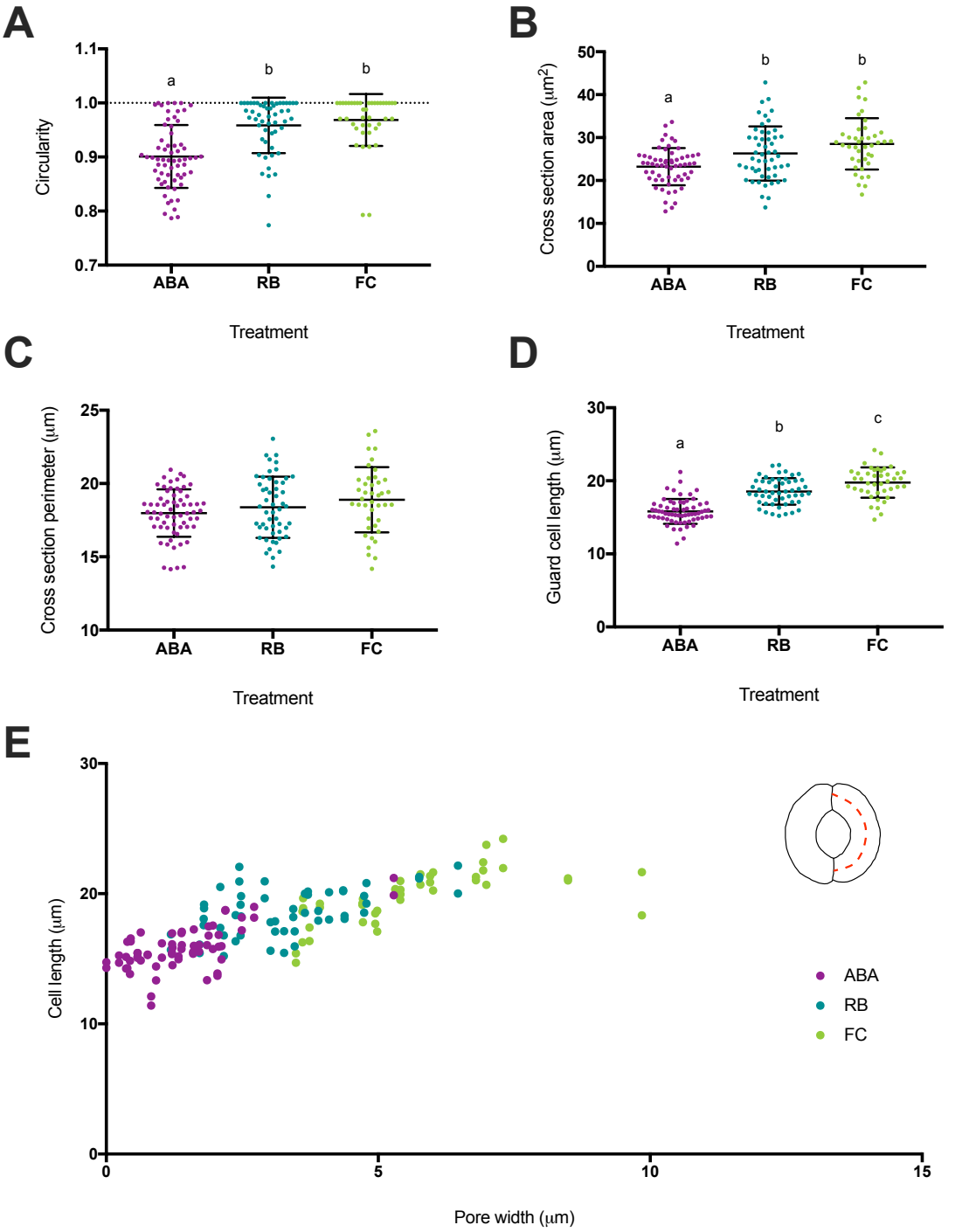

Figure 3.12 Changes in guard cell cross section shape and guard cell length when exposed to ABA (purple), resting buffer (RB; blue) or fusicoccin (FC; green). (A) Circularity of cross sections measured on a scale of 0-1 where 1 is a circle and the measured shape is increasingly ellipsoid as it tends towards 0. **(B)** Average cross section area and **(C)** average cross section perimeter. **(D)** Length of the arc of the guard cell. **(E)** Guard cell arc length plotted against pore area. Inset schematic shows the arc of the guard cell that was measured for cell length measurement in **D** and **E**. A Welch's ANOVA and pairwise t-test with Holm corrections was performed on **(A)** and a one-way ANOVA followed by Sidak's multiple comparisons test was performed (as appropriate) on datasets **B**-**D**. Within a dataset, samples indicated with the same letter cannot be distinguished from each other ($p<0.05$). Central horizontal line indicates mean and bars = SD. *n* = between 41 and 64 cells per treatment. Stomata were exposed to ABA, RB and FC (as indicated) with each datapoint representing a measurement from a single cell.

Figure 3.12A. Therefore, a Welch's ANOVA which accounts for heterogeneity in variance was used and showed that there was a significant ($F=33.023$, $p<0.05$) effect between treatments. A further post hoc pairwise t-test with Holm corrections showed that the difference in circularity was significantly different between cells treated with ABA and RB but not between RB and FC.

This reveals that as guard cells deflate to close the stomatal pore, a change of shape is occurring; the guard cells are not simply decreasing in size during closing, they are changing shape to become more elliptical.

3.5.6 Guard cell cross sections change in area but not perimeter during stomatal opening

To see whether this shape change was reflected in general cross section shape parameters, cross section area and perimeter was measured. The average area of a guard cell cross section in RB was $26.3 \pm 2.1\mu m^2$ ($n = 52$). After ABA treatment, the average area decreased to $23.4 \pm 4.5\mu m^2$ ($n = 60$) and in FC this increased to $28.5 \pm 6.0\mu m^2$ ($n = 41$) (Figure 3.12B). The difference in cross section area between RB and ABA was statistically significant but was not between RB and FC (Sidak's multiple comparisons test, $F=11.7$, $p<0.0001$). This could reflect the data of cross section circularity seen in Figure 3.12A which shows that cross sections in RB and FC share a similar more circular morphology, whereas in ABA the cross sections are less circular.

No statistical difference in guard cell cross section perimeter was found for any of the treatments (one-way ANOVA, $F=2.718$, $p>0.05$; Figure 3.12C). The average perimeter of cross sections in ABA, RB and FC were $18.0 \pm 1.6\mu m$ ($n = 64$), $18.4 \pm 2.1\mu m$ ($n = 52$) and $18.9 \pm 2.2\mu m$ ($n = 41$) respectively. This indicates that although there was some degree of cross-sectional shape change occurring between resting stomata and closed stomata, there was no difference in the average perimeter of the cross sections.

These data, along with the SA:V ratio data seen in section 3.5.3, demonstrate that cell shape changed between closed and resting stomata. During stomatal closure, the SA:V ratio of the guard cells increased, and the cross section of the cells became less circular while the cross-sectional area decreased but perimeter length remained constant.

3.5.7 Guard cells lengthen as stomata open

The data in Figure 3.12A-C shows that the overall change in surface area and volume of guard cells during opening and closing cannot solely be described by a change in cross sectional shape. Meckel et al., 2007 showed that there were significant changes in broad bean guard cell shape at the tips of the guard cells in the regions where the two paired guard cells meet, and Shope et al., 2003 measured guard cell lengthening during opening in broad bean stomata. Guard cell arc length was measured along the arc of the cell, ensuring equal space between each edge of the cell wall (inset in Figure 3.12E). The average arc length of a guard cell after ABA treatment was 15.81 ± 1.69µm (n = 64), which increased to 18.54 ± 1.81µm (n = 52) in RB and then increased again to 19.77 ± 2.07µm in FC (n = 42). These measurements were significantly different between treatments (Sidak's multiple comparisons test, F=65.7, p<0.0001) showing that guard cells increased in arc length as stomata opened (Figure 3.12D). Figure 3.12E shows pore width against guard cell arc length. There was a positive trend between cell arc length and pore width, showing that as stomata opened, the arc length of the guard cells increased.

3.5.8 Feret diameter of guard cell cross sections increases when stomata open

The Feret diameter is a measurement that represents the longest length of a specified shape, regardless of any shape irregularities. It is also known as the calliper diameter, which refers to the maximum measurement taken between two opposite sides of an object as if measured by callipers.

Feret diameter was calculated for guard cell cross sections using a programme in ImageJ to find the maximum diameter of the guard cell midpoint cross sections. This is illustrated in Figure 3.13. A number of cross sections have a circularity value of 1 (Figure 3.12A) and so these were discounted from the Feret analysis as there cannot be a single longest diameter of a circle as all diameters are equal in length.

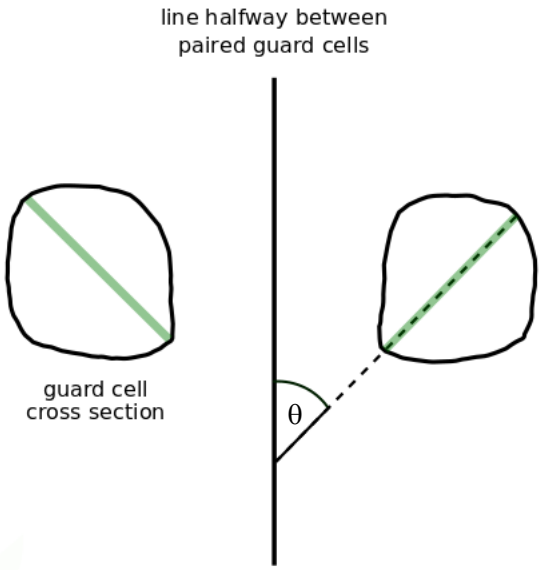

Figure 3.13 Feret diameter and angle for guard cell cross sections. The Feret diameter (green lines) is the longest length of a shape regardless of shape irregularities. Feret diameter of guard cell cross sections was measured using ImageJ. A hypothetical vertical line was drawn halfway between the two guard cells in ImageJ and then the angle at which the Feret diameter of each guard cell cross section intersects with the vertical line was calculated to give angle θ, a measure of guard cell tilt or angle.

Figure 3.14A shows the average Feret diameter of guard cell cross sections after treatment of stomata with ABA, RB or FC. The average Feret diameter for cells in ABA, RB and FC was 7.04 ± 0.71µm (n = 58), 6.72 ± 0.67µm (n = 38) and 7.55 ± 0.55µm (n = 22) respectively. There was no significant difference between the mean Feret diameter of guard cells in ABA or RB, however the mean Feret diameter of cross-sections from FC-treated samples was significantly higher than those taken from RB-treated stomata (Sidak's multiple comparisons test, F=10.23, p<0.0001). This indicates that as the stomata opened, the diameter of the longest length in the cell increased, again indicating a shape change occurring.

3.5.9 The angle of Feret diameter of guard cell cross sections changes as stomata open and close

The angle, θ, at which the Feret diameter meets a vertical line halfway between the two cross sections (Figure 3.13), was calculated to investigate the way in which guard cells change angle during opening and closing. The results are shown in Figure 3.14B.

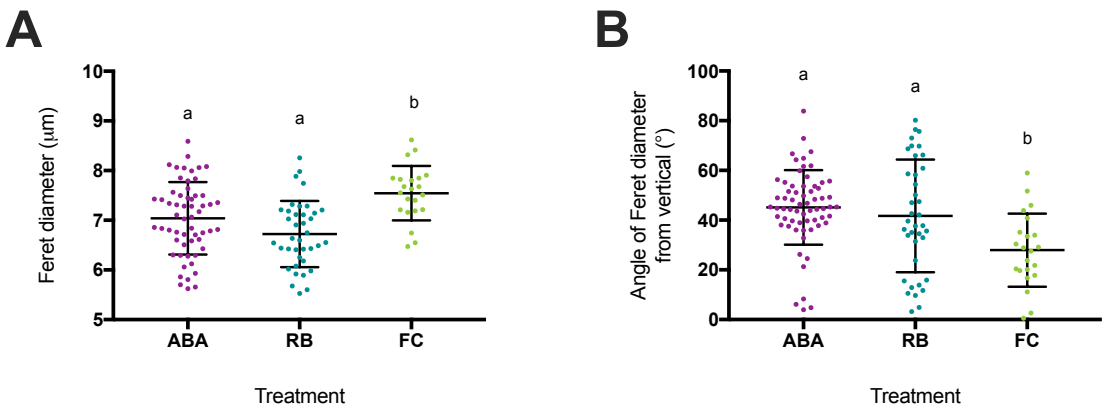

Figure 3.14 Feret diameter and angle changes when guard cells are exposed to ABA (purple), resting buffer (RB; blue) or fusicoccin (FC; green). (A) Feret diameter of guard cell cross sections and **(B)** the angle at which the Feret diameter of the guard cell cross section meets a vertical line between the two paired cells. For **(A)**, a one-way ANOVA was performed on each dataset followed by Sidak's multiple comparisons test ($F=10.23$, $p<0.0001$). For **(B)**, a Welch's ANOVA was performed with a Holm's t-test ($F=10.952$, $p<0.05$). Within a data set, samples indicated with the same letter cannot be distinguished from each other ($p<0.05$). Central horizontal line indicates mean and bars = SD. *n* = between 22 and 64 cells per treatment. Stomata were exposed to ABA, RB or FC (as indicated) with each data point representing a single guard cell.

Since the distribution of data points for RB shows multiple modal values, I tested for homogeneity of variance using a similar method to that discussed in section 3.5.5. A Shapiro-Wilk normality test interestingly showed non-normal distribution in the ABA treatment, and a Fligner-Killeen test revealed heterogeneity of variance (median chi-squared = 10.164, $p<0.05$). Therefore a non-parametric Welch's ANOVA was used ($F = 10.952$, $p<0.05$) with a post-hoc t-test with Holm corrections, which revealed that there was no significant difference between ABA- and RB-treated stomata but there was a significant difference between RB and FC. The average angle θ was 45° for cells in ABA ($n = 58$), 41° for cells in RB ($n = 38$) and 27° for cells in FC ($n = 22$).

3.6 Discussion

The aim of the research reported in this chapter was to develop a method of imaging stomata to gain 3D data on guard cell size and shape under changing environmental conditions. I hypothesised that guard cell shape changes when stomata are exposed to opening and closing stimuli, and that this shape change can be quantified using fluorescent microscopy and subsequent imaging processing software.

3.6.1 A novel method of imaging Arabidopsis guard cells in 3D using confocal microscopy

Imaging guard cells for 3D analysis has been done before with regards to guard cell shape change (Meckel et al., 2007), however this study focussed on broad bean leaf tissue, and not Arabidopsis leaf tissue. Developing a method of 3D imaging of guard cells with Arabidopsis tissue was considered beneficial for several reasons. Firstly, although Arabidopsis stomata have been thoroughly characterised and studied over the last few decades, there is still a traditional view of stomata being composed of sausage-shaped cells that swell and shrink proportionally in order to manipulate the aperture of the stomatal pore (Marom et al., 2017; Rui and Anderson, 2016; Yi et al., 2018). It is clear that this traditional view is incorrect but there is a surprising lack of quantitative data describing guard cell shape.

Secondly, there is a wealth of genetic resources available for Arabidopsis work. Studies of transgenic lines provide a comparison to results from investigations with wildtype tissue, allowing inferences on the function of genes either overexpressed or mutated in the transgenic lines. By taking advantage of the many knock-out lines available – for example from the Nottingham Arabidopsis Stock Centre (NASC) – one can expand the work done in this chapter into various mutant lines to characterise guard cell shape change when the plant lacks a specific genetic component thought or known to be involved in stomata function. Arabidopsis lends itself fairly easily to transformation using *Agrobacterium tumefaciens* and so more tailored genetic manipulation, targeting altered gene expression to guard cells whilst keeping the myr-YFP construct within the plant for confocal imaging of those guard cells, is possible.

However, this approach requires first that there is a solid description of the wildtype phenotype against which any change in shape can be quantified. The results reported in this chapter provide this baseline. Having an accurate representation of guard cell shape has become even more important with the advent of various mechanistic models of guard cell geometry and function (Carter et al., 2017; Woolfenden et al., 2018; Yi et al., 2018). These approaches depend upon accurate cell meshes, with changes in cell geometry having potentially large outcomes on modelled stomatal performance, yet to date most work on this area has used meshes based on idealised cell geometries. More realistic guard cell geometries are needed if this field is to progress.

Here I have analysed the Arabidopsis wildtype Col-0 to characterise guard cell shape change. The data support my first hypothesis by establishing a robust method that was reproducible on a fairly large scale. As a first step towards analysing how guard cell shape change might alter in different genetic backgrounds, I have taken steps to begin characterisation of a gene knock out in *ARP3*, the details of which are reported in Chapter 4.

3.6.2 Comparison of LSFM and CLSM to image stomata

LSFM as a method to image guard cells on live plants initially appeared to be a viable method of imaging stomata (Ovečka et al., 2015) due to its large field of view and quick scanning speed (Ovečka et al., 2018). It also offered the potential to automatically input different concentrations of CO_2 and to change the sample buffer without having to remove and re-load the sample, which could be used to manipulate stomatal aperture with minimal disruption to the sample and to the imaging process.

I used the protocol outlined by the above 2015 methods paper as a basis for my own work and I successfully developed a method to image stomata on the LSFM (Figure 3.3 and Figure 3.4). However, it became clear that this method would not be a reliable method of imaging stomata for 3D processing. Due to equipment constraints, automatically changing the internal CO_2 levels and sample buffer was not possible and manually changing the buffer led to multiple imaging difficulties, including the shifting of the sample in the sample buffer during image acquisition.

In contrast, confocal microscopy provided a more reliable and successful method of imaging stomata. Because of the method's ubiquity and versatility (Wymer et al., 1999)

there was more support and advice available during method development which may have contributed to its eventual success. On reflection, light sheet microscopy may not be the optimal choice for imaging stomata. The large field of view and speed of imaging that LSFM offers is a great benefit to long-term imaging of developmental processes in bigger tissues (e.g. Prunet, 2017), which I initially thought would be useful for imaging lots of stomata at once and capturing them opening or closing in real-time. However, multiple technical difficulties prevented the imaging of stomata in real-time which meant I did not need long-term imaging. Additionally it became clear that if I was to capture stomatal shape change using the software available, I would need high resolution images that could capture the intricacies of the cells changing shape, a resolution difficult to obtain with such large fields of view. Standard confocal microscopy provides higher resolution images from a smaller field of view suitable for this approach (Ovečka et al., 2018). In addition to these technical limits, choice of fluorescence marker was key to success and in the investigations reported here the myr-YFP transgenic line was central to the development of a robust protocol.

3.6.3 myr-YFP

myr-YFP stands for myristoylated YFP and refers to the addition of a short sequence to the protein which anchors it to the plasma membrane (in Willis et al., 2016, the line is referred to as acyl-YFP since anchoring of the protein to the membrane is strengthened through acylation).

The localisation of YFP to the stomatal cell membrane produced a strong and consistent signal that outlined the guard cells, as seen in Figure 3.9, as well as binding to some membrane structures internally. This often resulted in multiple "cells" being seeded inside each guard cell using the LGX software but these were easily merged during processing to form the whole guard cell shape. When compared to other methods of fluorescence marker that I tried, the process of segmenting cells labelled with myr-YFP was quick and easy.

3.6.4 Guard cell shape change

The successful development of a novel protocol to image stomata and to reconstruct the guard cell shape in 3D has provided useful and important information regarding changes in guard cell volume, surface area and cross-sectional shape as stomata open and close.

It is already well-documented that guard cells increase in volume when the stomata open and decrease in volume when they close (Franks et al., 2001). The data reported in this chapter provide quantitation of these values. Thus, from closed to open an Arabidopsis guard cell on average increases volume by 45%. This is accompanied by a change in surface area too, with a guard cell experiencing a 27% average increase in its surface area as a stomate shifts from closed to open. Clearly guard cells undergo a significant change in both surface area and volume during stomatal opening and closing.

When comparing these data with broad bean stomata, which see a volume change of 25% and a surface area change of 15% (Meckel et al., 2007), Arabidopsis undergo a comparatively greater size change than broad bean stomata do. This may be because Arabidopsis stomata are smaller on average than broad bean stomata and so any differences in volume and surface area are comparatively greater, or it could be because of the different experimental setup. Meckel et al. dark-adapted their stomata before exposing them to 10μM FC and imaging the same stomata over a 45 minute period, and so it is possible that the closing response following ABA is more extreme than from the stomata in the dark, so the starting 'closed' point for both experiments might be different. Although Meckel et al. note in the aforementioned paper, that paired guard cells of a single stomate often do not appear matched in size (an impression that I also gained from simple observation), my analysis of the quantitative data does not support the idea that paired guard cells differ in either volume or surface area, so this apparent visual difference in size does not reflect reality.

Closed stomata have a higher surface area to volume ratio than stomata in RB or opened stomata (FC-treated), which reflects the general geometric rule that smaller objects of a similar shape have a higher SA:V ratio than larger objects (as seen here with FC treatment). However, when looking at cross section shape changes, the data becomes more complex. For some of the parameters measured, the average RB sample measurement is statistically not different to FC-treatment (as seen when looking at

differences in Feret diameter) and for other parameters the RB samples cannot be distinguished from ABA-treated samples (for example cross section area). When looking at the range of guard cell cross section shapes found in RB-treated stomata, some cross sections appeared elliptical and slanting inwards (as for ABA treatments), whilst some seemed more circular (as observed after FC treatment), highlighted in Figure 3.11. This variation in guard cell shape in RB could represent how far along the opening-closing pathway that specific stomate was at the time of imaging. It is also possible that because there are no strong stimuli from the resting buffer for opening or closing, other stimuli in the experimental environment were having effects and effectively overriding the 'resting' status. For example, it is possible that in RB stomatal measurements depended on other factors, such as light or temperature in the room at the time when they were imaged. Because of this variation within the RB samples, when discussing cross sectional shape change I will mainly compare guard cells in ABA-treated stomata to cells from FC-treated stomata as these samples display a more consistent morphology within each dataset.

The smaller overall cell size of guard cells in ABA is reflected in the smaller area found in the midpoint cross-sections. However, interestingly, there is no difference seen in the perimeter of the cross-sections in any of the treatments, suggesting smaller changes in cell surface area in this region compared to volume changes of the cell. This could indicate some degree of unusual shape change. If the perimeter at the midsection of guard cells does not change during opening and closing, but the cell on the whole is changing volume and surface area, then there may be a perimeter change at a different part of the cell. In this analysis I did not look at cross sections at guard cell tips, but Meckel et al.,

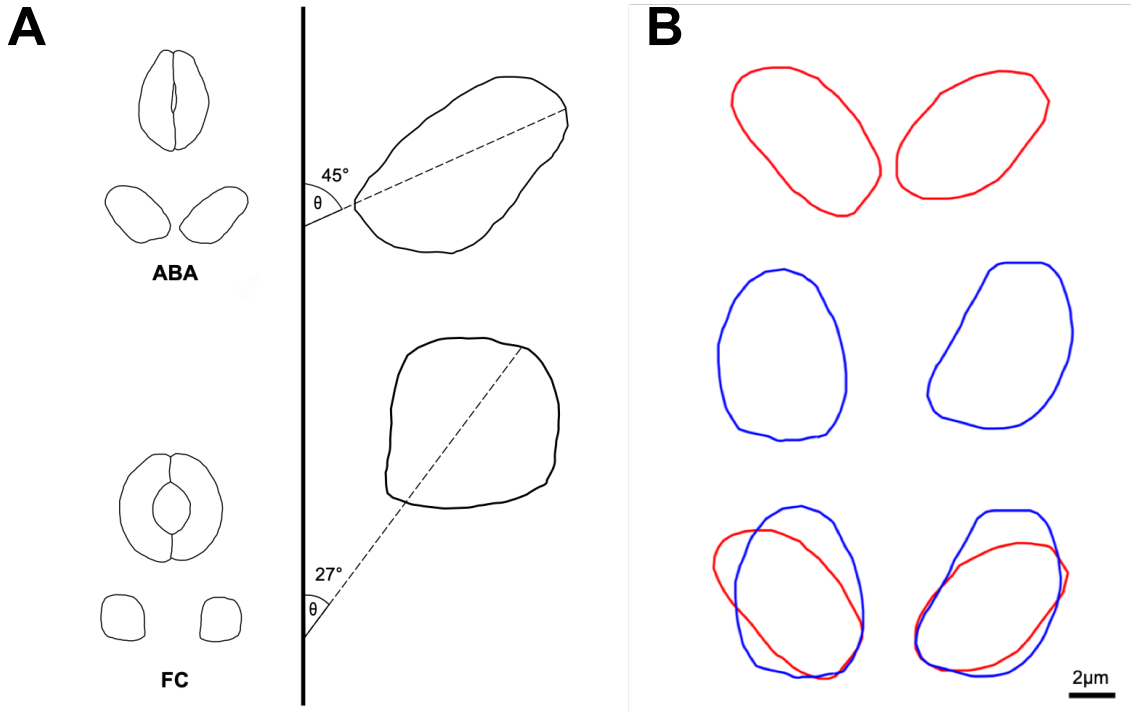

Figure 3.15 Guard cell cross sections change angle as stomata open and close. (A) Schematic to show that the angle at which the Feret diameter (dotted line) meets a vertical midpoint changes when stomata close (ABA) and open (FC). Cells and angles not to scale. **(B)** The differences in cross section shape change between open and closed stomata are seen when drawings of closed stomata (red) are overlaid with open stomata (blue). Drawings to scale but aperture not accurate due to overlaying in final row.

2007 observed significant shape change at the tips of their guard cells, consistent with the results reported here. My data also support the observation that guard cells lengthen as the pore opens, and so this also offers an explanation for the increases in surface area and volume.

Geometrically, the cross sections of guard cells in closed stomata treated with ABA were generally ellipsoid in shape and come together to touch, or almost touch, at the lower (inward) side of the stomatal pore (Figure 3.15). It is this touching that closes the stomata and reduces the aerial exchange of gases and water between the plant and the environment. In contrast, guard cell cross sections of open stomata are more circular than in ABA-treated stomata. These data unambiguously show that there is a significant change in the shape of the cross section of guard cells between open and closed stomata, which therefore supports Hypothesis II stated in the aims/objectives of this chapter which was that imaging methods can be used to quantify guard cell shape change. Differences in

cross sections has been noticed before in Meckel et al., 2007, who noted that guard cells in open stomata have a more circular cross section, and has been mentioned in some other papers (Bidhendi and Geitmann, 2018; Cooke et al., 1976; Shope et al., 2003) but the apparent "swinging" of the guard cells downwards as they lose turgor to close the stomata has not been described in such detail.

Cross sections of guard cells in open stomata being more circular is a pattern used in a computer model that looked at the aspect ratio of cell cross sections at the guard cell midpoint as turgor pressure increased within the cell, where an aspect ratio of 1 is a circle. As turgor pressure increased (and the stomate opens), the aspect ratio tended towards just below 1, regardless of whether the aspect ratio started above or below 1 (Woolfenden et al., 2017; supplimentary figures). My data showing that guard cell cross sections become more circular when the stomata open suggest that this model is consistent with reality in this aspect of stomatal geometry. However, the starting point of the different cross sections used in the computational model were different to the shapes seen in reality (and represented in Figure 3.11); the modellers used ellipses but the angle of the ellipse to the perpendicular was different to the angle that guard cells actually form, as demonstrated in the work presented here.

To characterise how much, if any, turning or slanting guard cell cross sections undergo during stomatal opening and closure, Feret diameter and the angle of this Feret diameter from a vertical midpoint was measured on guard cell cross sections. The angle of the ellipse in ABA-treated samples (the Feret angle θ) is significantly different to the angle measured in FC-treated samples. In ABA, the angle on average is at 45° from the vertical, whereas in FC-treated samples it is at 27° (Figure 3.15A). This suggests that when stomata open, the lower part of the cells (that create the bottom of the 'bowl') move away from each other to open the pore, which results in the angle of the cell getting more acute, and, simultaneously, the cells becoming rounder in cross section. This is in contrast to work in the literature suggesting that when stomata close there is a simple lateral movement of the cell edges to close of the outer pore and the cuticular ledge (Bourdais et al., 2019; Carter et al., 2017; Yi et al., 2018).

The results discussed in this chapter show that guard cell shape change (and, consequently, stomatal pore change) during stomatal opening and closing is far from

simple. There is a traditional view of a sausage-shaped cell proportionally increasing and decreasing in size, with its midpoint cross-section maintaining a perfect circle (Marom et al., 2017; Rui et al., 2016), and in some studies, guard cell cross section shape is not considered at all (Yi et al., 2018). It is true that at certain points of guard cell shape change (i.e. when cells are open) the cross-section of the cells is similar to a circle, however this is certainly not always the case and future models of stomatal function and guard cell geometry should reflect this. The assumption that guard cells have a consistently circular cross section can be rejected as we have seen that not only do guard cells vary significantly in cross-sectional shape, they also do not shrink and swell in a proportional manner.

There have been many previous investigations showing that guard cell shape change is anisotropic (Marom et al., 2017; Woolfenden et al., 2018, 2017; Yi et al., 2018) and the data presented here supports this. Many of these models characterise this anisotropy in terms of differences in cell wall thickness, which is important for normal stomatal function (Carter et al., 2017; Yi et al., 2018).

I propose a new general model of guard cell shape change. When stomata are closed, there is a relatively low internal turgor pressure in each guard cell which results in a decrease in overall cell volume and surface area. The cell essentially 'relaxes', and the decrease in turgor pressure means the periclinal ends of the guard cells swing down around the attachment to the neighbouring epidermal cell and touch, or almost touch, closing the pore. This results in the angle of the cell increasing as it flattens out. If this shape is extrapolated to the whole cell level – which I have observed while looking at the 3D stomata – it indicates that closed stomata are bowl-like, with the two guard cells

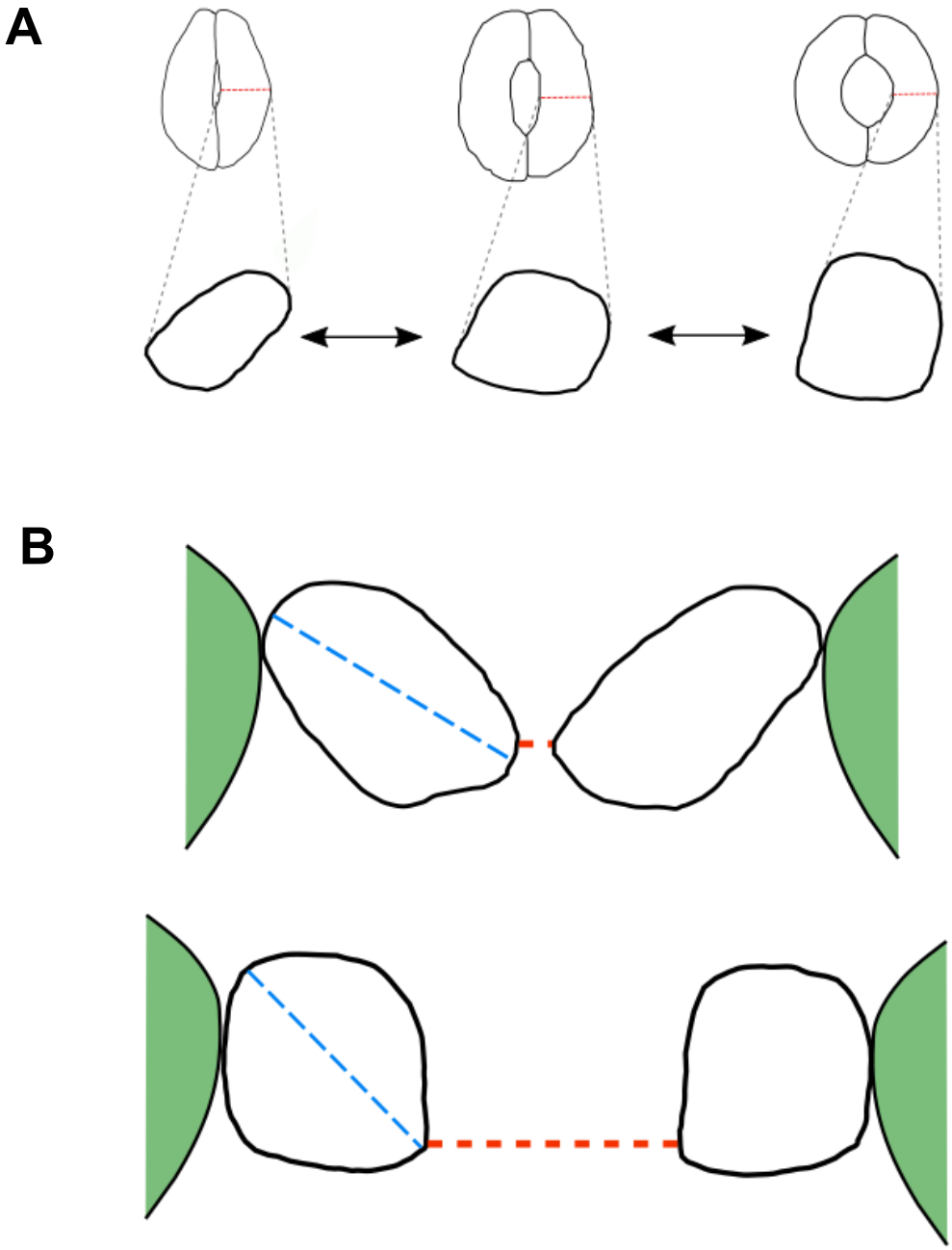

Figure 3.16 Schematics to show guard cell opening and closing. (A) As guard cells go from closed (left) to resting (centre) to open (right), the midpoint cross section shape changes. Red dashed line indicates the point along the midpoint guard cell at which the cross section was taken. **(B)** Cross section schematic illustrating side-on view of guard cell shape change as stomata go from closed (top) to open (bottom). The red line indicates minimum aperture of the stomatal pore which is increased significantly when stomata open. This corresponds to a change in cell angle (blue dashed line) as the cells 'twist' open. The green cells either side represent the neighbouring epidermal cells. This mechanism equates to minimal lateral movement of the guard cells into the adjacent epidermal cells while still opening the pore significantly.

touching at the lower (inside) end of each cell with a degree of space between the upper ends of the cells, creating a cavity. The images captured on the confocal microscope do not show the cuticular ledge (as the YFP was attached to the cell membrane) but if the cuticular ledge extends across the top of the pore as seen in multiple papers that have captures images of stomatal closure (Bourdais et al., 2019; Carter et al., 2017; Yi et al., 2018) then this could also provide another point of closure for the stomata.

To conclude, when stomata open, the internal turgor pressure of the guard cell increases and the cell swells to increase its volume by nearly half (45%) and its surface area by nearly a third (27%). Some of these volume and surface area changes can be explained by an increase in length of the cell. The pressure changes also force the cell to lose its ellipsoid cross-sectional shape and become more circular (Figure 3.16A). Whilst doing this, the shape twists, and the angle of the cell decreases so it becomes more 'upright'. This is likely due to the wall properties of the guard cells which constricts the cell and provides a means of an anisotropic cell growth. This also means that the midpoint of the cells may not actually move significantly further away from each other in order to open the pore: it is the shape change of the cells and the moving apart of the inner, lower parts of the two guard cells that causes the pore to open (Figure 3.16B). This may be a more energy efficient way of opening the pore as it does not require the guard cells to move into the adjacent epidermal cells to open but instead relies on the existing cell wall properties to change the shape of the cell as internal turgor pressure increases.

The 3D imaging protocol reported here has provided a new insight into stomatal opening and closing by providing detail on the shape change of guard cells. There is a great deal of variation in guard cell morphology (Figure 3.11), however trends in overall cell shape change and cross-section shape change show that the traditional 'sausage' model of guard cell shape does not capture reality. An alternative model (described here in Figure 3.16) is one in which change in guard cell shape and angle to the perpendicular is what opens the pore, and not simply the lateral movement of the two paired guard cells away from each other.

3.7 Limitations and future work

Despite the method described in this chapter providing novel insights into guard cell shape change, it has limitations, which are discussed below.

3.7.1 Fusicoccin as a toxin

Fusicoccin is a toxin produced by the fungal pathogen *Fusicoccum amygdali*, which causes wilt disease in almond and peach trees. It acts upon the H^+-ATPases located on plant plasma membranes (Johansson et al., 1993) to stimulate the extrusion of H^+ from the cells. This results in a rapid acidification of the area surrounding the plasma membrane and contributes to loosening of the cell walls under the acid growth theory (Rayle and Cleland, 1992). In stomata, this triggers an irreversible opening of the stomatal pore, which the fungus then uses to enter the plant, eventually causing plant death.

Fusicoccin can be used as a way to stimulate stomatal opening in order to test various parameters linked with stomatal movements. It was chosen as an opening trigger because it is quick and easy to administer to epidermal peels, and guarantees visible stomatal opening in a short space of time. However, fusicoccin is a plant toxin and there have been concerns that using it during physiological experiments is harmful to the plant, i.e., that it produces an unnatural opening result compared to other stomatal opening triggers, for example low CO_2. Indeed, when looking at the distribution of the data for guard cell volume in fusicoccin there seems to be a small spike in the number of cells with a high volume (data not shown) which could represent a number of guard cells being forced to inflate 'unnaturally'. However, when looking at data from guard cell pairs (Figure 3.10C), on average there is no difference in volume between paired guard cells of the same stomata. It is unlikely that a dead guard cell would maintain the same inflated volume as its living pair, which mitigates concerns that one cell is dying in each pair when exposed to fusicoccin

Concerns that administration of fusicoccin opens the stomata to the extreme and is therefore an unnatural representation of a true open stomatal measurement are valid. It may be one explanation for the unusual shapes seen in stomata that have been opened with fusicoccin (Figure 3.11). However, I would argue that for the purposes of this experiment, which is to assess the size and shape changes of guard cells when forced to close and open, using fusicoccin ensures that the stomata have opened within the time limits of the experiment, and also that the guard cells have been pushed to their extreme. This provides a clear point of comparison to closed stomata, and shows us to what degree of shape change guard cells have the capacity to adapt.

To fully confront concerns about the suitability of fusicoccin as a means of opening stomata, in future this method can be adapted in multiple ways for more physiologically natural and less potentially damaging methods of opening and closing. Two future alternatives to fusicoccin would be to dark-adapt the peels before exposing them to bright light before imaging them to trigger stomatal opening, or to treat the peels with low CO_2 for a period of time before imaging.

3.7.2 Accuracy of measurements in unnatural physiological conditions

Along the same lines as the previous argument, the fact that the method reported in this chapter uses epidermal peels and not whole leaf tissue could be seen as too unnatural from which to obtain any realistic physiological measurements. Considering that guard cells exchange water and solutes with neighbouring cells (Raschke and Fellows, 1971), as well as epidermal cells providing counteracting physical pressure (Franks and Farquhar, 2007), it is a valid argument that epidermal peels may not reflect accurately the degree of shape change that occurs during "normal" opening and closing of stomata. However, it is a method that is used frequently in stomatal studies and has been well established for a long period of time (Webb et al., 1996). The peels are quick and easy to prepare, and the removal of the underlying cells reduces the chances of detecting out-of-focus fluorescence during image acquisition which might disrupt image analysis.

3.7.3 Suggestions for future work

The method reported in this chapter represents a first step for 3D stomatal imaging to explore stomatal form and function, but I think there are several roads that this work can take in the future. For example, additional cross section data from different parts of the guard cell (e.g. the tips) would provide a more conclusive explanation of how the cross-section shape of guard cells changes during stomatal opening and closing.

Developing a method of imaging stomata shape change in real time would provide an interesting next step in this investigation. Significant attempts by myself were made into this using both the LSFM and the confocal microscope, however the many technical difficulties – such as movement of stomata during the timelapse imaging – meant that I had to prioritise other work over this. However, with enough time and optimisation this approach should be possible and would give us a wealth of data on not just the geometric

properties of guard cell shape change but also the dynamics of stomatal movement with time i.e. rate of opening and closing.

Using this method to simultaneously visualise epidermal cells surrounding the stomata and the guard cells, for example by using a membrane dye or stain such as FM4-64 or PI, would allow further investigation into the hypothesis put forward in Figure 3.16. Seeing to what degree the adjacent cells move with the guard cells would provide evidence to verify how much the guard cells move laterally during pore opening/closing. Developing this method to work with whole leaf samples instead of epidermal peels would also offer interesting information into the interaction between the guard cells and their surrounding leaf tissue in terms of volume and surface area changes, as well as any significant shape changes.

Another avenue which I began to explore was comparing data from Col-0 myr-YFP plants with transgenic mutant lines which have altered stomatal phenotypes. For example, I have transformed *arp3* knockout plants (Chapter 4) with the myr-YFP construct. Looking at more cell wall mutants or those with an interesting stomatal phenotype would provide an interesting comparison that could be used to see what effect altered different cell wall components have on guard cell shape and guard cell shape change.

Finally, the method could be expanded to many other plant species. Future development of 3D imaging of stomata in grass species would provide interesting information on the differences between monocot and dicot stomata. It would be particularly interesting if a line with fluorescently-labelled guard cells and subsidiary cells was available. One could then further investigate the unusual and complex shape changes that occur as the these 4-celled stomatal complexes open and close (Franks and Farquhar, 2007). In particular, one could examine the volume changes between guard cells in open and closed stomata and compare this to the volume changes of the subsidiary cells. This would allow an assessment of the degree that exchange of water and osmotic substances leads to reciprocal changes in volume of these cells, and the potential reciprocal changes in shape that occur between neighbouring cells.

3.8 Key findings

- Light sheet fluorescent microscopy can be used to image Arabidopsis guard cells, however for detailed shape change analysis such as the method described in this chapter, confocal microscopy is more appropriate.
- On average, paired guard cells are equal in volume and surface area.
- From closed to open, guard cells increase in volume by 45% and in surface area by 27%. They also undergo significant lengthening along the arc of the cell.
- From closed to open, guard cell cross section shape changes significantly too, with significant tilting and twisting during shape change. This is likely due to a combination of mechanical constraints provided by the cell wall, and the effects of adjacent epidermal cells, although further work into this is necessary. This 'twisting', as opposed to lateral movement of guard cells, to open the stomatal pore may improve efficiency of opening by reducing the energy expended on pushing back against the surrounding epidermal cells.

Chapter 4: Characterising the stomatal phenotype of *arp3* plants

4.1 Introduction

4.1.1 ARP2/3 and its role in plants

ARP2/3 (ACTIN RELATED PROTEIN COMPLEX) is a highly conserved protein complex derived of seven subunits involved in the formation of the actin cytoskeleton (Cooper et al., 2001). It acts as an actin binding protein (ABP) and is found in a broad range of eukaryotic organisms (Veltman and Insall, 2010) where it polymerises filamentous (F-) actin by binding to the side of an existing actin filament and initiating growth of a new filament at a 70° angle (Figure 4.1). Regulation and reorganisation of actin filaments is important to many cellular processes including cell division and vesicle movement (Mathur and Hülskamp, 2002).

In plants, it is thought that actin is involved mainly in transport and deposition of the plasma membrane and cell wall components to the cell wall (as opposed to microtubules

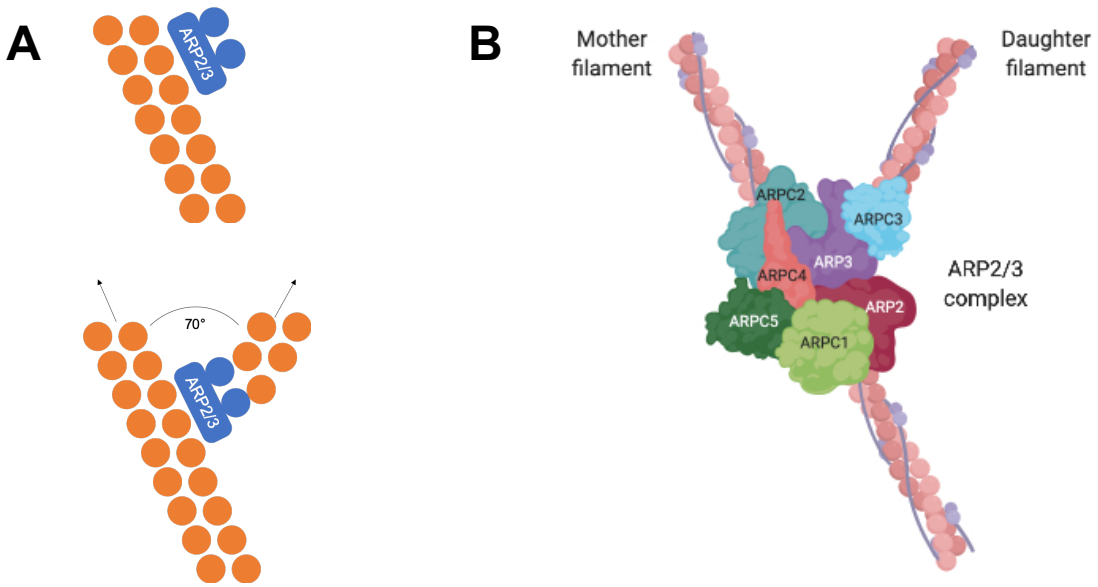

Figure 4.1 Simplified schematic of ARP2/3 complex action and structure. (A) Schematic of actin filament branching and growth via the ARP2/3 complex. **(B)** Model of ARP2/3 structure bound to a branching actin filament, showing the 7 subunits, ARPC1-5, ARP2 and ARP3. Image B created with Biorender.

that determine cell polarity) (Mathur and Hülskamp, 2002). ARP2/3 and homologs of its subunits have all been found in plants (Mathur et al., 2003) and have been characterised to some extent. For example, mutants of ARP2/3 subunits ACTIN-RELATED PROTEIN 2 and ACTIN-RELATED PROTEIN 3 (ARP2 and ARP3) exhibit epidermal defects including distorted trichomes, less lobed 'jigsaw' epidermal cells and reduced cell-cell adhesion in hypocotyls (Li et al., 2003; Mathur et al., 2003). Mutants of these two subunits as well as two other ARP2/3 subunits, ACTIN-RELATED PROTEIN COMPLEX SUBUNIT 2 and ACTIN-RELATED PROTEIN COMPLEX SUBUNIT 5 (ARPC2 and ARPC5), also lack the ability to properly form a central vacuole in some plant cells (Li et al., 2013; Mathur et al., 2003).

4.1.2 Role of ARP2/3 in stomatal function

The branching, lengthening and organisation of F-actin filaments has been previously visualised in plant cells (Smertenko et al., 2010) and these actin movements can be attributed at least in part to the ARP2/3 complex. Actin filaments have also been imaged in guard cells (Gao et al., 2008) and are thought to play an important role in stomatal function, with some evidence showing that actin regulates and modifies vacuolar morphology (Gao et al., 2008, 2005; MacRobbie and Kurup, 2007; Mathur et al., 2003) which is essential for guard cell function. Pharmacological disruption of actin filaments results in inhibited stomatal response to signalling stimuli such as ABA and light (Hwang et al., 1997; Kim et al., 1995), and other ABPs, such as STOMATAL CLOSURE-RELATED ACTING BINDING PROTEIN1 (SCAB1), have been found to be required for stomatal closure (Zhao et al., 2011).

Previous work has linked ARP2/3 mutants to unusual stomatal phenotypes. A paper describing a mutant in the ARPC2 subunit of the ARP2/3 complex – dubbed *high sugar response 3* (*hsr3*) as it was discovered in an Arabidopsis screen of seedlings showing a high sugar response – showed that this mutant exhibited reduced stomatal sensitivity to a variety of stimuli such as ABA, $CaCl_2$ and light (Jiang et al., 2012), providing a link between the ARP2/3 complex and stomatal function. Furthermore, using confocal microscopy to look at GFP-tagged actin, they observed that upon application of ABA the actin filament organisation in guard cells was disrupted in this mutant when compared to wildtype. Li et al., 2014 also looked at the ARP2/3 mutants *arpc4* and *arpc5* (ACTIN-

RELATED PROTEIN COMPLEX SUBUNIT 4 and ACTIN-RELATED PROTEIN COMPLEX SUBUNIT 5) and showed that these too had more limited stomatal response to stimuli such as ABA and H_2O_2.

ARP3 is one of the seven subunits of the ARP2/3 complex. It has been previously reported that *arp3* plants have slower light-stimulated stomatal opening and a smaller stomatal aperture compared to Col-0, reflecting impaired vacuolar fusion in guard cells found in this mutant line (Li et al., 2013). As there is an increasing risk globally of drought and hot temperatures, a reduced stomatal pore width could be seen as beneficial to a plant to conserve water in stressful environmental conditions, although altered stomatal opening may also lead to a penalty in terms of assimilation rate. Indeed, a previous member of the Fleming group, Alice Baillie, used an infrared gas analyser (IRGA) to look at the response (in terms of carbon assimilation) of Col-0 and *arp3* to increasing internal CO_2 concentration and to increasing irradiance (Alice Baillie, PhD thesis, University of Sheffield). She observed that *arp3* leaves responded to internal CO_2 similarly to Col-0, but they were not able to maximally utilise high light. The results showed that stomatal conductance of *arp3* was lower than that of Col-0 up to the highest concentrations of CO_2. Critically, at ambient CO_2 (the concentration at which the light curves were carried out), stomatal conductance was lower in *arp3* than Col-0. This suggests that the limiting factor in the assimilation/light curves was the CO_2 concentration and not light.

Further investigation into *arp3* and related mutants and stomatal phenotypes may provide insight both into the function of actin in stomatal function and potential targets for engineering future crop improvements.

4.1.3 Characterising *arp3* stomatal function and investigating the guard cell wall

The unpublished data described above suggest that the *arp3* mutant has abnormal stomatal conductance in response to CO_2. Furthermore, Li et al., 2013 investigated stomatal response of an *arp3* mutant to light using a stomatal aperture bioassay and found that *arp3* responded slower to light-induced opening. However, detailed investigation of *arp3* stomatal function is lacking. In this section of the thesis, I aim to investigate and characterise in greater detail the differences between *arp3* and Col-0 stomata.

Additionally, *arp3* may be a good candidate line for further investigation using the confocal method optimised during this thesis to describe guard cell shape changes (Chapter 3). Evidence for an interesting stomatal phenotype means 3D characterisation of the guard cells may provide more information on *arp3* stomatal function. It would be particularly interesting to explore the 3D shape changes of *arp3* guard cells considering it has been shown they have impaired vacuolar fusion (Li et al., 2013).

Whilst impaired vacuolar fusion will likely be responsible – at least in part – for any abnormal stomatal behaviour of *arp3* mutants (Li et al., 2013), I also sought to explore the potential role of an altered cell wall structure in *arp3* guard cells. The guard cell wall is important for normal stomatal function (e.g. Jones et al., 2003; Amsbury et al., 2016; Carter et al., 2017) and it is thought that actin is involved mainly in transport and deposition of plasma membrane and cell wall components to the cell wall (Mathur and Hülskamp, 2002). Although to date there has been no published evidence of *ARP3* involvement in cell wall deposition, it has been previously suggested (Daher and Braybrook, 2015), and mutants of other subunits of the ARP2/3 complex have been linked to altered levels of cell wall components, including cellulose and pectin (Pratap Sahi et al., 2017). Indeed, abnormal cell wall deposition during plant growth and development has been linked to the characteristic distorted trichome phenotype of some ARP2/3 mutants (Yanagisawa et al., 2015). Therefore there is a possibility that aberrant *arp3* stomatal behaviour can be explained by an abnormal composition of cell wall materials in *arp3* guard cell walls.

Therefore, my hypotheses for this chapter are:

I. *ARP3* is expressed in guard cells.
II. The mutant *arp3* has abnormal stomatal function.
III. This altered stomatal function can be explained by differences in the guard cell wall.
IV. Aberrant *arp3* stomatal function results in differences in whole plant physiology.

My aims for this chapter are:

I. To characterise stomatal function in *arp3* plants.
II. To investigate the link between altered *arp3* stomatal function and components of the guard cell wall using antibody labelling.

III. To investigate if the altered stomatal function in *arp3* plants can be linked to differences in whole plant physiology.

4.2 Results

4.2.1 *ARP3* is expressed in guard cells

To confirm that the *ARP3* gene (At1G13180) is expressed in guard cells, the online Arabidopsis EFP browser (Winter et al., 2007) was used to look at transcriptomic data. It showed that expression of *ARP3* was higher in mature guard cells than in the surrounding mesophyll cells (Figure 4.2).

4.2.2 The mutant *arp3* has a smaller rosette area and a lower rate of viable seedling germination

A T-DNA insertion mutant knockout of *arp3* in a Col-0 background was obtained from Firas Bou Daher (Sainsbury Laboratory, Cambridge) and was previously genotyped by Alice Baillie (from the Fleming lab group). After 5 weeks growth on soil, *arp3* plants had a significantly smaller rosette area than Col-0 (Figure 4.3A, B and C; unpaired t-test, df=8, $p<0.01$). It was also noted that *arp3* leaves looked rounder in comparison to Col-0, which corroborates data showing that *arp3* had a greater length to width ratio than Col-0 (Alice Baillie PhD thesis, unpublished data). It was noted that there seemed to be a lower

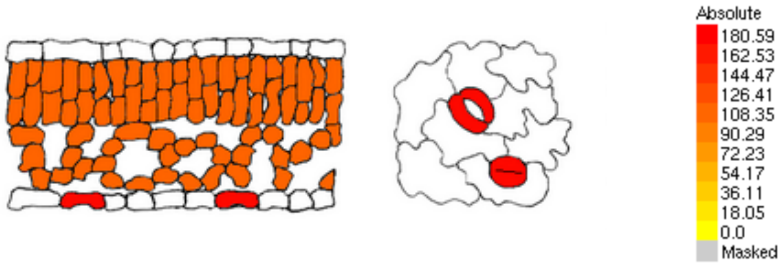

Figure 4.2 Data from EFP Browser showing expression levels of *ARP3* in guard cells compared with mesophyll tissue. Darker colours represent higher expression, with a maximum of 180.59. Guard cell tissue has an expression level of 174.35 and the whole leaf tissue has a level of 109.89 (Winter et al., 2007).

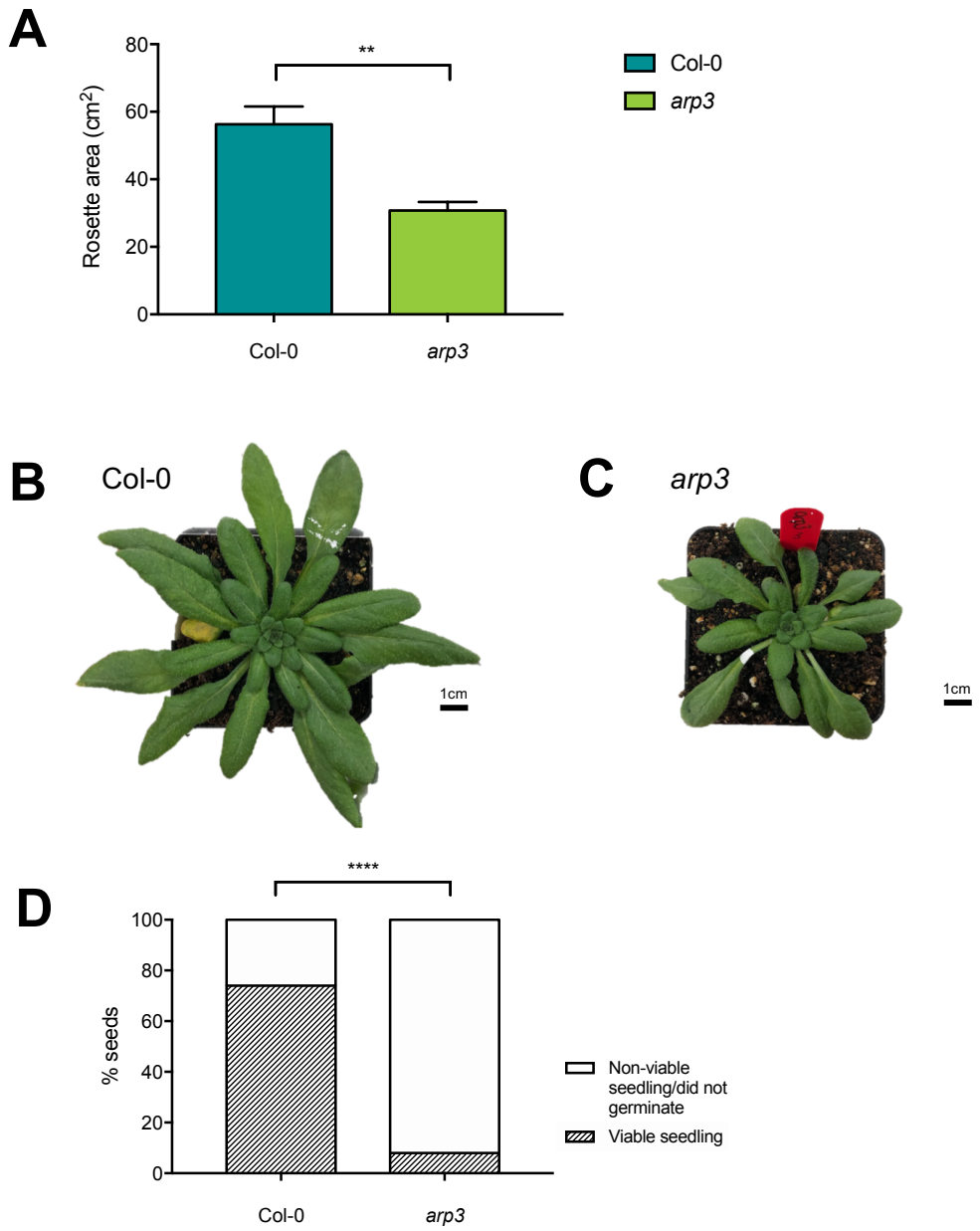

Figure 4.3 Rosette size and germination rate of Col-0 and *arp3* plants. (A) Rosette area of Col-0 and *arp3* plants was measured 5 weeks after sowing. An unpaired t-test was performed on dataset A (t=3.734, df=8, p<0.01), two stars indicate significance at p<0.01. *n* = 4 (*arp3*) and 6 (Col-0). Mean ± SEM. **(B)** and **(C)** Representative images of Col-0 and *arp3* plants at 5 weeks after sowing from which rosette measurements were taken. Scale bars = 1cm. **(D)** Number of seeds sowed was recorded and then seedlings were counted 14 days after sowing. Seedlings that were non-viable were grouped with seeds that did not germinate for this analysis (white) whereas plants that reached a certain size (stage 1.02; 2 rosette leaves >1mm in length) were counted as 'viable' (sketched). A two-way chi-squared test was performed on the dataset (chi-square = 90.04, df = 1, p<0.0001) and four stars indicate significance at p<0.0001. *n* = 58 (Col-0) and 64 (*arp3*).

germination rate of *arp3* seeds compared to Col-0 and so I decided to explore this further by doing a germination assay.

To do this, I stratified seeds as normal and then counted how many seeds were sown onto the soil in each pot and made a note of pot number. At 17 days after sowing, approximately the time that seedlings are big enough to 'thin' the seedlings out to ensure there is only 1 plant per pot, I made a note of how many plants were at the developmental stage that was consistent with other plants in the pots. This was approximately developmental stage 1.08 (8 rosette leaves >1mm in length) according to the Arabidopsis growth stages described in Boyes et al. (2001). These were classed as 'viable' seedlings, instead of 'germinated' seedlings, because I observed that for both Col-0 and *arp3* there were a few smaller seedlings at around stage 1.02 (2 rosette leaves >1mm in length) that were much smaller than the 'viable' seedlings. These were yellow or purple in colour and were clearly not healthy seedlings. For the purposes of this analysis, these were grouped along with seedlings that did not germinate.

Figure 4.3D shows the results of this analysis. 8% of *arp3* seeds germinated to produce a viable seedling compared to 74% of Col-0 seeds. A statistically significant difference is seen in the proportion of viable plants between Col-0 and *arp3* (chi-squared test, chi-square = 90.04, df=1, $p<0.0001$), showing that *arp3* seeds do not germinate comparably to Col-0, and when they do germinate, they are more frequently non-viable.

4.2.3 The mutant *arp3* exhibits distorted trichomes

To confirm the reported phenotype of the *arp3* mutant, SEM imaging was used to obtain images of the trichomes (Li et al., 2003; Mathur et al., 2003; Yanagisawa et al., 2015). These

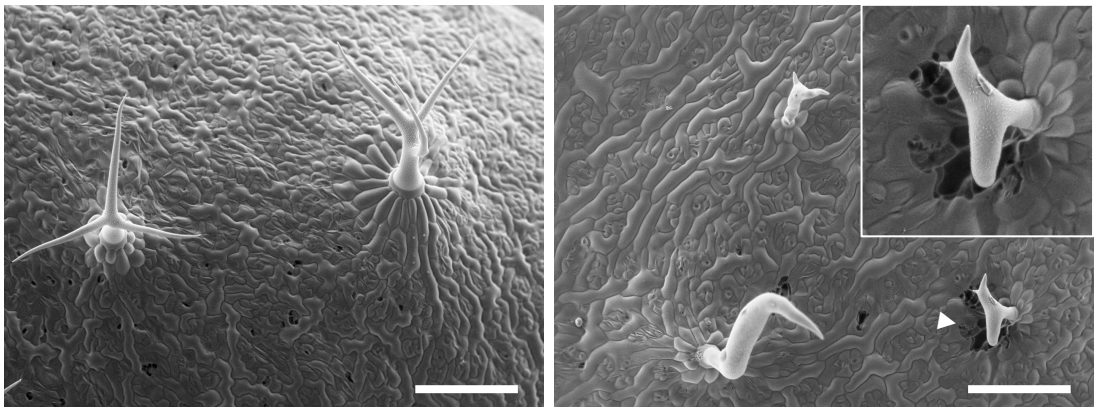

Figure 4.4 SEM images showing the distorted trichome trait in *arp3* mutants. Col-0 (left) trichomes display the normal stellate morphology, whereas *arp3* (right) trichomes are distorted. Triangular arrowhead indicates presence of defects in cell-cell adhesion which is shown on a larger scale in the inset. Scale bars = 300μm.

are shown in Figure 4.4. The mature wildtype three-pointed stellate (star-shaped) trichomes (Hülskamp et al., 1994) in Col-0 were clearly seen, whereas in *arp3* the trichomes are distorted, as previously described. This was the case for all trichomes observed.

What is also notable in these images is the evidence for defective cell-cell adhesion in the *arp3* epidermis, which has been observed before (Li et al., 2003; Mathur et al., 2003; Firas Bou Daher, personal communication). In the example image above there appears to be large gaps in the epidermis and cells pulling away from each other where the trichome meets the epidermis. There also appear to be small holes in the Col-0 epidermis, but this may be an artefact of using SEM imaging, which can be potentially destructive on softer epidermal tissue. Overall, the *arp3* mutant displays a disruption of epidermal adhesion, particularly around the base of the trichomes.

4.2.4 There is no difference in stomatal density between *arp3* and Col-0

To assess if knocking out *ARP3* had any impact on stomatal development, stomatal density was measured in *arp3* and Col-0 plants grown in identical conditions (Figure 4.5). The stomatal density of Col-0 plants was 232 ± 67 (mean ± SD, n = 27) and the stomatal density of *arp3* plants was 238 ± 69 (n = 27). Statistical analysis indicated that there is no significant impact of knocking out *arp3* on stomatal density (unpaired t-test, t=0.7348, df=72, p=0.4648).

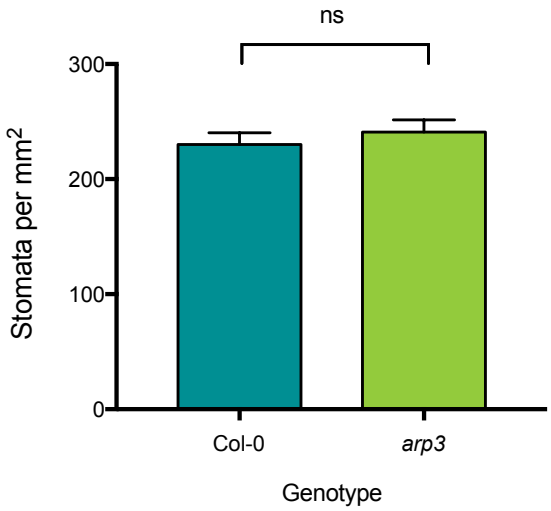

Figure 4.5 Stomatal density of the abaxial side of Col-0 and *arp3* leaves. An unpaired t-test revealed no significant difference between Col-0 (blue) and *arp3* (green) leaves (t=0.7348, df=72, p=0.4648). ns = not significant. Bars represent mean ± SEM. n = 27.

4.2.5 *arp3* exhibits differences in stomatal response to CO_2

There have been several previous papers that use stomatal bioassays to assess stomatal function in ARP2/3 mutants. ABA stomatal bioassays have shown that stomata from ARP2/3 mutants *arpc4* and *arpc5* close more slowly than wildtype stomata in response to ABA and H_2O_2 (Li et al., 2014), both known stimuli for stomatal closure. Bioassays testing *arp3* light-induced stomatal opening found that *arp3* mutants exhibited a slower opening response to light than the wildtype control (Li et al., 2013). To date, however, there have been no bioassays on *arp3* mutants that look at stomatal response to other stomatal opening/closing stimuli such as CO_2 or fusicoccin.

To assess stomatal function in the *arp3* mutant, a CO_2 stomatal bioassay was performed on epidermal peels of Col-0 and *arp3* plants (data collected by Sarah Carroll). This aims to measure the degree of stomatal opening and closing in response to different concentrations of CO_2 – low (0ppm), ambient (approx. 400ppm) and high (1000ppm) – on epidermal peels. The results are shown in Figure 4.6A.

Stomata on Col-0 epidermal peels opened in low CO_2 and closed in high CO_2, as shown by the increased and decreased pore width. The changes in pore width between low, ambient and high CO_2 were statistically significant for Col-0 (Tukey test, $p<0.05$, $n = 8$ plants). A similar step-wise pattern was seen in *arp3*, where the pores opened in response to low CO_2 and closed in response to high CO_2. The differences in *arp3* pore width were again statistically different (Tukey test, $p<0.05$, $n = 8$ plants) between the three CO_2 treatments.

Comparing the pore width between genotypes, there was no significant difference in pore width in high or ambient CO_2, however in low CO_2 the average pore width on *arp3* peels was significantly higher than on Col-0 peels under similar CO_2 conditions. This difference reflected an abnormal stomatal phenotype observed on *arp3* peels under low CO_2 conditions (Figure 4.6C compared to Figure 4.6B). A bowed-out "doughnut" stomatal shape was observed to some extent in all CO_2 treatments and in both *arp3* and Col-0, however, it was seen much more frequently in *arp3* leaves, especially in low CO_2 where nearly a quarter (23.4%, $n = 42$) of the stomata exhibited this phenotype (Figure 4.6D). The bowed-out *arp3* stomatal pores looked shorter than Col-0 pores, so I investigated this phenotype further.

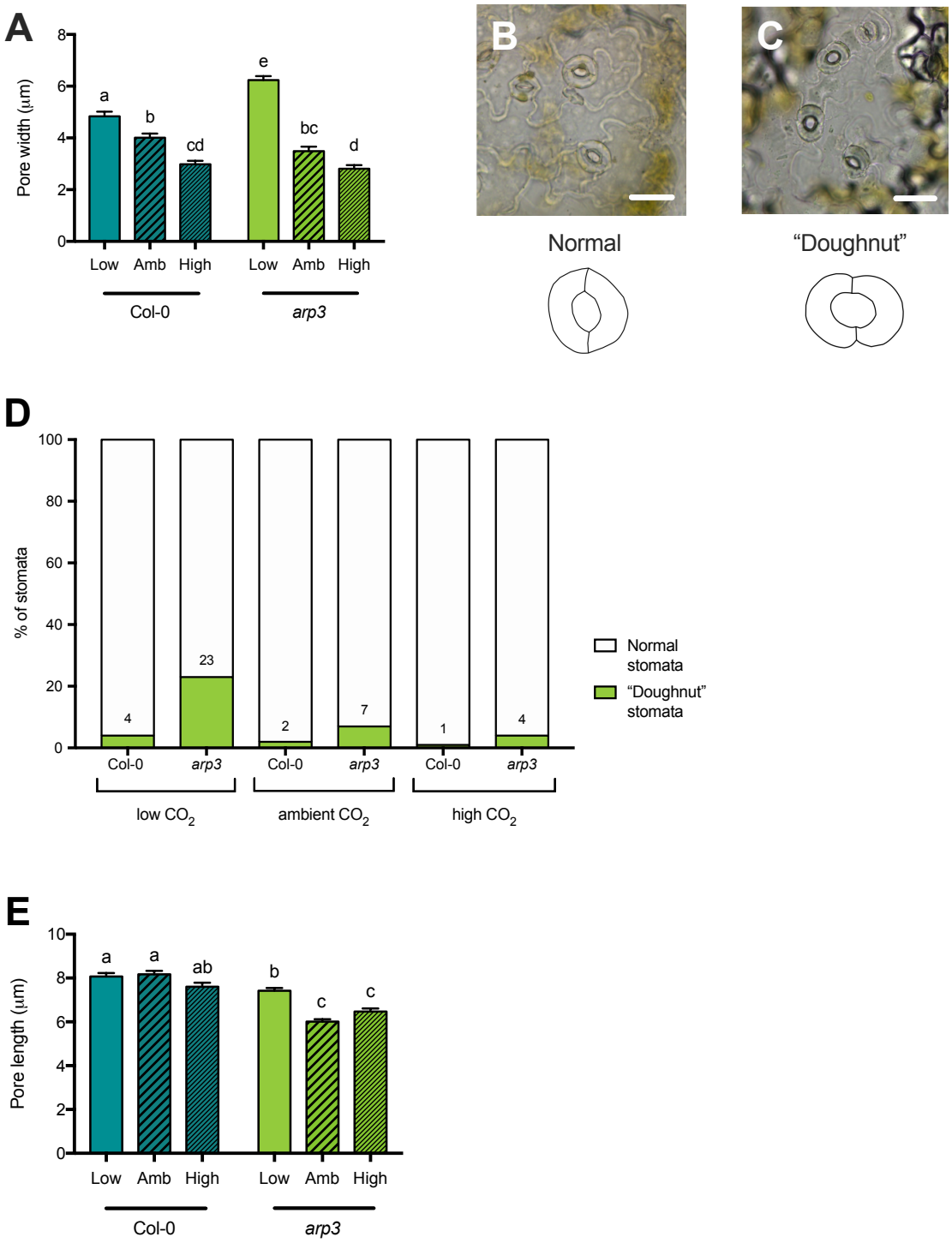

Figure 4.6 Assessing stomatal opening and closing in response to high CO_2 (1000ppm), ambient CO_2 (400ppm) and low CO_2 (CO_2-scrubbed air) in Col-0 and *arp3* epidermal peels. (A) Pore width was measured after epidermal peels of Col-0 (blue bars) and *arp3* (green bars) plants were exposed to each CO_2 treatment for 2.5 hours. **(B)** Representative image from a Col-0 epidermal peel in low CO_2 conditions and **(C)** representative image from an *arp3* epidermal peel in low CO_2 conditions showing the bowed-out "doughnut"-shaped stomata. Underneath are schematics showing differences in guard cell shape. **(D)** Percentage of "doughnut" shaped stomata was counted on *arp3* and Col-0 epidermal peels in the 3 different CO_2 treatments. Green bars represent % of "doughnut" stomata and white bars represent normal stomata. Numbers above green bars represent % of "doughnut" stomata rounded to the nearest whole number. **(E)** Pore length was measured after 2.5 hours of treatment with each CO_2 level in Col-0 (blue bars) and *arp3* (blue bars)epidermal peels. For (A) and (E), a two-way ANOVA was performed followed by a Tukey multiple comparisons test. Within each dataset, samples indicated with the same letter cannot be distinguished from each other ($p<0.05$). Bars indicate mean ± SEM. $n = 8$ plants. Scale bars = 20µm.

The average pore length of Col-0 stomata did not change between CO_2 treatments (Tukey test, F=35.03, p>0.05) (Figure 4.6E). This supports literature which hypothesises that the 'pinning down' of the stomatal tips assists stomata attaining maximum opening (Carter et al., 2017). However, in *arp3*, pore length changed with changes in CO_2 concentration. When exposed to ambient and high CO_2 concentrations, the average pore length of *arp3* stomata decreased significantly (Tukey test, F=35.03, p<0.05) compared to the pore length of *arp3* stomata under low CO_2. *arp3* stomatal pores were shorter under ambient and high CO_2 conditions than Col-0 stomata under equivalent conditions (Tukey test, F=35.03, p<0.05).

This data suggests that there is a difference in the way *arp3* and Col-0 stomata change pore width and length in response to varying CO_2 concentration. This is reflected in the abnormal stomatal phenotype seen in low CO_2-treated *arp3* epidermal peels where the guard cells bow out to make a doughnut-shaped extra-wide pore. This wider pore also results in a decrease in pore length. Indeed, in ambient and high CO_2 conditions, *arp3* also exhibits a smaller pore length although there is no difference in pore width when compared to wildtype. It appears that *arp3* stomata lack the mechanism that pins the stomatal tips into place during movement, or that the bowing outwards of the guard cells pulls together the pore tips, resulting in a misshapen stomatal pore seen under low CO_2 conditions.

4.2.6 *arp3* stomata respond like Col-0 to fusicoccin

Fusicoccin (FC) induces an extreme stomatal opening response. To further investigate the extra-wide pore phenotype seen in response to low CO_2 on *arp3* epidermal peels, a FC bioassay was performed on Col-0 and *arp3* epidermal peels. Epidermal peels of mature Col-0 and *arp3* leaves were floated in either opening buffer or 2µM FC and opening buffer solution for 2.5 hours in ambient light and CO_2 concentration.

Figure 4.7 shows the results. Average pore width of Col-0 stomata showed a significant increase between opening buffer and FC-treated epidermal peels (Tukey test, F=18.1, p<0.0001). *arp3* pore width also increased significantly from opening buffer to FC. However, pores of *arp3* stomata in opening buffer without fusicoccin were significantly wider than the pores of Col-0 stomata in the same treatment.

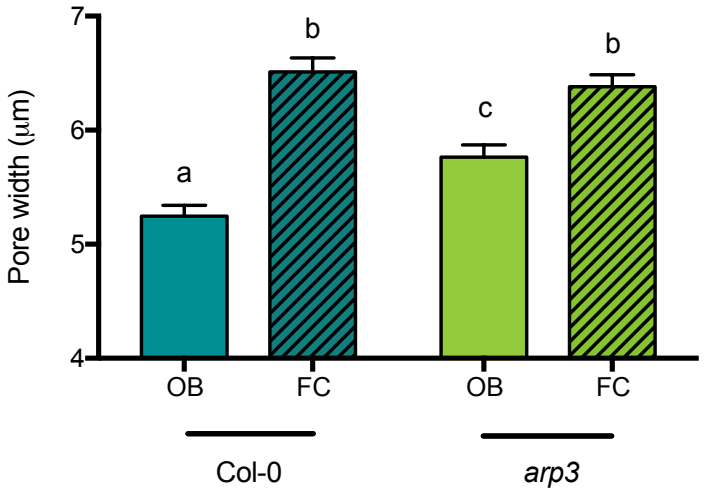

Figure 4.7 Effects of fusicoccin on stomatal pore width on Col-0 (blue) and *arp3* (green) epidermal peels. Col-0 and *arp3* epidermal peels were incubated for 2.5 hours in ambient light and CO_2 with either opening buffer (OB) or opening buffer with 2µM fusicoccin in (FC). A two-way ANOVA was performed on the data followed by a Tukey test. Samples indicated with the same letter cannot be distinguished from each other at the p = 0.05 confidence limit ($F=18.1$, $p<0.05$). $n = 9$. Mean ± SEM.

Interestingly, the average stomatal pore width in fusicoccin-treated peels was not statistically different between Col-0 and *arp3*. This was not expected because in the previous CO_2 bioassay stomata on *arp3* peels displayed a much wider pore width when stimulated to open with low CO_2. Upon further analysis, in the CO_2 bioassay (Figure 4.6A) average pore width in low CO_2 in Col-0 was 4.84µm and in *arp3* it was 6.23µm. In the FC bioassay (Figure 4.7), the average pore width of Col-0 in FC was 6.51µm and for *arp3* this was 6.38µm. This shows that in FC, Col-0 stomata are being forced to open wider than observed under low CO_2 conditions, whereas under both FC and low CO_2 treatments the *arp3* stomata are triggered to open to a similar, maximal width, i.e. the *arp3* stomata are more prone to maximal opening, irrespective of the "strength" of the opening stimulus.

The proportion of "doughnut" stomata to normal stomata was calculated for the FC-treated samples shown in Figure 4.7 (data not shown). In Col-0 this remained less than 5% of stomata in both opening buffer and FC. In *arp3*, the number of stomata exhibiting the "doughnut" shape was 5.3% in opening buffer and 13.2% in FC, which represents an overall decrease of 10% compared to the same results from the CO_2 bioassay (Figure 4.6D), although for one technical replicate the proportion of doughnut-shaped stomata was 25%.

Together with the results from the CO_2 bioassay in section 4.2.5, this data suggests that *arp3* plants have a wider stomatal aperture than Col-0 when exposed to moderate opening stimuli, such as opening buffer and low CO_2. However, when Col-0 and *arp3* peels are exposed to extreme opening stimuli (like fusicoccin), this forces the stomata in both genotypes to open maximally to a similar extent. Therefore, in more 'natural' conditions, *arp3* stomata may open as if exposed to extreme stimuli.

4.2.7 *arp3* temperature change in response to ABA

The above data shows that *arp3* stomata exhibit a more extreme opening response to some stimuli than control Col-0 plants. To instead assess the closing response of *arp3* stomata, thermal imaging was conducted of plants treated with ABA, a hormone that stimulates stomata to close. Col-0 and *arp3* plants were imaged with a thermal imaging camera for 1 hour and then plants were sprayed with either an ABA solution or a mock solution. The plants were then thermally imaged for another 80 minutes to see what effect ABA had on plant temperature. When stomata close, cooling of the plant is reduced and, therefore, a measurable plant temperature increase should occur.

Figure 4.8 displays a graph of the change in average plant temperature over time for this experiment. For the first 60 minutes, temperatures of both *arp3* and Col-0 plants remained constant at around 20°C. When either ABA or the mock treatment was applied to the plants, plant temperature rapidly dropped, followed by a temperature increase in all treatments. In those plants sprayed with ABA, temperature increased to above the pre-treatment level, i.e. to around 21-21.5°C. There was no difference in temperature response between *arp3* and Col-0 plants sprayed with ABA, suggesting an equivalent rate and extent of stomatal closure. Therefore these data, along with the CO_2 bioassay data, indicate that closure response is similar in Col-0 and *arp3*. However, in plants sprayed with a mock treatment, there was a difference in mean plant temperature between the mutant and the wildtype. This may be because of the wider pore displayed by stomata in

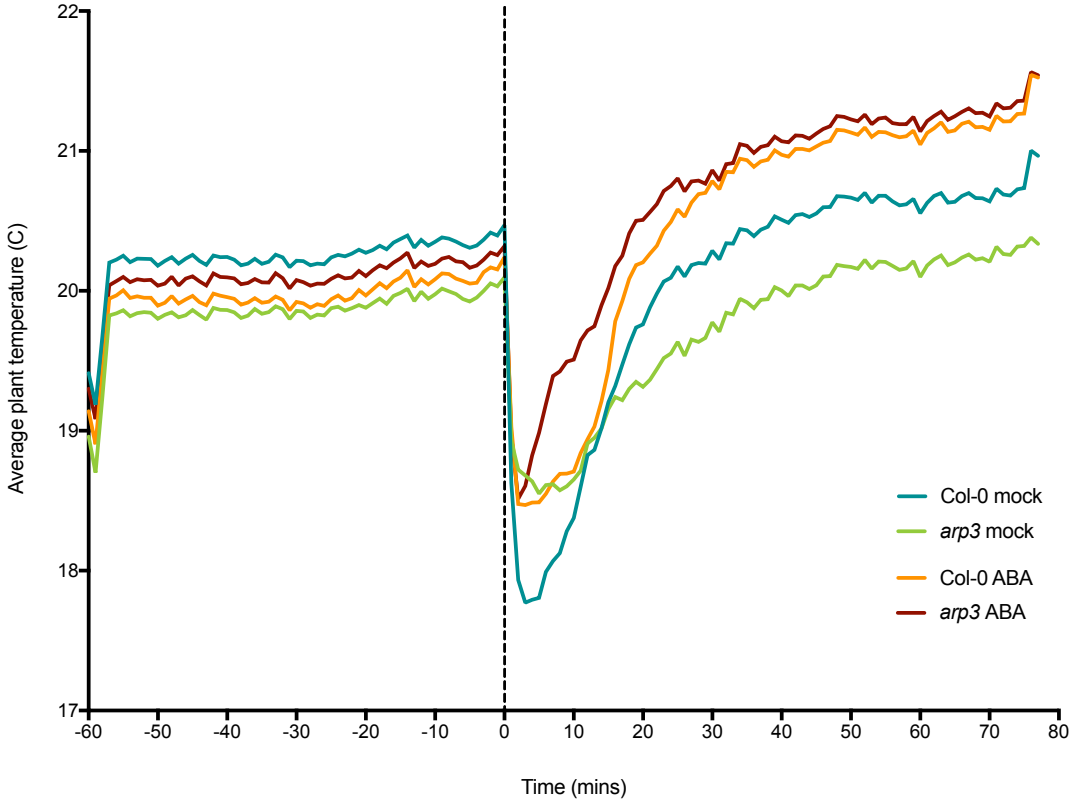

Figure 4.8 Temperature response of Col-0 and *arp3* plants to ABA or mock treatment. Col-0 and *arp3* plants were imaged for 60 minutes and then either a mock solution or a solution containing 5µM ABA was sprayed on at time point 0, indicated by the dashed line. Plants were then imaged for a further 80 minutes. Col-0 mock is represented by the blue line, *arp3* mock by the green line, Col-0 with ABA treatment in orange and *arp3* with ABA treatment in red. Mean plant temperature was calculated using 3 leaves per plant and 6 plants per treatment. $n = 6$.

the *arp3* mutant (Figure 4.6 and Figure 4.7), which would increase transpiration compared to Col-0 and, therefore, result in lower leaf temperature. However, it is worth noting that there was a ~0.2°C difference in plant temperature between *arp3* and Col-0 before the mock treatment and this difference is maintained after the treatment. The *arp3* mutant displayed a larger temperature range than Col-0, which might reflect the greater range in pore width between these lines, as shown in Figure 4.6A.

4.2.8 *arp3* stomatal conductance and assimilation in response to shifting CO_2

Previous data has suggested that *arp3* plants have a lower rate of stomatal conductance in ambient CO_2 and light conditions. To further assess the aberrant stomatal phenotype of *arp3* plants, CO_2 shifts on an Licor 6800 IRGA were conducted on Col-0 and *arp3* plants. During this process, stomatal conductance and assimilation of a leaf were measured in real-time, with a measurement being taken every two minutes. For the first 40 minutes,

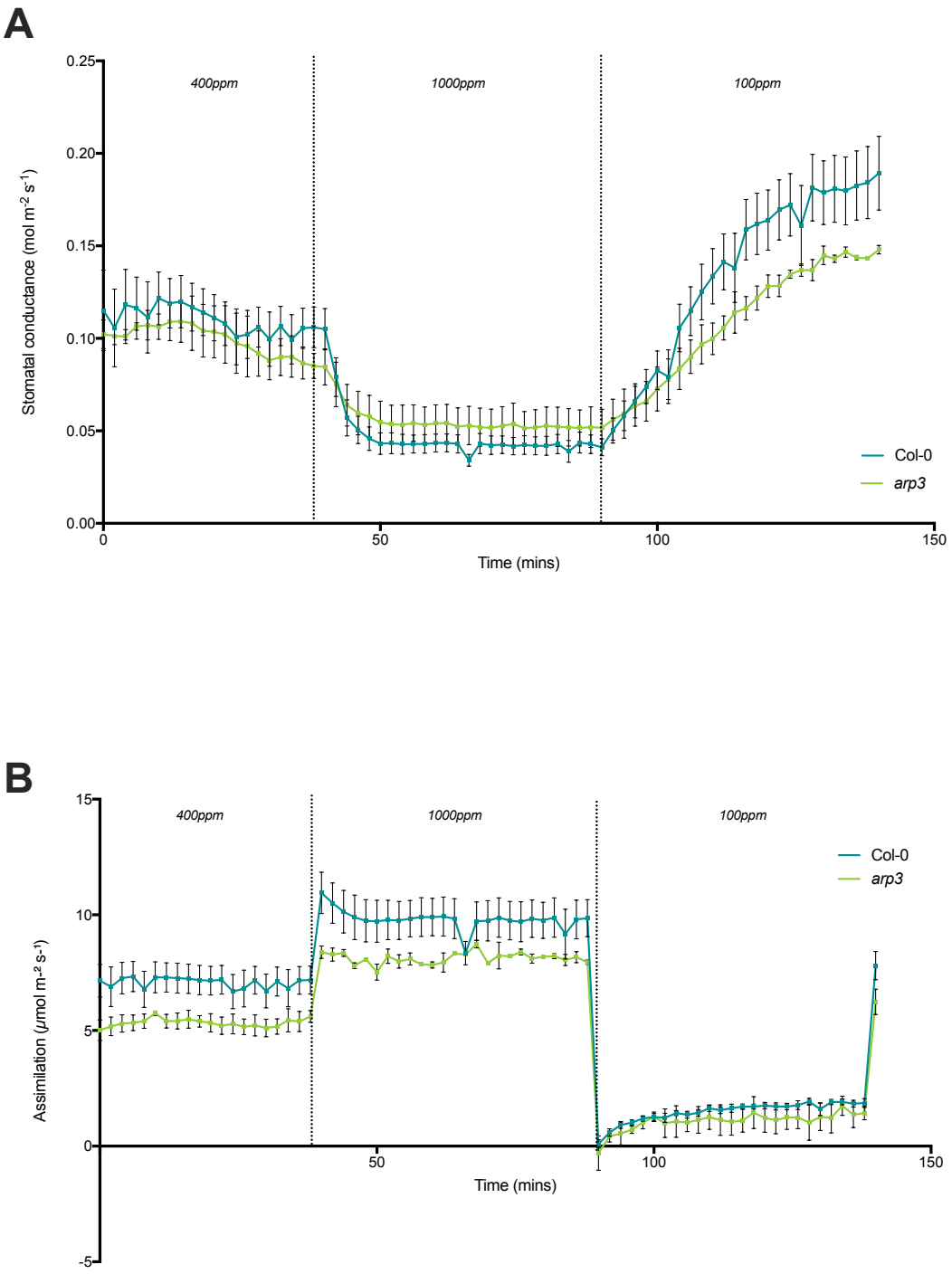

Figure 4.9 Stomatal conductance (A) and assimilation rate (B) of *arp3* (green) and Col-0 (blue) plants in response to shifts in CO_2 on an IRGA. (A) *arp3* shows a reduced dynamic range in response to CO_2 shifts when compared to Col-0. **(B)** Assimilation is lower in *arp3* than Col-0 under ambient and high CO_2 conditions, however there seems to be very little difference in assimilation in low CO_2. Light during this experiment was kept at 300 µmol m^{-2} s^{-1}. Error bars = SEM, *n*=6 (Col-0) or 2 (*arp3*).

the external CO_2 conditions were 400ppm, mimicking an ambient condition. This was increased to 1000ppm for 50 minutes for high CO_2 measurements, and then decreased to 100ppm for low CO_2 measurements. These concentrations are broadly comparable to the

low, ambient and high CO_2 conditions used in the CO_2 stomatal aperture bioassays. This allowed the identification of whether differences in stomatal pore width observed in the bioassay were reflected in differences in leaf stomatal conductance.

Figure 4.9A shows stomatal conductance over time of Col-0 and *arp3* plants. In ambient conditions, *arp3* had a slightly lower mean stomatal conductance than Col-0, although the variance in values suggests no difference between the genotypes. When CO_2 was increased to 1000ppm, stomatal conductance of both lines decreased, reflecting the closing of stomatal pores. Under these conditions *arp3* had a higher conductance than Col-0, suggesting their stomata were not as closed. When CO_2 was decreased to 100ppm, stomatal conductance of both *arp3* and Col-0 increased, however stomatal conductance in Col-0 plants increased faster than *arp3* and reached a much higher maximum level. This is in contrast to the results of the CO_2 bioassay in section 4.2.5 which indicated that *arp3* stomata have a wider pore under low CO_2 conditions, which might be expected to lead to a higher stomatal conductance.

With respect to assimilation rate, under ambient (400ppm) conditions *arp3* had a lower assimilation rate than Col-0 (Figure 4.9B) by around 40%. When CO_2 was increased to 1000ppm, there was an increase in assimilation rate for both *arp3* and Col-0 plants, although again, *arp3* had a lower rate of assimilation. When CO_2 was decreased to 100ppm, assimilation dropped rapidly in both lines, with a marginally higher mean rate measured in Col-0 leaves than in the *arp3* mutant. These data are consistent with the lower stomatal conductance under low CO_2 conditions observed in the *arp3* line (Figure 4.9A) but, again, inconsistent with the bioassay data shown in Figure 4.6.

Instantaneous water use efficiency (iWUE) was calculated from this data (Equation 4).

Equation 4 Equation for instantaneous water use efficiency.

$$iWUE = \frac{Assimilation}{Stomatal\ conductance}$$

There was no discernible difference in iWUE between Col-0 and *arp3* plants in both ambient and low CO_2 conditions (Figure 4.10). In high CO_2 conditions *arp3* plants showed

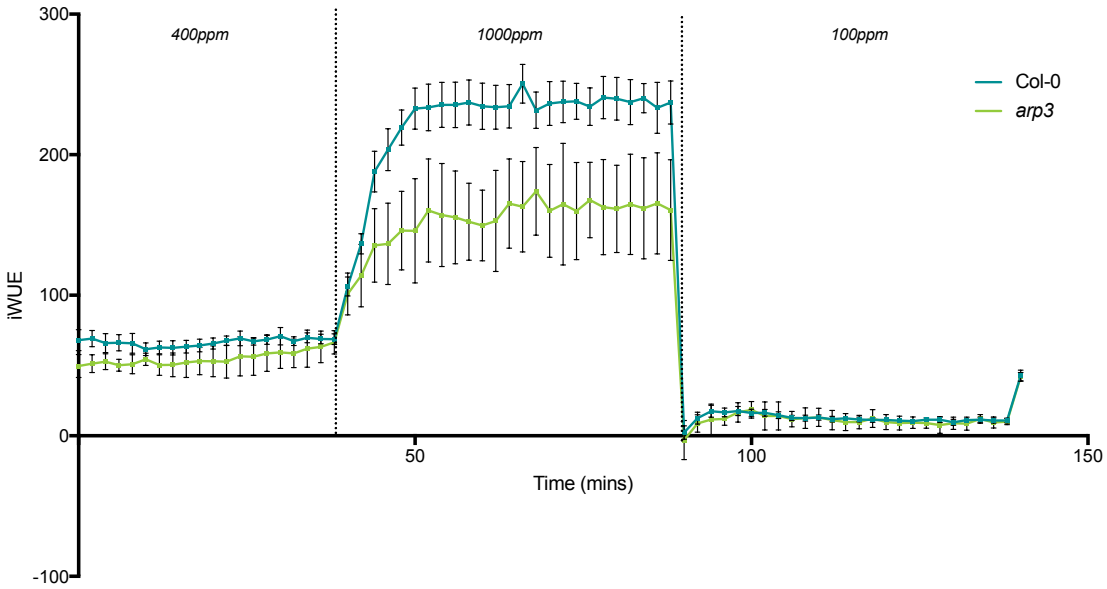

Figure 4.10 Instantaneous water use efficiency (iWUE) of Col-0 and *arp3* plants in response to CO_2 shifts. Error bars = SEM, *n*=6 (Col-0) or 2 (*arp3*).

a much lower iWUE, reflecting both an increase in stomatal conductance and decreased assimilation rate (Figure 4.9).

4.2.9 *arp3* stomata respond similarly to Col-0 after shifts in light intensity

Li et al., 2013 found that *arp3* stomata had a slower opening response to light exposure than Col-0. To investigate this further, I used an IRGA to record stomatal conductance of *arp3* and Col-0 leaves when cycling between darkness and saturating light conditions, following a similar method to one reported in Penfield et al., 2012. For this experiment, leaves were acclimatised at 200 µmol m^{-2} s^{-1} of light for 10 minutes, and then stomatal conductance was measured. The leaf was exposed to darkness (0 µmol m^{-2} s^{-1}) for 5 minutes and a reading was taken at the end of the dark period, and then light intensity increased to 1500 µmol m^{-2} s^{-1} (high light) for 5 minutes after which a measurement was taken. This was repeated for ten 5-minute intervals of dark/light switching, with the results shown in Figure 4.11.

After the initial 5-minute acclimation time, both Col-0 and *arp3* had a relatively high stomatal conductance which decreased after the first dark period. The starting measurement of stomatal conductance for *arp3* plants was significantly higher than Col-0 (Tukey test, $p<0.001$), at nearly double the rate (approximately 11 mol m^{-2} s^{-1} for Col-0 and

20 mol m^{-2} s^{-1} for *arp3*), which may reflect the extreme opening stomatal phenotype seen in *arp3* plants.

After an initial plateau, Col-0 stomatal conductance rose in response to saturating light and decreased in response to darkness. Col-0 sustained an overall increase in stomatal conductance from the start of the experiment to the end, which suggests that the stomata opened more in response to a 5-minute period of high light than they closed in response to a 5-minute period of darkness.

arp3 also responded to high light through an increase in stomatal conductance, and to darkness by decreasing stomatal conductance. The differences between stomatal conductance in Col-0 and *arp3* were not significantly different for all data points except

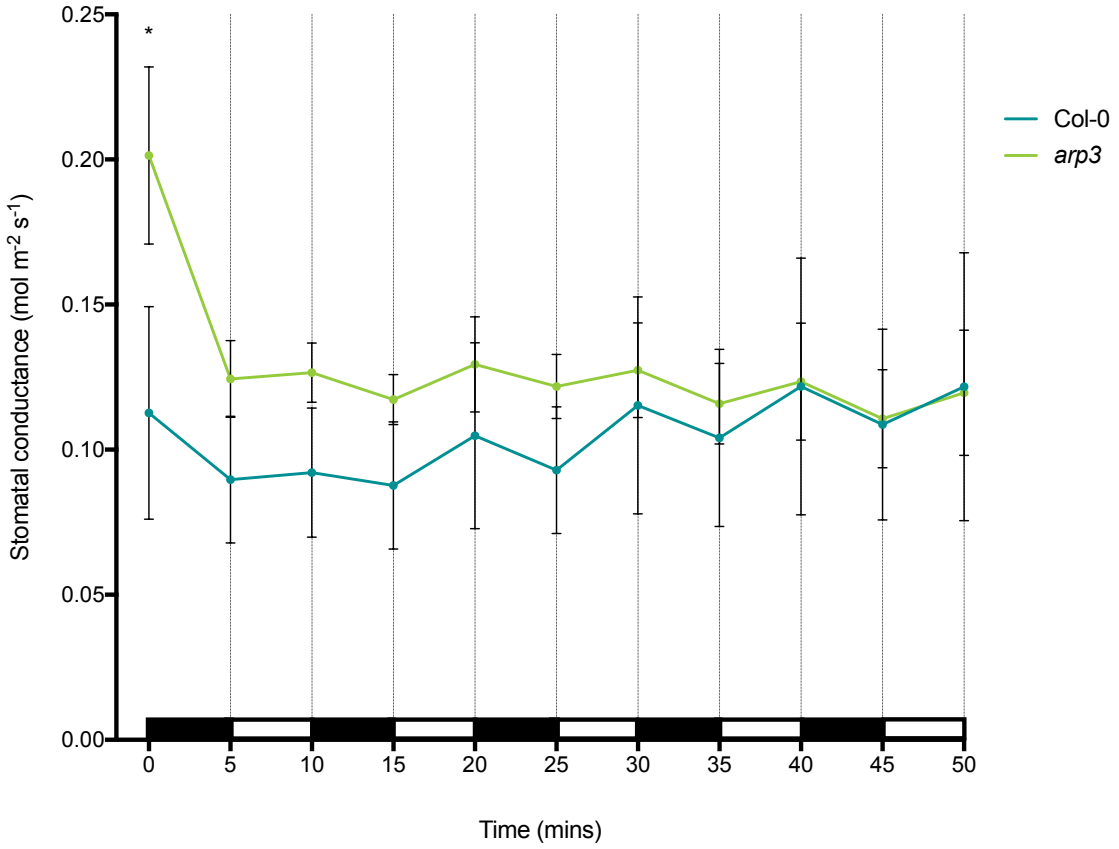

Figure 4.11 Stomatal conductance of Col-0 and *arp3* in response to shifting light concentration. After a 5-minute period of acclimation at 200µmol m^{-2} s^{-1}, a measurement of stomatal conductance was taken (time point 0). Thereafter, the leaf was exposed to alternating high light (white box) and darkness (black box) every 5 minutes. Stomatal conductance of Col-0 is shown with a blue line and stomatal conductance of *arp3* is in green. A 2-way ANOVA was performed on the data set followed by a Tukey's multiple comparison test. Stars indicate values that are significantly different from each other ($p<0.001$). Error bars = SEM. $n = 4$ (*arp3*) or 6 (Col-0).

the first (Tukey test, $p>0.05$). However, looking at the overall trends of the data, it appears that *arp3* stomata had a consistently higher rate of stomatal conductance than Col-0, until the final 10 minutes of the experiment. This suggests that *arp3* stomatal conductance is generally higher than Col-0 under ambient CO_2, contrary to the results in Figure 4.9A.

In contrast to Col-0, the overall trend of *arp3* stomatal conductance across the experiment showed no overall increase or decrease in mean stomatal conductance (apart from the initial drop after the first dark period). This may indicate that *arp3* stomata are slower to open than Col-0 in response to increased irradiance, which corroborates the report of Li et al., 2013, although care should be taken when interpreting these results due to the lack of statistical difference between the two samples.

4.2.10 Linking the *arp3* stomatal phenotype with altered cell wall deposition

Although some of the data described above is conflicting, overall they indicate that stomatal function in *arp3* mutants is altered compared with control plants, especially with regards to the extreme opening response to low CO_2 in the bioassay. This raises the question of how, mechanistically, this might occur. Actin is involved in the delivery and distribution of cell wall components, including pectin (Mathur and Hülskamp, 2002; Ridley et al., 2001). Since pectin has been shown to be important in stomatal function (Amsbury et al., 2016; Jones et al., 2003), I proceeded to investigate whether the aberrant stomatal phenotype seen in *arp3* mutant plants was linked to differential distribution of pectin in the guard cell wall.

Pectin makes up 35% of dicot primary cell walls, and of this, homogalacturonan (HG) accounts for over 60% (Mohnen, 2008). HG comprises long chains of galacturonic acid which, when newly synthesised in the Golgi apparatus and transported to the plasma membrane, is highly methylesterified (Ridley et al., 2001). At the plasma membrane HG is deposited to form the primary cell wall where methyl groups can be removed by pectin methylesterase (PME) enzymes. This means that a range of methylesterified and demethylesterified pectins are found in the cell wall, and their amount and distribution can provide some idea as to the function of cell wall. For example, Arabidopsis guard cells are rich in unesterified pectins which are required for normal stomatal function (Amsbury et al., 2016).

The distribution of pectins in plant cell walls can be detected using monoclonal antibody (mAb) labelling of fixed tissue. Previous work (Firas Bou Daher, personal communication) using mAb labelling of Arabidopsis stem tissue suggested that there was an increase in abundance of de-methylesterified pectins in *arp3* compared with Col-0, and a decrease in the amount of methylesterified pectin. As *arp3* is a mutant in which actin filament organisation is disrupted (Jiang et al., 2012), and pectins are transported via the Golgi apparatus that operates in tandem with intercellular microfilaments such as actin (Kim and Brandizzi, 2014), it was possible that the *arp3* mutants displayed altered cell wall pectin distribution in guard cells and that this underpinned changes in guard cell function.

To investigate this possibility, a series of immunolabelling experiments were performed using a variety of mAbs specific for different types of pectin. JIM7, LM19 and LM20 are all anti-HG mAbs, with JIM7 binding broadly to HG (Majewska-Sawka et al., 2002), whereas LM19 binds to unesterified HG and LM20 to only highly methylesterified HG (Amsbury et al., 2016). Transverse sections of mature Col-0 and *arp3* leaf tissue were incubated with the above mAbs, with the results shown in Figure 4.12.

In general there were no substantial differences in antibody distribution between *arp3* and Col-0 in either mesophyll tissue or in the guard cells. JIM7 and LM19 were both broadly distributed in both lines, whereas there was less signal for LM20 in both lines, with some intense signal at cell junctions. There was a slight increase in LM20 signal in *arp3*, especially on the epidermis, which would suggest the presence of more highly methylesterified pectin in these cells.

One notable difference between Col-0 and *arp3* images in Figure 4.12 is that there are apparent accumulations of pectin on the epidermis of *arp3* sections which are not present in Col-0 (Figure 4.12D and F). As indicated in Figure 4.4, *arp3* mutants display epidermal defects and so if the abnormal signal in the epidermis does reflect the distribution of pectin, this might be linked to this aspect of the *arp3* phenotype. Future investigation into the unusual epidermal pectin deposits would be interesting.

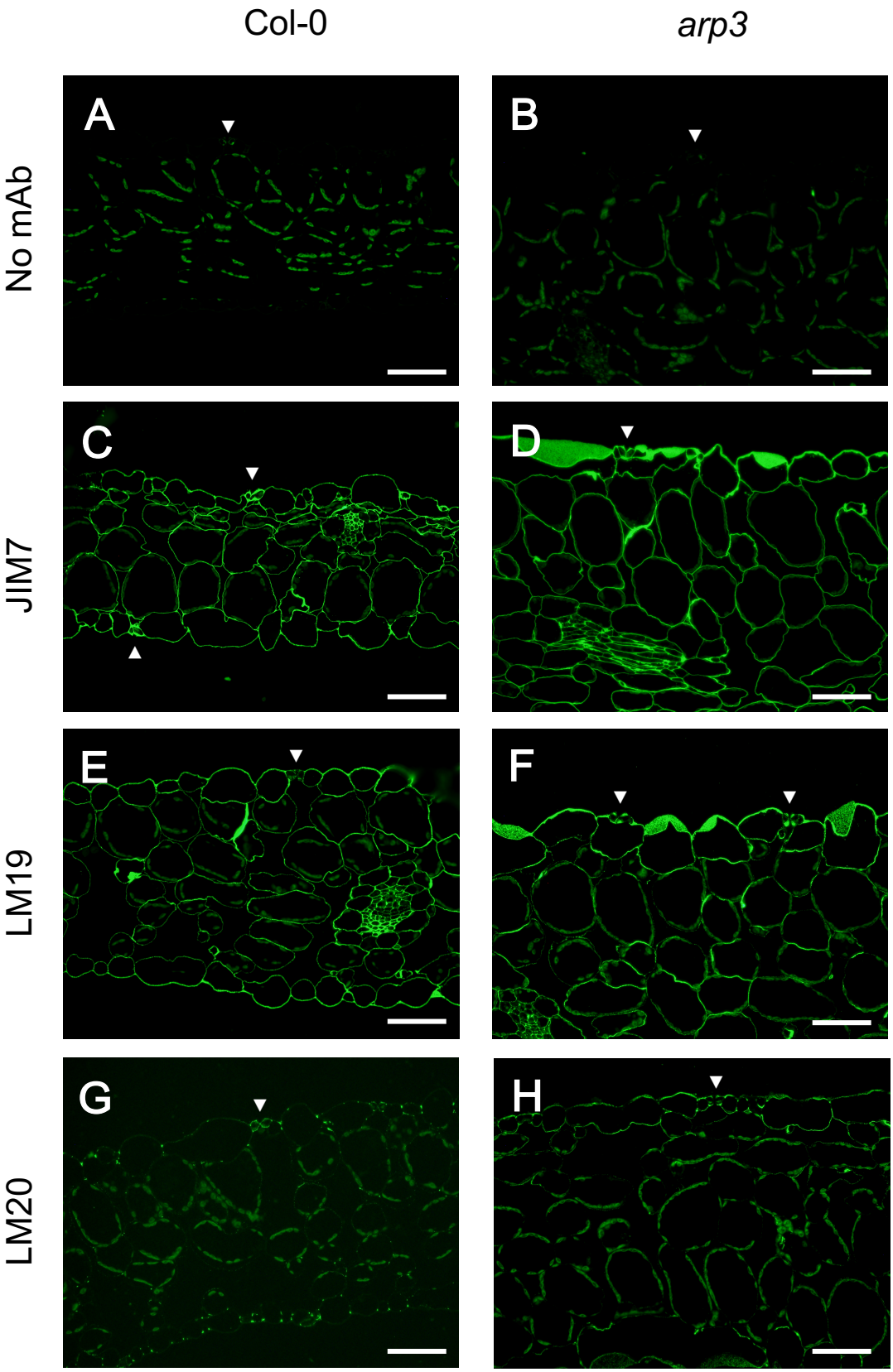

Figure 4.12 Immunolabelling of Col-0 (A, C, E and G) and *arp3* (B, D, F and H) leaf sections. (A) and **(B)** is a negative control, where the tissue was processed in the same way but without an antibody added. **(C)** and **(D)** were labelled with JIM7, an anti-homogalacturonan antibody. **(E)** and **(F)** were labelled with LM19, an antibody which binds to unesterified pectin. **(G)** and **(H)** were labelled with LM20, which binds to methylesterified pectin. Arrowheads point to stomata. Scale bars = 50μm. Representative images from 2 technical replicates and 2 biological replicates.

4.2.11 Transforming *arp3* plants with the myr-YFP construct to create lines for 3D guard cell analysis

The "doughnut" stomata seen in Figure 4.6 represent a quarter of *arp3* stomata treated with low CO_2. This shape is highly unusual and does not adhere to conventional ideas of guard cell structure (Meckel et al., 2007). At the same time, these images are taken using 2D microscopy, so it is difficult to fully compare this novel shape with that of "normal" stomata, i.e. it lacks a 3D view which would provide a better idea of how guard cell (and thus stomatal function) shape is altered in the *arp3* mutant. I therefore initiated experiments to generate *arp3* lines incorporating the myr-YFP construct described in Chapter 3 with the eventual aim of creating transgenic lines which could be used to characterise 3D shape change in the *arp3* mutant background. The myr-YFP construct (gifted from Raymond Wightman, Sainsbury Laboratory Cambridge) was transformed into *arp3* Arabidopsis using agrobacteria via a floral dip method. Seeds have been collected for the T3 generation but, due to time limitations of the project, have not yet been characterised. These seeds provide a useful resource for the future investigation of the unusual guard cell shape observed in the *arp3* mutant.

4.3 Discussion

The work in this chapter aimed to characterise an *arp3* mutant in terms of its stomatal phenotype, and to investigate the impacts on whole plant physiology level. I hypothesised that because mutants of the ARP2/3 complex have a significant impact on cellular actin and display defects in vacuolar fusion in guard cells (Li et al., 2013), knocking out *ARP3* would have an effect on guard cell morphology and stomatal function. I also aimed to investigate the possibility that abnormal *arp3* stomatal function was linked to differences in cell wall deposition caused by the *arp3* mutation.

4.3.1 *arp3* displays an abnormal guard cell phenotype with enhanced stomatal opening

After having established that *ARP3* was expressed in guard cells and that an *arp3* knockout line had been obtained (Hypothesis I), I carried out multiple assessments to evaluate *arp3* stomatal function in comparison to its wildtype counterpart Col-0.

A CO_2 bioassay revealed that the opening response to low CO_2 in *arp3* plants was different to Col-0 as pore width was significantly wider in low CO_2-treated epidermal peels (Figure 4.6), providing evidence supporting Hypothesis II. This finding seemingly contradicts previous literature (Li et al., 2013) that found *arp3* stomata did not open as widely or as fast during opening when compared to Col-0. The 2013 Li et al. paper used dark-adapted epidermal peels and then exposed them to light, taking pore width measurements at 30-minute time periods up to 2 hours after initial light exposure. Their method of taking epidermal peels, leaving them in a buffer for a set period of time in exposure to a stomatal opening/closing trigger, and then imaging the peels on a light microscope to obtain stomatal pore and complex measurements, is very similar to the CO_2 and fusicoccin bioassays I have performed in this thesis and therefore facilitates comparison of results.

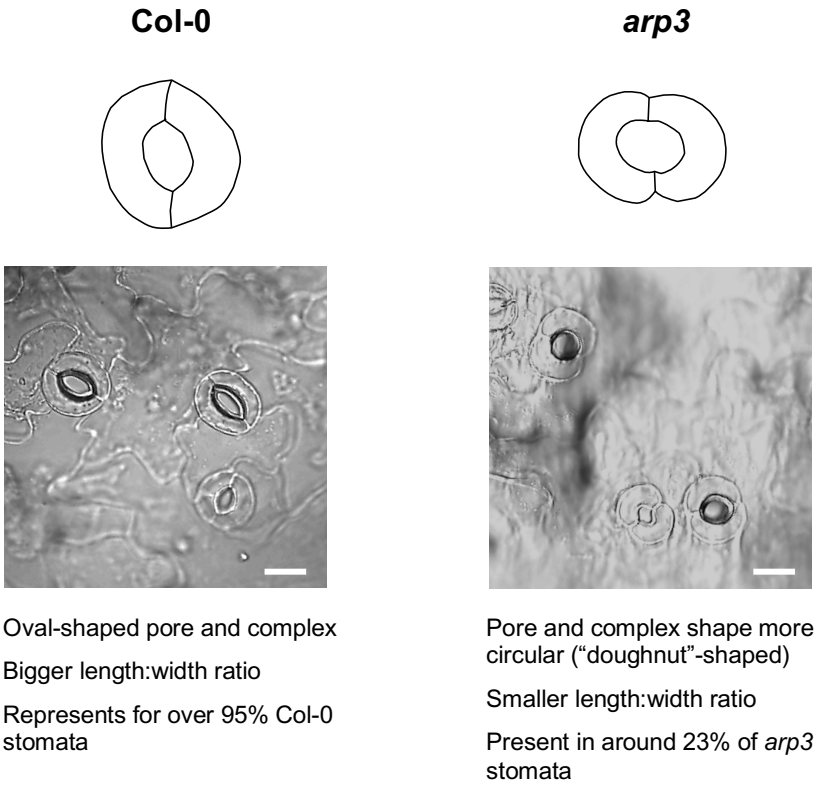

Figure 4.13 Summary of the differences between opened *arp3* and Col-0 stomata. Top, schematics showing differences in stomatal appearance in Col-0 and *arp3*. Bottom, light micrographs of Col-0 (left) and *arp3* (right) epidermal peels treated with fusicoccin, showing the differences in stomatal phenotype. Scale bars = 10μm.

Li et al. used a light intensity of 200μmol m^{-2} s^{-1} to stimulate stomatal opening, which would probably not be strong enough to trigger a "fully open" stomatal response as this light intensity is similar to the ambient conditions used for normal Arabidopsis growth. Additionally, 2 hours after being exposed to the light, the average pore width of both Col-0 and *arp3* stomata in the Li et al. paper was around 3μm, which is lower than maximum average stomatal pore width in the CO_2 bioassay reported in this chapter, where average pore width in response to low CO_2 was around 5μm in Col-0 and 6μm in *arp3*. Therefore, the fact that Li and colleagues did not observe the extremely open pores described in this chapter is likely due to the fact that they did not use stimuli that would induce a fully open response. As I did not measure rate of opening or closing in my bioassay, the two sets of results are not mutually exclusive, but together provide us a bigger and more cohesive picture of *arp3* stomatal opening.

In particular, my investigations of *arp3* stomatal response to low CO_2 levels revealed that 23% of stomata formed an unusual "doughnut" phenotype consisting of an extra-wide

pore and abnormal guard cell shape (Figure 4.13). As far as I am aware, this doughnut stomatal phenotype has not been described before and is a novel contribution to the phenotypic characterisation of ARP2/3 mutant plants. Another interesting finding from the CO_2 bioassay was the observation that there was a smaller pore length seen in both ambient CO_2- and high CO_2-treated *arp3* stomata but that they otherwise responded similarly to Col-0 in terms of pore width under these conditions. Other data in the literature has shown that the tips of the stomata contain areas of increased cell wall stiffness (Carter et al., 2017) and it was postulated that this enables a "pinning" of the stomatal pores so that the length of the pore as it opens and closes does not change (also observed in Rui and Anderson, 2016). It is possible that the *arp3* mutation is in some way preventing the deposition of de-esterified pectin to the poles of the guard cells, which therefore results in the shortening of the pore length during aperture changes. This remains to be further explored.

Although the *arp3* stomata displayed enhanced pore opening in response to low CO_2, a similar difference between *arp3* and Col-0 was not observed in response to FC. However, my analysis suggests that these observations can be reconciled if the strength of the stimuli used to trigger opening is taken into account. FC triggers extreme pore opening (to an extent that it may almost be considered non-physiological), whereas low CO_2 is a weaker trigger of opening. If the *arp3* mutation leads to guard cells which are mechanically more sensitive to opening/closing stimuli, then although the final maximal stomatal aperture (after FC treatment) might be the same, the system might achieve this maximum at a lower stimulation threshold.

The differences in guard cell shape and stomatal function between Col-0 and *arp3* plants described in this chapter could be explained – at least in part – by the impaired vacuolar fusion in *arp3* guard cells observed by Li et al. (2013). Polymerisation and assembly of actin filaments by ARP2/3 is known to be disrupted in *arp3* mutants (Mathur et al., 2003) which resulted in small unfused vacuoles adjacent to the central vacuole in Li et al. (2013). The fusion of vacuoles in guard cells is one of the main mechanisms driving guard cell expansion and stomatal opening, which, as discussed, Li et al. showed was impaired in *arp3*. Although vacuole morphology and fusion was not explored in this work, this provides another mechanism to explain the results described in this chapter. The possibility of aberrant guard cell wall component deposition in ARP2/3 mutants also

remained to be explored as another potential mechanism, which is discussed later in section 4.3.3.

4.3.2 *arp3* plants have a smaller rosette size and a lower photosynthetic capacity

At a whole-plant level, *arp3* mutants displayed significantly smaller rosette areas and a reduced germination rate. Our data also indicate that loss of *ARP3* leads to a lower photosynthetic capacity, certainly at higher CO_2 levels, and are consistent with this being at least partially linked to abnormal stomatal function. The iWUE of *arp3* plants was lower than Col-0, especially in high concentrations of CO_2, which suggests that *arp3* plants cannot utilise high concentrations of CO_2. This is consistent with the smaller size of the rosette plants observed in the *arp3* mutant, and provides evidence in support of Hypothesis IV.

With respect to the comparison of the stomatal phenotype observed in the epidermal strip bioassays and measured by IRGA, there is a discrepancy between the two methods. IRGA measurements indicated a slightly lower stomatal conductance at low CO_2, whereas the bioassay indicated a larger pore size (and thus inferred a potentially larger stomatal conductance). It is difficult to simply reconcile these two approaches. Although epidermal bioassays are widely used in stomatal biology (e.g. Li et al., 2013, 2014) they clearly represent an artificial system in which the potential influence of, for example, subtending mesophyll tissue on stomatal function is removed. On the one hand, this simplifies the dissection of guard cell function, but on the other hand one must be cautious in inferring whole leaf gas exchange function from such in vitro measurements (Roelfsema and Hedrich, 2005). These data supports the hypothesis that the loss of *ARP3* does lead to loss of normal stomatal function, but the assessment of significance on whole organ/plant physiology is best done using techniques which best assess behaviour at this scale.

4.3.3 *arp3* and guard cell wall composition

There are multiple sources that have shown a link between mutants of the ARP2/3 complex and cell wall defects. For example, Yanagisawa et al., 2015 showed that abnormalities in the delivery of cell wall components during development resulted in the characteristic *ARP2/3* distorted trichomes, seen in Figure 4.4. *arp2*, *arpc4* and *arpc5* mutants

exhibit reduced thickness of lignified cell walls and an increase in homogalacturonan (HG) content in inflorescence stems (Pratap Sahi et al., 2017). In contrast, Dyachok et al., 2008 quantified sugars from seedling roots using gas chromatography and found no difference in the amount of sugars that comprise the pectin backbone (including galactose, the main constituent of HG) in *arp2* compared to wildtype, although they did find that there were occasional differences in cell wall junctions between *arp2* and Col-0 root tip tissue, where the cell junctions were enlarged in *arp2* and filled with an "abnormal texture".

The immunolabelling data reported in this chapter did not suggest any major differences between *arp3* and Col-0 in terms of guard cell wall pectin amount and distribution. Therefore, the link between the *arp3* mutant and altered guard cell wall composition remains inconclusive and no data can be put forward in support of Hypothesis III. Of course, although I focussed on pectin composition, guard cell walls contain many more components, so future work could involve a wider screen of the array of cell wall antibodies now available. It should also be noted that high levels of particular epitopes can sometime mask the access to probes for less abundant (but potentially cell specific) epitopes. This problem can be overcome by pre-treating sections with enzymes to remove the masking elements, but the combinatorial approach of an array of pre-enzymes with specific antibodies to a range of epitopes makes the size of the task quite large. It is interesting that the incubations reported here with general probes for pectin did suggest some abnormal pectin distribution across the epidermal layer. Taken in conjunction with the overt disruption to the epidermis in SEM images of the *arp3* surface, it is tempting to speculate whether this more general alteration to the leaf surface might impinge on the gas exchange data obtained for this mutant, i.e. how does a general epidermal shift in pectin amount/distribution influence gas exchange, either directly or indirectly? Overall, my data does support a change in cell structure/adhesion in the *arp3* mutant, but the precise changes in cell wall composition underpinning these changes remains open to discussion.

One difference that was noticed (but was not guard cell related) was the large accumulations of pectin on *arp3* epidermises. Thicker epidermal cell walls could impair gas diffusion pathways, which offers another explanation towards the low iWUE and low assimilation rate of *arp3* mutants. This remains to be explored further.

4.3.4 Future work

This chapter presents new and interesting findings on the stomatal phenotype of *arp3* plants. However, it is not a complete story and there are still more discoveries to be made.

Firstly, more in-depth characterisation into the unusual doughnut shape of fully-opened *arp3* stomata would be interesting. For this thesis, I attempted to use confocal microscopy to obtain images of *arp3* guard cells crossed with actin-tagged fluorophores in order to explore any differences that may arise in actin organisation in *arp3* guard cells compared to Col-0. Unfortunately, these lines did not display sufficient fluorescent signal for this to be possible (data not shown), which is likely due to the segregating nature of the plants.

Additionally, if one could cross *arp3* with a tonoplast- or vacuole-tagged line in order to visualise the extent to which vacuoles are disrupted in low CO_2-treated stomata, this would extend work done in Li et al., 2013 and could provide some elucidation of the internal mechanism by which the doughnut shape is obtained.

Along similar lines, the doughnut shape of *arp3* stomata makes it an exciting candidate for the 3D guard cell analysis method I optimised in Chapter 3. Unfortunately, I ran out of time with this project but I think it would be very interesting to see to what extent the *arp3* guard cell doughnut shape is reflected in changes to cell volume and surface area, and/or changes to its cross-sectional shape, especially now a thorough description of the wildtype has been produced.

As previously discussed, antibody labelling of fixed tissue is not a quantitative nor comprehensive method of identifying the composition of plant cell wall tissue: a more quantifiable method of cell wall analysis may be required in future work. Plant cell wall quantification has been done by using mass spectrometry and liquid chromatography (e.g. Alonso et al., 2010; Fang et al., 2015), but a method of cell wall extraction and quantification of esterification based on methods used in Müller et al. (2013) may clear up the inconclusive nature of the immunolabelling experiments, although the amounts of tissue required may prove challenging.

In the *arp3* mutant used in this project the ARP3 protein is lost throughout the plant. A project in which the wildtype *ARP3* gene is inserted behind a guard cell-specific promoter and transformed into the *arp3* mutant to produce a guard cell complemented line would provide more insight into whether the physiological differences observed at a whole-

plant level, such as a lower assimilation rate at ambient and high CO_2 levels, are due solely to the differences in stomatal function, or whether the *ARP3* knockout has a broader effect on leaf photosynthesis.

4.4 Key findings

- *arp3* mutants display a significant guard cell shape phenotype after treatment with low CO_2. The guard cells swell and bow outwards and a circular, hyper-opened "doughnut"-shaped pore occurs in approximately 25% of stomata.
- Some experiments suggest that *arp3* mutants achieve an opened pore with a weaker stimulation threshold i.e. they are more sensitive to opening stimuli and are quick to form the doughnut pore.
- From immunolabelling experiments, there is no evidence to suggest that there are any differences between *arp3* and Col-0 in pectin distribution in the leaf cell walls contributing to the unusual guard cell shape phenotype.
- At a whole-plant level, *arp3* exhibits significant phenotypic defects when compared to wildtype, such as a reduced rosette area and a lower plant water use efficiency. However, more work is needed to investigate whether these differences are due to aberrant *arp3* stomatal function, or whether there are broader effects of the *arp3* gene mutation throughout the plant.

Chapter 5: Investigation into the role of α-expansins in guard cell function

5.1 Introduction

Expansins are cell wall proteins that are involved in the loosening of the plant cell wall. They do so in a pH-dependent manner (Cosgrove, 2000; McQueen-Mason et al., 1992) and were first described in studies into the acid growth phenomenon (Li et al., 1993; McQueen-Mason et al., 1992). They are thought to function non-enzymatically by breaking the hydrogen bonds that link cellulosic and non-cellulosic components of the cell wall (McQueen-Mason and Cosgrove, 1994), allowing the separation of cellulose microfibrils and other components which contributes to cell wall creep (Marga et al., 2005). When coupled with increases in the cell's internal pressure, this allows turgor-driven expansion and growth of the cell.

Expansins have been found across plant taxa. In each group there is generally a large family of expansin genes, split into four main subfamilies (here listed from the largest family to the smallest): α-expansins, β-expansins (Li et al., 2002), expansin-like A and expansin-like B (Sampedro and Cosgrove, 2005). Both α- and β-expansins have been experimentally proven to be involved in cell wall loosening and modification (more so for α- than β-) but the expansin-like A and expansin-like B proteins are identified as such only from their gene sequences and similarities in protein structure. The significance of the observed differences in sequence have yet to be further examined and so little is known about the function of these subfamilies.

In Arabidopsis, there are 26 α-expansins and five β-expansins. α- and β-expansins differ in both their protein structure and their distribution – for example, β-expansins are highly expressed in pollen – although online databases show that both families are present in most tissues (Winter et al., 2007). Interestingly, β-expansins have been found to be homologous to group I allergens contained in pollen, and are therefore thought to play a role in pollen tube penetration using a wall-loosening mechanism (Cosgrove et al., 1997). There are many more β-expansin proteins in grasses than in Arabidopsis (Lee et al., 2001) which is believed to be due to the difference in composition of monocot cell walls

(Cosgrove et al., 2002), and indeed it has been observed that β-expansins are more highly active in grass cell walls than α-expansins (Lee et al., 2001).

The role of expansins in cell wall loosening means that expansins are often associated with cell growth. α-expansins are commonly located in vegetative tissue across multiple plant taxa and are often found in growing and developing tissues and organs. For example, they have been shown to be involved in ripening of tomatoes (Brummell et al., 1999) and strawberries (Harrison et al., 2001); root elongation in soybean (Lee et al., 2003), and root initiation in pine (Hutchison et al., 1999); and leaf expansion in tobacco (Sloan et al., 2009).

5.1.1 *EXPA1* has been implicated in stomatal function

Plant cell wall growth can be characterised into two broad types. The first is a reversible, short-term loosening of the plant cell wall (Cosgrove, 1999), as seen in auxin-induced growth for example, which can take just minutes to occur (Green and Cummins, 1974). Long term cell wall growth is associated with whole cell growth and division, in which longer-term (hours or longer) remodelling of the cell wall occurs. It is thought that expansins are involved in both processes (Cosgrove, 1999).

As stomata can react to changes in external or internal signals within minutes, guard cell wall extension and contraction often falls into the first category. Indeed, changes to guard cell walls are reversible, allowing guard cells to expand and deflate, thus allowing the stomatal aperture formed between the guard cells to adapt to constant fluctuations in the plants' environment. The relatively rapid expansion and deflation of the guard cells suggests that their cell walls have a specific structure/function, and it seems highly plausible that expansins might be involved in regulating the unusual extensibility of the guard cell wall.

There has so far been some evidence linking expansin activity to the guard cell wall. In Zhang et al. (2011), stomatal function was assessed using a stomatal aperture bioassay in a transgenic Arabidopsis line in which the Arabidopsis α-expansin *AtEXPA1* was overexpressed. The plants were dark-adapted and epidermal peels taken. The peels were then exposed to 200 mol m^{-2} s^{-1} light and stomatal aperture was measured every 30 minutes for 2 hours. This revealed that the transgenic *AtEXPA1* over-expressing lines reached a wider stomatal pore aperture faster than the wildtype control upon exposure to

light. After 2 hours, the average aperture of both the transgenic line and wildtype was the same. The authors followed this up with a similar experiment in which peels were incubated with an anti-EXPA1 antibody which showed that inhibition of AtEXPA1 decelerated light-induced opening in a pH-dependent manner. Evidence for expansin activity was further provided through measuring the elastic modulus of tobacco guard cells in both an *AtEXPA1-OE* transgenic line and the wildtype line through the use of a cell pressure probe. The elastic modulus indicates how much turgor pressure would be required to achieve a volume change. It was found that guard cells from the mutant line had a smaller elastic modulus than the wildtype, suggesting that the guard cells in the *AtEXPA1-OE* line would need less turgor pressure to change cell volume, indicating that they had a more flexible cell wall.

Additional work by the same group suggested that the same transgenic line in which *AtEXPA1* is overexpressed had a higher rate of photosynthesis and a higher transpiration rate than wildtype (Wei et al., 2011). This indicates that expansin activity in the guard cells influenced stomatal function and, thus, may have had an impact on whole plant physiology.

The authors also proposed a mechanism for how altered expansin activity in guard cells might lead to the observed phenotype (although this has yet to be proven). It is known that activity of the H^+-ATPase in the guard cell plasma membrane is required for stomatal opening: it helps to create an electrochemical gradient across the plasma membrane which drives K^+ ion accumulation and, therefore, movement of water into the guard cell, which increases turgor pressure and leads to stomatal opening. They proposed that because hyperpolarisation of the guard cell plasma membrane also increases acidification of the guard cell wall (Rayle and Cleland, 1992), this results in a rise in expansin activity and therefore cell wall loosening which assists in the swelling of the guard cells.

Although the data from the experiments exploring the effects of the overexpression of *AtEXPA1* on stomatal function are intriguing, they are based on ectopic expression of a gene. This raises the potential for pleiotropic effects on phenotype, i.e., the question is raised as to what extent the observed stomatal phenotype is a direct or indirect outcome of a very broad increase in *AtEXPA1* expression. More convincing evidence for a role of expansins in guard cell function would come from an analysis of lines in which expansin

activity was lost or decreased. If loss of expansin activity leads to an abrogation or a disturbance of stomatal opening/closing, this would be strong evidence that expansins do play a role in normal guard cell function.

5.1.2 Hypotheses and objectives

My hypotheses for this chapter are as follows:

I. Guard cell function depends on cell wall structure.
II. Specific α-expansin proteins are expressed in guard cells.
III. Changing the expression of the relevant α-expansin genes will result in altered stomatal function.
IV. Altered stomatal function as a result of changing expression of α-expansin genes will result in differences between mutants and wildtype in plant physiology.

Therefore, my aims are:

I. To identify α-expansin genes that are expressed in the Arabidopsis guard cell.
II. To characterise loss-of-function mutations in the genes to see if there is any effect on stomatal function.
III. To investigate whether differences in stomatal function as a result of altered guard cell expansin gene expression can be linked to changed plant physiology.

5.2 Results

5.2.1 Identification of α-expansins with a potential role in the guard cell wall

There are 26 proteins in the Arabidopsis α-expansin protein family. To assess which α-expansin proteins would be suitable candidates for investigation into their role in guard cell wall function, I first looked at the results from a microarray analysis conducted by Lee Hunt (Julie Gray lab, University of Sheffield) using NASCARRAYS29 data, in which expression levels of genes in guard cell-enriched *A. thaliana* tissue were compared to that from whole leaf tissue. This data, although not guard cell specific, provides an indication of genes that are more highly expressed in guard cell-enriched tissue and which therefore may play an important role in guard cells.

I narrowed down the microarray data to look at only α-expansin genes, then plotted the fold change between whole leaf tissue and guard cell enriched tissue (Figure 5.1A). Clearly a number of expansin genes are expressed to some extent in guard cells, but two genes stood out as the most highly expressed in guard cell tissue when compared to whole leaf tissue: AT2G39700 (α-expansin 4; *EXPA4*) and AT3G55500 (α-expansin 16; *EXPA16*).

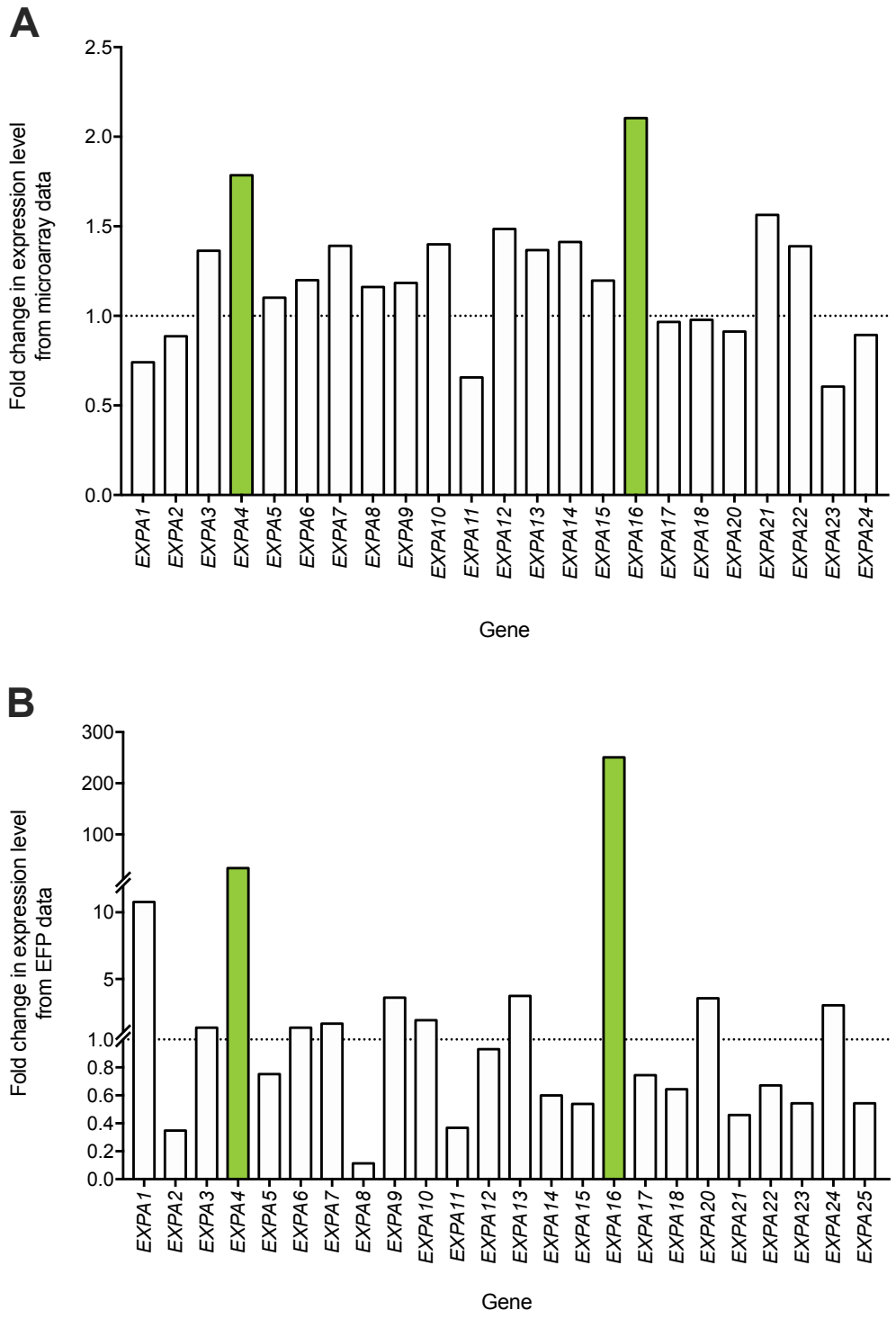

Figure 5.1 Expression of α-expansin genes in guard cell enriched tissue. (A) Fold change in expression levels of α-expansin genes in guard cell-enriched tissue compared to whole leaf tissue from a microarray dataset. **(B)** Fold change in expression levels of the same genes in guard cells compared to mesophyll tissue from the EFP Browser (Winter et al., 2007). Dotted lines represent a ratio of 1 where expression level in guard cell enriched tissue and whole leaf tissue are equal. *EXPA4* and *EXPA16* are highlighted in green on both graphs. *EXPA19*, *EXPA25* (microarray only) and *EXPA26* have been excluded from this analysis due to lack of available data.

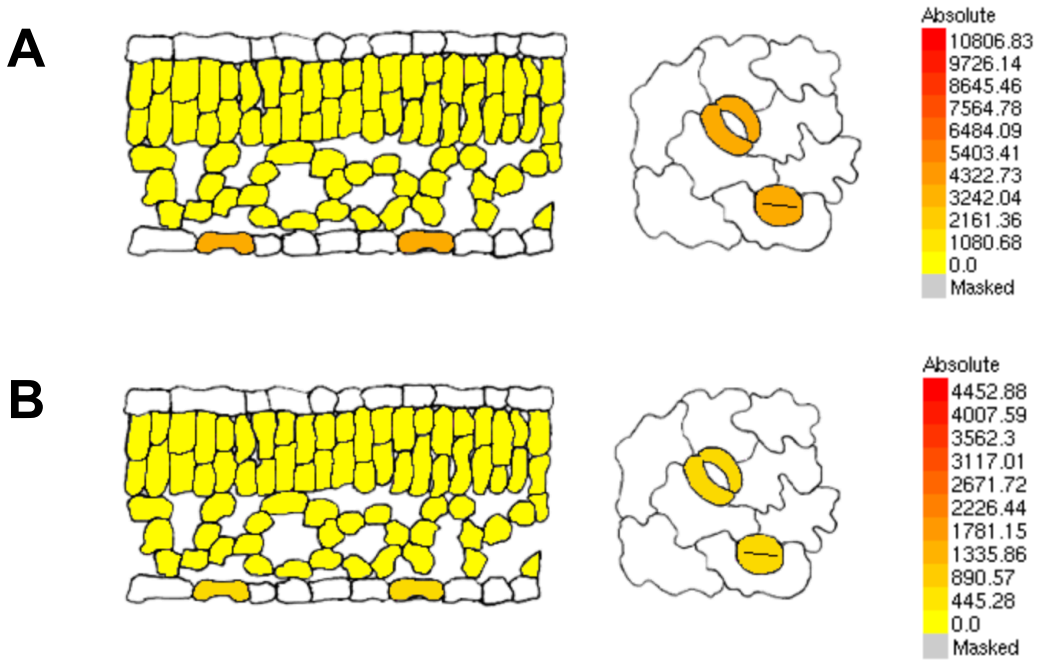

Figure 5.2 Data from EFP browser showing expression levels of *EXPA16* (A) and *EXPA4* (B) in guard cells compared with mesophyll cells. (A) Expression levels of *EXPA16* in guard cells and mesophyll (GC = 3400.6; M = 13.56). **(B)** Expression levels of *EXPA4* in guard cells and mesophyll (GC = 677.58; M = 19.72). Darker colours represent higher expression levels. Data taken from the online EFP browser (Winter et al., 2007).

An additional dataset was used to verify the results from the microarray analysis. Data taken from the online Arabidopsis EFP browser (Winter et al., 2007) was used to compare expression of α-expansin genes in guard cells to their expression in mesophyll tissue (Figure 5.2). Figure 5.1B shows that according to the EFP browser *EXPA4* and *EXPA16* are

Table 5.1 Expression levels of *EXPA4* and *EXPA16* in guard cells from different databases. Data from the EFP browser and the microarray are measured in terms of signal intensity from separate microarray experiments.

Gene	Database	Guard cell expression level (signal intensity)	Whole leaf tissue expression level (microarray) (signal intensity)	Mesophyll expression level (EFP browser) (signal intensity)
EXPA4	Microarray data	54.80	30.70	-
	EFP browser	677.58	-	19.72
EXPA16	Microarray data	28.53	13.56	-
	EFP data	3400.6	-	13.56

both expressed highly in guard cells when compared to mesophyll tissue, which corroborates the microarray data, with *EXPA16* being particularly notable in that its expression level in guard cells is 250x higher than that in mesophyll tissue. These results are summarised in Table 5.1.

The high expression of *EXPA4* and *EXPA16* in guard cell tissue when compared to general leaf tissue makes these two α-expansin genes interesting candidates for investigation into the role of α-expansins in guard cell walls. These genes were taken forward for further analysis.

Seeds from the following T-DNA insertion mutants were obtained from NASC (Alonso et al., 2003; Scholl et al., 2000): SALK_134337 and GK-061D02. The former is T-DNA insertion mutant of *expa16* and the latter of *expa4*.

5.3 Analysis of *expa16* stomatal function

5.3.1 Characterising an *expa16* insertion mutant

Salk-134337 seeds were sown and grown in long day conditions and at 3 weeks leaves were harvested from which DNA was extracted. Primers were designed (see Appendix 8.1) to genotype the plants using the extracted DNA, and PCR reactions were performed to confirm zygosity of the mutants. Only plants that were homozygous for the mutation in *EXPA16* were carried forward for further analysis.

The genotyping process and resulting electrophoresis gel images are shown in Figure 5.3. Figure 5.3A is a diagram showing where the primers bound in wildtype genomic DNA (gDNA) and in gDNA with the T-DNA insertion in the gene of interest. If a plant was homozygous negative (wildtype), then a band would form in the lane between the left primer (LP) and the right primer (RP) within the gene. If a plant was homozygous positive, there would be a band in the left border (LB) and RP lane, and none in the LP and RP lane as the sequence would be too long to amplify with the inserted T-DNA. Heterozygous plants would have a band in both lanes. Figure 5.3B shows the gel image from Salk_134337 gDNA (a T-DNA insertion in the *EXPA16* gene). Here, *expa16* has a band in the reaction with the border (LB) primer and does not have one in the lane with

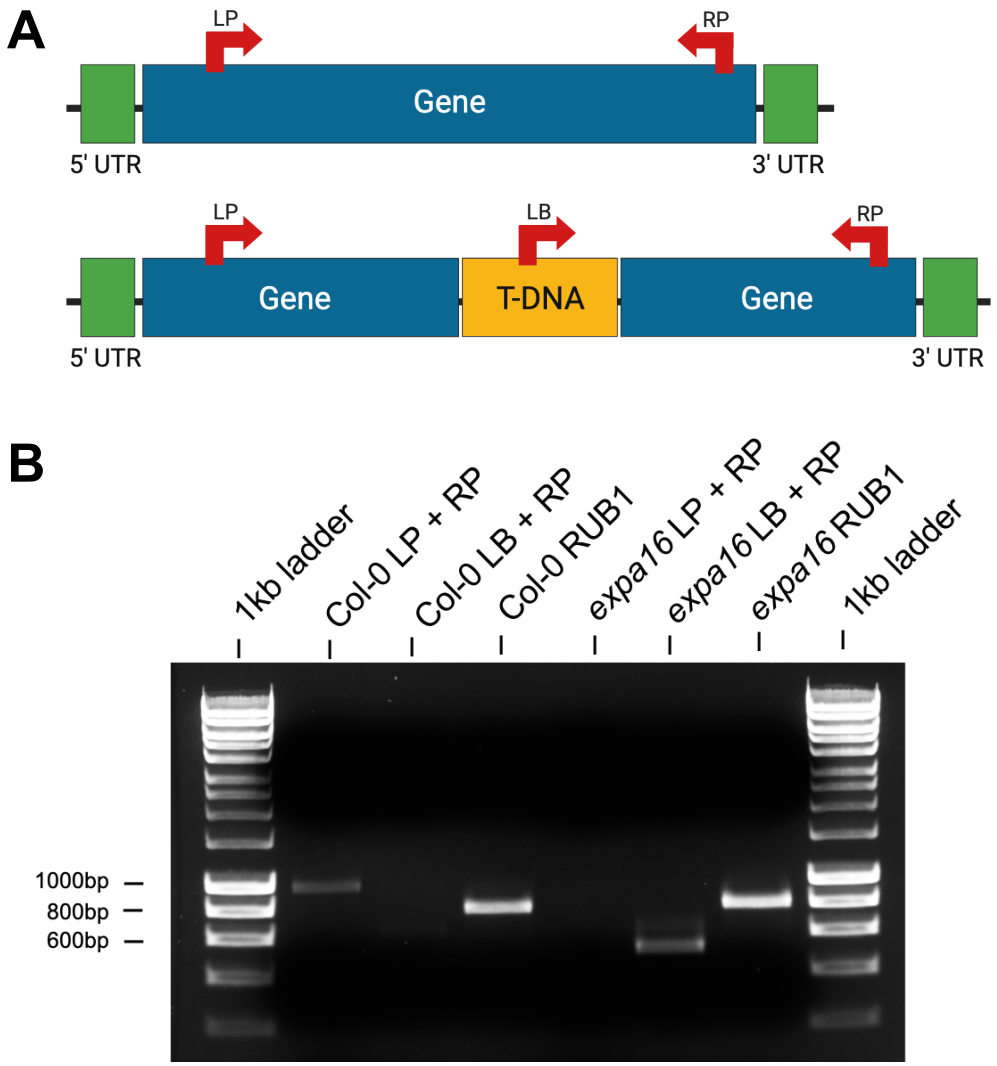

Figure 5.3 PCR genotyping of an *expa16* transgenic line. (A) Schematic showing position of primers used in a genotyping PCR reaction. Image created using Biorender. **(B)** Gel image of Col-0 and Salk-134337 gDNA after PCR. A band in the LP + RP column for Col-0 shows that this is the wildtype for *AtEXPA16*. A band in the LB + RP column in Salk_134337 (*AtEXPA16*) shows that it has the T-DNA insertion and therefore a mutation in the *EXPA16* gene. The RUB1 used rubisco primers (At4G36800) as a positive control. Expected fragment sizes were: LP+RP = 982bp, LB+RP = 500bp, RUB1 = 800bp.

the wildtype left primer (LP). This confirms that this line is homozygous with the insertion.

5.3.2 Assessing *expa16* stomatal aperture in response to differences in CO_2 level

Stomata close in response to higher CO_2 concentrations whereas they open under low concentrations to increase gas exchange. This can be used to stimulate stomata to open and close in a laboratory setting, which is useful to assess stomatal opening and closing in

different plants and genetic backgrounds. Therefore a bioassay was performed to assess stomatal opening and closing of *expa16* plants in response to shifts in CO_2.

Abaxial epidermal peels from Col-0 and *expa16* plants were placed into buffer through which different concentrations of CO_2 were pumped: 1000ppm for 'high' CO_2, 400ppm for 'ambient' CO_2 and 0ppm for 'low' CO_2. After 2.5 hours, peels were imaged on a light microscope and then stomatal apertures were measured from the images.

Figure 5.4 shows the results from this experiment. Col-0 stomata had a significantly higher mean pore aperture in low CO_2 when compared to ambient CO_2, which in turn was significantly higher than in high CO_2 (Tukey test, df=27.05, $p<0.0001$). This shows that the pore was opening and closing as expected in the control tissue.

In the *expa16* knockout line, this pattern changed. There was no significant difference in pore aperture between peels in either low, ambient and high CO_2 conditions. This shows that there was a more limited stomatal response in this transgenic line that has the *EXPA16* gene knocked out when compared to wildtype, which suggests that *EXPA16* has a role in stomatal opening and closing.

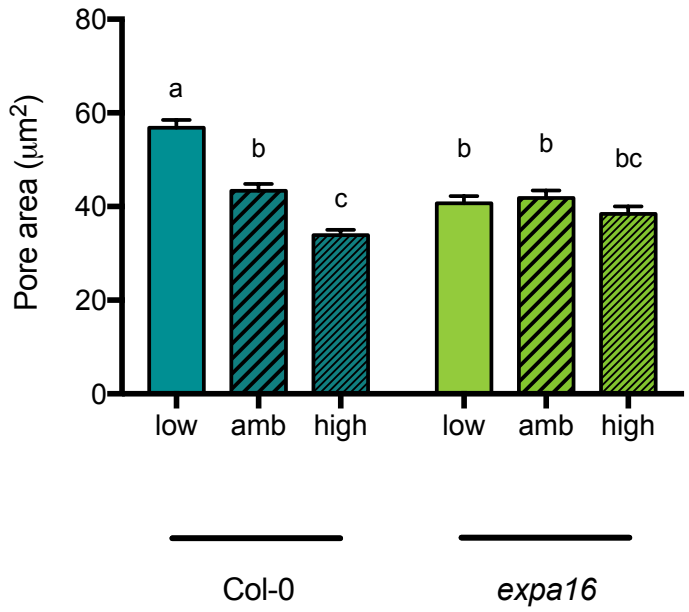

Figure 5.4 Assessing stomatal opening and closing response to differing concentrations of CO_2 in *expa16* (green bars) and Col-0 (blue bars) plants. Epidermal peels were taken from Col-0 and *expa16* plants and were left in buffer through which high CO_2 (1000ppm), ambient CO_2 (400ppm) and CO_2-scrubbed air (low CO_2) was bubbled through for 2.5 hours. A two-way ANOVA was performed followed by a Tukey multiple comparisons test. Samples indicated with the same letter cannot be distinguished from each other ($p<0.05$). Bars indicate mean ± SEM. Per treatment $n = 8$ plants. This was repeated twice with the same results found both times.

5.3.3 Assessing *expa16* whole plant response to ABA

Opening and closing of stomata will alter stomatal conductance and, as a consequence, transpiration from the leaf surface. This will alter surface temperature which can be captured by thermal imaging. Therefore, to assess the impact of the koockout of *expa16* on stomatal function in intact plants (as opposed to the epidermal strips used above), a thermal imaging method (described in Chapter 2) was used. To regulate stomatal closure, exogenous ABA was used as a trigger, with the results shown in Figure 5.5.

In the hour before the plants were spray-treated, plant temperature very slowly increased by around 1°C, which is likely due to the plants acclimatising to natural fluctuations in their environment. Once sprayed with a 5μM ABA or a mock spray, the mean plant temperature decreased from around 21.4° rapidly by approximately 5°. Regardless of which treatment was applied to the plant, each shows a similar rate of recovery of temperature for the first 10 minutes after spraying. 50 minutes after spraying the average plant temperatures reached a plateau and stopped increasing. This is where some differences between the genotypes are seen.

After an hour, plants sprayed with the mock treatment had recovered to match their original temperature, with Col-0 plants reaching a mean temperature of 21.51° (n = 6) and *expa16* 21.49° (n = 6). Both genotypes when sprayed with ABA reached a higher temperature than the mock treatment. An hour after application of ABA, Col-0 plants had a mean temperature of 21.87°, which is 0.36° hotter than the mock treated Col-0. *expa16* plants treated with ABA had a mean temperature of 22.16° after an hour, 0.67° above the mock treated *expa16*, which demonstrates a larger plant temperature range.

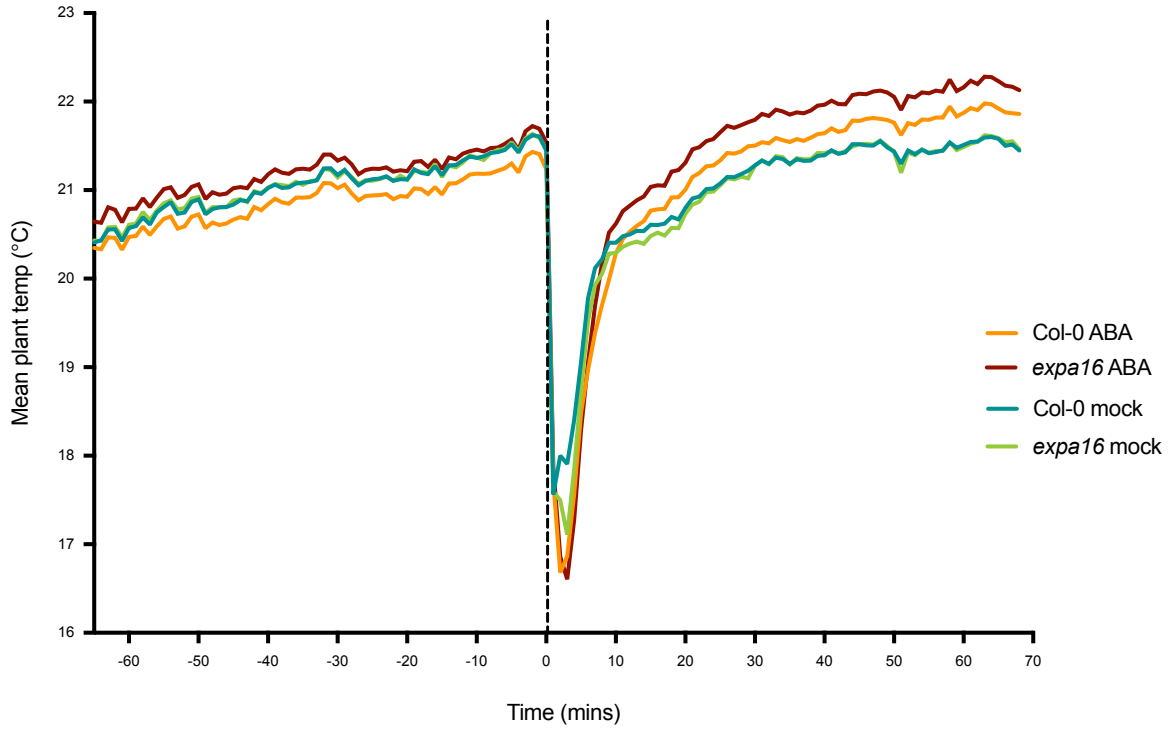

Figure 5.5 *expa16* plants show an increase in leaf temperature after application with ABA. Mean plant temperature was calculated using an average of 3 leaf spots per plant using the genotypes indicated (*expa16* and Col-0). After approximately 60 minutes in ambient conditions, either a 5µM ABA solution or a mock solution (without ABA) was sprayed onto the plants (at the time indicated by the dashed line) and then plants were imaged for a further 60 minutes. Col-0 mock is represented by the blue line, *expa16* mock by the green line, Col-0 with ABA treatment in orange and *expa16* with ABA treatment in red. $n = 6$ plants per genotype.

Although the differences in plant temperature are small, there is a clear increase in the temperature of plants when applied with ABA when compared to plants applied with a mock solution. There is also a difference between genotypes when ABA is applied, with *expa16* plants increasing more in temperature than Col-0 plants. These data imply that transpiration and plant cooling in *expa16* plants is less effective than in Col-0, which suggests that the stomata on *expa16* leaves are more closed than on Col-0 leaves. This contrasts with the earlier stomatal aperture bioassay suggesting that stomata on *expa16* plants close to a lesser extent than Col-0.

5.3.4 Assessing *expa16* plant response to drought

To further investigate the potential role of *EXPA16* in stomatal function we examined the thermal response of Col-0 and *expa16* mutant plants to imposed drought, a known environmental trigger of stomatal closure (Leung and Giraudat, 1998). Col-0 and *expa16* plants grown at the same time under identical conditions were imaged using a thermal

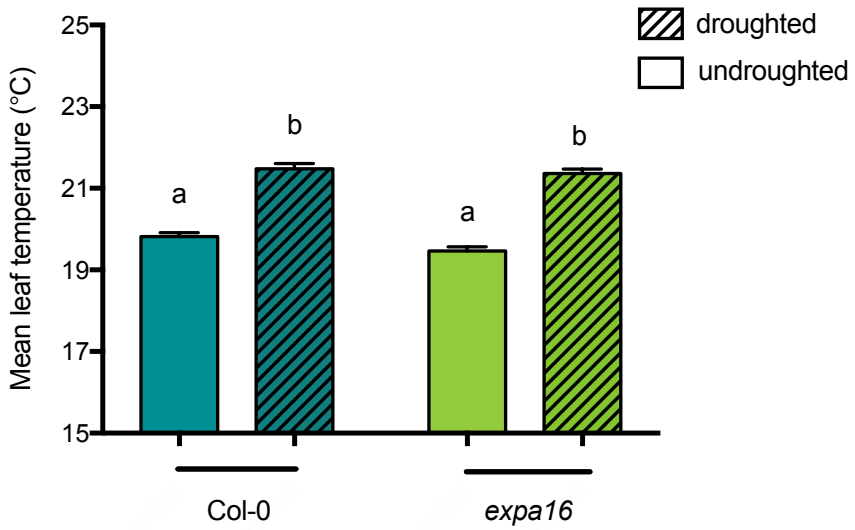

Figure 5.6 Mean leaf temperature of Col-0 (blue) and *expa16* (green) plants in response to drought treatment. Well-watered Col-0 and *expa16* plants were imaged on a thermal imaging camera, left without watering for 5 days, and then imaged again. A two-way ANOVA was performed on the data set followed by a Tukey test (F=91.41, p<0.0001). Samples indicated by the same letter cannot be differentiated (df=86, p<0.05). *n* = 7 (*expa16*) and 8 (Col-0).

imaging camera ('Undroughted' treatment). Plants were then left in normal growth conditions without watering, and 5 days later were imaged again ('Droughted' treatment). Leaf temperature from 6 leaves was measured from 4 plants per genotype, both before and after the drought treatment. The results are shown in Figure 5.6.

Before droughting, mean Col-0 leaf temperature was 19.81 ± 0.45°C (mean ± SD, *n* = 8) and mean *expa16* leaf temperature was 19.46 ± 0.47°C (*n* = 7). After 5 days of no watering, temperatures were measured again. The temperature of Col-0 leaves had increased significantly from the undroughted leaves to 21.48 ± 0.62°C (Tukey test, df=86, p<0.0001). A significant increase in leaf temperature was also seen in *expa16* leaves, to 21.36 ± 0.47 (Tukey test, df=86, p<0.0001). However, there were no significant differences seen between *expa16* and Col-0 mean leaf temperatures, in either the undroughted or the droughted sample sets. This indicates that the *expa16* plants were responding to drought stress in the same way as Col-0.

5.3.5 *expa16* stomatal conductance and assimilation in response to shifting CO_2

To further investigate stomatal function of *expa16* plants, stomatal conductance was measured under shifting CO_2 conditions using an IRGA (infrared gas exchange analyser).

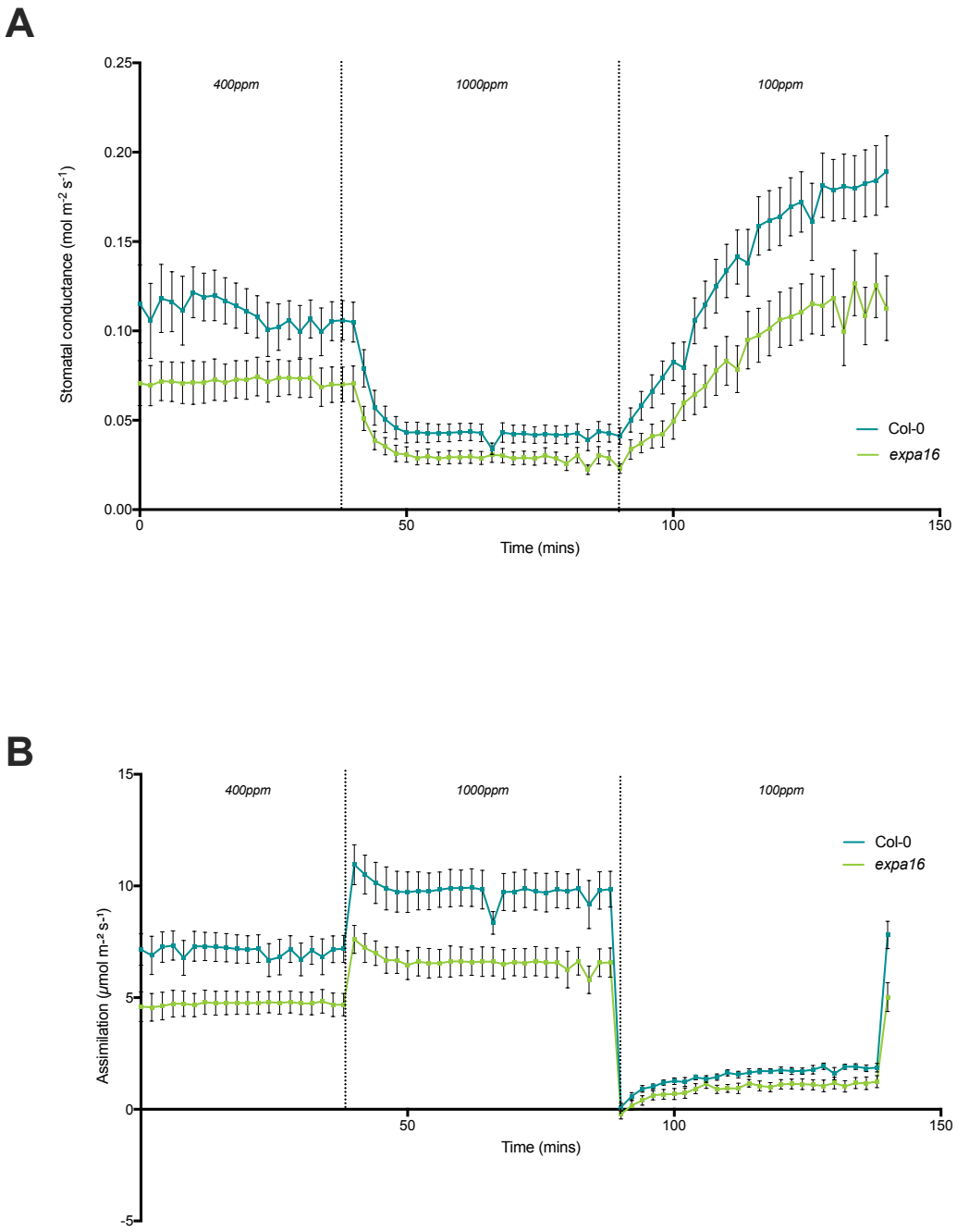

Figure 5.7 Stomatal conductance and assimilation rate of *expa16* (green) and Col-0 (blue) plants in response to shifts in CO_2 on an IRGA. (A) Stomatal conductance is lower in *expa16* than in Col-0 under all CO_2 conditions. **(B)** Assimilation rate is lower in *expa16* than Col-0 under ambient and high CO_2 conditions, however, there seems to be very little difference in assimilation rate in low CO_2. Light levels remained constant at 300 µmol m^{-2} s^{-1}. Error bars = SEM, $n = 6$ for each genotype.

A Li-cor 6800 was programmed to take measurements of stomatal conductance and assimilation every 2 minutes as the external CO_2 concentration changed, first from 400ppm (ambient) to 1000ppm (high) and then to 100ppm (low).

At 400ppm CO_2, stomatal conductance of *expa16* plants was about a third of that in Col-0 (Figure 5.7A). When CO_2 was increased to 1000ppm, stomatal conductance of both lines decreased but again *expa16* had a lower stomatal conductance than Col-0. When CO_2 was decreased, plants of both genotypes increased stomatal conductance, but *expa16* reached a lower maximum than Col-0 by a large amount – the maximum conductance reached in low CO_2 of *expa16* plants matched that observed in Col-0 plants in ambient CO_2.

The assimilation rate of both lines increased when CO_2 concentration increased from 400ppm to 1000ppm (Figure 5.7B). However, *expa16* had a lower rate of assimilation in both 400ppm CO_2 and 1000ppm CO_2 than Col-0. This may be because the stomatal conductance was lower in both of these conditions. When CO_2 decreased to 100ppm, assimilation rate decreased in both lines and was similar for Col-0 and *expa16* leaves.

Overall, it is noticeable that for both assimilation rate and stomatal conductance, the range recorded in *expa16* plants was less than that observed in Col-0. This supports the data in Figure 5.4 which shows abrogated stomatal function of *expa16* under differing CO_2 conditions.

5.3.6 *expa16* stomatal response to rapid light shifting

Zhang et al., 2011 used light to assess the speed of stomatal opening in a line in which *EXPA1* was overexpressed and found that stomata in the overexpressor line opened faster than wildtype. To investigate whether the *EXPA16* knock-out line showed an altered rate of opening/closing response, I used an IRGA to measure stomatal conductance of *expa16* and Col-0 leaves when rapidly shifting between darkness (0 μmol m^{-2} s^{-1}) and light saturation (1500 μmol m^{-2} s^{-1}). This method is similar to one reported in Penfield et al., 2012. The results of the experiment are shown in Figure 5.8.

After the initial 5-minute acclimation time at 200 μmol m^{-2} s^{-1} (ambient) light, both Col-0 and *expa16* had a similar rate of stomatal conductance. During the first three dark and light cycles both lines seemed to plateau without much change in stomatal conductance. Then, stomatal conductance of Col-0 leaves began to increase in response to high light and decrease in response to darkness. The same was seen for *expa16*, although it is worth noting that the decreases in stomatal conductance after periods of darkness were not as sharp as the decreases seen after darkness in Col-0.

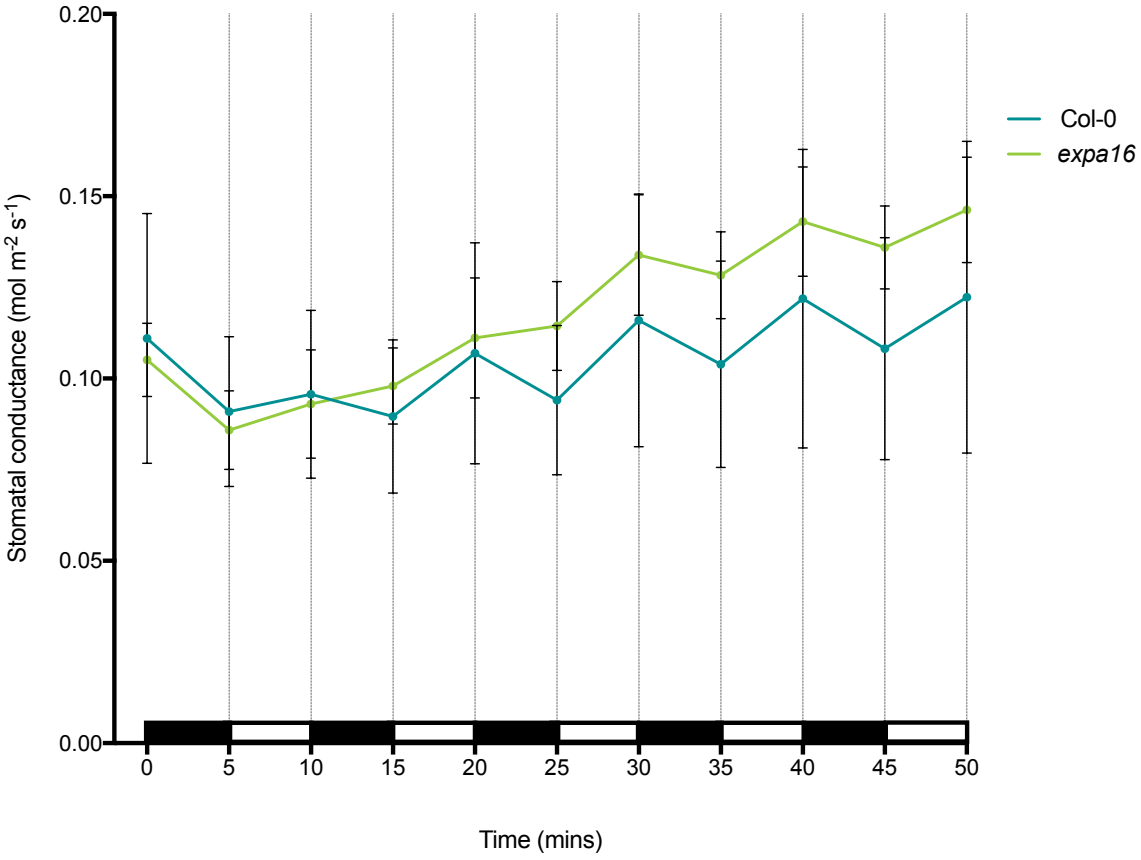

Figure 5.8 Stomatal conductance of *expa16* (green) and Col-0 (blue) leaves in response to shifting light concentrations. After a 5-minute period of acclimation at 200µmol m^{-2} s^{-1}, a measurement of stomatal conductance was taken (time point 0). Thereafter, the leaf was exposed to alternating high light (1500 µmol m^{-2} s^{-1}) (white box) and darkness (black box) every 5 minutes. A two-way ANOVA was performed on the data set followed by a Tukey's multiple comparison test which found there were no significant differences between the two datasets (n>0.05). Error bars = SEM. *n* = 7 (*expa16*) or 6 (Col-0).

Looking at overall trends from the data, it appears that *expa16* opened more on average over the experiment, as there is a larger difference between the two lines at the end than at the start of the experiment. However, the differences between the two lines were not statistically significantly different at any point on the graph.

5.3.7 Rosette size and stomatal density in *expa16* plants

To test whether the differences seen between *expa16* and Col-0 would have any effect of whole plant size, rosette area was measured from *expa16* and Col-0 plants 5 weeks after sowing. There was no significant difference between the two in terms of rosette area (Figure 5.9A; unpaired t-test, p=0,9849, *n*=6) and no visible differences could be seen in plant growth or form (Figure 5.9B and C). Stomatal density was also measured from

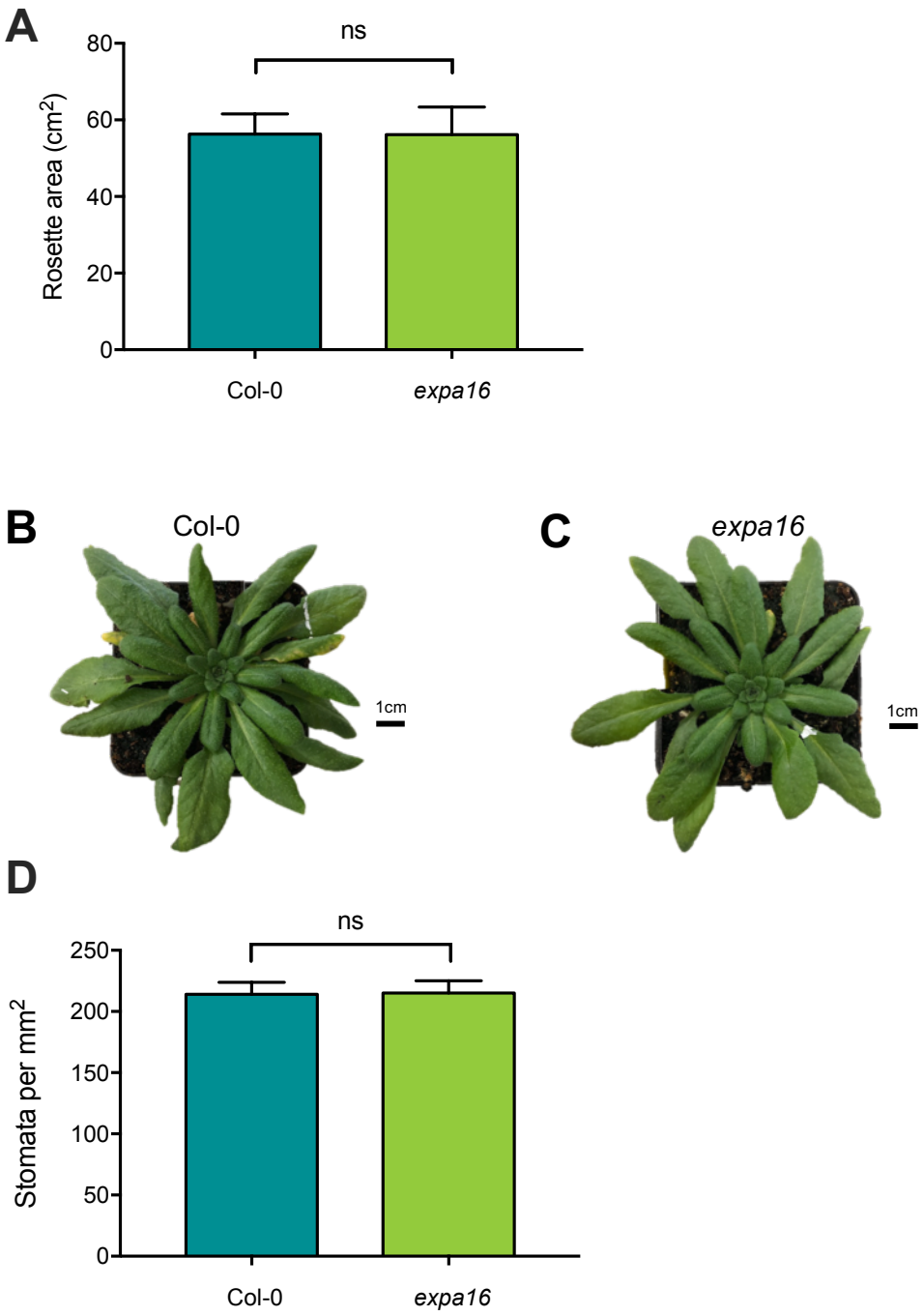

Figure 5.9 Rosette size and stomatal density of *expa16* (green) and Col-0 (blue) plants. (A) Rosette area of Col-0 and *expa16* plants was measured 5 weeks after sowing. Unpaired t-test, p=0.9849, ns = not significant. Mean ± SEM, *n* = 6 for each genotype. Representative images of **(B)** Col-0 and **(C)** *expa16* plants 5 weeks after sowing. Scale bars = 1cm. **(D)** Stomatal density measurements taken from the abaxial side of leaves of *expa16* and Col-0 plants. Unpaired t-test, p=0.9425, ns = not significant. Mean ± SEM, *n* = 3 views per leaf, 3 leaves per plant.

leaves of 5-week-old Col-0 and *expa16* plants. The results are shown in Figure 5.9D. There was no significant difference in stomatal density between Col-0 and *expa16* (unpaired t-test, p>0.05, *n*=9), with 214 ± 50 stomata per mm² of abaxial leaf surface, and *expa16*, with

214 ± 51 stomata per mm^2 of abaxial leaf surface. This means that any difference in stomatal function described in this section is unlikely due to differences in stomatal density.

5.4 Analysis of *expa4* stomatal function

5.4.1 Assessing *expa4* stomatal aperture in response to CO_2 level

To investigate the role of *AtEXPA4* (the second expansin gene identified by my expression analysis to have a potential role in stomatal function, Section 5.2.1), seeds of a putative T-DNA knock-out line (GK-061D02) were obtained from the NASC stock centre. Seeds were grown and were genotyped using the method shown in Figure 5.3. Plants homozygous with the insertion in were grown for seed.

To examine whether there was a difference in stomatal function between the *expa4* mutant and the control, a stomatal aperture bioassay was carried out. Figure 5.10 shows stomatal response to different CO_2 levels in *expa4* plants and Col-0, the wildtype control. Epidermal peels taken from mature leaves were exposed to buffers provided with a low concentration of CO_2 (0ppm), ambient CO_2 (approximately 400ppm), or a high concentration of CO_2 (1000ppm). The results from three independent experiments are shown as separate graphs because of the variation seen between datasets, as discussed below.

In Figure 5.10A, B and C, mean pore aperture increased in response to low CO_2 treatment and decreased in response to high CO_2 treatment for Col-0 epidermal peels, and in each of these cases the differences in stomatal aperture between low-, ambient- and high-CO_2 treated peels was statistically significant (Tukey test, $p<0.05$, $n = 9$).

The technical repeat described in Figure 5.10A, indicated that *expa4* had a limited response to different concentrations of CO_2 compared to Col-0. Neither high- nor low-treated *expa4* epidermal peels showed any significant differences in pore aperture compared with ambient-treated peels (Tukey test, $p>0.05$, $n = 9$), although the difference between low and high was significant (Tukey test, $p<0.0001$, $n = 9$), indicating that the response to CO_2 was limited but not totally inhibited.

Similarly, in Figure 5.10B, there was evidence of a reduced closing response to high CO_2, as the mean pore aperture of *expa4* stomata was not statistically different between high-

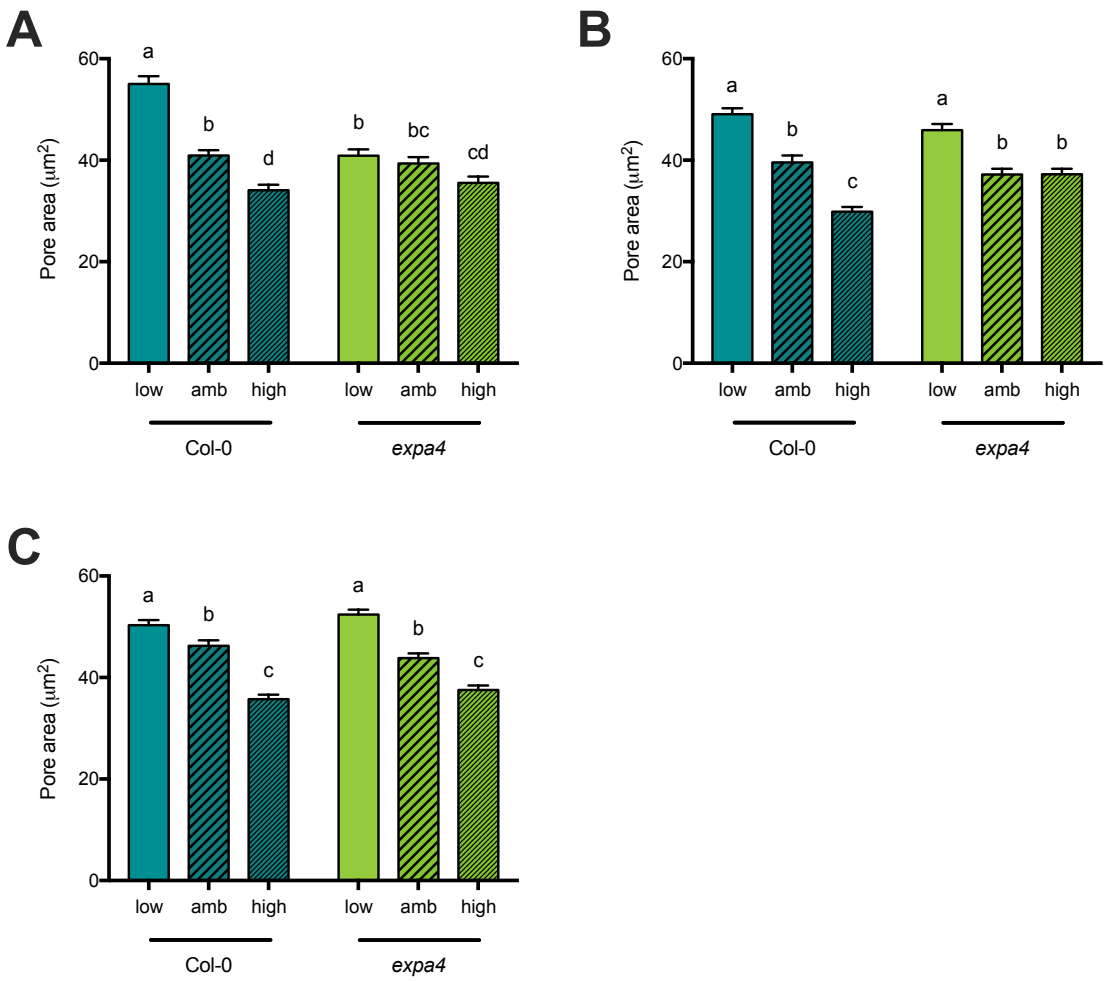

Figure 5.10 Assessing stomatal response to differing concentrations of CO_2 in Col-0 (blue) and *expa4* (green) leaf epidermal peels. (A-C) Each graph represents a different technical replicate. For each graph, epidermal peels were taken from Col-0 and *expa4* plants and were left in buffer through which high CO_2 (1000ppm), ambient CO_2 (400ppm) and CO_2-scrubbed air (low CO_2) was bubbled through for 2.5 hours. A two-way ANOVA was performed followed by a Tukey test. Within a dataset, samples indicated with the same letter cannot be distinguished from each other ($p<0.05$). Bars indicate mean ± SEM. Per treatment $n = 9$ plants.

and ambient-treated peels (Tukey test, $p>0.9999$, $n = 9$). However this time, the stomata opened similarly to Col-0 in response to low CO_2.

The third repeat seen in Figure 5.10C shows no difference in opening or closing response between Col-0 and *expa4* (Tukey test, $p>0.05$, $n = 9$).

The data suggest that there might be a stomatal phenotype in *expa4* but there is variation between individual experiments. Two independent experiments indicated that closure of *expa4* stomata in response to high CO_2 was decreased compared to Col-0, however one repeat showed no such differences and suggested that *expa4* stomata functioned similarly to wildtype. This variation between experiments means alternative independent data

must be attained before attempting to draw conclusions, therefore it was decided that other methods of assessing *expa4* stomatal function should be used to investigate further the effects of knocking out *expa4* on stomatal function.

5.4.2 Assessing *expa4* whole plant response to ABA

To gauge whether the *expa4* stomata showed an altered closing response to ABA, measurement of plant temperature was performed in a similar experiment to that described in section 5.3.3 where 5 µM ABA was applied to *expa16* and Col-0 plants and thermal imaging data collected. The results are shown in Figure 5.11.

60 minutes prior to the application of ABA, the mean plant temperature for both WT and *expa4* plants remained fairly consistent at 20.7°C (n = 12). The plants were then sprayed with either a mock solution or a 5µM ABA solution. After an initial drop in temperature, the mean plant temperature of plants sprayed with either solution increased at the same rate. The plants sprayed with the mock solution regain a similar temperature to before they were sprayed after 35 minutes and remain at 21.10 ± 0.07°. The plants sprayed with

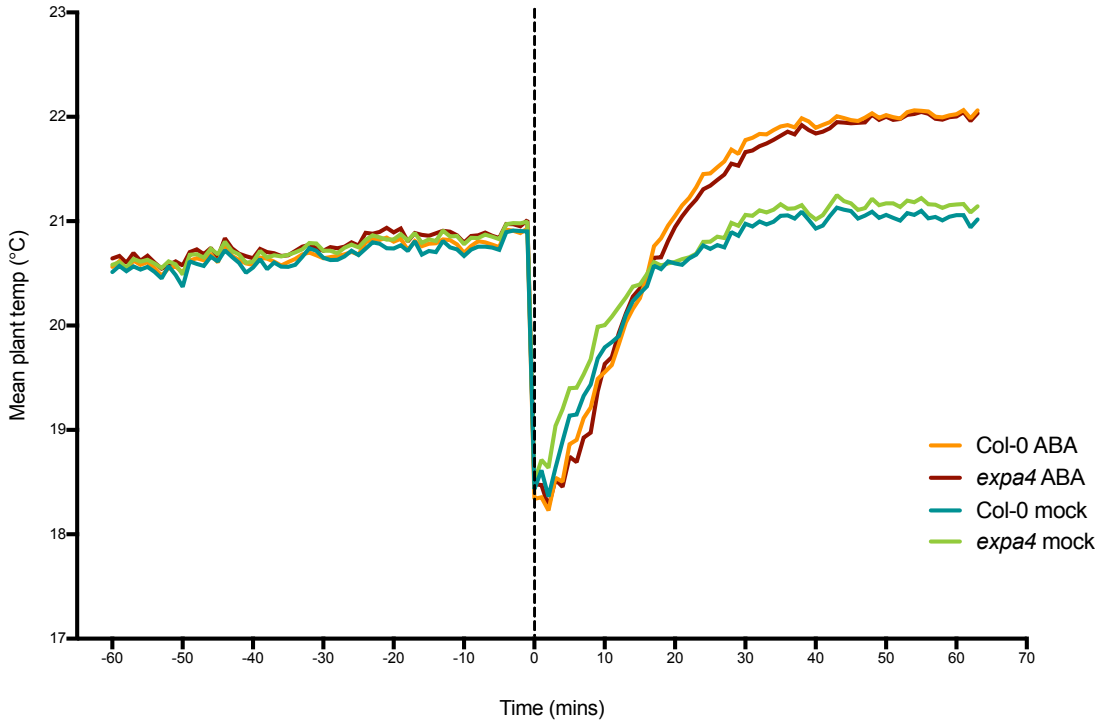

Figure 5.11 There is no difference between *expa4* and WT leaf thermal response to ABA. Mean plant temperature was calculated using an average of 3 leaf spots per plant using the genotypes indicated (*expa4* and Col-0 WT). After 60 minutes in ambient conditions, either a 5µM ABA solution or a mock solution (without ABA) was sprayed onto the plants (at the time indicated by the dashed line) and then plants were imaged for a further 60 minutes. Col-0 mock is represented by the blue line, *expa4* mock by the green line, Col-0 with ABA treatment in orange and *expa4* with ABA treatment in red. n = 12 plants per genotype from 2 technical replicates.

ABA reach a plateau 35 minutes after application of the solution and at a higher temperature of 22.00 ± 0.06°. There is no difference between the WT plants and *expa4* plants with either mock treatment or ABA treatment.

These results show that after ABA application, the mean temperature of the plants increased by an average of 1.3°, compared to plants that were sprayed with a mock solution which saw an increase in temperature of 0.4°. ABA causes stomata to close, reducing transpiration and therefore causing an increase in average leaf temperature.

However, there was no difference observed in plant temperature between WT and *expa4* samples, for either ABA or mock treatment. This supports some of the earlier data presented in section 5.4.1 which showed mixed results for the impact of CO_2 on *expa4* stomatal function using bioassays. Some of the data from CO_2 stomatal aperture bioassays also suggested there is no phenotypic difference in stomatal function between *expa4* and wildtype plants.

5.4.3 *expa4* plant response to drought

To further assess the impact of the reduced stomatal opening/closing range of *expa4* plants, a droughting experiment was performed similar to the one on *expa16* plants in section 5.3.4. Mean plant temperature of *expa4* and Col-0 plants was measured before and after a 5-day droughting treatment using a thermal imaging camera.

Figure 5.12 shows the results of this experiment. Before droughting, the average temperature of Col-0 leaves was 21.38 ± 0.25°C (mean ± SD, n = 6) and *expa4* leaves was 21.68 ± 0.28° (n = 6). After the 5 days without watering, the mean temperature of Col-0 leaves rose significantly when compared to the undroughted mean plant temperature to 22.44 ± 0.36° (Tukey test, df=45, $p<0.05$). The mean leaf temperature of *expa4* leaves also increased significantly, to 22.14 ± 0.36°. Stomata close in response to drought stress as a

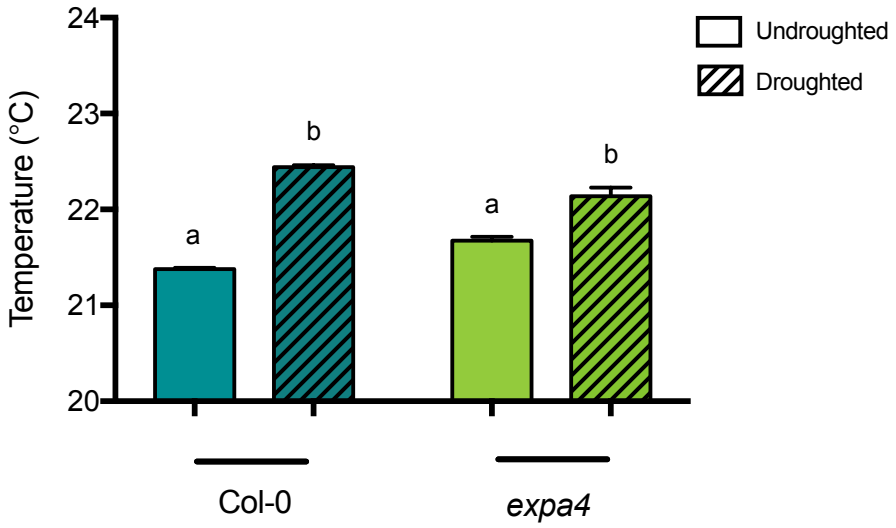

Figure 5.12 The mean leaf temperature of Col-0 (blue) and *expa4* (green) plants change in response to drought. Plants were imaged using a thermal imaging camera and mean leaf temperature was measured. The plants were then left for 5 days without watering and mean leaf temperature was measured via thermal imaging again. A two-way ANOVA was performed on the data set followed by a Tukey test and samples indicated by the same letter cannot be distinguished from each other ($p<0.05$). Mean ± SEM, $n = 4$ leaves from 6 plants per treatment.

way to conserve water, and so this increase in temperature after droughting is likely due to the stomata on the leaves closing.

However, when comparing treatment means across genotypes, there were no significant differences in plant temperature between Col-0 and *expa4*, either before or after the drought treatment. This suggests that *expa4* was behaving the same as wildtype Col-0 in terms of its stomatal response to drought and subsequent mean leaf temperature.

5.4.4 *expa4* stomatal conductance in response to shifting CO_2

In order to more precisely measure stomatal response to CO_2 on *expa4* leaves, CO_2 shifts on an IRGA were conducted on *expa4* and Col-0 plants (as performed on *expa16* plants in section 5.3.5). The results are shown in Figure 5.13. In ambient CO_2 conditions, the stomatal conductance of *expa4* was lower than that of Col-0, and when CO_2 increased to 1000ppm, the stomatal conductance in *expa4* halved and in Col-0 it decreased by about a two-thirds, with both lines reaching a similar level of conductance after a similar time. When the CO_2 was decreased to 100ppm, the level of stomatal conductance in both lines increased to above that measured in ambient CO_2, however the rate of increase was faster

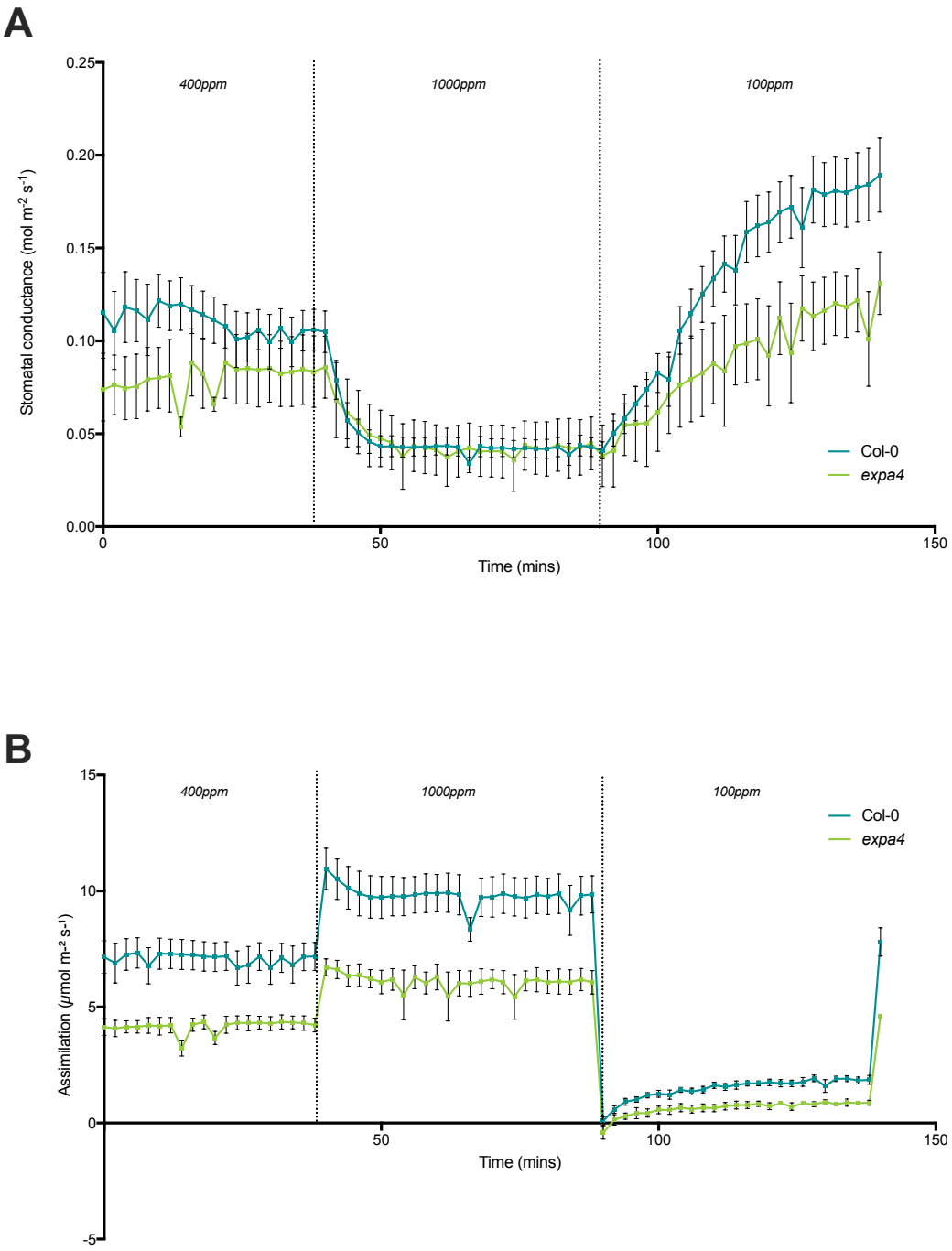

Figure 5.13 Stomatal conductance and assimilation of *expa4* (green) and Col-0 (blue) plants in response to shifting CO_2. (A) *expa4* plants do not have as high a stomatal conductance as Col-0 plants under ambient and low CO_2 conditions suggesting that they do not open as much as Col-0. **(B)** *expa4* plants generally have an assimilation rate lower than that of Col-0 regardless of the environmental CO_2 concentration. This is most notable at ambient and high CO_2 concentrations. Error bars = SEM, *n*=3 for *expa4*, *n*= 6 for Col-0.

in Col-0 than in *expa4*, suggesting that *expa4* stomata are slower to respond in decreases in CO_2. *expa4* also achieved a lower maximum of stomata conductance than Col-0.

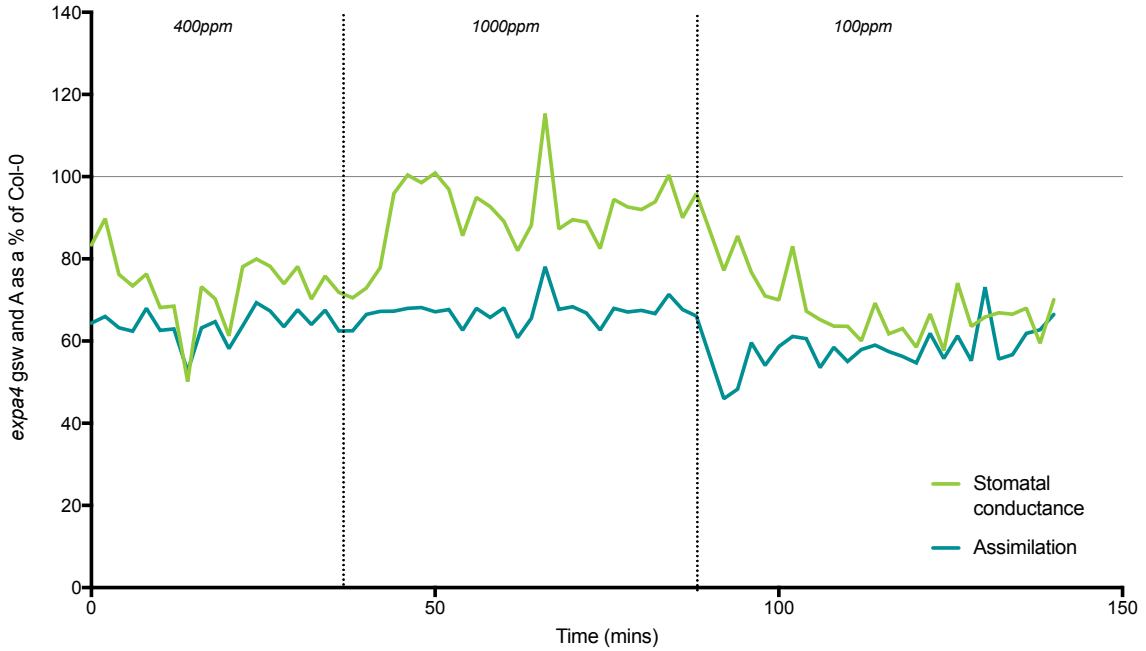

Figure 5.14 Stomatal conductance (green) and assimilation (blue) of *expa4* expressed as a percentage of Col-0 under a range of CO_2 levels. Data taken from the CO_2 shifts in Figure 5.13. A = assimilation (blue line), gsw = stomatal conductance (green line). *n*=3 for *expa4*, *n*= 6 for Col-0.

In all CO_2 conditions, assimilation was lower in *expa4* leaves than Col-0 although this difference was less pronounced under low CO_2 and more pronounced under high CO_2 (Figure 5.13B). *expa4* also exhibited a smaller range of stomatal conductance and assimilation than Col-0.

In Figure 5.14, the data from the CO_2 shift experiment shown in Figure 5.13 are arranged to express *expa4* stomatal conductance and assimilation as a percentage of Col-0 stomatal conductance and assimilation. Here it is clearer that *expa4* leaves have a consistently lower assimilation rate than the wildtype at around 60-70% of Col-0. Stomatal conductance in *expa4* differs more than assimilation rate, reaching around 90% of Col-0 stomatal conductance in high CO_2 conditions and decreasing to 60% of Col-0 conductance in low CO_2. These data indicate that the loss of *expa4* results in a reduced range of stomatal movement under different CO_2 conditions, especially with respect to the opening response.

5.4.5 Stomatal density in *expa4* plants

Stomatal density was calculated to assess if this was altered in the *expa4* leaves. The average stomata per mm^2 on WT leaves was 219 ± 50 (mean ± SD, *n* = 9), and on *expa4*

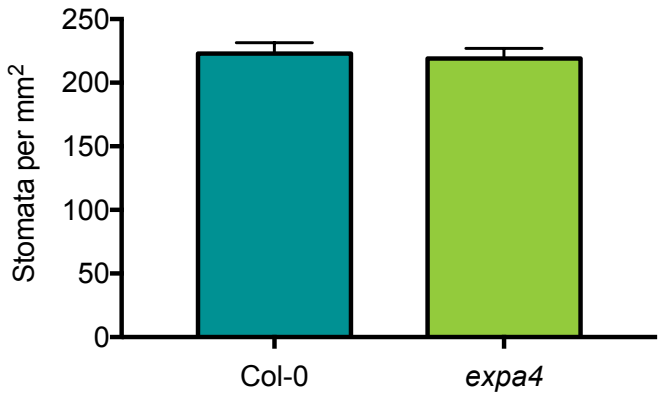

Figure 5.15 Stomatal density from the abaxial side of leaves of WT and *expa4* plants. Unpaired t-test, p>0.05. Mean ± SEM, *n* = 3 views per leaf, 3 leaves per plant, 3 plants per genotype.

leaves this was 224 ± 55 (*n* = 9) (Figure 5.15). There was no significant difference observed between average stomata per mm^2 on WT leaves and *expa4* leaves (unpaired t-test, df=72, p>0.05).

5.4.6 Repeat PCR genotyping of *expa4* plants

The results detailed in this section exhibited high levels of variation both within experiments and between experiments, meaning that *expa4* was difficult to robustly characterise in terms of its stomatal function. Towards the end of this series of experiments I re-visited the *expa4* mutant line to try and identify potential reasons for the observed variability recorded.

DNA was extracted from four *expa4* plants and two Col-0 plants and a genotyping PCR was performed as described in section 5.3.1, using the primers appropriate to the gene and T-DNA insertion, as well as actin primers as a positive control. The results are shown in Figure 5.16. Each gDNA sample showed a PCR product when the actin primers were used as a positive control. The two Col-0 gDNA samples showed a band in the LP + RP sample, indicating that the endogenous *EXPA4* sequence was present. Three out of four of

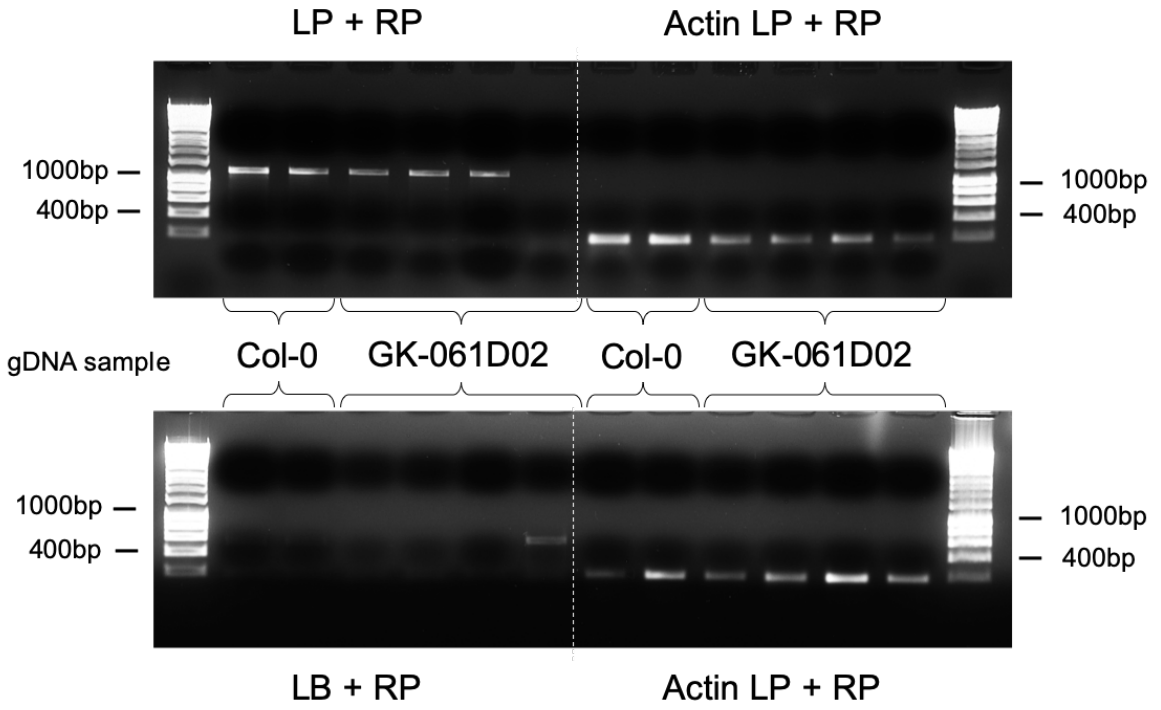

Figure 5.16 PCR genotyping of transgenic line GK-061D02 (*expa4*). Above left, the PCR reactions using *expa4* left primer (LP) and right primer (RP) (a band indicates presence of the wildtype allele). Below left, the PCR reactions using the Salk left border (LB) primer and *expa4* RP (a band indicates presence of the T-DNA insertion). Above and below right, the PCR reactions using an actin LP and RP as a positive control. The first two lanes in each section represent Col-0 gDNA, and the last four lanes represent *expa4* gDNA. Ladders on both are 1kb ladders from Bioline with relevant band sizes pointed out. Expected product sizes were: LP+RP = 1186; LB+RP = 600; Actin = 200bp.

the GK-061D02 (putative *expa4* samples) gDNA samples had a band in the LP + RP column and not the LB + RP column, and one sample had a band in the LB + RP column and not in the LP + RP column. This indicates that three out of four of the GK-061D02 plants did not have the T-DNA insertion but did have the *EXPA4* sequence and, therefore, were not *expa4* knock down mutants, i.e., the plants were from a segregating population.

5.5 Discussion

The work in this chapter first of all aimed to identify α-expansins with a relatively higher transcript level in guard cells than leaf tissue based on in-house and public databases. The data suggested that many expansins are expressed in guard cells but two are expressed to a high level in guard cells, *EXPA4* and *EXPA16*. I then took the approach of identifying mutant lines lacking specific α-expansin expression, as this method would provide evidence for endogenous function. As α-expansins are a multi-gene family, there is always potential for gene redundancy, but analysis of single gene knock-outs is a valid first approach before using more complicated approaches aimed at reducing or removing expression of multiple expansin genes (e.g. Goh et al., 2012).

The analysis described here identified *EXPA4* and *EXPA16* as lead expansin genes with a potential role in guard cell function, providing data in support of Hypothesis II, that expansins were expressed in some levels in guard cells. To analyse stomatal function in mutant lines of these genes, *expa4* and *expa16*, I took a combined functional approach to measure stomatal function both directly and indirectly. This included assays based on direct viewing of stomata in isolated epidermal strips triggered to open or close through altered CO_2 levels and an indirect assay of stomatal function (thermal imaging of intact plants after treatment with a chemical (ABA) or environmental (drought) stomatal-closure inducer), as well as stomatal gas exchange in intact leaves using an IRGA.

The results of these analyses led to data suggesting that stomatal function was abrogated in at least one of the mutants, which supports Hypothesis III, that loss of expansins would lead to altered stomatal function. However, the mechanistic interpretation of the data was complicated both by a degree of variability in the data obtained (particularly with *expa4*) and by some of the phenotypes observed being difficult to reconcile within the analysis of each mutant line. The data for each line is discussed below.

5.5.1 The role of *EXPA16* in stomatal function and plant physiology

The CO_2 stomatal aperture bioassay performed on *expa16* and Col-0 epidermal peels provided strong evidence that stomatal opening is abrogated in *expa16* when compared to Col-0 in response to low CO_2, providing data to support Hypothesis III in the aims/objectives of this chapter. This experiment also showed that the *expa16* closing

response was more limited, but not absent, in response to high CO_2. This was in contrast to the thermal imaging experiment in which *expa16* and Col-0 plants were exposed to ABA, the results of which showed that *expa16* plants were hotter after being ABA-treated. This suggests that *expa16* stomata were more closed in response to ABA which therefore reduced transpirational cooling, which is not the same closing response seen after high CO_2 treatment in the bioassay.

It was expected that drought treatment would encourage plants to close their stomata, so to further test the closing response in *expa16*, a thermal imaging drought experiment was conducted. This showed that there was no difference in whole plant temperature between *expa16* and Col-0 after 5 days of drought, which indicates that any stomatal abnormality seen in *expa16* is having little effect on its drought tolerance. It also provides evidence that the closing response of *expa16* stomata is not dissimilar to that of Col-0, or, in context of the previous data, that whether or not the *expa16* stomata are more or less closed than wildtype, the response evens out at a whole plant level.

The data from the CO_2 shifts on the IRGA shows that there are some differences in gas exchange parameters between Col-0 and *expa16*, providing evidence supporting Hypothesis IV in the aims/objectives of this chapter. Stomatal conductance in *expa16* was consistently lower than Col-0, especially in low CO_2 conditions, which contradicts the results from the bioassay. This suggests that even though the stomata were not closing as much in response to high CO_2, the stomatal conductance is lower. Assimilation of *expa16* plants was lower than Col-0 in ambient and high CO_2 conditions but not low CO_2 conditions.

Overall, these data indicate that there is a change of stomatal properties compared to wildtype when *expa16* is put under strong stimuli, such as high and low CO_2 concentrations in epidermal strips, but that when the stomata are in intact leaves under less extreme conditions the differences from control plants is obscured. The bioassay data indicates a smaller dynamic stomatal range (similar to *expa4*), as do the measurements of stomatal conductance under different CO_2 concentrations, yet there is also evidence for *expa16* stomata being more closed than wildtype under certain conditions.

The data suggest that knocking out *EXPA16* may result in a poorer performance in terms of stomatal conductance and carbon assimilation in the leaves, but that this is not enough

to have any significant effect on whole-plant physiology such as its resistance to drought or overall plant growth. *expa16* stomata may be more sensitive to closing stimuli, but this closing response comes with a relative decrease in assimilation, so conclusions about water use efficiency are difficult to make.

There is no literature that I am aware of that links *EXPA16* to stomatal function. One study into peach domestication and fruit edibility found that a peach *EXPA16* ortholog had increased its genetic copy number during domestication (Yu et al., 2018) and the paper suggested it may have a role in fruit texture and ripening, consistent with previous data on the role of expansins in fruit ripening (Brummell et al., 1999; Harrison et al., 2001).

5.5.2 The role of *EXPA4* in stomatal function and plant physiology

Investigation into stomatal function in *expa4* plants revealed high levels of variation both between and within experiments. Although initial analysis at the start of the project indicated the seed stock used was a homozygous T-DNA knock-out insertion in the *EXPA4*, upon further investigation it was apparent that it was in reality segregating (Figure 5.16). For this analysis four GK-061D02 plants were genotyped and three were revealed to be wildtype, so although this is too small a sample size to say for certain that 75% of the GK-061D02 seeds do not contain the mutation, it is likely that a significant proportion do not contain the T-DNA insertion in the *EXPA4* gene. This provides a probable explanation for the high degree of variability seen in the *expa4* data, because if only some of the plants used in these experiments were true knock out mutants and the rest were either heterozygous or wildtype, then this would reduce or remove any potential differences seen between *expa4* and Col-0. Therefore any interpretation of the *EXPA4* data must at this stage be treated with caution.

Thus, although the stomatal aperture bioassays on *expa4* (Figure 5.10) indicated a loss of stomatal closure in response to high CO_2, one replicate showed no difference in stomatal aperture response of *expa4* relative to Col-0. Thermal imaging revealed that there was no temperature difference between *expa4* and Col-0 plants before or after ABA treatment, and there was no difference between *expa4* and Col-0 in overall plant temperature after 5 days of drought treatment. Finally, IRGA data indicated that stomatal conductance of *expa4* plants was lower in ambient and low CO_2 conditions than Col-0, which suggests stomata are more shut in *expa4* than Col-0. This contrasts to the bioassay data showing a

decreased closing response in *expa4*. Assimilation of *expa4* plants in all three CO_2 conditions was 40% lower than that of Col-0 plants.

Previously, there has been no evidence linking *EXPA4* to stomatal function and so this data, while difficult to interpret, is a novel contribution to the collective knowledge of α-expansins.

Overall, although the data presented here on the role of *EXPA4* on stomatal function are inconclusive, they do provide some indicators on the general role of (and challenges of investigating) expansins in guard cell function. This is discussed in the following section.

5.5.3 The role of α-expansins in stomatal function

Expansins are an interesting candidate for studying in relation to stomatal function because it is known that guard cell wall properties can have huge effects on stomatal movement and expansins are established modulators of cell wall extensibility (Amsbury et al., 2016; Carter et al., 2017; Jones et al., 2003; Wei et al., 2011; Zhang et al., 2011). However, there has been little work published so far linking the two. A group investigating the effects of *EXPA1* overexpressed in Arabidopsis found that stomata in the transgenic overexpressor line opened faster in response to light and also had an increased photosynthetic and transpiration rate (Wei et al., 2011; Zhang et al., 2011), but otherwise there are no functional data implicating expansins in stomatal function.

The data presented in this chapter indicate that if some α-expansins which are highly expressed in guard cells are knocked out (e.g. *EXPA16* and *EXPA4*), this results in a more limited stomatal range in certain conditions which, in turn, can have an effect on plant assimilation. These data make sense when considered in the context of previous investigations into expansins and guard cell function. As a general rule, if expansins are over expressed, increased expansin activity means the stomata can respond faster to opening stimuli which results in an increase in photosynthetic rate. If expansins are knocked out, stomatal response is abrogated and stomatal conductance and assimilation of the plants is more limited. This implies that expansins may provide elasticity and stretch to the guard cell walls, contributing to some degree to the stomatal response to opening and closing stimuli and having an effect on overall plant gas exchange.

However expansin over-expression also leads to an increase in transpiration (Wei et al., 2011) and therefore water loss, which is likely due to the stomata being open wider and for longer than normal. Therefore, it is possible that the amount of expansin activity in the guard cell wall is a fine balance: too much activity and water use efficiency decreases due to the increase in transpiration rate caused by the flexible cell wall opening the pore too much or too early; too little expansin activity and the guard cell wall is so rigid that the pore cannot change and therefore assimilation rate drops.

5.5.4 Limitations and future work

The work done in this chapter builds upon previous work (Wei et al., 2011; Zhang et al., 2011) investigating the role of α-expansins in stomatal function. By investigating two more α-expansin genes – *EXPA4* and *EXPA16* – through functional analysis of single gene knock-outs, I have found that at least one of these genes (*EXPA16*) may have a role in stomatal function. However, there are a number of lines of future work required to fully substantiate these data, discussed below.

The two α-expansins studied here were identified as having a potentially important role in guard cells due to their relatively high expression following an analysis of a microarray data set. Consultation of a second independent online dataset (EFP browser) revealed a similar pattern of expression of *EXPA4* and *EXPA16*, validating the microarray data. However, there is evidence that expansin proteins are turned over and can be up- or down-regulated quickly (Cosgrove, 1999; Harrison et al., 2001; Lee et al., 2003). Thus even though it appeared that they were highly expressed in guard cell tissue compared to whole leaf tissue, this does not mean guard cells have this level of expansin expression continuously. In addition, transcript expression does not always correlate with protein level, so just because *EXPA16* and *EXPA4* show a high level of gene expression in certain tissues, this does not mean that this translates to expansin protein activity. Nevertheless, measuring expansin transcript levels and distribution is a common and valid way of estimating expansin activity (Cho and Kende, 1998).

Unfortunately, during this project it was discovered that the seed stock of *expa4* used was in fact segregating (Figure 5.16), so the data for this mutant line may not reflect the true reality of stomatal function in *expa4* knock-out mutants. Identifying a true homozygous mutant line for *expa4* is essential, followed by revisiting the experimental procedures

outlined in this chapter to see if any different – potentially stronger – and more reliable phenotypes are seen in terms of stomatal function in *expa4*.

It should also be noted that in this chapter only one mutant line for *EXPA16* and *EXPA4* were analysed. Confirmation of the phenotypes observed in independent knock-out or knock-down lines is required. This could be achieved by identifying further T-DNA lines or by generating RNAi or CRISPR-CAS9 mutants. In addition, formal complementation of the *EXPA16* and *EXAPA4* mutants is required to demonstrate that any phenotype observed is due to the loss of the mutated gene.

Further proof in support of this hypothesis would require restoration of normal (wildtype) stomatal function by restoration of *EXPA16* or *EXPA4* gene expression to guard cells. Identification and characterisation of complemented *expa4* and *expa16* lines would provide a more complete view of these. During the PhD, I made a start on complementing the *expa4* line by using both the wildtype *EXPA4* promoter and also using a guard cell-specific promoter, however I ran out of time before completion of this project. In addition, the mutants studied in this chapter lack relevant *EXPA* gene expression throughout the plants, so it is theoretically possible that any phenotype observed is not directly related to loss of expansin gene expression only in the guard cells. Complementation or RNAi experiments using guard cell specific promoters would be an ideal way of exploring this possibility.

A further limitation of the study is that α-expansins are encoded by fairly large gene family and the data indicate that several of these genes are expressed in Arabidopsis guard cells, i.e., *EXPA16* and *EXPA4* are highly expressed but they are by no means the only expansins expressed in these cells. The loss of a single gene, *EXPA1*6, is likely to lead to a quantitative outcome rather than total loss of expansin activity. Thus, a quantitative effect on guard cell function might be expected. The data in this chapter therefore supports the hypothesis that α-expansins are required for normal stomatal function (Hypothesis III), but in future work an attempt to make multiple knock-downs to see if this leads to a more dramatic phenotype (such as its drought response) could be attempted. This could be done by crossing *expa4* and *expa16* to create a double mutant, or using an artificial microRNA (amiRNA) system to more specifically silence multiple α-expansin genes, as demonstrated in Goh et al., 2012.

In this chapter a number of methods, both direct and indirect, were used to assay stomatal function, with the different approaches sometimes producing apparently contradictory results. For example, the bioassays in this chapter have been performed on mature leaf epidermal peels. This is a well-established method in the field of stomatal biology (e.g. Webb and Hetherington, 1997; Li et al., 2013; Elhaddad et al., 2014), however as discussed in Chapter 4, there are valid concerns about the structural integrity of these peels. Whole leaf or whole leaf segment bioassays are a potential method to explore in future when directly assessing stomatal function through bioassays such as these. It is possible that the use of epidermal peels reveals elements of altered stomatal opening/closing which are obscured or dampened in a physiologically more realistic situation where intact leaves are used. Again, the use of multiple knock-outs or amiRNA constructs might lead to larger changes in expansin expression level and, thus, a more dramatic phenotype.

Despite these limitations, the data presented in this chapter indicate that loss of *EXPA16* gene expression does lead to altered stomatal function. Stomatal function in *expa16* plants generally results in a lower photosynthetic rate than their wildtype counterpart, and they have a smaller dynamic range in terms of stomatal aperture. It is likely that these phenotypes are only be seen after exposure of stomata to extreme stimuli, such as in very high or low concentrations of CO_2, or under extreme physiological conditions, for example when measurements are taken from epidermal strips. Future work to corroborate these data and to extend the analysis to other members of the expansin gene family are required.

5.6 Key findings

- Expansins are a likely candidate for short-term modification of the guard cell wall. Two expansin genes, *EXPA4* and *EXPA16* are highly expressed in guard cells.
- In extreme conditions, *expa16* mutants display a reduced dynamic stomatal range, and have a lower photosynthetic rate than wildtype plants. However, these differences do not have a significant effect on whole-plant physiology e.g. plant growth.
- Some data suggest that *expa4* plants may also display differences in stomatal function, however further work is necessary to describe to what extent.
- The data in this chapter combined with previous work into the link between altered expansin expression and differences in stomatal function suggest that expansins do

play a role in stomatal function. It is likely that expansins provide a degree of elasticity to the guard cell wall which, upon an increase in guard cell turgor pressure, increases loosening of the guard cell wall and allowing cell wall stretch, cell expansion and therefore opening the pore.

Chapter 6: Discussion

Guard cell shape change is a product of the interaction between internal turgor pressure of the cell and the guard cell wall, and is essential for guard cell function (Carter et al., 2017; Meckel et al., 2007; Woolfenden et al., 2018, 2017; Yi et al., 2018). The research presented in this thesis provides novel insights into shape change of Arabidopsis guard cells and the role of the cell wall in guard cell shape and stomatal function.

In Chapter 3, the development of a new method is described to image stomata on live plant tissue and to use these images to generate 3D data about guard cell shape change during stomatal opening/closing. It was concluded that light sheet fluorescence microscopy (LSFM) could successfully be used to take images of stomata on Arabidopsis seedlings, and the images taken from early experiments in this project were in line with the quality of previously published LSFM images of the leaf surface (Ovečka et al., 2018, 2015). Despite this, these images were unsuitable for the 3D reconstruction of guard cells. Since there has been no evidence to date of guard cells imaged to the level of detail needed for this analysis using LSFM, it is likely that this is simply a limitation of this technique. This should be taken into account when planning future microscopy experiments to generate data for computational 3D reconstruction. It was decided that confocal microscopy was a more suitable method for generating the higher resolution images required for 3D reconstruction.

Z-stacks of stomata were taken on a confocal microscope and processed in LithographX (Barbier de Reuille et al., 2015). Although this programme, and its sister programme MorphographX, have been used to reconstruct various plant cells in 3D (e.g. Montenegro-Johnson et al., 2015; Kirchhelle et al., 2016; Kiss et al., 2017; see Appendix 8.2 for more details), to my knowledge this method has never been used before to segment and reconstruct guard cells in 3D. The application of this processing method to reconstruct stomata fulfils one of the aims of this thesis and further reinforces confocal microscopy as a dominant method for imaging plant cells to high resolution (Ovečka et al., 2018).

Once I had optimised this method, stomata were imaged in either a closed, open or a resting state and data extracted from the guard cells to describe differences in volume, surface area, and other shape change parameters between the three treatments. Whilst

guard cell shape change has been observed by those studying stomatal biology for a long time (Cooke et al., 1976), this thesis presents the first detailed characterisation of this shape change in Arabidopsis and one of the few to do so in 3D.

The results from this work supported previous observations that guard cells change shape significantly during opening and closing. Both the volume and surface area of the cells increased during the transition from a closed to an open state, echoing previous observations (Meckel et al., 2007; Shope et al., 2003). Interestingly, surface area: volume ratio decreased during opening. This suggests a shape change was occurring during this process, and that the growth of the guard cell is anisotropic (Marom et al., 2017; Woolfenden et al., 2018, 2017), which was supported when cross section shape was characterised. When closed, guard cells were ellipsoid in cross section, whereas open stomata had more circular guard cell cross sections. This has not been experimentally tested before but provides evidence in accordance with previous suggestions (Bidhendi and Geitmann, 2018; Cooke et al., 1976; Shope et al., 2003). However, despite this significant shape change, the perimeter length of the cross-sections did not change during opening/closing, further suggesting a degree of shape change in the cells not captured in the midpoint cross sections. In order to explain the difference in surface area seen at a whole cell level, the length of guard cells when stomata were open and closed was measured which showed that guard cells lengthen significantly as the pore widens (also seen in Meckel et al., 2007).

A significant discovery related to the ellipsoid/circular cross-sectional shape change was that the guard cells shifted angle as they opened or closed, pivoting downwards as the cells increased in turgor pressure and opened the pore. These findings contradict the traditional view of sausage-shaped guard cells moving laterally to open and close the pore, and highlights the importance of accounting for more complex shapes in models of stomatal function. Although simplified guard cell geometries, both in terms of shape and cell wall composition, allows for exploration of specific parameters within the simplified model (Cooke et al., 1976; Shope et al., 2003; Woolfenden et al., 2018, 2017), the data presented in this chapter shows that models of guard cell shape need updating. This presents a useful and novel insight into guard cell shape which will likely advance future stomatal modelling, and fulfils another thesis aim.

As discussed in Chapter 3, this imaging method is not without its limitations. A recurring theme in this thesis has been that epidermal peels may not necessarily reflect stomatal function or guard cell shape change in the intact leaf (see also the *arp3* phenotype in Chapter 4, and the expansin knockouts in Chapter 5), therefore care must be taken when interpreting these results. However, the imaging results offer quantifiable support for previous observations on guard cell shape from other studies (e.g. cross-section shape and guard cell lengthening) suggesting that they hold validity.

The importance of guard cell shape is highlighted in Chapter 4, in which I investigated the stomatal characteristics and function of a knockout of a gene encoding an ARP2/3 subunit, ARP3. This transgenic line exhibited an abnormal opening phenotype in which about a quarter of *arp3* stomata bowed outwards to form a hyper-opened "doughnut"-shaped pore in response to low CO_2. This this was seen in epidermal peels, and there were also differences in assimilation and stomatal conductance between *arp3* and wildtype measured at the whole-plant level. Gas exchange measurements indicated that under low CO_2 conditions *arp3* had a lower stomatal conductance than Col-0, which is difficult to reconcile within the bioassay analysis in which the strong phenotype of the hyper-opened stomata seen on epidermal peels was under low CO_2 conditions. The gas exchange data also suggested that the loss of *ARP3* function led to a lower plant water use efficiency than the wildtype, especially under high CO_2. These results further highlight the importance of using multiple techniques at different scales to fully assess stomatal function.

I also investigated the possibility that the abnormal stomatal phenotype seen in *arp3* peels was caused by guard cell wall defects, as previous literature has linked mutants of the ARP2/3 complex with abnormality in the delivery of components to the cell wall (Pratap Sahi et al., 2017; Yanagisawa et al., 2015). I used immunolabelling of pectin components in fixed and sectioned *arp3* leaf tissue but found no evidence to suggest that there was any difference in guard cell wall composition between *arp3* and the wildtype. Therefore, the mechanism causing the doughnut-shaped *arp3* stomatal phenotype remains to be explored. There is a possibility that the impaired vacuolar fusion previously observed in *arp3* stomata (Li et al., 2013) is contributing to this phenotype, as vacuoles are important in maintaining guard cell shape through hydrostatic pressure (Eisenach et al., 2015; Gao et al., 2005). Indeed, the ARP2/3 complex has been linked to the morphology of other cell

types, such as pavement cells (Li et al., 2003; Qian et al., 2009). This provides an interesting route for future investigations into *arp3* stomatal function and the role of the ARP2/3 complex in the guard cell.

In Chapter 5 I identified two Arabidopsis α-expansin genes that were highly expressed in guard cells when compared with mesophyll tissue – *EXPA16* and *EXPA4* – and characterised knockouts of these in terms of their stomatal function.

I found evidence to suggest that *expa16* plants have abrogated stomatal function which translated to reduced stomatal conductance and a lower rate of assimilation at a whole-plant level under differing levels of CO_2. However, this did not convert into any differences in plant growth or drought response. Considering that the α-expansin family in Arabidopsis is large, and that these expansins are not the only expansins expressed within the guard cells, it is highly likely that there is some degree of functional redundancy within this gene family.

I also characterised an *expa4* mutant in terms of its stomatal function and the impact of losing *EXPA4* function on whole plant physiology using similar techniques to those used to investigate *expa16*. A high degree of variability within these datasets was later explained by the fact the seed population was in reality a segregating population, and therefore the plants used for these experiments were a mixture of *expa4* (likely both homozygous and heterozygous) and wildtype. Although an unfortunate discovery, this highlights the importance of regular PCR genotyping within transgenic experiments to ensure seed stocks and plants are what they say they are. Whether the occasional stomatal phenotype observed in this segregating population of *expa4* mutants was indeed linked to loss of expansin function remains to be tested.

The results presented in Chapter 5 do to some extent suggest expansins play a role in stomatal function. As discussed in Chapter 1, endogenous proteins might allow modification of the plant cell wall in response to short-term stimuli (Braidwood et al., 2014) and expansins could provide this short-term modification (Cosgrove, 2005, 1999). As the guard cell wall expands and contracts repeatedly and often within minutes of a stimuli, expansins are a likely candidate for providing some of this short-term extensibility. Previous research found that stomata from a transgenic line overexpressing *AtEXPA1* opened faster and wider than wildtype, and that these plants had a higher

transpiration rate and increased photosynthetic capacity (Wei et al., 2011; Zhang et al., 2011). My results fit with these findings. If overexpressing an α-expansin gene results in faster and wider opening and knocking out an expansin gene decreased stomatal range (section 5.3.2), this suggests that expansins are indeed providing elasticity to the guard cell wall.

6.1 Future perspectives

The data presented in this thesis provide significant advances into what we know about stomatal function and guard cell shape. However, some critical questions remain, and this thesis has opened up the potential for more areas of study. In this section I will propose more experiments to follow up the work I have done here.

The development of the confocal method into a reproducible technique for large scale (>50 stomata per treatment) quantification of guard cells in 3D offers significant opportunity for future work. Here I have provided data of plasma membrane-tagged myr-YFP guard cells in a Col-0 background, but characterising other transgenic mutants labelled with this YFP membrane marker would be an ideal way of measuring guard cell shape change in other lines. Towards the end of this thesis I transformed *arp3* with the myr-YFP construct in order to characterise the doughnut-shaped stomata that occur upon application with low CO_2 in 3D. Unfortunately, these plants were not ready for analysis within the time frame of this thesis, but they provide an experimental tool to characterise guard cell shape change in an *arp3* background in the future. Other interesting stomatal phenotypes that have significant cell wall deformations or known opening/closing impairments could be further examined. Additionally, using another type of membrane dye, e.g. FM4-64, to visualise the epidermal cells adjacent to the stomata on the confocal and then using the same process on LithographX to reconstruct these pavement cells would be interesting, allowing examination of shape and volume changes of pavement cells during stomatal movement.

This technique also has potential for dynamic imaging. Using this method to image stomata had a time restraint as each guard cell z-stack took approximately 5 minutes, but this method could potentially be further refined to make each z-stack quicker. Experimentation with image size and speed would be useful to do this. This would then lend itself to time-lapse experiments, wherein a 3D stomata could be viewed and imaged

whilst opening and closing, which could answer further questions on stomatal opening/closing rate and more detailed characterisation of shape change.

Applying the imaging technique beyond Arabidopsis is another route future work could take. However, due to the relative difficulty I had with optimising this method, careful choice of species would prove beneficial as some plants are thought to be more difficult to manipulate than others. Grasses with subsidiary cells flanking the stomata provide an attractive area of study, as it would be interesting to explore volume changes between guard cells and subsidiary cells, and also to investigate changes in shape/volume within the grass guard cells to see by how much, if any, the mechanisms of stomatal opening and closing differs between dicots and monocots.

Previous work found a link between the ARP2/3 complex and stomatal function (Jiang et al., 2012; Li et al., 2014) and my work reinforces this idea. To explore the possibility that the unusual guard cell shape seen in *arp3* epidermal peels is caused by altered vacuolar function, a fluorescent-tagged (e.g. GFP) tonoplast line could be crossed or transformed into the *arp3* mutant and vacuolar number/shape visualised by fluorescence microscopy. Application of different stomatal triggers may illuminate differences in vacuole morphology between *arp3* and the wildtype background, which may explain this unusual guard cell shape.

There is potential for cloning work in the *arp3* and expansin projects. A common way of validating results produced by experiments on T-DNA knockouts (such as the CO_2 bioassays in Chapters 4 and 5) is to make complemented lines in which the wildtype gene is reintroduced to the transgenic line. This could be under a more general promoter, such as 35S promoter, under the native promoter of that gene, or under a tissue-specific promoter, such as a guard cell-specific promoter. The *arp3* line has a significant physiological phenotype, especially its smaller rosette size and gas exchange differences, so I would therefore be interested to introduce the *ARP3* gene under a guard cell-specific promoter in an *arp3* background and studying it in terms of its stomatal function and whole plant physiology. This would indicate to what extent these whole-plant phenotypic differences are as a result of impaired stomatal function. For example, the distorted trichomes seen in *arp3* mutants may not be remediated but the differences in stomatal conductance might, which may therefore have an effect on plant growth and leaf/rosette

size. In the case of *expa16*, using an *EXPA16* promoter or a guard cell-specific promoter would both be useful in similar complementation experiments.

Repeating the genotyping of *expa4*, and the replication of the experiments done in Chapter 5, is of course an obvious continuation of this project. Furthermore, due to the high chances of functional redundancy within the α-expansin gene family, transgenic lines with multiple expansins knocked out may provide a more dramatic phenotype to explore in more detail the effects of knocking out expansins on stomatal function.

To conclude, this thesis provides significant advances into the characterisation of shape and shape change in Arabidopsis guard cells. It has been shown that the ARP3 subunit of the stomatal complex contributes to normal guard cell shape and that the knockdown *arp3* has substantial phenotypic defects at the whole-plant level. Both my work presented here and previous work into expansins and stomatal function (Wei et al., 2011; Zhang et al., 2011) indicate that expansins play a role in the guard cell wall. The study of expansins in particular provides a potential target for further manipulation of the guard cell wall to optimise water use efficiency. As assimilation and stomatal conductance often prove to be asynchronous, meaning more water may be lost than necessary (Lawson and Blatt, 2014; Lawson and Vialet-Chabrand, 2018), finding cell wall mechanisms by which stomata open or close more rapidly provides a potential target for future crop improvements.

In the future, my data from the 3D reconstructions of guard cells will feed into stomatal mechanical models that are being developed to provide a deeper understanding of the control of gas exchange in plants, a key problem in plant biology of relevance to food security and climate change. Investigations into altering guard cell wall components integrated with cell shape data contribute to a more comprehensive view of the specialised guard cell wall and its effects on guard cell mechanics, laying the groundwork for future exploration into the structure and function of stomata.

6.2 Key messages

- Stomata are incredibly important to plant survival and a significant amount of research has gone into different aspects of the stomatal system including stomatal development, signalling and physiology. However, despite the fact that stomata are so

well-studied, we have very little knowledge about a fundamental aspect of guard cells: their 3-dimensional shape.

- Several stomatal function models have indicated that shape change of guard cells during stomatal opening and closing is essential to stomatal function. This thesis provides a detailed method of guard cell shape quantification in 3D which provides characterisation of Arabidopsis wildtype guard cells, and also has a great amount of potential for future work. This can then be used as a point of comparison to characterise, for example, known stomatal mutants or stomata after enzyme modification.
- Understanding guard cell shape change in Arabidopsis lays the groundwork for translation into crop research. Learning more about genetic contributors to guard cell shape change allows us to identify target genes for guard cell wall/geometry optimisation. Developing methods of quantifying guard cell shape in Arabidopsis encourages the movement of these methods into plant species that may be more complex e.g. stomata with subsidiary cells.
- Stomatal opening and closing is key to the instantaneous water use efficiency of plants. Altered cell wall geometry may lead to variant dynamics of stomatal conductance which may therefore further provide targets for crop improvements.

Chapter 7: References

Albenne, C., Canut, H., Hoffmann, L., Jamet, E., 2014. Plant Cell Wall Proteins: A Large Body of Data, but What about Runaways? Proteomes 2, 224–242.

Alonso, A.P., Piasecki, R.J., Wang, Y., LaClair, R.W., Shachar-Hill, Y., 2010. Quantifying the labeling and the levels of plant cell wall precursors using ion chromatography tandem mass spectrometry. Plant Physiol. 153, 915–24.

Alonso, J.M., Stepanova, A.N., Leisse, T.J., Kim, C.J., Chen, H., Shinn, P., Stevenson, D.K., Zimmerman, J., Barajas, P., Cheuk, R., Gadrinab, C., Heller, C., Jeske, A., Koesema, E., Meyers, C.C., Parker, H., Prednis, L., Ansari, Y., Choy, N., Deen, H., Geralt, M., Hazari, N., Hom, E., Karnes, M., Mulholland, C., Ndubaku, R., Schmidt, I., Guzman, P., Aguilar-Henonin, L., Schmid, M., Weigel, D., Carter, D.E., Marchand, T., Risseeuw, E., Brogden, D., Zeko, A., Crosby, W.L., Berry, C.C., Ecker, J.R., 2003. Genome-wide insertional mutagenesis of Arabidopsis thaliana. Science 301, 653–7.

Amsbury, S., Hunt, L., Elhaddad, N., Baillie, A., Lundgren, M., Verhertbruggen, Y., Scheller, H. V., Knox, J.P., Fleming, A.J., Gray, J.E., 2016. Stomatal Function Requires Pectin De-methyl-esterification of the Guard Cell Wall. Curr. Biol. 26, 2899–2906.

Anderson, C.T., Carroll, A., Akhmetova, L., Somerville, C., 2010. Real-time imaging of cellulose reorientation during cell wall expansion in Arabidopsis roots. Plant Physiol. 152, 787–96.

Asai, N., Nakajima, N., Kondo, N., Kamada, H., 1999. The Effect of Osmotic Stress on the Solutes in Guard Cells of Vicia faba L. Plant Cell Physiol. 40, 843–849.

Barbier de Reuille, P., Routier-Kierzkowska, A.-L., Kierzkowski, D., Bassel, G.W., Schüpbach, T., Tauriello, G., Bajpai, N., Strauss, S., Weber, A., Kiss, A., Burian, A., Hofhuis, H., Sapala, A., Lipowczan, M., Heimlicher, M.B., Robinson, S., Bayer, E.M., Basler, K., Koumoutsakos, P., Roeder, A.H., Aegerter-Wilmsen, T., Nakayama, N., Tsiantis, M., Hay, A., Kwiatkowska, D., Xenarios, I., Kuhlemeier, C., Smith, R.S., 2015. MorphoGraphX: A platform for quantifying morphogenesis in 4D. Elife 4, e05864.

Bashline, L., Lei, L., Li, S., Gu, Y., 2014. Cell Wall, Cytoskeleton, and Cell Expansion in

Higher Plants. Mol. Plant 7, 586–600.

Bassel, G.W., Stamm, P., Mosca, G., Barbier de Reuille, P., Gibbs, D.J., Winter, R., Janka, A., Holdsworth, M.J., Smith, R.S., 2014. Mechanical constraints imposed by 3D cellular geometry and arrangement modulate growth patterns in the Arabidopsis embryo. Proc. Natl. Acad. Sci. U. S. A. 111, 8685–90.

Bergmann, D.C., Sack, F.D., 2007. Stomatal development. Annu. Rev. Plant Biol. 58, 163–81.

Bernal, A.J., Jensen, J.K., Harholt, J., Sørensen, S., Moller, I., Blaukopf, C., Johansen, B., de Lotto, R., Pauly, M., Scheller, H.V., Willats, W.G.T., 2007. Disruption of *ATCSLD5* results in reduced growth, reduced xylan and homogalacturonan synthase activity and altered xylan occurrence in Arabidopsis. Plant J. 52, 791–802.

Berthet, B., Maizel, A., 2016. Light sheet microscopy and live imaging of plants. J. Microsc. 263, 158–164.

Bertolino, L.T., Caine, R.S., Gray, J.E., 2019. Impact of Stomatal Density and Morphology on Water-Use Efficiency in a Changing World. Front. Plant Sci. 10, 225.

Bhosale, R., Boudolf, V., Cuevas, F., Lu, R., Eekhout, T., Hu, Z., Van Isterdael, G., Lambert, G.M., Xu, F., Nowack, M.K., Smith, R.S., Vercauteren, I., De Rycke, R., Storme, V., Beeckman, T., Larkin, J.C., Kremer, A., Höfte, H., Galbraith, D.W., Kumpf, R.P., Maere, S., De Veylder, L., 2018. A Spatiotemporal DNA Endoploidy Map of the Arabidopsis Root Reveals Roles for the Endocycle in Root Development and Stress Adaptation. Plant Cell 30, 2330–2351.

Bidhendi, A.J., Geitmann, A., 2018. Finite Element Modeling of Shape Changes in Plant Cells. Plant Physiol. 176, 41–56.

Bird, S.M., Gray, J.E., 2003. Signals from the cuticle affect epidermal cell differentiation. New Phytol. 157, 9–23.

Bolte, S., Cordelières, F.P., 2006. A guided tour into subcellular colocalization analysis in light microscopy. J. Microsc. 224, 213–232.

Bourdais, G., McLachlan, D.H., Rickett, L.M., Zhou, J., Siwoszek, A., Häweker, H., Hartley, M., Kuhn, H., Morris, R.J., MacLean, D., Robatzek, S., 2019. The use of

quantitative imaging to investigate regulators of membrane trafficking in Arabidopsis stomatal closure. Traffic 20, 168–180.

Bouton, S., Leboeuf, E., Mouille, G., Leydecker, M.-T., Talbotec, J., Granier, F., Lahaye, M., Höfte, H., Truong, H.-N., 2002. QUASIMODO1 Encodes a Putative Membrane-Bound Glycosyltransferase Required for Normal Pectin Synthesis and Cell Adhesion in Arabidopsis. Am. Soc. Plant Biol. 14, 2577–2590.

Boyes, D.C., Zayed, A.M., Ascenzi, R., McCaskill, A.J., Hoffman, N.E., Davis, K.R., Görlach, J., 2001. Growth stage-based phenotypic analysis of Arabidopsis: a model for high throughput functional genomics in plants. Plant Cell 13, 1499–510.

Braidwood, L., Breuer, C., Sugimoto, K., 2014. My body is a cage: mechanisms and modulation of plant cell growth. Source New Phytol. 201, 388–402.

Brummell, D.A., Harpster, M.H., Dunsmuir, P., 1999. Differential expression of expansin gene family members during growth and ripening of tomato fruit. Plant Mol. Biol. 39, 161–169.

Caffall, K.H., Mohnen, D., 2009. The structure, function, and biosynthesis of plant cell wall pectic polysaccharides. Carbohydr. Res. 344, 1879–1900.

Caine, R.S., Yin, X., Sloan, J., Harrison, E.L., Mohammed, U., Fulton, T., Biswal, A.K., Dionora, J., Chater, C.C., Coe, R.A., Bandyopadhyay, A., Murchie, E.H., Swarup, R., Quick, W.P., Gray, J.E., 2019. Rice with reduced stomatal density conserves water and has improved drought tolerance under future climate conditions. New Phytol. 221, 371–384.

Cannon, M.C., Terneus, K., Hall, Q., Tan, L., Wang, Y., Wegenhart, B.L., Chen, L., Lamport, D.T.A., Chen, Y., Kieliszewski, M.J., 2007. Self-assembly of the plant cell wall requires an extensin scaffold. PNAS 105, 2226–2231.

Carpita, N.C., Gibeaut, D.M., 1993. Structural models of primary cell walls in flowering plants: consistency of molecular structure with the physical properties of the walls during growth. Plant J. 3, 1–30.

Carter, R., Woolfenden, H., Baillie, A., Amsbury, S., Carroll, S., Healicon, E., Sovatzoglou, S., Braybrook, S., Gray, J.E., Hobbs, J., Morris, R.J., Fleming, A.J., 2017. Stomatal Opening Involves Polar, Not Radial, Stiffening Of Guard Cells. Curr. Biol. 27, 2974–

2983.

Casson, S., Gray, J.E., 2008. Influence of Environmental Factors on Stomatal Development. New Phytol. 178, 9–23.

Castilleux, R., Plancot, B., Ropitaux, M., Carreras, A., Leprince, J., Boulogne, I., Follet-Gueye, M.-L., Popper, Z.A., Driouich, A., Vicré, M., 2018. Cell wall extensins in root–microbe interactions and root secretions. J. Exp. Bot. 69, 4235–4247.

Cavalier, D.M., Lerouxel, O., Neumetzler, L., Yamauchi, K., Reinecke, A., Freshour, G., Zabotina, O.A., Hahn, M.G., Burgert, I., Pauly, M., Raikhel, N. V., Keegstra, K., 2008. Disrupting two Arabidopsis thaliana xylosyltransferase genes results in plants deficient in xyloglucan, a major primary cell wall component. Plant Cell 20, 1519–37.

Chater, C., Peng, K., Movahedi, M., Dunn, J.A., Walker, H.J., Liang, Y.-K., McLachlan, D.H., Casson, S., Isner, J.C., Wilson, I., Neill, S.J., Hedrich, R., Gray, J.E., Hetherington, A.M., 2015. Elevated CO2-Induced Responses in Stomata Require ABA and ABA Signaling. Curr. Biol. 25, 2709–16.

Chater, C.C.C., Caine, R.S., Fleming, A.J., Gray, J.E., 2017. Origins and Evolution of Stomatal Development. Plant Physiol. 174, 624–638.

Cho, H.-T., Kende, H., 1998. Tissue localization of expansins in deepwater rice. Plant J. 15, 805–812.

Clough, S.J., Bent, A.F., 1998. Floral dip: a simplified method forAgrobacterium-mediated transformation ofArabidopsis thaliana. Plant J. 16, 735–743.

Coneva, V., Frank, M.H., Balaguer, M.A. de L., Li, M., Sozzani, R., Chitwood, D.H., 2017. Genetic Architecture and Molecular Networks Underlying Leaf Thickness in Desert-Adapted Tomato Solanum pennellii. Plant Physiol. 175, 376–391.

Cooke, J.R., De Baerdemaeker, J.G. De, Rand, R.H., Mang, H.A., 1976. A Finite Element Shell Analysis of Guard Cell Deformations. Trans. ASAE 19, 1107–1121.

Cooper, J.A., Wear, M.A., Weaver, A.M., 2001. Arp2/3 complex: Advances on the inner workings of a molecular machine. Cell 107, 703–705.

Cosgrove, D.J., 1999. Enzymes and other agents that enhance cell wall extensibility. Annu. Rev. Plant Physiol. Plant Mol. Biol. 50, 391–417.

Cosgrove, D.J., 2000. Loosening of plant cell walls by expansins. Nature 407, 321–326.

Cosgrove, D.J., 2005. Growth of the plant cell wall. Nat. Rev. Mol. Cell Biol. 6, 850–61.

Cosgrove, D.J., Bedinger, P., Durachko, D.M., 1997. Group I allergens of grass pollen as cell wall-loosening agents. Proc. Natl. Acad. Sci. U. S. A. 94, 6559–64.

Cosgrove, D.J., Li, L.C., Cho, H.-T., Hoffmann-Benning, S., Moore, R.C., Blecker, D., 2002. The Growing World of Expansins. Plant Cell Physiol. 43, 1436–1444.

Daher, F.B., Braybrook, S.A., 2015. How to let go: pectin and plant cell adhesion. Front. Plant Sci. 6, 523.

Derbyshire, P., McCann, M.C., Roberts, K., 2007. Restricted cell elongation in Arabidopsis hypocotyls is associated with a reduced average pectin esterification level. BMC Plant Biol. 7, 31.

Dittrich, M., Mueller, H.M., Bauer, H., Peirats-Llobet, M., Rodriguez, P.L., Geilfus, C.-M., Carpentier, S.C., Al Rasheid, K.A.S., Kollist, H., Merilo, E., Herrmann, J., Müller, T., Ache, P., Hetherington, A.M., Hedrich, R., 2019. The role of Arabidopsis ABA receptors from the PYR/PYL/RCAR family in stomatal acclimation and closure signal integration. Nat. Plants 1–10.

Doheny-Adams, T., Hunt, L., Franks, P.J., Beerling, D.J., Gray, J.E., 2012. Genetic manipulation of stomatal density influences stomatal size, plant growth and tolerance to restricted water supply across a growth carbon dioxide gradient. Philos. Trans. R. Soc. Lond. B. Biol. Sci. 367, 547–55.

Dyachok, J., Shao, M.R., Vaughn, K., Bowling, A., Facette, M., Djakovic, S., Clark, L., Smith, L., 2008. Plasma membrane-associated SCAR complex subunits promote cortical F-actin accumulation and normal growth characteristics in arabidopsis roots. Mol. Plant 1, 990–1006.

Easlon, H.M., 2013. Easy Leaf Area.

Eckardt, N.A., Cominelli, E., Galbiati, M., Tonelli, C., 2009. The Future of Science: Food and Water for Life. Plant Cell 21, 368–372.

Eisenach, C., Francisco, R., Martinoia, E., 2015. Plant vacuoles. Curr. Biol. 25, R136–R137.

Elhaddad, N.S., Hunt, L., Sloan, J., Gray, J.E., 2014. Light-induced stomatal opening is

affected by the guard cell protein kinase APK1b. PLoS One 9, e97161.

Eun, S.-O., Lee, Y., 2000. Stomatal opening by fusicoccin is accompanied by depolymerization of actin filaments in guard cells. Planta 210, 1014–1017.

Fang, J., Qin, G., Ma, J., She, Y.-M., 2015. Quantification of plant cell wall monosaccharides by reversed-phase liquid chromatography with 2-aminobenzamide pre-column derivatization and a non-toxic reducing reagent 2-picoline borane. J. Chromatogr. A 1414, 122–128.

Fischer-Parton, S., Parton, R.M., Hickey, P.C., Dijksterhuis, J., Atkinson, H.A., Read, N.D., 2000. Confocal microscopy of FM4-64 as a tool for analysing endocytosis and vesicle trafficking in living fungal hyphae. J. Microsc. 198, 246–259.

Fischer, R.A., 1968. Stomatal opening: role of potassium uptake by guard cells. Science 160, 784–5.

Flurotherm.com, 2019. FEP Tubing | Properties | Fluorotherm.com [WWW Document]. URL https://www.fluorotherm.com/technical-information/materials-overview/fep-properties/ (accessed 1.4.19).

Food and Agriculture Organization of the United Nations., 2013. The State of Food and Agriculture 2013.

Franks, P.J., 2003. Use of the pressure probe in studies of stomatal function. J. Exp. Bot. 54, 1495–1504.

Franks, P.J., Beerling, D.J., 2009. Maximum leaf conductance driven by CO2 effects on stomatal size and density over geologic time. Proc. Natl. Acad. Sci. U. S. A. 106, 10343–7.

Franks, P.J., Buckley, T.N., Shope, J.C., Mott, K.A., 2001. Guard Cell Volume and Pressure Measured Concurrently by Confocal Microscopy and the Cell Pressure Probe. Plant Physiol. 125, 1577–1584.

Franks, P.J., Drake, P.L., Beerling, D.J., 2009. Plasticity in maximum stomatal conductance constrained by negative correlation between stomatal size and density: an analysis using Eucalyptus globulus. Plant. Cell Environ. 32, 1737–1748.

Franks, P.J., Farquhar, G.D., 2007. The Mechanical Diversity of Stomata and Its

Significance in Gas-Exchange Control. Plant Physiol. 143, 78–87.

Franks, P.J., W Doheny-Adams, T., Britton-Harper, Z.J., Gray, J.E., W. Doheny-Adams, T., Britton-Harper, Z.J., Gray, J.E., W Doheny-Adams, T., Britton-Harper, Z.J., Gray, J.E., 2015. Increasing water-use efficiency directly through genetic manipulation of stomatal density. New Phytol. 207, 188–95.

Gao, X.-Q., Chen, Jing, Wei, P.-C., Ren, F., Chen, Jia, Wang, X.-C., 2008. Array and distribution of actin filaments in guard cells contribute to the determination of stomatal aperture. Plant Cell Rep. 27, 1655–1665.

Gao, X.-Q., Li, C.-G., Wei, P.-C., Zhang, X.-Y., Chen, J., Wang, X.-C., 2005. The dynamic changes of tonoplasts in guard cells are important for stomatal movement in Vicia faba. Plant Physiol. 139, 1207–16.

Geisler, M., Nadeau, J., Sack, F.D., 2000. Oriented Asymmetric Divisions That Generate the Stomatal Spacing Pattern in Arabidopsis Are Disrupted by the too many mouths Mutation. Plant Cell 12, 2075–2086.

Geisler, M.J., Sack, F.D., 2002. Variable timing of developmental progression in the stomatal pathway in Arabidopsis cotyledons. New Phytol. 153, 469–476.

Geitmann, A., 2010. Mechanical modeling and structural analysis of the primary plant cell wall. Curr. Opin. Plant Biol. 13, 693–699.

Glass, G. V, Peckham, P.D., Sanders, J.R., 1972. Consequences of Failure to Meet Assumptions Underlying the Fixed Effects Analyses of Variance and Covariance. Rev. Educ. Res. 42, 237–288.

Godfray, H.C.J., Beddington, J.R., Crute, I.R., Haddad, L., Lawrence, D., Muir, J.F., Pretty, J., Robinson, S., Thomas, S.M., Toulmin, C., 2010. Food security: the challenge of feeding 9 billion people. Science 327, 812–8.

Goh, H.-H., Sloan, J., Dorca-Fornell, C., Fleming, A., 2012. Inducible repression of multiple expansin genes leads to growth suppression during leaf development. Plant Physiol. 159, 1759–70.

Goubet, F., Misrahi, A., Park, S.K., Zhang, Z., Twell, D., Dupree, P., 2003. AtCSLA7, a cellulose synthase-like putative glycosyltransferase, is important for pollen tube

growth and embryogenesis in Arabidopsis. Plant Physiol. 131, 547–57.

Grant, G.T., Mon, E.R., Rees, D.A., Smith, P.J.C., Thom, D., 1973. Biological interactions between polysaccharides and divalent cations: the egg-box model. FEBS Lett. 32, 195–198.

Green, P.B., Cummins, W.R., 1974. Growth rate and turgor pressure: auxin effect studies with an automated apparatus for single coleoptiles. Plant Physiol. 54, 863–9.

Greger, K., Swoger, J., Stelzer, E.H.K., 2007. Basic building units and properties of a fluorescence single plane illumination microscope. Rev. Sci. Instrum. 78, 0237051–0237057.

Hall, Q., Cannon, M.C., 2002. The Cell Wall Hydroxyproline-Rich Glycoprotein RSH Is Essential for Normal Embryo Development in Arabidopsis. Plant Cell 14, 1161–1172.

Hamant, O., Heisler, M.G., Jönsson, H., Krupinski, P., Uyttewaal, M., Bokov, P., Corson, F., Sahlin, P., Boudaoud, A., Meyerowitz, E.M., Couder, Y., Traas, J., 2008. Developmental patterning by mechanical signals in Arabidopsis. Science 322, 1650–5.

Hara, K., Kajita, R., Torii, K.U., Bergmann, D.C., Kakimoto, T., 2007. The secretory peptide gene EPF1 enforces the stomatal one-cell-spacing rule. Genes Dev. 21, 1720–5.

Harrison, E.P., McQueen-Mason, S.J., Manning, K., 2001. Expression of six expansin genes in relation to extension activity in developing strawberry fruit. J. Exp. Bot. 52, 1437–1446.

Hashimoto, M., Negi, J., Young, J., Israelsson, M., Schroeder, J.I., Iba, K., 2006. Arabidopsis HT1 kinase controls stomatal movements in response to CO2. Nat. Cell Biol. 8, 391–397.

Haworth, M., Elliott-Kingston, C., McElwain, J.C., 2011. Stomatal control as a driver of plant evolution. J. Exp. Bot. 62, 2419–23.

Helper, P.K., Newcomb, E.H., 1964. Microtubules and fibrils in the cytoplasm of Coleus cells undergoing secondary cell wall deposition. J. Cell Biol. 20, 529–32.

Hetherington, A.J., Dolan, L., 2018. Stepwise and independent origins of roots among land plants. Nature 561, 235–238.

Hetherington, A.M., Woodward, F.I., 2003. The role of stomata in sensing and driving

environmental change. Nature 424, 901–8.

Hongo, S., Sato, K., Yokoyama, R., Nishitani, K., 2012. Demethylesterification of the Primary Wall by PECTIN METHYLESTERASE35 Provides Mechanical Support to the Arabidopsis Stem. Source Plant Cell 24, 2624–2634.

Horrer, D., Flü, S., Pazmino, D., Leonhardt, N., Lawson, T., Santelia, D., 2016. Blue Light Induces a Distinct Starch Degradation Pathway in Guard Cells for Stomatal Opening. Curr. Biol. 26, 362–370.

Horstmann, M., Topham, A.T., Stamm, P., Kruppert, S., Colbourne, J.K., Tollrian, R., Weiss, L.C., 2018. Scan, extract, wrap, compute—a 3D method to analyse morphological shape differences. PeerJ 6.

Houston, K., Tucker, M.R., Chowdhury, J., Shirley, N., Little, A., 2016. The Plant Cell Wall: A Complex and Dynamic Structure As Revealed by the Responses of Genes under Stress Conditions. Front. Plant Sci. 7.

Hu, H., Boisson-Dernier, A., Israelsson-Nordström, M., Böhmer, M., Xue, S., Ries, A., Godoski, J., Kuhn, J.M., Schroeder, J.I., 2010. Carbonic anhydrases are upstream regulators of CO2-controlled stomatal movements in guard cells. Nat. Cell Biol. 12, 87–93.

Hughes, J., Hepworth, C., Dutton, C., Dunn, J.A., Hunt, L., Stephens, J., Waugh, R., Cameron, D.D., Gray, J.E., 2017. Reducing Stomatal Density in Barley Improves Drought Tolerance without Impacting on Yield. Plant Physiol. 174, 776–787.

Huisken, J., Swoger, J., Del Bene, F., Wittbrodt, J., Stelzer, E.H.K., 2004. Optical sectioning deep inside live embryos by selective plane illumination microscopy. Science (80-.). 305, 1007–9.

Hülskamp, M., Miséra, S., Jürgens, G., 1994. Genetic dissection of trichome cell development in Arabidopsis. Cell 76, 555–566.

Hutchison, K.W., Singer, P.B., McInnis, S., Diaz-Sala, C., Greenwood, M.S., 1999. Expansins are conserved in conifers and expressed in hypocotyls in response to exogenous auxin. Plant Physiol. 120, 827–32.

Hwang, J.U., Suh, S., Yi, H., Kim, J., Lee, Y., 1997. Actin Filaments Modulate Both

Stomatal Opening and Inward K+-Channel Activities in Guard Cells of Vicia faba L. Plant Physiol. 115, 335–342.

Jackson, M.D.B., Duran-Nebreda, S., Kierzkowski, D., Strauss, S., Xu, H., Landrein, B., Hamant, O., Smith, R.S., Johnston, I.G., Bassel, G.W., 2019. Global Topological Order Emerges through Local Mechanical Control of Cell Divisions in the Arabidopsis Shoot Apical Meristem. Cell Syst. 8, 53-65.e3.

Jezek, M., Blatt, M.R., 2017. The Membrane Transport System of the Guard Cell and Its Integration for Stomatal Dynamics. Plant Physiol. 174, 487–519.

Jiang, K., Sorefan, K., Deeks, M.J., Bevan, M.W., Hussey, P.J., Hetherington, A.M., 2012. The ARP2/3 complex mediates guard cell actin reorganization and stomatal movement in Arabidopsis. Plant Cell 24, 2031–40.

Johansson, F., Sommarin, M., Larsson, C., 1993. Fusicoccin Activates the Plasma Membrane H + -ATPase by a Mechanism Involving the C-Terminal Inhibitory Domain. Plant Cell 5, 321.

Jones, A.R., Forero-Vargas, M., Withers, S.P., Smith, R.S., Traas, J., Dewitte, W., Murray, J.A.H., 2017. Cell-size dependent progression of the cell cycle creates homeostasis and flexibility of plant cell size. Nat. Commun. 8, 15060.

Jones, L., Milne, J.L., Ashford, D., McCann, M.C., McQueen-Mason, S.J., 2005. A conserved functional role of pectic polymers in stomatal guard cells from a range of plant species. Planta 221, 255–264.

Jones, L., Milne, J.L., Ashford, D., McQueen-Mason, S.J., 2003. Cell wall arabinan is essential for guard cell function. Proc. Natl. Acad. Sci. U. S. A. 100, 11783–11788.

Keller, B., 1993. Structural Cell Wall Proteins. Plant Physiol. 101, 130.

Kim, M., Hepler, P.K., Eun, S.O., Ha, K.S., Lee, Y., 1995. Actin Filaments in Mature Guard Cells Are Radially Distributed and Involved in Stomatal Movement. Plant Physiol. 109, 1077–1084.

Kim, S.-J., Brandizzi, F., 2014. The Plant Secretory Pathway: An Essential Factory for Building the Plant Cell Wall. Plant Cell Physiol. 55, 687–693.

Kim, T.-H., Böhmer, M., Hu, H., Nishimura, N., Schroeder, J.I., 2010. Guard Cell Signal

Transduction Network: Advances in Understanding Abscisic Acid, CO2 , and Ca2+ Signaling. Annu. Rev. Plant Biol. 61, 561–591.

Kirchhelle, C., Chow, C.-M., Foucart, C., Neto, H., Stierhof, Y.-D., Kalde, M., Walton, C., Fricker, M., Smith, R.S., Jérusalem, A., Irani, N., Moore, I., 2016. The Specification of Geometric Edges by a Plant Rab GTPase Is an Essential Cell-Patterning Principle During Organogenesis in Arabidopsis. Dev. Cell 36, 386–400.

Kirschner, G.K., Stahl, Y., Imani, J., von Korff, M., Simon, R., 2018. Fluorescent reporter lines for auxin and cytokinin signalling in barley (Hordeum vulgare). PLoS One 13, e0196086.

Kiss, A., Moreau, T., Mirabet, V., Calugaru, C.I., Boudaoud, A., Das, P., 2017. Segmentation of 3D images of plant tissues at multiple scales using the level set method. Plant Methods 13, 114.

Klemm, D., Heublein, B., Fink, H.-P., Bohn, A., 2005. Cellulose: Fascinating Biopolymer and Sustainable Raw Material. Angew. Chemie Int. Ed. 44, 3358–3393.

Kollist, H., Nuhkat, M., Roelfsema, M.R.G., 2014. Closing gaps: linking elements that control stomatal movement. New Phytol. 203, 44–62.

Lake, J.A., Quick, W.P., Beerling, D.J., Woodward, F.I., 2001. Plant development. Signals from mature to new leaves. Nature 411, 154.

Lamport, D.T.A., Kieliszewski, M.J., Chen, Y., Cannon, M.C., 2011. Update on the Extensin Superfamily Role of the Extensin Superfamily in Primary Cell Wall Architecture. Plant Physiol. 156, 11–19.

Lawson, T., Blatt, M.R., 2014. Stomatal Size, Speed, and Responsiveness Impact on Photosynthesis and Water Use Efficiency. Plant Physiol. 164, 1556–1570.

Lawson, T., Vialet-Chabrand, S., 2018. Speedy stomata, photosynthesis and plant water use efficiency. New Phytol. 221, 93–98.

Lee, D.-K., Ahn, J.H., Song, S.-K., Choi, Y. Do, Lee, J.S., 2003. Expression of an expansin gene is correlated with root elongation in soybean. Plant Physiol. 131, 985–97.

Lee, Y., Choi, D., Kende, H., 2001. Expansins: ever-expanding numbers and functions. Curr. Opin. Plant Biol. 4, 527–532.

Leung, J., Giraudat, J., 1998. Abscisic acid signal transduction. Annu. Rev. Plant Physiol. Plant Mol. Biol. 49, 199–222.

Leymarie, J., Vavasseur, A., Lascéve, G., 1998. CO2 sensing in stomata of abi1-1 and abi2-1 mutants of Arabidopsis thaliana. Plant Physiol. Biochem. 36, 539–543.

Li, L.J., Ren, F., Gao, X.-Q., Wei, P.C., Wang, X.C., 2013. The reorganization of actin filaments is required for vacuolar fusion of guard cells during stomatal opening in Arabidopsis. Plant, Cell Environ. 36, 484–497.

Li, S., Blanchoin, L., Yang, Z., Lord, E.M., 2003. The Putative Arabidopsis Arp2/3 Complex Controls Leaf Cell Morphogenesis. Plant Physiol. 132, 2034.

Li, X., Li, J.-H., Wang, W., Chen, N.-Z., Ma, T.-S., Xi, Y.-N., Zhang, X.-L., Lin, H.-F., Bai, Y., Huang, S.-J., Chen, Y.-Li., 2014. ARP2/3 complex-mediated actin dynamics is required for hydrogen peroxide-induced stomatal closure in Arabidopsis. Plant. Cell Environ. 37, 1548–1560.

Li, Y., Darley, C.P., Ongaro, V., Fleming, A., Schipper, O., Baldauf, S.L., McQueen-Mason, S.J., 2002. Plant expansins are a complex multigene family with an ancient evolutionary origin. Plant Physiol. 128, 854–64.

Li, Z.-C., Durachko, D.M., Cosgrove, D.J., 1993. An oat coleoptile wall protein that induces wall extension in vitro and that is antigenically related to a similar protein from cucumber hypocotyls. Planta 191, 349–356.

Liang, Y.-K., Xie, X., Lindsay, S.E., Wang, Y.B., Masle, J., Williamson, L., Leyser, O., Hetherington, A.M., 2010. Cell wall composition contributes to the control of transpiration efficiency in Arabidopsis thaliana. Plant J. 64, 679–686.

Liu, X., Wolfe, R., Welch, L.R., Domozych, D.S., Popper, Z.A., Showalter, A.M., 2016. Bioinformatic Identification and Analysis of Extensins in the Plant Kingdom. PLoS One 11, e0150177.

Lohse, G., Hedrich, R., 1992. Characterization of the plasma-membrane H+-ATPase from Vicia faba guard cells. Planta 188, 206–214.

Louveaux, M., Julien, J.-D., Mirabet, V., Boudaoud, A., Hamant, O., 2016. Cell division plane orientation based on tensile stress in Arabidopsis thaliana. Proc. Natl. Acad.

Sci. U. S. A. 113, E4294-4303.

MacRobbie, E.A.C., Kurup, S., 2007. Signalling mechanisms in the regulation of vacuolar ion release in guard cells. New Phytol. 175, 630–640.

Maizel, A., von Wangenheim, D., Federici, F., Haseloff, J., Stelzer, E.H.K., 2011. High-resolution live imaging of plant growth in near physiological bright conditions using light sheet fluorescence microscopy. Plant J. 68, 377–385.

Majewska-Sawka, A., Münster, A., Rodríguez-García, M.I., 2002. Guard cell wall: immunocytochemical detection of polysaccharide components. J. Exp. Bot. 53, 1067–1079.

Marga, F., Grandbois, M., Cosgrove, D.J., Baskin, T.I., 2005. Cell wall extension results in the coordinate separation of parallel microfibrils: evidence from scanning electron microscopy and atomic force microscopy. Plant J. 43, 181–90.

Marom, Z., Shtein, I., Bar-On, B., 2017. Stomatal Opening: The Role of Cell-Wall Mechanical Anisotropy and Its Analytical Relations to the Bio-composite Characteristics. Front. Plant Sci. 8, 2061.

Mathur, J., Hülskamp, M., 2002. Microtubules and Microfilaments in Cell Morphogenesis in Higher Plants. Curr. Biol. 12, R669–R676.

Mathur, J., Mathur, N., Kernebeck, B., Hülskamp, M., 2003. Mutations in actin-related proteins 2 and 3 affect cell shape development in Arabidopsis. Plant Cell 15, 1632–45.

McAinsh, M.R., Brownlee, C., Hetherington, A.M., 1990. Abscisic acid-induced elevation of guard cell cytosolic Ca2+ precedes stomatal closure. Nature 343, 186–188.

McFarlane, H.E., Döring, A., Persson, S., 2014. The Cell Biology of Cellulose Synthesis. Annu. Rev. Plant Biol. 65, 69–94.

McKim, S.M., Routier-Kierzkowska, A.-L., Monniaux, M., Kierzkowski, D., Pieper, B., Smith, R.S., Tsiantis, M., Hay, A., 2017. Seasonal Regulation of Petal Number. Plant Physiol. 175, 886–903.

McLachlan, D.H., Lan, J., Geilfus, C.-M., Dodd, A.N., Larson, T., Baker, A., Hõrak, H., Kollist, H., He, Z., Graham, I., Mickelbart, M.V., Hetherington, A.M., 2016. The Breakdown of Stored Triacylglycerols Is Required during Light-Induced Stomatal

Opening. Curr. Biol. 26, 707–712.

McQueen-Mason, S., Cosgrove, D.J., 1994. Disruption of hydrogen bonding between plant cell wall polymers by proteins that induce wall extension. Proc. Natl. Acad. Sci. 91, 6574–6578.

McQueen-Mason, S., Durachko, D.M., Cosgrove, D.J., 1992. Two Endogenous Proteins That Induce Cell Wall Extension in Plants. Plant Cell 4, 1425.

Meckel, T., Gall, L., Semrau, S., Homann, U., Thiel, G., 2007. Guard Cells Elongate: Relationship of Volume and Surface Area during Stomatal Movement. Biophys. J. 92, 1072–1080.

Meents, M.J., Watanabe, Y., Samuels, A.L., 2018. The cell biology of secondary cell wall biosynthesis. Ann. Bot. 121, 1107–1125.

Melotto, R., 2010. Assessing Stomatal Response to Live Bacterial Cells using Whole Leaf Imaging. J. Vis. Exp 2185.

Mohnen, D., 2008. Pectin structure and biosynthesis. Curr. Opin. Plant Biol. 11, 266–277.

Monniaux, M., Pieper, B., McKim, S.M., Routier-Kierzkowska, A.-L., Kierzkowski, D., Smith, R.S., Hay, A., 2018. The role of APETALA1 in petal number robustness. Elife 7, e39399.

Montenegro-Johnson, T.D., Stamm, P., Strauss, S., Topham, A.T., Tsagris, M., Wood, A.T.A., Smith, R.S., Bassel, G.W., 2015. Digital Single-Cell Analysis of Plant Organ Development Using 3DCellAtlas. Plant Cell 27, 1018–33.

Moore, P.J., Staehelin, L.A., 1988. Immunogold localization of the cell-wall-matrix polysaccharides rhamnogalacturonan I and xyloglucan during cell expansion and cytokinesis inTrifolium pratense L.; implication for secretory pathways. Planta 174, 433–445.

Mueller, S.C., Brown, R.M., 1980. Evidence for an intramembrane component associated with a cellulose microfibril-synthesizing complex in higher plants. J. Cell Biol. 84, 315–26.

Müller, K., Levesque-Tremblay, G., Bartels, S., Weitbrecht, K., Wormit, A., Usadel, B., Haughn, G., Kermode, A.R., 2013. Demethylesterification of cell wall pectins in

Arabidopsis plays a role in seed germination. Plant Physiol. 161, 305–16.

Newman, R.H., Hill, S.J., Harris, P.J., 2013. Wide-angle x-ray scattering and solid-state nuclear magnetic resonance data combined to test models for cellulose microfibrils in mung bean cell walls. Plant Physiol. 163, 1558–67.

Niklas, K.J., 2004. The Cell Walls that Bind the Tree of Life. Bioscience 54, 831.

Nishiyama, Y., 2009. Structure and properties of the cellulose microfibril. J. Wood Sci. 55, 241–249.

Ovečka, M., Vaškebová, L., Komis, G., Luptovčiak, I., Smertenko, A., Šamaj, J., 2015. Preparation of plants for developmental and cellular imaging by light-sheet microscopy. Nat. Protoc. 10, 1234–1247.

Ovečka, M., von Wangenheim, D., Tomančák, P., Šamajová, O., Komis, G., Šamaj, J., 2018. Multiscale imaging of plant development by light-sheet fluorescence microscopy. Nat. Plants 4, 639–650.

Paddock, S.W., 2000. Principles and Practices of Laser Scanning Confocal Microscopy. Mol. Biotechnol. 16, 127–150.

Palevitz, B.A., Hepler, P.K., 1976. Cellulose microfibril orientation and cell shaping in developing guard cells of Allium: The role of microtubules and ion accumulation. Planta 132, 71–93.

Parry, M.., Rosenzweig, C., Iglesias, A., Livermore, M., Fischer, G., 2004. Effects of climate change on global food production under SRES emissions and socio-economic scenarios. Glob. Environ. Chang. 14, 53–67.

Parry, M.L., Canziani, O.F., Palutikof, J.P., van der Linden, P.J., Hanson, C.E., 2007. IPCC Fourth Assessment Report: Climate Change 2007.

Peaucelle, A., Braybrook, S., Höfte, H., 2012. Cell wall mechanics and growth control in plants: the role of pectins revisited. Front. Plant Sci. 3, 121.

Peaucelle, A., Braybrook, S.A., Le Guillou, L., Bron, E., Kuhlemeier, C., Höfte, H., 2011. Pectin-induced changes in cell wall mechanics underlie organ initiation in Arabidopsis. Curr. Biol. 21, 1720–6.

Peaucelle, A., Louvet, R., Johansen, J.N., Höfte, H., Laufs, P., Pelloux, J., Mouille, G., 2008.

Arabidopsis Phyllotaxis Is Controlled by the Methyl-Esterification Status of Cell-Wall Pectins. Curr. Biol. 18, 1943–1948.

Pelletier, S., Van Orden, J., Wolf, S., Vissenberg, K., Delacourt, J., Ndong, Y.A., Pelloux, J., Bischoff, V., Urbain, A., Mouille, G., Lemonnier, G., Renou, J.-P., Höfte, H., 2010. A role for pectin de-methylesterification in a developmentally regulated growth acceleration in dark-grown Arabidopsis hypocotyls. New Phytol. 188, 726–39.

Pelloux, J., Rusterucci, C., Mellerowicz, E.J., Rustérucci, C., Mellerowicz, E.J., 2007. New insights into pectin methylesterase structure and function. Trends Plant Sci. 12, 267–277.

Peña, M.J., Carpita, N.C., 2004. Loss of highly branched arabinans and debranching of rhamnogalacturonan I accompany loss of firm texture and cell separation during prolonged storage of apple. Plant Physiol. 135, 1305–13.

Penfield, S., Clements, S., Bailey, K.J., Gilday, A.D., Leegood, R.C., Gray, J.E., Graham, I.A., 2012. Expression and manipulation of PHOSPHOENOLPYRUVATE CARBOXYKINASE 1 identifies a role for malate metabolism in stomatal closure. Plant J. 69, 679–688.

Pillitteri, L.J., Torii, K.U., 2012. Mechanisms of Stomatal Development. Annu. Rev. Plant Biol. 63, 591–614.

Popper, Z.A., 2008. Evolution and diversity of green plant cell walls. Curr. Opin. Plant Biol. 11, 286–292.

Popper, Z.A., Michel, G., Hervé, C., Domozych, D.S., Willats, W.G.T., Tuohy, M.G., Kloareg, B., Stengel, D.B., 2011. Evolution and Diversity of Plant Cell Walls: From Algae to Flowering Plants. Annu. Rev. Plant Biol. 62, 567–590.

Pratap Sahi, V., Cifrová, P., García-González, J., Kotannal Baby, I., Mouillé, G., Gineau, E., Müller, K., Baluška, F., Soukup, A., Petrášek, J., Schwarzerová, K., 2017. Arabidopsis thaliana plants lacking the ARP2/3 complex show defects in cell wall assembly and auxin distribution. Ann. Bot. 122, 777–789.

Prunet, N., 2017. Live Confocal Imaging of Developing Arabidopsis Flowers. J. Vis. Exp. 122, e55156.

Qian, P., Hou, S., Guo, G., 2009. Molecular mechanisms controlling pavement cell shape in Arabidopsis leaves. Plant Cell Rep. 28, 1147–1157.

Raschke, K., Fellows, M.P., 1971. Stomatal movement in Zea mays: Shuttle of potassium and chloride between guard cells and subsidiary cells. Planta 101, 296–316.

Rayle, D.L., Cleland, R.E., 1992. The Acid Growth Theory of auxin-induced cell elongation is alive and well. Plant Physiol. 99, 1271–4.

Ridley, B.L., O'Neill, M.A., Mohnen, D., 2001. Pectins: structure, biosynthesis, and oligogalacturonide-related signaling. Phytochemistry 57, 929–967.

Roeder, A.H.K., Chickarmane, V., Cunha, A., Obara, B., Manjunath, B.S., Meyerowitz, E.M., 2010. Variability in the control of cell division underlies sepal epidermal patterning in Arabidopsis thaliana. PLoS Biol. 8, e1000367.

Roelfsema, M.R.G., Hedrich, R., 2005. In the light of stomatal opening: new insights into 'the Watergate.' New Phytol. 167, 665–691.

Roelfsema, M.R.G., Hedrich, R., 2010. Making sense out of Ca^{2+} signals: their role in regulating stomatal movements. Plant. Cell Environ. 33, 305–321.

Roelofsen, P.A., Houwink, A.L., 1951. Cell wall structure of staminal hairs ofTradescantia virginica and its relation with growth. Protoplasma 40, 1–22.

Rowe, M.H., Bergmann, D.C., 2010. Complex signals for simple cells: the expanding ranks of signals and receptors guiding stomatal development. Curr. Opin. Plant Biol. 13, 548–555.

Rubin, E.M., 2008. Genomics of cellulosic biofuels. Nature 454, 841–5.

Rui, Y., Anderson, C.T., 2016. Functional analysis of cellulose and xyloglucan in the walls of stomatal guard cells of Arabidopsis thaliana. Plant Physiol. 170, 1398–1419.

Rui, Y., Yi, H., Kandemir, B., Wang, J.Z., Puri, V.M., Anderson, C.T., 2016. Integrating cell biology, image analysis, and computational mechanical modeling to analyze the contributions of cellulose and xyloglucan to stomatal function. Plant Signal. Behav. 11, e1183086.

Sampedro, J., Cosgrove, D.J., 2005. The expansin superfamily. Genome Biol. 6.

Sapala, A., Runions, A., Routier-Kierzkowska, A.-L., Das Gupta, M., Hong, L., Hofhuis,

H., phane Verger, S., Mosca, G., Li, C.-B., Hay, A., Hamant, O., Roeder, A.H., Tsiantis, M., Prusinkiewicz, P., Smith, R.S., 2018. Why plants make puzzle cells, and how their shape emerges. Elife 7, e32794.

Scheller, H.V., Ulvskov, P., 2010. Hemicelluloses. Annu. Rev. Plant Biol. 61, 263–89.

Scheuring, D., Löfke, C., Krüger, F., Kittelmann, M., Eisa, A., Hughes, L., Smith, R.S., Hawes, C., Schumacher, K., Kleine-Vehn, J., 2016. Actin-dependent vacuolar occupancy of the cell determines auxin-induced growth repression. Proc. Natl. Acad. Sci. U. S. A. 113, 452–7.

Schindelin, J., Arganda-Carreras, I., Frise, E., Kaynig, V., Longair, M., Pietzsch, T., Preibisch, S., Rueden, C., Saalfeld, S., Schmid, B., Tinevez, J.-Y., White, D.J., Hartenstein, V., Eliceiri, K., Tomancak, P., Cardona, A., 2012. Fiji: an open-source platform for biological-image analysis. Nat. Methods 9, 676–682.

Schmidt, C., Schroeder, J.I., 1994. Anion Selectivity of Slow Anion Channels in the Plasma Membrane of Guard Cells. Plant Physiol. 106, 383–391.

Schneider, C.A., Rasband, W.S., Eliceiri, K.W., 2012. NIH Image to ImageJ: 25 years of image analysis. Nat. Methods 9, 671–5.

Schoch, P.G., Jaques, R., Lecharny, A., Sibi, M., 1980. Dependence of the Stomatal Index on Environmental Factors during Stomatal Differentiation in Leaves of Vigna sinensis L. J. Exp. Bot. 31, 1211–1216.

Scholl, R.L., May, S.T., Ware, D.H., 2000. Seed and molecular resources for Arabidopsis. Plant Physiol. 124, 1477–80.

Schroeder, J.I., Allen, G.J., Hugouvieux, V., Kwak, J.M., Waner, D., 2001. Guard cell signal transduction. Annu. Rev. Plant Physiol. Plant Mol. Biol. 52, 627–658.

Schroeder, J.I., Hagiwara, S., 1989. Cytosolic calcium regulates ion channels in the plasma membrane of Vicia faba guard cells. Nature 338, 427–430.

Schroeder, J.I., Hedrich, R., Fernandez, J.M., 1984. Potassium-selective single channels in guard cell protoplasts of Vicia faba. Nature 312, 361–362.

Schroeder, J.I., Raschke, K., Neher, E., 1987. Voltage dependence of K+ channels in guard-cell protoplasts. Proc. Natl. Acad. Sci. 84, 4108–4112.

Schuetz, M., Smith, R., Ellis, B., 2013. Xylem tissue specification, patterning, and differentiation mechanisms. J. Exp. Bot. 64, 11–31.

Shimazaki, K., Doi, M., Assmann, S.M., Kinoshita, T., 2007. Light Regulation of Stomatal Movement. Annu. Rev. Plant Biol. 58, 219–247.

Shope, J.C., DeWald, D.B., Mott, K.A., 2003. Changes in surface area of intact guard cells are correlated with membrane internalization. Plant Physiol. 133, 1314–21.

Sinclair, T.R., Tanner, C.B., Bennett, J.M., 1984. Water-Use Efficiency in Crop Production. Bioscience 34, 36–40.

Sloan, J., Backhaus, A., Malinowski, R., McQueen-Mason, S., Fleming, A.J., 2009. Phased control of expansin activity during leaf development identifies a sensitivity window for expansin-mediated induction of leaf growth. Plant Physiol. 151, 1844–54.

Smertenko, A.P., Deeks, M.J., Hussey, P.J., 2010. Strategies of actin reorganisation in plant cells. J. Cell Sci. 123, 3019–28.

Somerville, C., Bauer, S., Brininstool, G., Facette, M., Hamann, T., Milne, J., Osborne, E., Paredez, A., Persson, S., Raab, T., Vorwerk, S., Youngs, H., 2004. Toward a systems approach to understanding plant cell walls. Science (80-.). 306, 2206–11.

Souza, N.M., Topham, A.T., Bassel, G.W., 2017. Quantitative analysis of the 3D cell shape changes driving soybean germination. J. Exp. Bot. 68, 1531–1537.

Stanislas, T., Platre, M.P., Liu, M., Rambaud-Lavigne, L.E.S., Jaillais, Y., Hamant, O., 2018. A phosphoinositide map at the shoot apical meristem in Arabidopsis thaliana. BMC Biol. 16, 20.

Sticklen, M.B., 2008. Plant genetic engineering for biofuel production: towards affordable cellulosic ethanol. Nat. Rev. Genet. 9, 433–443.

Sumigray, K.D., Terwilliger, M., Lechler, T., 2018. Morphogenesis and Compartmentalization of the Intestinal Crypt. Dev. Cell 45, 183–197.

Tauriello, G., Meyer, H.M., Smith, R.S., Koumoutsakos, P., Roeder, A.H.K., 2015. Variability and Constancy in Cellular Growth of Arabidopsis Sepals. Plant Physiol. 169, 2342–58.

Tieman, D.M., Handa, A.K., 1994. Reduction in Pectin Methylesterase Activity Modifies

Tissue Integrity and Cation Levels in Ripening Tomato (Lycopersicon esculentum Mill.) Fruits. Plant Physiol. 106, 429–436.

Tierney, M.L., Varner, J.E., 1987. The Extensins. Am. Soc. Plant Biol. 84, 1–2.

Tomer, R., Khairy, K., Amat, F., Keller, P.J., 2012. Quantitative high-speed imaging of entire developing embryos with simultaneous multiview light-sheet microscopy. Nat. Methods 9, 755–763.

Topham, A.T., Taylor, R.E., Yan, D., Nambara, E., Johnston, I.G., Bassel, G.W., 2017. Temperature variability is integrated by a spatially embedded decision-making center to break dormancy in Arabidopsis seeds. Proc. Natl. Acad. Sci. U. S. A. 114, 6629–6634.

Truernit, E., Bauby, H., Dubreucq, B., Grandjean, O., Runions, J., Barthélémy, J., Palauqui, J.-C., 2008. High-resolution whole-mount imaging of three-dimensional tissue organization and gene expression enables the study of Phloem development and structure in Arabidopsis. Plant Cell 20, 1494–503.

Tsugawa, S., Hervieux, N., Hamant, O., Boudaoud, A., Smith, R.S., Li, C.-B., Komatsuzaki, T., 2016. Extracting Subcellular Fibrillar Alignment with Error Estimation: Application to Microtubules. Biophys. J. 110, 1836–1844.

Vahisalu, T., Kollist, H., Wang, Y.-F., Nishimura, N., Chan, W.-Y., Valerio, G., Lamminmäki, A., Brosché, M., Moldau, H., Desikan, R., Schroeder, J.I., Kangasjärvi, J., 2008. SLAC1 is required for plant guard cell S-type anion channel function in stomatal signalling. Nature 452, 487–491.

Veltman, D.M., Insall, R.H., 2010. WASP Family Proteins: Their Evolution and Its Physiological Implications. Mol. Biol. Cell 21, 2880–2893.

Vergara, C.E., Carpita, N.C., 2001. β-D-Glycan synthases and the CesA gene family: lessons to be learned from the mixed-linkage (1→3),(1→4)β-D-glucan synthase. Plant Mol. Biol. 47, 145–160.

Verger, S., Long, Y., Boudaoud, A., Hamant, O., 2018. A tension-adhesion feedback loop in plant epidermis. Elife 7, e34460.

Vischer, N., Nastase, S., 2009. ObjectJ: Non-destructive marking and linked results in

ImageJ [WWW Document]. URL https://sils.fnwi.uva.nl/bcb/objectj/index.html

von Wangenheim, D., Daum, G., Lohmann, J.U., Stelzer, E.K., Maizel, A., 2014. Live imaging of Arabidopsis development. Methods Mol. Biol. 1062, 539–50.

Vuolo, F., Kierzkowski, D., Runions, A., Hajheidari, M., Mentink, R.A., Gupta, M. Das, Zhang, Z., Vlad, D., Wang, Y., Pecinka, A., Gan, X., Hay, A., Huijser, P., Tsiantis, M., 2018. LMI1 homeodomain protein regulates organ proportions by spatial modulation of endoreduplication. Genes Dev. 32, 1361–1366.

Wang, M., Yuan, D., Gao, W., Li, Y., Tan, J., Zhang, X., 2013. A Comparative Genome Analysis of PME and PMEI Families Reveals the Evolution of Pectin Metabolism in Plant Cell Walls. PLoS One 8, e72082.

Wang, W., Sijacic, P., Xu, P., Lian, H., Liu, Z., 2018. Arabidopsis TSO1 and MYB3R1 form a regulatory module to coordinate cell proliferation with differentiation in shoot and root. Proc. Natl. Acad. Sci. U. S. A. 115, E3045–E3054.

Webb, A.A., Hetherington, A.M., 1997. Convergence of the abscisic acid, CO2, and extracellular calcium signal transduction pathways in stomatal guard cells. Plant Physiol. 114, 1557–60.

Webb, A.A.R., McAinsh, M.R., Mansfield, T.A., Hetherington, A.M., 1996. Carbon dioxide induces increases in guard cell cytosolic free calcium. Plant J. 9, 297–304.

Wei, P.-C., Zhang, X.-Q., Zhao, P., Wang, X.-C., 2011. Regulation of stomatal opening by the guard cell expansin AtEXPA1. Plant Signal. Behav. 6, 740–2.

Wendrich, J.R., Möller, B.K., Li, S., Saiga, S., Sozzani, R., Benfey, P.N., De Rybel, B., Weijers, D., 2017. Framework for gradual progression of cell ontogeny in the Arabidopsis root meristem. Proc. Natl. Acad. Sci. U. S. A. 114, E8922–E8929.

Weyers, J.D.B., Johansen, L.G., 1985. Accurate estimation of stomatal aperture from silicone rubber impressions. New Phytol. 101, 109–115.

Willats, W.G.T., McCartney, L., Knox, J.P., 2001. In-situ analysis of pectic polysaccharides in seed mucilage and at the root surface of Arabidopsis thaliana. Planta 213, 37–44.

Willis, L., Refahi, Y., Wightman, R., Landrein, B., Teles, J., Huang, K.C., Meyerowitz, E.M., Jönsson, H., 2016. Cell size and growth regulation in the Arabidopsis thaliana apical

stem cell niche. Proc. Natl. Acad. Sci. U. S. A. 113, E8238–E8246.

Winter, D., Vinegar, B., Nahal, H., Ammar, R., Wilson, G. V., Provart, N.J., 2007. An "Electronic Fluorescent Pictograph" Browser for Exploring and Analyzing Large-Scale Biological Data Sets. PLoS One 2, e718.

Wolf, S., Greiner, S., 2012. Growth control by cell wall pectins. Protoplasma 249, S169-75.

Woodward, F.I., 1987. Stomatal numbers are sensitive to increases in CO2 from pre-industrial levels. Nature 327, 617–618.

Woolfenden, H.C., Baillie, A., Gray, J.E., Hobbs, J.K., Morris, R.J., Fleming, A.J., 2018. Models and Mechanisms of Stomatal Mechanics. Trends Plant Sci. 23, 822–832.

Woolfenden, H.C., Bourdais, G., Kopischke, M., Miedes, E., Molina, A., Robatzek, S., Morris, R.J., 2017. A computational approach for inferring the cell wall properties that govern guard cell dynamics. Plant J. 92, 5–18.

Wu, Y., Ghitani, A., Christensen, R., Santella, A., Du, Z., Rondeau, G., Bao, Z., Colón-Ramos, D., Shroff, H., 2011. Inverted selective plane illumination microscopy (iSPIM) enables coupled cell identity lineaging and neurodevelopmental imaging in Caenorhabditis elegans. Proc. Natl. Acad. Sci. U. S. A. 108, 17708–13.

Wymer, C.L., Beven, A.F., Boudonck, K., Lloyd, C.W., 1999. Confocal Microscopy of Plant Cells. Confocal Microsc. 103–130.

Yanagisawa, M., Desyatova, A.S., Belteton, S.A., Mallery, E.L., Turner, J.A., Szymanski, D.B., 2015. Patterning mechanisms of cytoskeletal and cell wall systems during leaf trichome morphogenesis. Nat. Plants 1, 1–8.

Yi, H., Rui, Y., Kandemir, B., Wang, J.Z., Anderson, C.T., Puri, V.M., 2018. Mechanical Effects of Cellulose, Xyloglucan, and Pectins on Stomatal Guard Cells of Arabidopsis thaliana. Front. Plant Sci. 9, e1566.

Yu, Y., Fu, J., Xu, Y., Zhang, J., Ren, F., Zhao, H., Tian, S., Guo, W., Tu, X., Zhao, Jing, Jiang, D., Zhao, Jianbo, Wu, W., Wang, G., Ma, R., Jiang, Q., Wei, J., Xie, H., 2018. Genome re-sequencing reveals the evolutionary history of peach fruit edibility. Nat. Commun. 9, 5404.

Žádníková, P., Wabnik, K., Abuzeineh, A., Gallemi, M., Van Der Straeten, D., Smith, R.S.,

Inzé, D., Friml, J., Prusinkiewicz, P., Benková, E., 2016. A Model of Differential Growth-Guided Apical Hook Formation in Plants. Plant Cell 28, 2464–2477.

Zhang, X.-Q., Wei, P.-C., Xiong, Y.-M., Yang, Y., Chen, J., Wang, X.-C., 2011. Overexpression of the Arabidopsis α-expansin gene AtEXPA1 accelerates stomatal opening by decreasing the volumetric elastic modulus. Plant Cell Rep. 30, 27–36.

Zhao, L., Sack, F.D., 1999. Ultrastructure of stomatal development in *Arabidopsis* (Brassicaceae) leaves. Am. J. Bot. 86, 929–939.

Zhao, Y., Zhao, S., Mao, T., Qu, X., Cao, W., Zhang, L., Zhang, W., He, L., Li, S., Ren, S., Zhao, J., Zhu, G., Huang, S., Ye, K., Yuan, M., Guo, Y., 2011. The Plant-Specific Actin Binding Protein SCAB1 Stabilizes Actin Filaments and Regulates Stomatal Movement in Arabidopsis. Plant Cell 23, 2314.

Chapter 8: Appendix

8.1 Primers

8.1.1 Genotyping *expa16* and *expa4* T-DNA insertion mutants

Primer name	Sequence
SALK left border (LB) 1.3	ATTTTGCCGATTTCGGAAC
GABI left border (LB)	ATATTGACCATACTCATTGC
SALK_134337 FP	CAAAACCAAGAGGTTACCGTC
SALK_134337 RP	CGATACTTGTTGCTGTAGCCC
GABI-471E10 FP	TGAAACGCCTCAAATAAGGTC
GABI-471E10 RP	GGCTAGGTCAAAGTGTTCACG
RUB1 FP	GCGAACTTCGTCTTCACAA
RUB1 RP	GGAAAAAGGTCTGACCGACA
ACTIN2 FP	CCAGAAGGATGCATATGTTGGTG
ACTIN2 RP	GAGGAGCCTCGGTAAGAAGA

8.2 Literature review of LGX methodology

In order to give me the best chance of successful segmentation on LGX, a brief literature review was conducted to assess which sample preparation techniques were most common in order to successfully produce 3D cell segmentation on LGX (Table 8.1).

Out of all the papers reviewed, none looked specifically at stomata, with many focussing on embryos, flowers and roots, likely due to their small and/or transparent tissue. However, one paper looked at the patterning of Arabidopsis epidermal cells (Sapala et al., 2018) which showed stomata in their images, proving that cells on the leaf epidermis of plants can be successfully imaged and processed using LGX. What was clear across all the papers, and indeed the original article by Barbier de Reuille et al. (2015) is that one of the most important factors in successful 3D segmentation in LGX is the quality and strength of the cell outline signals.

Table 8.1 A literature review of papers using LithographX or MorphographX to image plant cells in 3D. Entries are in alphabetical order. PI = propidium iodide.

Paper	What imaging	Fluorophore(s) used	Processing notes
Bassel *et al.*, 2014	Arabidopsis embryos	PI (final concentration 100µg/ml) for 1-2 hours	Fixed and cleared tissue, chloral hydrate; confocal method from Truernit *et al.*, 2008
Bhosale *et al.*, 2018	Arabidopsis roots and cell nuclei	GFP and PI	Live tissue
Coneva *et al.*, 2017	Tomato leaf	0.002% PI for 2 hours in fixing/clearing steps	Fixed and cleared tissue
Hamant *et al.*, 2008	Arabidopsis shoot apex	GFP FM 4-64 dsRED	Merryproj (original paper); MGX review (Barbier de Reuille et al., 2015) Live tissue
Hetherington and Dolan, 2018	Arabidopsis root meristems	Likely autofluorescence	Sectioned tissue Live tissue
Jackson *et al.*, 2019	Arabidopsis SAMs	YFP plasma membrane marker	Live tissue
Kirchhelle *et al.*, 2016	Arabidopsis root	YFP (plasma membrane marker)	Live tissue
Kirschner *et al.*, 2018	Arabidopsis SAM	mVENUS	Live tissue
Kiss *et al.*, 2017	Arabidopsis stem and flower buds	Live tissue FM4-64	Live tissue
Louveaux *et al.*, 2016	Arabidopsis shoot apex	GFP (LTi6B – membrane protein)	Live tissue
McKim *et al.*, 2017	Arabidopsis flowers	0.1% PI for 2-5 minutes	Live tissue
Monniaux *et al.*, 2018	Arabidopsis flower development	YFP and PI	Live tissue
Prunet *et al.*, 2017	Arabidopsis flower development	Recommends either: a PM fluorescent protein; FM4-64 (20 mins); PI (2 mins).	Live tissue
Prunet, 2017	Arabidopsis flower development	PI (1mg/ml for 2 minutes before washing) FM4-64 (80µg/µl for 20 minutes before washing)	Live tissue
R Jones *et al.*, 2017	Arabidopsis stems	GFP FM 4-64 (30-60 seconds)	Live tissue
Sapala *et al.*, 2018	Arabidopsis cotyledon epidermis	pUBQ10::myr-YFP?! PI	Live tissue
Scheuring *et al.*, 2016	Arabidopsis roots – vacuolar morphology	PI used for segmenting cell boundaries MDY-64 (membrane marker), GFP, YFP, FM4-64, and PI for other aspects	Live tissue PI only stain used for MGX analysis

Souza, Topham and Bassel, 2017	Soybean hypocotyl during germination	PI 100µg/µl	Fixed and cleared tissue
Stanislas *et al.*, 2018	Arabidopsis shoot apical meristem	Various transgenics e.g. mCitrine, TdTomato, CFP FM4-64 for membrane staining	Live tissue
Tauriello *et al.*, 2015	Arabidopsis sepal	YFP epidermal fluorescent marker; mCitrine membrane marker	Live tissue Confocal method described in Roeder *et al.*, 2010 PI staining revealed dead/damaged cells
Topham *et al.*, 2017	Arabidopsis embryos	PI	Fixed and cleared tissue
Tsugawa *et al.*, 2016	Arabidopsis sepal	GFP mCherry	Microtubule marker (for study) and membrane marker (for cell segmentation) Mounted in agarose or culture medium on microscope **Used unspecified blurring and smoothing in MGX**
Verger *et al.*, 2018	Arabidopsis cotyledon epidermis Shoot apex	PI mCitrine GFP	**Live tissue**
Vuolo *et al.*, 2018	Arabidopsis shoots	DAPI, PI, mVENUS, GFP	Live tissue
Wang *et al.*, 2018	Arabidopsis roots and flowers	Live tissue Roots – PI for 2 mins Flowers – PI and GFP	Live tissue
Wendrich *et al.*, 2017	Arabidopsis root apical meristem	Fixed and used PI	Fixed and cleared tissue
Žádníková *et al.*, 2016	Arabidopsis embryos – apical hook	GFP	Fixed and cleared tissue